Kinetic Theory For Dilute And Concentrated Polymer Solutions: Study Of Nonhomogeneous Effects

by

Aparna Vasant Bhave

Submitted to the Department of Chemical Engineering
in partial fulfillment of the requirements for the degree of

Doctor of Philosophy in Chemical Engineering

at the

MASSACHUSETTS INSTITUTE OF TECHNOLOGY

October 1992

Author . . . . ⌄.┤. . . . . ⌐. . . . .┤. . . . .
Department of Chemical Engineering
October 22, 1992

Certified by. . . . .,. . . . .
Robert C. Armstrong
Professor
Thesis Supervisor

Certified by. . . . . ⌐. . ⌐. ⌐. .⸱. ⸱⸱ . . . . . . ⸱⸱ ⸱⸱⌐⸻.. . . . .
Robert A. Brown
Professor
Thesis Supervisor

Accepted by . . . . . ,⸱ ⸱⸱ . . . . ⸱ . . . . ⸱ . . . .
Robert E. Cohen
Chairman, Committee for Graduate Students

Kinetic Theory For Dilute And Concentrated Polymer Solutions: Study Of Nonhomogeneous Effects

by

Aparna Vasant Bhave

Abstract

Constitutive equations for dilute and concentrated polymer solutions are developed by using phase space kinetic theory in this thesis. The focus is on the study of spatial nonhomogeneities that are important in systems involving large gradients in stress and velocity, geometries with small spatial dimensions such as porous media and problems involving phase-separating systems. The modifications to classical kinetic theory that must be made in order to study such nonhomogeneous problems involve explicitly taking into account the spatial dependence of the polymer configurational distribution function and the finite spatial extent of the polymer molecules.

The nonhomogeneous dilute solution theory developed using a Hookean dumbbell model is a nonsimple viscoelastic fluid theory with diffusive coupling between stress at all points in the flow. Solution of any fluid mechanical problem with this theory involves imposing orientational boundary conditions. A generalized flux expression is derived that predicts molecular migration due to concentration, stress and velocity gradients. The stress diffusion terms are shown to scale as $\sqrt{D_{tr}\lambda_H}$, where D_{tr} is the polymer translational diffusivity and λ_H is the polymer relaxation time. Solution of a rectilinear shear flow problem was carried out and ties together ideas such as apparent slip in polymer solutions and the development of polymer depletion layers near solid walls. The apparent slip coefficient scaled as $\sqrt{D_{tr}\lambda_H}/L$, where L is the characteristic length scale of the system. The thickness of the depletion layers also scales as $\sqrt{D_{tr}\lambda_H}$.

The nonhomogeneous concentrated solution theory developed using a rigid dumbbell model incorporates the effects of hard-body polymer-polymer interactions and predicts a transition from a randomly-ordered isotropic phase to a prolate nematic phase with increasing concentration. The isotropic-nematic transition in spatially homogeneous systems was studied at equilibrium and in the presence of shear and shearfree flows. Material functions in these flows were also calculated. Multiple nematic phases were shown to coexist depending on the imposed kinematics and the initial molecular orientation. The existence of oblate symmetry was predicted in biaxial stretching flow and a two-dimensional in-planar oblate to prolate transition was

predicted with increasing concentration.

The development of structure by spinodal decomposition at the isotropic-nematic transition point was studied with a linear stability analysis. The effects of alternative forms of the intermolecular potential on the formation of structure were explored. In the absence of rotational diffusivity effects, the characteristic domain size λ_{dom} was shown to scale as the range of interaction between the interacting molecules and the growth rate scaled as D_{tr}/λ_{dom}^2, in agreement with the classical theory of spinodal decomposition. In the presence of rotational diffusivity, no spatial pattern develops for a range of concentrations within the unstable spinodal region. At higher concentrations, classical behavior and domain formation is again seen. The effect of flow on the onset of instability was also studied with the linear stability analysis and the critical concentration for change in stability in the presence of flow $\mathcal{N}'$ scaled such that $\mathcal{N}_c - \mathcal{N}' \sim \delta^{1/2}$, where $\delta \equiv \dot{\epsilon}/D_r$ in shearfree flow and $\delta \equiv \dot{\gamma}/D_r$ in shear flow.

Thesis Supervisor: Robert C. Armstrong
Title: Professor

Thesis Supervisor: Robert A. Brown
Title: Professor

Acknowledgements

It's so difficult to describe what all the different people here have meant to me.

Let me start at the beginning. Aai and Baba, I want to dedicate this thesis (for what it is worth) to you. You have been with me from the beginning, through all my fits of elation and depression. Your belief in your daughter has always been and always will be a point of support for me. Tai and Brett, you have stood by me and supported me always. I know I aggravate you at times, but deep down you know what your love means to me. And Subodh, I will save the best for last.

All my friends here – three names stand out – Bhavik, Ramnath and Vishak. Should I say thanks? For your willing ears and your words of support. I have special memories of our friendship. And Vivek, your superb sense of the ridiculous never failed to cheer me up. Bhattu, you give me courage with your patience and endurance. And Sudhakar, maybe we'll see you in iceberg-land.

And all the folks in 246 and 254 – the older ones who are out there somewhere and the younger ones who soon will be. Dilip, don't let your cynicism about Mobil make you bitter, there is bound to be change. Paul C., I have great respect for your sense of the "correct" and your strange sense of humor. The office has been a quiet place since you graduated. Jeff, hang in there ... Todd, you too. Remember you guys are the next ones to jump the boat. Mike and Lars, good luck and all that. Sureshman, keep at it, sir. Good luck to you and Shanti. And Radha, it's good to have you as part of the group. Dimitris, I know I'll be reading about you. And Angelos, good luck to you in your job search – don't aim low. Costas, a special word of thanks for not rebuffing me on the countless occasions that I came and bothered you. Howard, good luck in wrapping up at MIT. Dr. B., I'll remember your advice about the cold! Keep in touch, all of you, and visit us in Minnesota.

Bob and Bob, thanks for your guidance and support. You once said that this was my chance to reach out for the best – it is for you to decide the measure of my success. A special note for Arline: thanks for all your help, and your cheerful smile. Remember you promised to visit me in MN. And Nancy, what would we do without

you?

It is the end of a phase of my life now. I am at a new beginning, with you, Subodh, as my partner. With you by my side, I will reach my goals ... come, let us walk together.

Contents

List of Figures

List of Tables

Chapter 1

Introduction

1.1 Issues in the Development of Molecular Theories for Polymeric Liquids

Low-molecular-weight fluids, such as water, that display Newtonian behavior have been the focus of many intensive studies in the area of fluid mechanics. Such fluids are characterized by a constant viscosity, and have flow behavior that is accurately described by the Navier-Stokes equations. However, many other fluids, such as polymer solutions and melts, fiber and colloidal suspensions, liquid crystals and foams do not obey this description. These fluids form a large and important segment of today's chemical process industries. In 1988, for instance, 30 billion tons of synthetic polymers were produced in the United States, with a value of approximately $240 billion (Standard and Poors, 1989). It is crucial to extend our understanding of Newtonian fluid mechanics to encompass this vast array of materials that are generally called *non-Newtonian* fluids.

The first step in the study of non-Newtonian fluid mechanics is obtaining a rheological equation of state or *constitutive model* for the fluid that describes precisely the relations between the stress τ and strain-rate $\dot{\gamma}$ of an arbitrary material element, regarded as part of a flowing continuum. This is the counterpart of the Newtonian constitutive equation $\tau = -\mu\dot{\gamma}$, where μ is the constant Newtonian viscosity. The

constitutive equation, in general, is a relation between the kinematic, dynamic and thermodynamic variables associated with a material element and also involves physical constants of the material. The development of a compact constitutive equation for any non-Newtonian fluid is complicated by the vast range of complex rheological responses displayed by these fluids. This complex rheology is a consequence of the internal microstructure possessed by non-Newtonian fluids, that can be deformed by the imposed flow field. In turn, the fluid stresses are strongly dependent on the microstructure and any change in the microstructure also affects the flow field and results in the complex rheology. The close coupling between the internal microstructure and the imposed flow fields can, in fact, be used to "tailor" the microstructure to specifications, and thereby achieve desired material properties in the final material. A good constitutive model should be capable of describing the relationship between the internal microstructure and the imposed flow field, by capturing the essence of the underlying dynamical processes on the scale of the internal microstructure.

The early constitutive models were phenomenological, often restricted to only a few classes of flows and incapable of describing all the rheological responses displayed by these fluids. In the last several decades, the close relation between the internal microstructure and rheological properties has been recognized, and the more recent constitutive equations are based on micromechanical descriptions of macromolecular systems. This approach is referred to as *kinetic theory* and uses the principles of nonequilibrium statistical mechanics to obtain the relation between the microscopic mechanical model parameters and the macroscopic flow properties of the system. Kinetic theory is applied in this thesis to focus on the development of constitutive equations for polymeric liquids.

Early kinetic theories for polymeric liquids used crude models for the polymer chain that did not account for the details of the molecular architecture; subsequently, more complex models were introduced to account for chain branching and steric hindrances between two different molecules and between parts of the same molecule. Such realistic complex models are used in the study of equilibrium properties of the polymer solutions, *e.g.*, differences in chain conformation in the presence of different

solvents. However, the study of microstructure in the presence of flow is a much more complex problem; as a result, kinetic theory developments of constitutive equations aimed at describing the rheology of polymer solutions and melts are generally restricted to simpler micromechanical models.

Kinetic theory development of constitutive equations can be broadly divided into two categories: dilute solution theories and theories for concentrated solutions or melts. In the dilute solution theories, the polymer molecule is considered to interact only with the surrounding solvent molecules, which are considerably smaller than the polymer chain. On the scale of the macromolecule, the *average* behavior of a single polymer chain in a *mean field* due to the surrounding solvent particles provides an accurate description of the system. Theories for concentrated solutions are much more complex than the dilute solution theories. A primary reason is that polymer-polymer interaction must be explicitly considered for an accurate representation of the system. However, a mean field approach is necessary to keep the problem mathematically tractable. The goal of such a theory is to capture the essence of the intermolecular interactions in a mean field description, so as to predict the behavior of concentrated systems with some degree of accuracy.

Some of the problems studied using these constitutive theories include the effect of chain flexibility on rheological properties (Armstrong, 1974a & 1974b; Wedgewood *et al.*, 1991), the effect of incorporating *hydrodynamic interaction*, *i.e.*, perturbation of the solvent velocity due to the local chain motion (Öttinger, 1985, 1986 & 1987), the effect of excluded volume interactions between different parts of the same polymer chain due to the finite volume occupied by the chain (Baldwin and Helfand, 1990; Öttinger, 1989b & 1990), effect of entanglements in concentrated systems (Lodge, 1985) and the effect of constraints imposed on the motion of a single polymer chain due to the surrounding polymer matrix (Doi and Edwards, 1978a, 1978b, 1978c & 1979; Curtiss and Bird, 1981a & 1981b). These and other developments in polymer kinetic theory have been reviewed recently by Bird and Öttinger (1992).

1.1.1 Importance of Incorporating Spatial Nonhomogeneities

The extensive use of kinetic theory for development of constitutive theories has given considerable insight into molecular processes underlying the complex rheological features exhibited by polymer solutions and melts and it is sometimes possible to relate specific molecular features to a characteristic rheological response. However, for simplicity, most theories have been aimed at elucidating *bulk* properties of the system, and at the very outset in their development, the system is taken to be unbounded and *spatial homogeneity* is assumed. This implies an assumption of uniform concentration through the system, as well as uniform stress and velocity gradients on the length scale of the macromolecule. These homogeneous, unbounded constitutive theories are sufficient in problems where the assumptions of spatial homogeneity hold, such as in the calculation of bulk rheological properties in an imposed flow field. However, in coupling fluid rheology and fluid mechanics, specific flow geometries and boundaries are introduced that can lead to a breakdown of the assumption of spatial homogeneity. Consequently, the *homogeneous* theories are unsuitable for the study of intrinsically nonhomogeneous problems, *e.g.*, problems involving sharp gradients in stress and velocity fields, possibly on length scales comparable to macromolecular length, descriptions of phase-separating systems and models of systems involving small spatial dimensions such as flow through porous media where wall effects could play a major role. These systems are often encountered in the processing of polymer solutions, as described next.

The advisability of using intrinsically homogeneous models for studying problems involving large gradients in the stress and velocity fields has often been questioned (Brown *et al.*, 1986; Lipscomb *et al.*, 1987). The difficulty is clear from studies of the flow through an abrupt contraction (Coates, 1992; Marchal and Crochet, 1987), as shown in Fig. 1-1. For both Newtonian and non-Newtonian fluids, the stresses in the fluid become infinite as one approaches the reentrant corner singularity. For the Newtonian fluid, the stress is *square integrable* and leads to a finite force on the wall (Dean and Montagnon, 1949; Moffatt, 1964; Coates *et al.*, 1992); for the homogeneous viscoelastic fluid models that have been used, the *integrability* of the
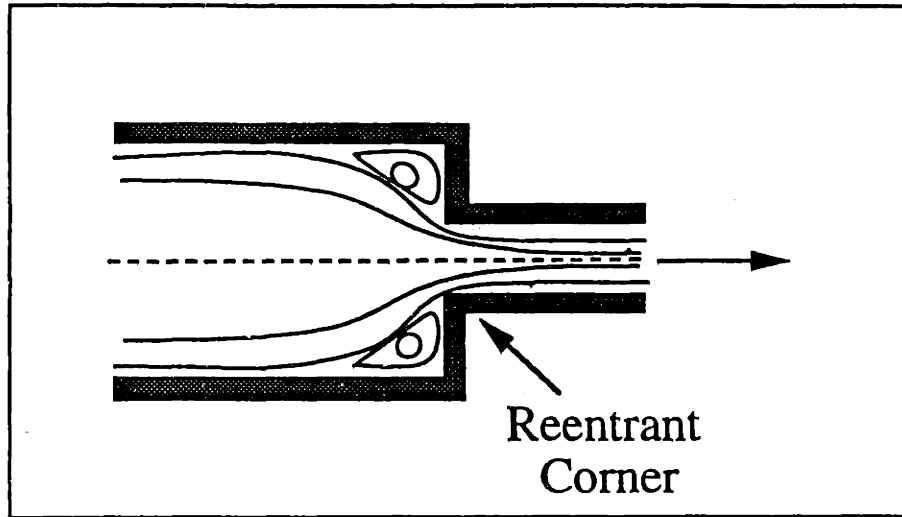
Figure 1-1: Flow through an abrupt contraction.

stresses is not necessarily guaranteed. A number of homogeneous viscoelastic models have been studied by Coates (1992); in most cases, integrability is guaranteed only in the presence of a Newtonian solvent or by suitable modification of the constitutive theory in the vicinity of the singularity. In these models, however, the effect of the large stress and velocity gradients on the fluid microstructure in the vicinity of the reentrant corner singularity has not been rigorously examined.

It has been suggested that development of large gradients in stress and velocity on length scales comparable to the length of the polymer chain can result in segregation between solvent and polymer molecules or between polymer molecules of different molecular weight (Tirrell and Malone, 1977; Aubert and Tirrell, 1980; Aubert et al., 1980). The hypothesis of Tirrell and Malone, termed as "stress-induced diffusion", suggests that polymer molecules migrate from regions of higher stress gradients to regions of lower stress gradients, due to an entropic driving force. Extending this hypothesis to the contraction flow problem, it can be speculated that polymer molecules migrate away from the corner singularity and leave only the Newtonian solvent behind.

19
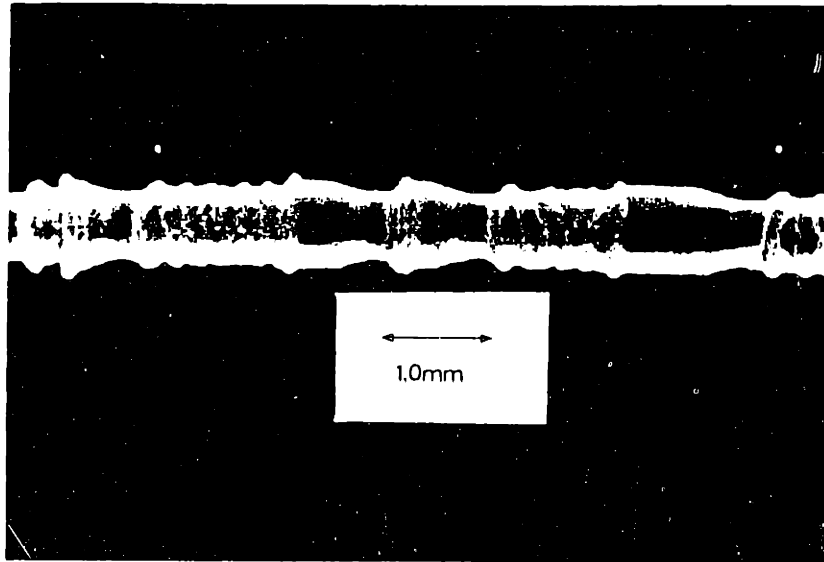
Figure 1-2: Extrudate distortion in the melt fracture instability (*reproduced from* Denn, 1990).

Thus, at the reentrant corner, the integrable stress condition would be automatically satisfied. A constitutive theory that consistently accounts for the effects of such stress and velocity gradients on the microstructure is necessary to prove or disprove this micromechanical picture of the polymer solution in a high stress gradient.

The presence of solid boundaries is an ubiquitous source of nonhomogeneities; in flow problems involving small spatial dimensions, wall effects can have a significant impact on the bulk flow. For instance, in problems of enhanced oil recovery, polymer solutions have to flow through natural porous media where the pore dimension $(1 - 20\mu m)$ is often comparable to macromolecular sizes $(0.4 - 1\mu m)$; molecular orientation imposed as a result of steric hindrances with the wall lead to a reduced apparent viscosity that depends on pore size and increased flow rate through the porous medium (Chauveteau, 1982). The interaction between the polymer and wall also has been invoked to explain the melt *fracture* instability, illustrated in Fig. 1-2. When the throughput of polymer melt from an extruder exceeds a material-dependent

critical value, the surface of the extrudate develops wave-like periodic oscillations, as seen from Fig. 1-2. It has been suggested that adhesion of the polymer to the wall breaks down beyond a critical throughput, and leads to the onset of the melt fracture instability (Ramamurthy, 1986; Denn, 1990). The data collected by Ramamurthy indicate that the point of onset of the instability is modified by changing the material of the die and thus, by changing the adhesion properties at the solid-melt interface. The mechanism for the lack of adhesion leading to the instability is not at all clear.

Spatial nonhomogeneities that are introduced either due to the presence of solid boundaries or due to the effect of nonhomogeneous stress and velocity fields can be viewed as nonhomogeneities that are extrinsic to the dynamics of the internal microstructure. In addition to these extensive sources, spatial nonhomogeneities are intrinsic to and an important consequence of the dynamics of phase-separating systems. The problem of treating such spatial nonhomogeneities is of particular importance in polymeric liquid crystalline systems, where the development of *uniform* orientational order is key to exploiting the unique properties of these materials.

A schematic of the disorder-order transition that occurs with increasing concentration in liquid crystalline systems is illustrated in Fig. 1-3. The solution makes the transition from an isotropic state to an ordered nematic one through a metastable region of coexistence as the concentration is increased. In the metastable region, orientational order develops via *nucleation and growth*, whereby a nucleus of well-defined order is first formed and then grows in wavelength with fixed amplitude. In the unstable region, orientational order spontaneously develops by *spinodal decomposition* over the entire system (Cahn, 1961 & 1965); in this case, direction of ordering is correlated over a fixed wavelength and the amplitude or degree of ordering increases gradually with time. Both processes lead to the development of a so-called *polydomain* texture, where the molecular orientation is relatively uniform over a region identified as the *domain*, although orientation between domains is entirely uncorrelated. The surfaces between domains eventually decay to point and line defects (de Gennes, 1974); the defects represent very rapid changes in orientational order over very small distances. These defects are persistent, especially in liquid crystalline polymers, and can have a
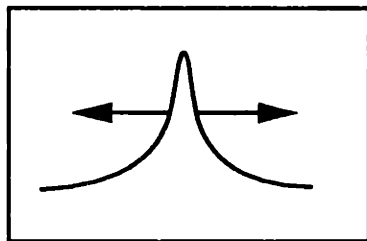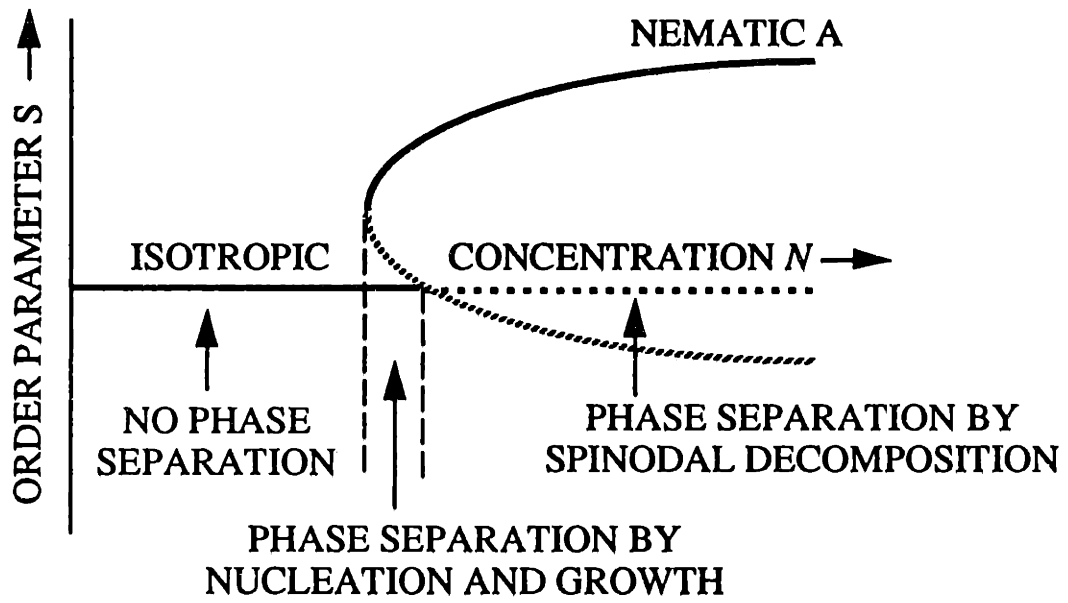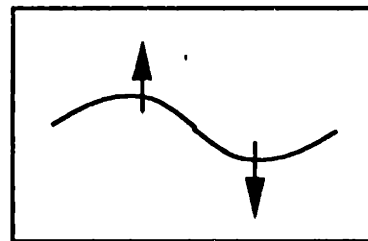
Figure 1-3: Schematic of the disorder-order transition in liquid crystalline systems.

significant effect on the properties of these systems.

In order to consider these and the descriptions of other systems with nonhomogeneous structure, it is necessary to develop a comprehensive theory that considers the effects of nonhomogeneities on a macromolecular length scale. The goal of this thesis is to construct a rigorous and consistent kinetic theory framework that allows the incorporation of spatial nonhomogeneities into constitutive equations that describe polymer and liquid crystalline solutions.

1.2   Thesis Goals

The role of spatial nonhomogeneities in different physical systems is examined in this thesis using the concepts of phase-space kinetic theory, as laid out in Bird *et al.* (1987b). Two problems have been studied. The first problem is the extension of the homogeneous dilute solution theories to incorporate nonhomogeneities and to understand the coupling between polymer concentration, stress and velocity fields. The theory is based on explicitly retaining the spatial dependence of the field variables and allowing for rapid changes in the concentration, stress and velocity fields on the length scale of the polymer molecule. This nonhomogeneous theory allows the incorporation of polymer-wall interactions, by way of explicit boundary conditions. The effect of boundary conditions on the bulk flow behavior can thus be easily studied. A very simple molecular model is used to keep other complications to a minimum.

The development of structure at the order-disorder transition in liquid crystalline polymers eventually leads to the formation of defects that have a significant impact on the material properties. The second problem is therefore concerned with the extension of the nonhomogeneous dilute solution theory to a highly concentrated solution of rigid rods that undergoes a transition from a randomly ordered phase to an orientationally ordered liquid crystalline phase with increasing concentration. In such concentrated systems, the intermolecular interaction between polymer molecules plays a key role in determining the properties of the system. In the description of the rigid-rod system, pairwise *excluded volume* interactions between two rigid rods

prevent the intersection of two rigid rods and leads to the disorder-order transition with increasing concentration (Onsager, 1949). Here, *excluded volume* refers to the volume occupied by a rigid rod that is inaccessible to any other rigid rod. The goal of this study is to understand the role of the intermolecular potential in the development of structural order at the critical concentration.

A nonhomogeneous theory for the concentrated rigid rod system is developed within the kinetic theory framework. A mean-field version of the hard-rod interaction potential is developed; the potential is a nonhomogeneous generalization of the mean-field Maier-Saupe potential that has been used in previous homogeneous theories for liquid crystalline polymers (Maier and Saupe, 1958 & 1959; Doi, 1980 & 1981, Menon, 1990). The potential accounts for the increased importance of the excluded volume interactions between the molecules with increasing concentration and incorporates the effects of a finite range of interaction between two rigid rods. The homogeneous aspects of the theory are first studied by ignoring all spatial gradients in the description of the microstructure. The equilibrium phase transition from a disordered to an ordered phase is studied, along with the effect of different flow fields on the development of microstructure and the associated rheological properties of the system in steady and transient flows.

The formation of oriented domains at the disorder-order transition point by spinodal decomposition is a result of a short-range ordering process between the rigid-rod-like molecules, and as such can be regarded as an example of *cooperative phenomena* (Stanley, 1971). It crucially depends on the manner in which the interactions propagate order from one particle to another, and the interaction potential plays an important role in determining the dynamics of this ordering process. The final goal in the study of these concentrated systems is to understand the role of the interaction potential on spinodal decomposition, and identify the details that must be incorporated into the nonhomogeneous theory in order to correctly model the phase transition. Linear stability theory is adopted to study the structure that develops at the equilibrium phase transition point and to predict the characteristic domain sizes at the onset.

1.3   Thesis Outline

The internal microstructure possessed by polymer solutions is responsible for its complex flow behavior that differs greatly from that exhibited by small-molecular-weight Newtonian fluids. The close relationship between the microstructure and fluid rheology has lead to the development of constitutive theories based on micromechanical models and nonequilibrium statistical mechanics to describe non-Newtonian behavior. An introduction to the development of micromechanical-model-based constitutive theories for polymeric or viscoelastic fluids is given in Chapter 2. The structure of the macromolecule, and the ideas of *relaxation time* and *fading memory* are introduced in Section 2.1. The behavior of polymeric liquids is contrasted with ordinary Newtonian fluids, with the goal of illustrating the complex rheology displayed by the polymeric fluids. The different flow fields and material functions that are used to characterize the complex rheological behavior are described in Section 2.2. Finally, the basic concepts behind kinetic theory of viscoelastic constitutive equations are introduced in Section 2.3. The molecular models that are commonly used to model complex polymer molecules are described in Section 2.3.1, and concepts of configurational distribution functions and ensemble averaging are introduced in Section 2.3.2. Some of the common problems encountered in most kinetic theory developments are also discussed, such as the mean-field treatment of the intermolecular forces and the need to use closure approximations. This section serves as an introduction to much of the notation that is used in the subsequent development of the nonhomogeneous theories. The *Oldroyd-B* constitutive equation is derived in Section 2.3.3 using the kinetic theory ideas described in the previous sections, and the derivation serves as an illustration of the underlying assumptions in traditional kinetic theory developments. The ideas of spatial homogeneity that makes the traditional theories unsuitable to the study of inherently nonhomogeneous problems also are discussed.

The development of a consistent kinetic theory framework for the treatment of nonhomogeneous problems is described in Chapter 3. An introduction to the nonhomogeneous problem is given in Section 3.1. Other theories that have been suggested

to explain the anomalous behavior observed in nonhomogeneous systems also are reviewed in this section. The changes that must be made to a homogeneous kinetic theory in order to incorporate spatial nonhomogeneities are discussed in Section 3.2. The constitutive equation for nonhomogeneous systems is developed in Section 3.3 using phase space kinetic theory. At the outset, the choice of the molecular model and the notation are described. The hydrodynamic equations of change are obtained first. Next, simplified expressions for the mass flux vector and stress tensor are developed involving averages with respect to the distribution functions. Finally, evolution equations for the distribution function are obtained in order to close the equation set. On simplification, a coupled set of equations are obtained for the polymer concentration and stress contribution. These equations are compared to the corresponding homogeneous constitutive equation, the *Oldroyd B fluid* model, and the significance of the new terms in the constitutive theory is discussed. The nonhomogeneous constitutive theory is a *non-simple* fluid theory, because the stress at a point in the flow couples, in a diffusive manner, to all other points in the flow. There is need to impose boundary conditions on molecular orientation which allows determination of stress at the boundary. Suitable boundary conditions are also discussed in this section. A simple problem of rectilinear shear flow is solved to illustrate the significant features of this constitutive equation. The main development in Chapter 3 ignores the effect of all external forces and neglects the effects of bead inertia. The effect of incorporating external forces and bead inertia is studied in Section 3.5.

The development in Chapter 3 accounts for the effect of spatial nonhomogeneities that arise due to factors external to the dynamics of the molecules. In addition, spatial nonhomogeneities develop as a result of phase separation, and the structure of the nonhomogeneity in these systems is closely related to the interactions between individual macromolecules that comprise the internal microstructure. These problems are of special importance in polymeric liquid crystalline systems, as discussed in Section 1.1.1. The nonhomogeneous theory for dilute polymer solutions developed in Chapter 3 is extended in Chapter 4 to concentrated systems of rigid-rod-like molecules that undergo a transition to liquid crystalline nematic phases with increasing concen-

tration. An introduction to liquid crystalline systems is presented in Section 4.1, along with the significant rheological features displayed by these systems. The rheology of liquid crystalline polymers is also compared to isotropic polymer rheology to illustrate the effects of molecular ordering. A review of existing theories for liquid crystalline polymers is presented in Section 4.2.

The development of Chapter 3 is paralleled in Section 4.3, where the nonhomogeneous liquid crystalline constitutive theory is developed. The theory differs from the development presented in Chapter 3 in that the molecular model is chosen to be a rigid dumbbell to account for the stiff backbones of molecules that have a tendency to form ordered phases. Moreover, intermolecular interactions that were neglected in the dilute solution theory of Chapter 3 are now included. The presence of a rigid dumbbell model makes it convenient to use *generalized coordinates*, which are described in Section 4.3.1. The importance of correctly capturing the essence of the intermolecular interaction into a mean-field type potential has already been emphasized in this chapter. The homogeneous mean-field Maier-Saupe potential has been used in the early homogeneous theories for liquid crystalline polymers and is generalized here to account for spatial nonhomogeneities by including the effects of a finite interaction range between the interacting rigid-rods. One such generalization, the hard-rod potential, that is used to model the excluded volume effects is discussed in Section 4.3.2. An alternative form for the interaction potential was recently developed (Marrucci and Greco, 1991; Greco and Marrucci, 1992a & 1992b) by using a similar development, and is compared in this section with the hard-rod potential. The relevant equations of change and the constitutive equation are developed in Section 4.3.3 for a general potential. Closure approximations that are required to obtain a closed set of equations also are described in detail.

The homogeneous aspects of the liquid crystal problem are studied in Chapter 5. A considerably simpler set of equations is obtained in Section 5.1 by making an assumption of spatial homogeneity in the equations developed in Chapter 4. The phase behavior and microstructure predictions at equilibrium and in the presence of shear and elongational flow fields is studied in Section 5.2. The different phases that can

coexist are obtained in the different flow fields. The rheological predictions in steady and transient flows are studied in Section 5.3. The use of closure approximations has a significant effect on some rheological predictions. The conditions that must be imposed on any closure approximation and the possibility of using alternative closure approximations is explored in Section 5.5.

The nonhomogeneous aspects of the liquid crystalline problem are studied in Chapter 6. With increasing concentration, the randomly ordered isotropic state becomes unstable due to the increased effect of excluded volume interactions that prevent two molecules from intersecting each other. In the unstable region, orientational order spontaneously develops by spinodal decomposition. The classical theory of spinodal decomposition in binary alloys and glasses developed by Cahn (1961 & 1965) is presented in Section 6.1. Linear stability theory is adopted in Section 6.2 to study the predictions of the nonhomogeneous governing equations developed in Chapter 4. A dispersion equation that gives the relation between growth rate and spatial wavenumber is used to obtain the characteristic domain sizes at any given concentration in Section 6.2.1. The effect of closure on the dispersion relation is also examined in this section. The predictions for the two forms of the intermolecular potential, developed in Section 4.3, are compared in Section 6.2.2. The predictions for characteristic domain size are related to the interaction range of the intermolecular potential. In classical spinodal decomposition, the separation of phases is accomplished purely due to translational diffusivity of the separating molecules. In the liquid crystal problem, rotational diffusivity D_r also can be significant compared to the translational diffusivity D_{tr}. The role played by D_r in spinodal decomposition is explored in Section 6.2.3. The effect of flow on the dispersion relation and on the critical concentration for the onset of instability is studied in Section 6.3.

Chapter 2

Viscoelastic Constitutive Theories

The internal microstructure possessed by polymer solutions and melts leads to complex rheological behavior. It is inadequate to define a single viscosity for these materials and other *material functions* are needed to characterize the fluid completely. The behavior of Newtonian and viscoelastic materials is compared in Section 2.1, and some of the commonly used material functions are defined in Section 2.2. Our goal is to be able to describe the complex rheology of polymeric fluids with the help of closed form constitutive models. Recognizing the close relation between the rheology and the internal microstructure, recent constitutive models are based on micromechanical models of the macromolecular system and are developed by using a formal kinetic theory framework. The basic ideas behind the kinetic theory of polymer solutions are presented in Section 2.3. The different molecular models that have been used for the development of constitutive equations are discussed in this section.

2.1   Viscoelastic Phenomena

A polymer or macromolecule consists of a long backbone of smaller monomer units joined together, with attached side-groups that are often bulky and complicated. Typical molecular weights range from $10^4 - 10^6$ gm/mol. Free rotation about the C-C bonds, that make up a hydrocarbon backbone, allows the molecule to exist in a large number of configurations. Furthermore, the molecule can change from one configura-

tion to another; such configurational changes may be either local rearrangements of the backbone or large overall changes in configuration. The preferred configuration depends on the different forces that act on the molecule. For instance, when subjected to a spatially or temporally varying flow field, the molecular configuration changes continuously so as to balance this applied force. As the molecule coils and stretches in an effort to change its configuration, there are a number of characteristic time constants (or scales) associated with the different molecular motions. These comprise the spectrum of relaxation times that characterize the polymer molecule. The relaxation spectrum gives the fluids a *fading memory* with the duration of the longest relaxation time. When this longest relaxation time is of the same order-of-magnitude as the characteristic time for the macroscopic flow system, marked deviations from Newtonian fluid mechanics are observed.

A measure of the deviation of the system from Newtonian behavior is best given in terms of a dimensionless group, the *Deborah number* (Reiner, 1964; Bird, 1965). The Deborah number is defined as the ratio of a characteristic time for the fluid relaxation λ to a characteristic time of the flow system t_{flow}, as

$$\mathrm{De} = \frac{\lambda}{t_{flow}}. \tag{2.1}$$

If the Deborah number is small, the polymer molecules retain their equilibrium configuration, and the polymeric fluid exhibits more or less Newtonian behavior. Thus, the limit $\mathrm{De} \to 0$ represents a viscous Newtonian fluid. Conversely, if the Deborah number is large, polymer molecules that are strongly distorted by the flow cannot relax to their equilibrium configuration during the time scale of the process or experiment. In the limit $\mathrm{De} \to \infty$, the experiment happens so fast that the polymer molecules have no time to change configuration, and the fluid behaves like an elastic solid. Polymeric liquids are therefore often referred to as *viscoelastic* fluids.

The deformability of the internal microstructure by external flow fields and the fading memory possessed by the constituent polymer molecules results in a number of interesting viscoelastic phenomena. For instance, if we insert rotating rods into two

30
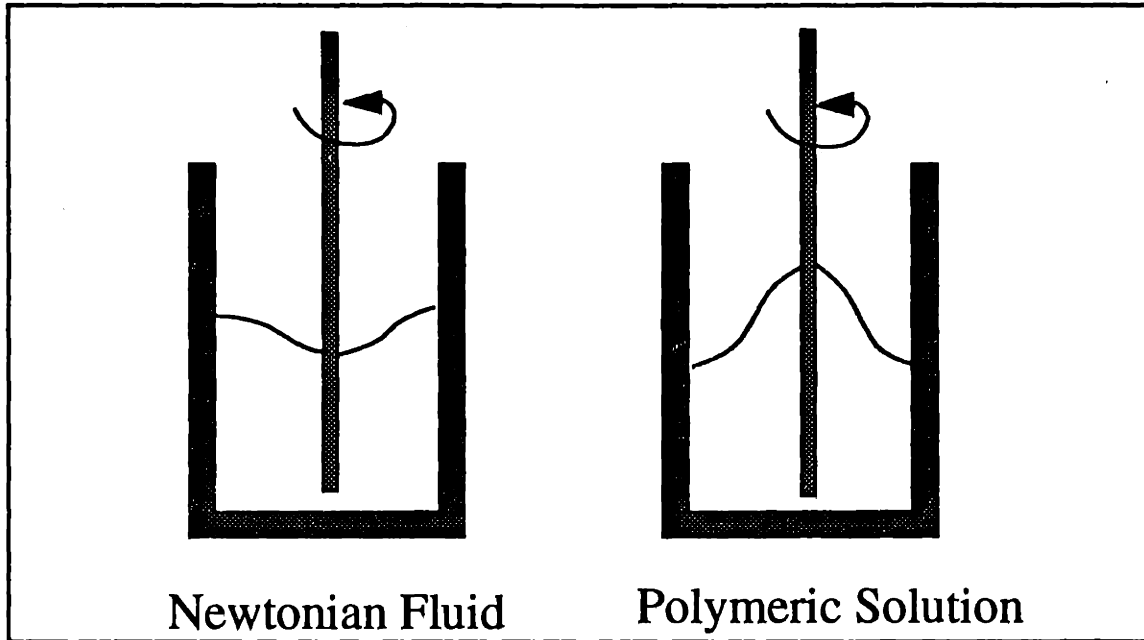
Figure 2-1: The Weissenberg effect.

beakers, filled with a Newtonian and a polymeric liquid, drastically different effects are seen; see Fig. 2-1. In the Newtonian case, the centrifugal forces push the liquid outward from the rotating rod, and a small dip in the free surface is seen at the center. On the other hand, for the polymeric solution, the fluid is pushed inwards and climbs up the rotating rod. This phenomenon is a direct consequence of the stretching and orientation of the polymer molecules along the circular streamlines that results in the development of normal stresses. These normal stresses oppose the centrifugal force on the fluid and are sufficiently strong to cause a net flow inwards, resulting in the rod-climbing phenomenon or the *Weissenberg effect*. Fluids comprised of small molecules that can be treated as point particles do not show such normal stress effects since the molecules are not capable of alignment with the flow.

This example illustrates the point that the deformable internal microstructure possessed by polymer solutions is responsible for effects that are unique to viscoelastic fluids. Other examples of such viscoelastic phenomena are described in Bird *et al.* (1987a). In order to accurately model the flow behavior of such polymeric fluids, a constitutive theory must be able to account for the stretching, rotation and

deformation of constituent molecules that changes the internal microstructure.

2.2 Material Functions for Polymeric Liquids

Fluids without microstructure, such as Newtonian fluids, are characterized by a single viscosity coefficient. Alternatively, due to the internal microstructure and its ability to get deformed in the presence of flow fields, a number of material functions that depend on shear rate, frequency and time must be defined in order to characterize completely the viscoelastic fluid.

The flow fields used most commonly to characterize non-Newtonian fluids are shear flow and shearfree flow. A simple shear flow is given by the flow field

$$v_x = \dot{\gamma}_{yx} y; \quad v_y = 0; \quad v_z = 0 \tag{2.2}$$

where the velocity gradient $\dot{\gamma}_{yx}$ may be a function of time. Based on measurements of the shear stress τ_{xy} in steady shear flow (i.e., $\dot{\gamma}_{yx}$ = constant), a steady-state non-Newtonian viscosity η is defined as

$$\tau_{yx} = -\eta(\dot{\gamma})\dot{\gamma}_{yx} \tag{2.3}$$

where the shear rate $\dot{\gamma} = \sqrt{1/2\dot{\gamma}:\dot{\gamma}}$. Viscoelastic fluids show non-zero normal stresses in simple shear flow, unlike Newtonian fluids which show no normal stresses. These normal stresses manifest themselves dramatically, as illustrated by the rod-climbing experiment, and must also be measured. For simple shearing flows of incompressible fluids, only two independent combinations of the normal stresses can be measured (Bird et al., 1987a), provided the fluid is isotropic. Also, it is not possible to distinguish between pressure and normal stresses from normal force measurements in experiments. Therefore, the two normal stress differences $\tau_{xx} - \tau_{yy}$ and $\tau_{yy} - \tau_{zz}$ are customarily measured. Based on these stress measurements, two other steady-state shear flow material functions are defined as the first and second normal stress
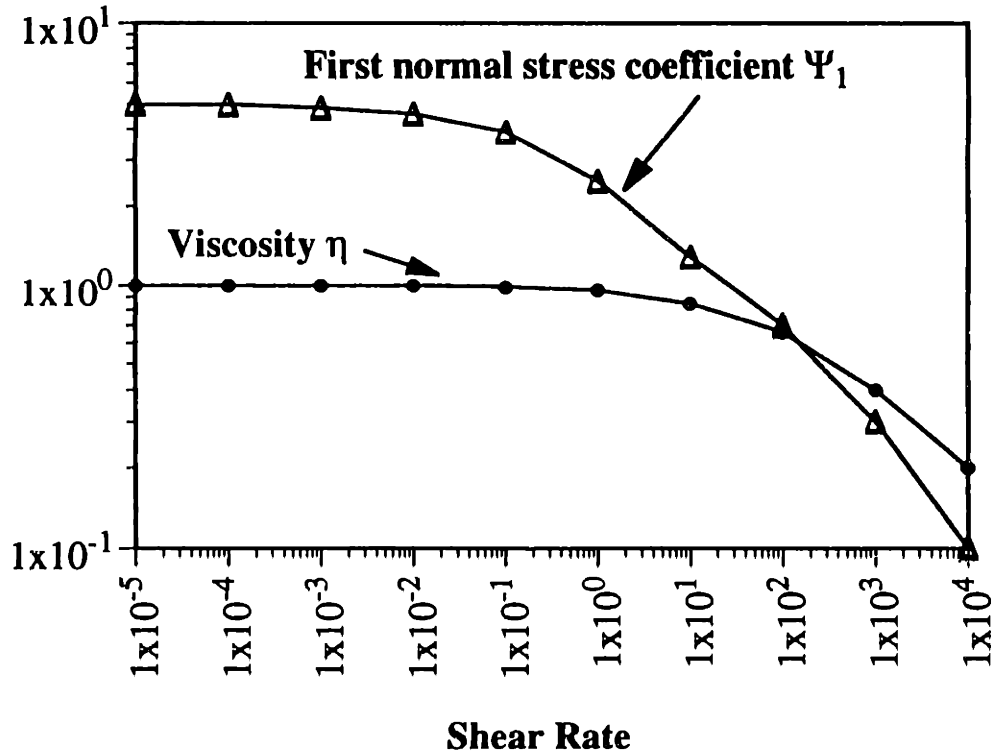
Figure 2-2: Typical viscosity and first normal stress coefficient for a polymer melt plotted as a function of shear rate.

coefficients, Ψ_1 and Ψ_2, respectively:

$$\tau_{xx} - \tau_{yy} \equiv -\Psi_1(\dot{\gamma})\dot{\gamma}_{yx}^2, \tag{2.4}$$

$$\tau_{yy} - \tau_{zz} \equiv -\Psi_2(\dot{\gamma})\dot{\gamma}_{yx}^2. \tag{2.5}$$

Generally, τ_{xx} is large and negative, as a consequence of molecular alignment along streamlines, and results in a large positive first normal stress coefficient. Typical behavior of the viscosity η and first normal stress coefficient Ψ_1 for isotropic fluids is shown schematically in Fig. 2-2 as a function of the shear rate $\dot{\gamma}$. The viscosity typically displays a constant viscosity plateau at low shear rates, called the zero-shear-rate viscosity η_0. At higher shear rates, the viscosity follows a linear power-law, where the viscosity could decrease by as much as two to three decades. The slope of this region, on a log-log plot, is typically between -0.4 and -0.9. Similar behavior is displayed by Ψ_1, although it decreases much more rapidly than η. The second normal

stress coefficient in isotropic fluids has not been studied much because it is very difficult to measure; it is generally believed to be about 10% of Ψ_1, and of opposite sign (Bird *et al.*, 1987a).

In the case of anisotropic fluids, such as liquid crystalline solutions, the first normal stress coefficient Ψ_1 decreases as $\dot\gamma^{-1}$ at low shear rates (Larson, 1988). A negative value of Ψ_1 also is reported in some systems over a substantial range of shear rates, and is accompanied by large second normal stress differences (Magda *et al.*, 1991).

The relaxation of the molecular configurations on time scales that are comparable to those in the experiment imparts an inherently temporal character to the problem. Therefore, it is insufficient to give only the steady-state material functions. It is also necessary to define material functions in time-dependent shear flows. Rheologists have devised a number of such unsteady shear flow experiments such as small-amplitude oscillatory shear and stress growth on start-up of steady shear flow. These experiments and the relevant material functions are described in the book by Bird *et al.* (1987a), and are summarized in Figs. 2-3 and 2-4.

Simple shearfree flows are given by the velocity field

$$
\begin{aligned}
v_x &= -\frac{1}{2}\dot\epsilon(1+b)x, \\
v_y &= -\frac{1}{2}\dot\epsilon(1-b)y, \\
v_z &= +\dot\epsilon z
\end{aligned}
\tag{2.6}
$$

where $0 \le b \le 1$ and $\dot\epsilon$ is the elongation rate. Special shearfree flows are defined for particular values of b. The flow for $b = 0$ and $\dot\epsilon > 0$ is uniaxial extension; $b = 0$ and $\dot\epsilon < 0$ corresponds to biaxial stretching flow; and all flows with $b = 1$ are planar elongational flows. The two normal stress differences of experimental interest in these flows are $\tau_{zz} - \tau_{xx}$ and $\tau_{xx} - \tau_{yy}$, and two viscosity functions, $\bar\eta_1$ and $\bar\eta_2$, are defined as

$$
\tau_{zz} - \tau_{xx} = -\bar\eta_1(\dot\epsilon, b)\dot\epsilon,
\tag{2.7}
$$

$$
\tau_{yy} - \tau_{xx} = -\bar\eta_2(\dot\epsilon, b)\dot\epsilon.
\tag{2.8}
$$

34
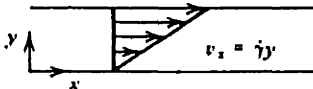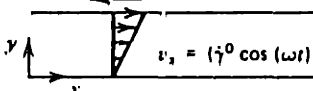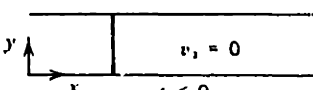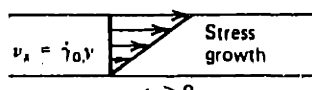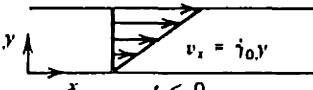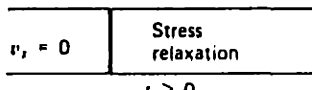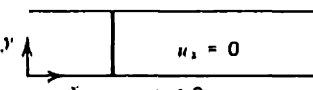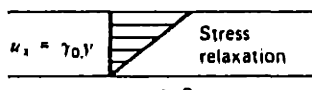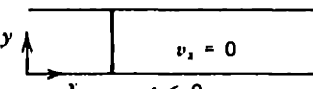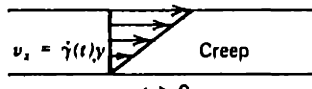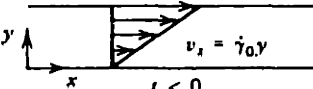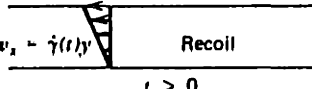
a Steady shear flow	$v_x = \dot{\gamma} y$	v_x = velocity in x–direction $\dot{\gamma}$ = shear rate
b Small–amplitude oscillatory shear	$v_x = (\dot{\gamma}^0 \cos{(\omega t)}) y$	$\dot{\gamma}^0$ = shear rate amplitude ω = angular frequency

	Fluid at rest	Steady shear flow
c Stress growth upon inception of steady shear flow	$v_x = 0$ $t < 0$	$v_x = \dot{\gamma}_0 y$ Stress growth $t > 0$

	Steady shear flow	Motion suddenly stopped
d Stress relaxation after cessation of steady shear flow	$v_x = \dot{\gamma}_0 y$ $t < 0$	$v_x = 0$ Stress relaxation $t > 0$

	Fluid at rest	Fluid at rest
e Stress relaxation after a sudden shearing displacement	$u_x = 0$ $t < 0$	$u_x = \gamma_0 y$ Stress relaxation $t > 0$

	Fluid at rest	Constant shear stress applied
f Creep	$v_x = 0$ $t < 0$	$v_x = \dot{\gamma}(t) y$ Creep $t > 0$

	Steady shear flow	Shear stress suddenly removed
g Constrained recoil after steady shear flow	$v_x = \dot{\gamma}_0 y$ $t < 0$	$v_x = \dot{\gamma}(t) y$ Recoil $t > 0$

Figure 2-3: Various types of simple shear flow experiments used in rheology (*reproduced from* Bird *et al.*, 1987a).

Material Functions in Simple Shearing Flows $v_x = \dot{\gamma}_{yx}\, y,\ v_y = v_z = 0$

Flow	Material Function	Defining Equation
a. Steady shear flow $\dot{\gamma}_{yx} = \dot{\gamma} = $ constant	$\eta(\dot{\gamma})$ $\Psi_1(\dot{\gamma})$ $\Psi_2(\dot{\gamma})$	$\tau_{yx} = -\eta\dot{\gamma}_{yx}$ $\tau_{xx} - \tau_{yy} = -\Psi_1\dot{\gamma}_{yx}^2$ $\tau_{yy} - \tau_{zz} = -\Psi_2\dot{\gamma}_{yx}^2$
b. Small-amplitude oscillatory shear $\dot{\gamma}_{yx} = \dot{\gamma}^0 \cos \omega t$ $\quad = \gamma^0 \omega \cos \omega t$	$\eta'(\omega)$ $\eta''(\omega)$ $G'(\omega) = \eta''\omega$ $G''(\omega) = \eta'\omega$	$\tau_{yx} = -\eta'\dot{\gamma}^0 \cos \omega t$ $\quad -\eta''\dot{\gamma}^0 \sin \omega t$ $\tau_{yx} = -G'\gamma^0 \sin \omega t$ $\quad -G''\gamma^0 \cos \omega t$
c. Stress growth upon inception of steady shear flow $\dot{\gamma}_{yx} = \begin{cases} 0 & t < 0 \\ \dot{\gamma}_0 & t \geq 0 \end{cases}$	$\eta^+(t, \dot{\gamma}_0)$ $\Psi_1^+(t, \dot{\gamma}_0)$ $\Psi_2^+(t, \dot{\gamma}_0)$	$\tau_{yx} = -\eta^+\dot{\gamma}_0$ $\tau_{xx} - \tau_{yy} = -\Psi_1^+\dot{\gamma}_0^2$ $\tau_{yy} - \tau_{zz} = -\Psi_2^+\dot{\gamma}_0^2$
d. Stress relaxation after cessation of steady shear flow $\dot{\gamma}_{yx} = \begin{cases} \dot{\gamma}_0 & t < 0 \\ 0 & t \geq 0 \end{cases}$	$\eta^-(t, \dot{\gamma}_0)$ $\Psi_1^-(t, \dot{\gamma}_0)$ $\Psi_2^-(t, \dot{\gamma}_0)$	$\tau_{yx} = -\eta^-\dot{\gamma}_0$ $\tau_{xx} - \tau_{yy} = -\Psi_1^-\dot{\gamma}_0^2$ $\tau_{yy} - \tau_{zz} = -\Psi_2^-\dot{\gamma}_0^2$
e. Stress relaxation after a sudden shearing displacement $\dot{\gamma}_{yx} = \gamma_0 \delta(t)$	$G(t, \gamma_0)$ $G_{\Psi 1}(t, \gamma_0)$	$\tau_{yx} = -G\gamma_0$ $\tau_{xx} - \tau_{yy} = -G_{\Psi 1}\gamma_0^2$
f. Creep $\tau_{yx} = \begin{cases} 0 & t < 0 \\ \tau_0 & t \geq 0 \end{cases}$	$J(t, \tau_0)$	$\gamma_{yx}(0, t) = -J\tau_0$
g. Constrained recoil after steady shear flow $\tau_{yx} = \begin{cases} \tau_0 & t < 0 \\ 0 & t \geq 0 \end{cases}$	$\gamma_r(0, t, \tau_0)$ $\gamma_\infty(\tau_0)$ $J_e^0(\tau_0)$	$\gamma_r = \int_0^t \dot{\gamma}_{yx}(t')\, dt'$ $\gamma_\infty = \lim_{t \to \infty} \gamma_r$ $\gamma_\infty = J_e^0(\tau_0)\tau_0$

Figure 2-4: Material functions in simple shearing flows (*reproduced from* Bird *et al.*, 1987a).

For isotropic fluids in steady-state shearfree flow with $b = 0$, $\bar{\eta}_2 = 0$ and $\bar{\eta}_1$ is simply called the *elongational viscosity* $\bar{\eta}$. However, for anisotropic fluids, such as liquid crystalline systems, both the viscosity functions are important. As in the case of shear flows, material functions in time-dependent shearfree flows also are defined and these have been summarized in Fig. 2-5.

A proper understanding of non-Newtonian fluid mechanics is critically dependent on our ability to develop accurate constitutive models for these fluids. The primary goal of theoretical studies is to incorporate that physics into the constitutive model which is responsible for the complex rheological behavior of the macromolecular fluids. The early constitutive models were phenomenological, often restricted to only a few classes of flows and incapable of describing all the rheological responses displayed by non-Newtonian fluids. Modifications of the models proceeded on an *ad hoc* basis, and gave no insight into the relation between rheology and the underlying molecular processes could be gained. Recognizing the strong coupling between the internal microstructure and the rheological response, recent constitutive theories are based on a micromechanical description of the macromolecular solution and a formal kinetic theory framework is used to rigorously derive the governing equations. It is interesting that a number of the early phenomenological models have been rederived using a more rigorous molecular theory. The basic concepts of polymer kinetic theory are discussed in the next section.

2.3 Constitutive Theories with a Micromechanical Basis: A Kinetic Theory Approach

The aim of kinetic theory is to use simple molecular models to describe the relevant statistical features of macromolecular configuration in nonequilibrium systems and to use this statistical description to deduce the associated transport and rheological properties. The biggest advantage of this approach is that it makes direct use of the fact that the rheology of macromolecular systems and suspensions, such as polymer solutions and melts, liquid crystal polymers and fiber suspensions, is intimately

Definitions of Material Functions in Shearfree Flows

$$v_x = -\tfrac{1}{2}\dot{\epsilon}(1+b)x, \quad v_y = -\tfrac{1}{2}\dot{\epsilon}(1-b)y, \quad v_z = \dot{\epsilon}z$$

Flow	Material Function	Defining Equation
a. Steady shearfree flow $\dot{\epsilon} = \text{constant}$	$\bar{\eta}_1(\dot{\epsilon})$ $\bar{\eta}_2(\dot{\epsilon})$	$\tau_{zz} - \tau_{xx} = -\bar{\eta}_1\dot{\epsilon}$ $\tau_{yy} - \tau_{xx} = -\bar{\eta}_2\dot{\epsilon}$
b. Stress growth on inception of steady shearfree flow $\dot{\epsilon} = \begin{cases} 0 & t < 0 \\ \dot{\epsilon}_0 & t \geq 0 \end{cases}$	$\bar{\eta}_1^+(t, \dot{\epsilon}_0)$ $\bar{\eta}_2^+(t, \dot{\epsilon}_0)$	$\tau_{zz} - \tau_{xx} = -\bar{\eta}_1^+\dot{\epsilon}_0$ $\tau_{yy} - \tau_{xx} = -\bar{\eta}_2^+\dot{\epsilon}_0$
c. Elongational creep $(b = 0)$ $(\tau_{zz} - \tau_{xx}) = \begin{cases} 0 & t < 0 \\ \sigma_0 & t \geq 0 \end{cases}$	$D(t, \sigma_0)$	$\epsilon(0, t) = -D\sigma_0$
d. Free recovery after steady elongational flow $(b = 0)$ $(\tau_{zz} - \tau_{xx}) = \begin{cases} \sigma_0 & t < 0 \\ 0 & t \geq 0 \end{cases}$	$\epsilon_r(0, t, \sigma_0)$ $\epsilon_\infty(\sigma_0)$	$\epsilon_r = \displaystyle\int_0^t \dot{\epsilon}(t')\,dt'$ $\epsilon_\infty = \lim_{t \to \infty} \epsilon_r$

Figure 2-5: Material functions in shearfree flows (*reproduced from* Bird *et al.*, 1987a).

related to the microstructure of these macromolecules and particles. The macro-molecules in polymer melts and solutions are represented by simplified mechanical models, and principles of nonequilibrium statistical mechanics are applied in order to obtain relations between the microscopic mechanical model parameters and the macroscopic properties of the fluids. Simplifying assumptions are made at different points of the development, but the physical basis behind these is well understood and clearly stated. A systematic improvement over existing theory is possible, and the addition of new terms to the constitutive model does not proceed on an *ad hoc* basis.

2.3.1 Micromechanical Models for Polymer Molecules

The first step in the development of a kinetic theory for polymer solutions is the mi-cromechanical representation of the polymer molecule. Micromechanical models that incorporate detailed structural features of the polymer molecule can be constructed. For instance, Flory and coworkers (Flory, 1969) modelled a polymer by a linear chain of beads and rods, with the rod length equal to the length of a C-C bond and with successive rods at angles appropriate to the molecular structure; the model has been used to study conformational properties of a single polymer molecule in a solvent bath at equilibrium. Such realistic models can be used if the ultimate goal is to obtain the detailed relationship between the molecular architecture and equilibrium bulk properties. However, if the objective is to study nonequilibrium flow systems and ob-tain the associated rheological properties, the problem is far more complicated, and it becomes necessary to use considerably simpler molecular models to obtain either analytical or numerical results (Bird and Öttinger, 1992).

Thus, in polymer kinetic theory, simple mechanical models are preferred. Each polymer molecule is modelled as a collection of *beads*, where each bead represents a collection of several monomer units. The beads are of finite size and arbitrary shape, or are restricted to point masses, which are referred to as structureless beads. The beads are then joined in an arbitrary manner, by *springs* or *massless rods*. A combination of connectors can also be used in the same molecule.

The simplest of these molecular models are the so-called *dumbbell models*, where

the number of beads is set equal to two. There are two kinds of dumbbell models: *rigid* and *elastic* dumbbells (Bird *et al.*, 1987b). In the former, the connector is a rigid rod, whereas in the latter, the beads are connected with a spring, as illustrated in Fig. 2-6. The simplest elastic dumbbell model is the *Hookean dumbbell*, where the beads are connected by a perfectly elastic or *Hookean* spring and the tension in the spring is proportional to the bead separation. The dumbbells are orientable in a solvent flow field, and stretchable (except the rigid dumbbell). These two properties – orientation and elastic stretching – are essential for the qualitative description of rheological properties of the fluid.

These dumbbell models are very crude representations of polymer molecules and do not account for the details of the molecular architecture. It is possible to improve on these models by adding more beads and connectors. This approach leads to the bead-rod chain model or the *pearl necklace model*, and the different bead-spring models such as the *Rouse-Zimm model* (Rouse, 1953; Zimm, 1956); see Fig. 2-6. The Rouse and Zimm theories use the same molecular model, but differ in the treatment of hydrodynamic interaction with the solvent. These models can depict the *bending* motions of a polymer molecule, in addition to the orientability and stretching motions described by the dumbbell models. The increased modes of cooperative motion in the multibead models lead to a more accurate description of spectrum of relaxation times exhibited by polymer solutions and melts. Therefore, the Rouse and Zimm models have been preferred over the simpler dumbbell models in the interpretation of linear viscoelastic data (Ferry, 1980). However, in flows involving large molecular deformations, the dumbbell models and their multibead analogues generally yield the same qualitative information; see Section 2.3.3. Furthermore, the attendant mathematics is much simpler in the case of dumbbell models, and with a minimum of mathematical effort, it is possible to go from molecular models to fluid dynamics. The effect of changes made at the molecular level, in either the micromechanical model or in the assumptions underlying the development, can be observed by solving simple flow problems, such as homogeneous shear and shearfree flows. A qualitative understanding of rheological phenomena is thus developed with the simple dumbbell models, and
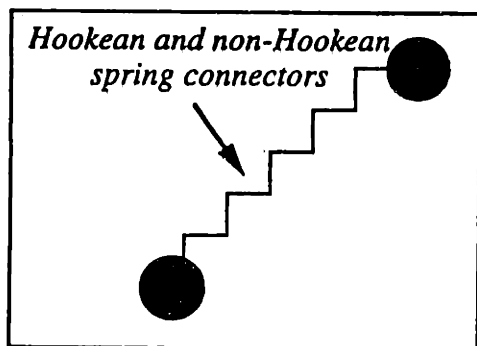
(a) ELASTIC DUMBBELL MODELS
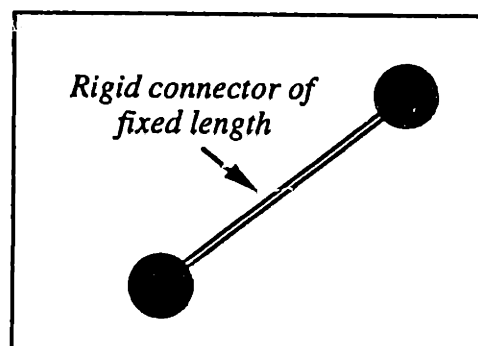
(b) RIGID DUMBBELL MODELS
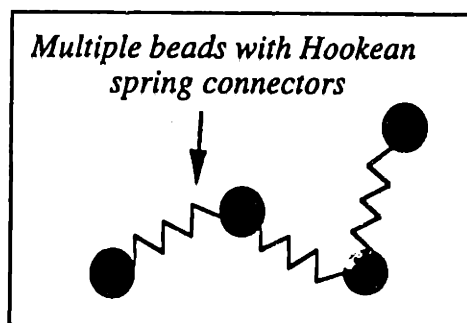
(c) MULTIBEAD ROUSE-ZIMM
CHAIN MODELS

Figure 2-6: Commonly used molecular models: (a) Elastic dumbbell; (b) Rigid dumbbell; (c) Rouse-Zimm chain model.

the main ideas can be extended to other molecular models, if necessary. Hence, the simpler dumbbell models have been used more extensively than multibead models in the study of viscoelastic fluid mechanics. In this thesis, only the Hookean and rigid dumbbell models have been used.

2.3.2 Basic Concepts of Kinetic Theory

In the most general description of a polymeric solution or melt, the system is viewed as a collection of a large number of molecules of various kinds. The polymer molecules are modelled with the different bead-rod-spring models discussed above and the smaller solvent molecules are treated as simple mass points. This allows an explicit description of the molecular motion of the solvent and polymer-solvent interactions. Typically, most kinetic theories treat the solvent as a continuum, specifically an incompressible Newtonian liquid of viscosity η_s that exerts a drag on the individual beads of the micromechanical model as macromolecule moves through the solvent. This description is reasonably accurate, considering the disparity in the molecular sizes of the polymer and solvent molecules. The contributions of the solvent and polymer to the stress tensor or mass flux vector are assumed to be additive.

The different species present in this system are denoted as $(\alpha, \beta, \ldots)$ and the different molecules are labelled $(i, j, \ldots)$. This notation is consistent with the development presented in Bird *et al.* (1987b). The center of mass position of molecule i of species α is then denoted as $r_c^{\alpha i}$ and the associated momentum is denoted as $p_c^{\alpha i}$. The internal configuration of the molecule in space is best described by generalized coordinates $(Q_1^{\alpha i}, Q_2^{\alpha i}, \ldots, Q_s^{\alpha i})$, $s \leq 3N - 3$ where N is the number of beads in the molecular model. The internal coordinates are independent and sufficient to describe the relative locations of all the constituent beads of the molecular model, and account for all constraints in the molecular model. These internal position coordinates are associated with the generalized conjugate momenta $\{P_s^{\alpha i}\}$ that are related to the time rate of change of the internal position coordinates. The generalized coordinates simplify considerably when the molecular model has no constraints, *e.g.*, in the Hookean dumbbell, the internal coordinates can be given by a single 3-dimensional connector

vector Q with three independent components; see Chapter 3. The presence of constraints in the molecular model decreases the degrees of freedom and the number of generalized coordinates, e.g., in the rigid dumbbell model, the two polar angles (θ, ϕ) are sufficient to describe the orientation of the molecule.

The dynamical state of this macroscopic system, consisting of the solvent and the micromechanical model of the polymer molecules, then is described by a *system point* in the associated phase space. The phase space is a multidimensional space with coordinates that are the configuration and momentum coordinates $\{r_c^{\alpha i}, Q_s^{\alpha i}, p_c^{\alpha i}, P_s^{\alpha i}\}$ of all molecules αi making up the macroscopic system of interest. In general, the dynamical state changes with time, and the system point traces out a trajectory in the phase space. This evolution of the dynamical state is governed by *Hamilton's equations of motion*. These equations are the equivalent of Newton's equations of motion in three-dimensional space, and are written as

$$\dot{r}_c^{\alpha i} = \frac{\partial \mathcal{H}^{(T)}}{\partial p_c^{\alpha i}}$$

$$\dot{Q}_s^{\alpha i} = \frac{\partial \mathcal{H}^{(T)}}{\partial P_s^{\alpha i}}$$

$$\dot{p}_c^{\alpha i} = -\frac{\partial \mathcal{H}^{(T)}}{\partial r_c^{\alpha i}}$$

$$\dot{P}_s^{\alpha i} = -\frac{\partial \mathcal{H}^{(T)}}{\partial Q_s^{\alpha i}} \qquad (2.9)$$

where $\mathcal{H}^{(T)}$ is the *Hamiltonian* of the entire system and is equal to the sum of the energies of the separate molecules and the intermolecular potential Φ, associated with the forces between the molecules. The energy of each molecule, in turn, is a sum of the kinetic energy of the motion of the center of mass, the kinetic energy $\mathcal{K}_{int}$ associated with the internal coordinates, the intramolecular potential ϕ and the external potential $\phi^{(e)\alpha i}$ acting on the system. The Hamiltonian $\mathcal{H}^{(T)}$ is written as

$$\mathcal{H}^{(T)} \equiv \sum_\alpha \sum_i \left[\frac{1}{2m^\alpha}(p_c^{\alpha i})^2 + \mathcal{K}_{int} + \phi + \phi^{(e)\alpha i} \right] + \Phi \qquad (2.10)$$

where m^α is the mass of a molecule of species α.

43

In order to obtain the average behavior of a macroscopic system, such as the one described above, the concept of *ensembles* is used. The ensemble consists of a large number of systems that are identical to the macroscopic system of interest. The probable behavior of the macroscopic system is then described by the average behavior of systems comprising the ensemble. Each system within the ensemble is represented by a system point in phase space, and each system evolves according to Hamilton's equations. The dynamical state of such an ensemble is described by a distribution of system points in the phase space, $f(x,t)$ and the average behavior of the system is described by the time evolution of such a distribution. Here, the system point x refers to the full set of configuration and momentum coordinates $\{r_c^{\alpha i}, Q_s^{\alpha i}, p_c^{\alpha i}, P_s^{\alpha i}\}$ of all the molecules in the system and $f(x,t)dx$ is the number of system points that lies in the $(6 + 2s)$-dimensional differential hypercube of volume dx in the phase space.

It is important to note that system points are neither lost nor created; as time evolves, they simply move through the phase space describing the time evolution of the dynamical state of each system in the ensemble. Thus, the conservation equation or *equation of continuity* in phase space is simply written as

$$\frac{\partial f}{\partial t} = -\sum_i \frac{\partial}{\partial x_i}(\dot{x}_i f). \tag{2.11}$$

The equation of continuity (2.11) combined with Hamilton's equations of motion (2.10) results in the *Liouville equation*, which is the starting point for all further development in nonequilibrium statistical mechanics.

In the formal development, the theory is usually restricted to two-body interactions, and it is unnecessary to deal with the complete phase-space distribution function f. Therefore, more tractable lower order distribution functions are defined. Thus, the singlet phase-space distribution function f_α is defined as

$$f_\alpha(r, Q, p, P, t) \equiv \langle \sum_i \delta(r_c^{\alpha i} - r)\delta(Q^{\alpha i} - Q)\delta(p_c^{\alpha i} - p)\delta(P^{\alpha i} - P) \rangle \tag{2.12}$$

where δ is the *Dirac delta function*. The argument Q represents the full set of gen-

eralized coordinates Q, and $\delta(Q^{\alpha i} - Q)$ represents the corresponding product of δ-functions; similarly, P represents the full set of generalized momenta P, and $\delta(P^{\alpha i} - P)$ represents the corresponding product of δ-functions. The angular brackets $\langle \ \rangle$ represent an ensemble average defined as

$$\langle B \rangle \equiv \int B f(x, t) dx \tag{2.13}$$

where x refers to all the phase-space coordinates and the dynamical variable $B \equiv B(x)$. The product $f_\alpha(r, Q, p, P, t) dr\, dQ\, dp\, dP$ gives the probable number of molecules of species α with center of mass in the region dr about r, internal configuration in a range dQ about Q and momenta in the ranges dp and dP about p and P, respectively. Integrating f_α over all momenta yields the singlet configurational distribution function

$$\Psi_\alpha(r, Q, t) \equiv \iint f_\alpha(r, Q, p, P, t) dp\, dP. \tag{2.14}$$

In a similar fashion, a *pair phase-space distribution function* is defined as

$$
\begin{aligned}
f_{\alpha\beta}(r', Q', r'', Q'', p', P', p'', P'', t) &\equiv \langle \sum_i \sum_{j, i \neq j} \delta(r_c^{\alpha i} - r') \\
\times \delta(Q^{\alpha i} - Q') \delta(r_c^{\beta j} - r'') \delta(Q^{\beta j} - Q'') \delta(p_c^{\alpha i} - p') \\
\times \delta(P^{\alpha i} - P') \delta(p_c^{\beta j} - p'') \delta(P^{\beta j} - P'') \rangle.
\end{aligned}
\tag{2.15}
$$

The product $f_{\alpha\beta}(r', Q', r'', Q'', p', P', p'', P'', t) dr'\, dQ'\, dr''\, dQ''\, dp'\, dP'\, dp''\, dP''$ gives the joint probable number of finding a molecule of species α in the range (dr', dQ', dp', dP') about (r', Q', p', P') with a molecule of species β in the range (dr'', dQ'', dp'', dP'') about (r'', Q'', p'', P''). Integrating $f_{\alpha\beta}$ over all momenta yields a *pair configurational distribution function* as

$$\Psi_{\alpha\beta}(r', Q', r'', Q'', t) = \iiiint f_{\alpha\beta}(r', Q', r'', Q'', p', P', p'', P'', t) dp'\, dP'\, dp''\, dP''. \tag{2.16}$$

Governing equations of change for these lower order distribution functions are then obtained from the Liouville equation by making suitable choices for the dynamical

45

variable B. Other choices for B lead to the hydrodynamic equations of change; from these, general expressions for the macroscopic fluxes of mass, momentum and energy are obtained in terms of the intermolecular forces. It also is possible to derive statistically averaged equations of motion for the polymer chain, where we can identify expressions for the different forces acting on the polymer such as the *Brownian* forces, the *hydrodynamic drag forces* on the beads, the intramolecular spring forces and intermolecular forces due to *excluded volume*. Force balances then can be obtained, and used to write general *diffusion equations* that govern the time evolution of the lower order distribution functions of interest. All the macroscopic variables of interest are given by averages over these lower order distribution functions.

In general, it is assumed in polymer kinetic theory that the velocity distribution is not much perturbed from equilibrium and can be given as

$$\Xi = \Xi_{eq} = \frac{\exp(-\mathcal{H}/kT)}{\int\int \exp(-\mathcal{H}/kT)dp_c dP}. \tag{2.17}$$

This assumption is referred to as the assumption of *equilibration in momentum space*. In addition, by taking averages over all the momentum coordinates, it is possible to reduce the problem to the configuration space of a single molecule. Evaluation of the singlet configurational distribution function Ψ_α becomes a central task in the further development of the theory. However, since the intermolecular potential Φ is approximated by a sum of two-body potentials, the time evolution equation for Ψ_α obtained from the Liouville equation also involves the pair distribution function $\Psi_{\alpha\beta}$. Terms involving $\Psi_{\alpha\beta}$ account for the two-body interaction of the polymer α with surrounding solvent and polymer molecules. This leads to a *closure problem*, that is a common feature in non-equilibrium kinetic theory development, and that is a direct consequence of trying to compress all the information present in a complete phase-space distribution function f into a lower-order distribution function f_α involving just one of the species present in the system.

The method generally employed to overcome this problem is to "smear out" the solvent-polymer and polymer-polymer interaction, and treat a single polymer

molecule as being acted upon by a *mean field* that would depend on Ψ_α alone. Thus, in dilute solution theories where no polymer-polymer interactions are considered, all solvent-polymer interactions are taken to result in a *hydrodynamic* force, that is given empirically by an expression modelled after Stokes' law for drag on a solid sphere in creeping flow. This is equivalent to treating the solvent as a continuum that exerts a *drag* on the beads of the molecular model. Such a mean field description is reasonably accurate since the polymer molecule is large compared to the solvent molecule.

The problem is more complex in concentrated systems, since polymer-polymer interactions are no longer negligible. A mean field approach is still adopted to keep the problem tractable. The goal is to capture the essence of the intermolecular interaction in the mean field description, and to depict accurately the behavior of the concentrated system. In one view of the problem, the motion of a single polymer chain within a matrix of surrounding polymer chains is taken to be anisotropic, such that the polymer can move more easily along its length rather than sideways. This effect is treated by means of an anisotropic friction tensor and anisotropic Brownian motion (Curtiss and Bird, 1981a & 1981b). Another view of the problem considers the polymer chain as being trapped in a tube formed by the constraints due to surrounding polymer molecules; the molecule moves by *reptation* such that on an average the velocity of an individual bead is along the length of the chain (de Gennes, 1971; Doi and Edwards, 1978a, 1978b, 1978c & 1979).

In some concentrated systems, other intermolecular interactions also are important. For example, in liquid crystalline systems, the excluded volume interactions between molecules with rigid backbones are directly responsible for a transition from an isotropic to a liquid-crystalline phase. Here, *excluded volume* refers to the volume occupied by a polymer molecule that is inaccessible to any other molecule. In these systems, the excluded volume interactions are modelled by the mean-field *Maier-Saupe* potential (Maier and Saupe, 1958 & 1959; Doi, 1980 & 1981) acting on the molecule of interest, over and above the hydrodynamic drag forces exerted by the surrounding medium. The Maier-Saupe potential is essentially a mean-field version of the hard-rod intermolecular potential and accurately describes the increased excluded

volume interactions between rigid rods with increasing concentration. The excluded volume interaction prevents the rods from intersecting each other and leads to spontaneous orientational ordering when the concentration is increased beyond a critical value. Such liquid crystalline systems are discussed in greater detail in Chapters 4, 5 and 6.

A simpler diffusion equation for Ψ_α is obtained after making these approximations. This form of the diffusion equation also is referred to as the *Smoluchowski equation* or the *Fokker-Planck equation* (Doi and Edwards, 1986). The rigorous phase space approach is not always used in the kinetic theory development of the constitutive models. A number of kinetic theories are set up directly in the configuration space of a single polymer molecule; *ad hoc* expressions for the different forces that act upon the molecule are then used to write a diffusion equation that governs the time evolution of Ψ_α. However, in problems where the details of intermolecular interaction are important or in problems involving spatial nonhomogeneities, it is preferable to use rigorous phase space kinetic theory so that all the relevant equations of change can be consistently derived. Thus, average properties of the macromolecular system can be determined by solving the diffusion equation for the distribution function.

An expression for the stress tensor must be obtained in order to make the connection with rheological behavior and bulk fluid mechanics. An expression for the total stress tensor π is obtained when phase space kinetic theory is used in developing the equation of conservation of momentum from the Liouville equation. The expression for the total stress π is simplified by making the assumption of equilibration in momentum space and approximating the polymer-solvent interactions by an average hydrodynamic drag force, as in deriving the diffusion equation. The final expression for the stress tensor typically involves ensemble averages with respect to the singlet configurational distribution function Ψ_α.

In a typical fluid mechanical problem, where the primary interest is in momentum transport alone, the hydrodynamic equations of motion and continuity, the expression for the stress tensor, and the diffusion equation for the configurational distribution function form a closed set of equations that must be solved simultaneously to ob-

tain the stress and velocity profiles. However, solving the evolution equation for the configurational distribution function is computationally intensive, especially in fluid mechanics problems involving two or three spatial dimensions (Advani and Tucker, 1987). Instead, a typical solution involves taking lower order moments of the diffusion equation with respect to the internal coordinates, and solving for them directly. This method is equivalent to expanding the distribution function in terms of its moments, and retaining only the lower order moments. Since the expression for the stress tensor also involves the lower order moments of the distribution function, this method is convenient and less computationally intensive. However, as in the case of obtaining lower order distribution functions from the phase-space distribution function, a closure problem results when we attempt to compress all the information present in the configurational distribution function into a limited number of lower order moments. Thus, the equation for the second moment involves the fourth, the equation for the fourth involves the sixth, and so on. *Closure approximations* are used to approximate the higher order moments in terms of the lower ones and thus obtain a closed set of equations. The advantages and disadvantages of such approximations are discussed at length in Chapter 5.

In recent years, with the advent of better computational facilities, exact evaluation of the lower order distribution functions in simple flow problems and in the evaluation of rheological properties has been attempted (Stewart and Sørensen, 1972; Fan, 1989). However, solving realistic fluid mechanics problems by using this approach is not yet feasible and direct evaluation of moments is still the method of choice. Thus, we strive to develop a closed set of equations consisting of the equations of motion and continuity, the stress tensor expression in terms of the lower order moments of the distribution function and governing equations for these lower order moments. These equations are simultaneously solved by a variety of numerical methods to get a solution to the flow problem. The major steps involved in going from the Liouville equation to the solution of flow problems are shown schematically in Fig. 2-7.

```
┌─────────────────────────────┐
│      PHYSICAL MODEL          │
│      Bead-Spring-Rod         │
│        Description           │
│      Of Polymer System       │
└─────────────────────────────┘
                │
                ▼
┌─────────────────────────────────────────────────┐
│            LIOUVILLE EQUATION                    │
│  General Phase Space Conservation Equation       │
└─────────────────────────────────────────────────┘
```

Special Choices Of Dynamical Variables

```
┌──────────────┐   ┌──────────────┐   ┌──────────────┐
│   Species    │   │   Equation   │   │  Diffusion   │
│ Conservation │   │  Of Motion   │   │  Equation    │
│   Equation   │   │              │   │              │
└──────────────┘   └──────────────┘   └──────────────┘
```

$$\mathbf{j}_p \qquad\qquad \tau_p \quad \langle QQ \rangle, \langle QQQQ \rangle$$

```
┌─────────────────────────────────────────────────┐
│            CONSTITUTIVE MODEL                    │
└─────────────────────────────────────────────────┘
```
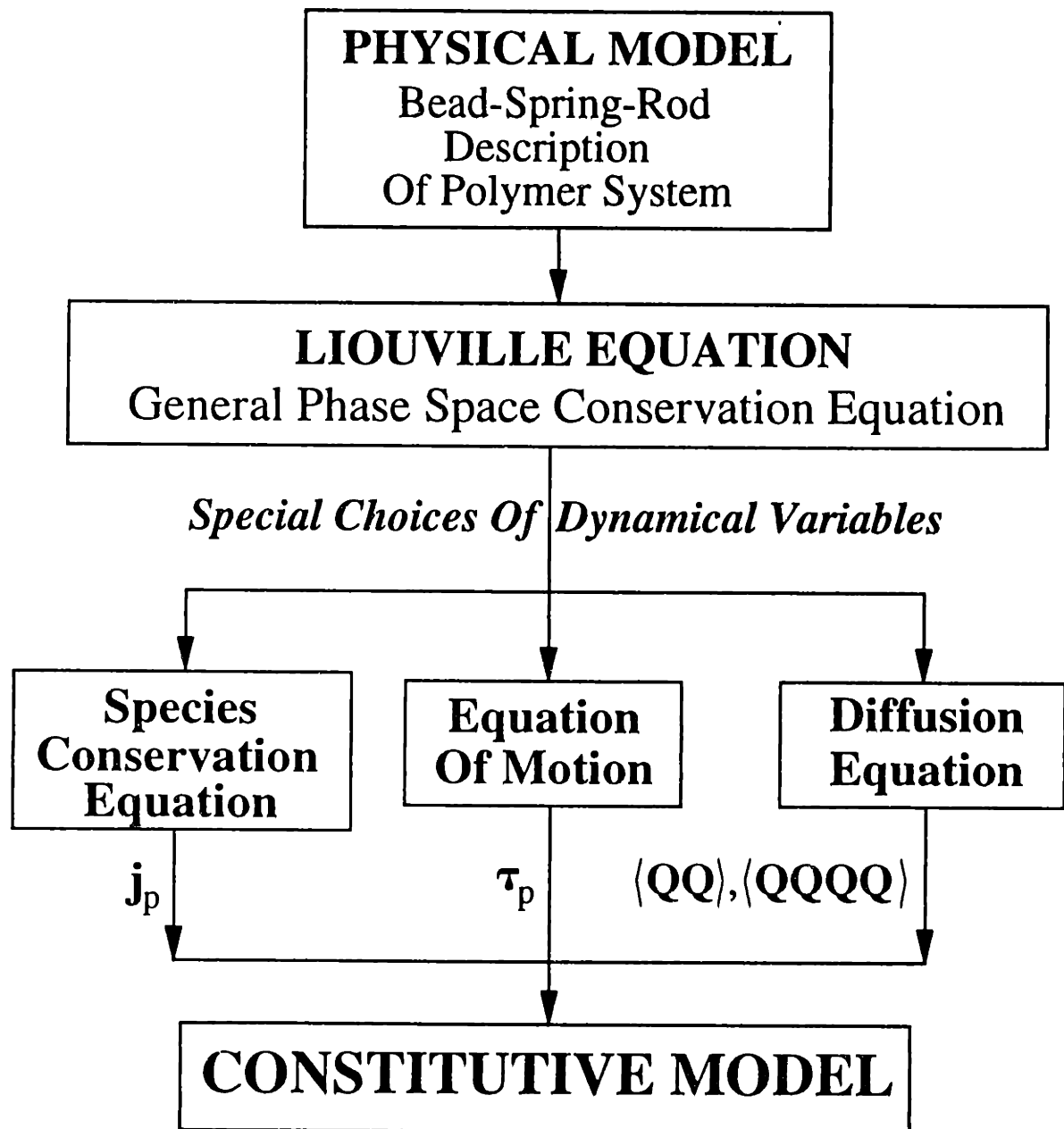
Figure 2-7: Schematic diagram of development of the constitutive equation.

2.3.3 Development of the Oldroyd-B Fluid Model from Kinetic Theory

The classical kinetic theory development of the Oldroyd-B fluid model is considered as an example of the development of micromechanical-model-based constitutive equations. The Oldroyd-B model results from a *dilute* solution theory that is derived for a Hookean dumbbell model of a polymer molecule, illustrated in Fig. 2-6(a). The configuration of the dumbbell is specified by its center-of-mass position vector r_c and the connector vector Q. Since the molecular model has no internal constraints, generalized coordinates can be avoided. The average behavior of the system can be described in terms of the singlet configurational distribution function $\Psi_p(r, Q, t)$. The product $\Psi_p(r, Q, t) dr dQ$ gives the number of dumbbells in the configuration range (dr, dQ) about (r, Q). Since the number of dumbbells is constant, an *equation of continuity* for Ψ_p is written in the six-dimensional configurational hyperspace, in a manner analogous to writing the equation of continuity in hydrodynamics, to give

$$\frac{\partial \Psi_p}{\partial t} = -\frac{\partial}{\partial r} \cdot ([[\dot{r}]]^p \Psi_p) - \frac{\partial}{\partial Q} \cdot ([[\dot{Q}]]^p \Psi_p). \tag{2.18}$$

Equations of motion for the momentum-space-averages $[[\dot{r}]]^p$ and $[[\dot{Q}]]^p$ are obtained by setting up a force balance over the Hookean dumbbell, accounting for hydrodynamic drag, Brownian, intramolecular spring and external forces on the dumbbell. Neglecting the effect of external forces yields

$$[[\dot{r}]]^p = v(r) - \frac{kT}{2\zeta} \frac{\partial \ln \Psi_p}{\partial r} \tag{2.19}$$

and

$$[[\dot{Q}]]^p = [\kappa \cdot Q] - \frac{2kT}{\zeta} \frac{\partial \ln \Psi_p}{\partial Q} - \frac{2H}{\zeta} Q. \tag{2.20}$$

where ζ is a scalar frictional drag coefficient and H is the Hookean spring constant. The drag experienced by the beads of the dumbbell moving through the solvent is taken to be isotropic, and is characterized by a single drag coefficient. The transposed velocity gradient tensor κ is taken to be constant, and implicitly assumes that velocity

51

variations over the length scale of the molecules can be neglected. The expression for the Brownian forces used in Eqs. (2.19) and (2.20) is derived from rigorous kinetic theory using the *equilibration in momentum space* assumption. No intermolecular forces are considered, since the Oldroyd-B fluid model is a dilute solution theory.

Further development of the constitutive theory is based on the assumption of *spatial homogeneity*. Classical kinetic theory assumes that the configurational distribution function Ψ_p has no dependence on the location of the center of mass of the molecule. Thus, the distribution of configurations and the number density of the molecules are independent of spatial position. This hypothesis is consistent with the assumption that the system is infinite and unbounded, as well as subject to a homogeneous flow field. The configuration distribution function Ψ_p is then factored as

$$\Psi_p(r, Q, t) = n\psi_p(Q, t) \tag{2.21}$$

where n is the *constant number density of dumbbells* and $\psi_p(Q, t)$ describes the internal molecular configuration.

Substituting Eqs. (2.21), (2.19) and (2.20) into Eq. (2.18) gives the *diffusion equation* in terms of the distribution function ψ_p as

$$\frac{\partial \psi_p}{\partial t} = -\frac{\partial}{\partial Q} \cdot \left[(\kappa \cdot Q)\psi_p - \frac{2kT}{\zeta} \frac{\partial \psi_p}{\partial Q} - \frac{2H}{\zeta} Q\psi_p \right]. \tag{2.22}$$

An expression for the stress tensor is required to relate the changes in the configurational distribution function due to imposed flow fields, as given by Eq. (2.22), to fluid mechanics and rheology. An elementary derivation of the stress tensor was given by Kramers (1944) and accounted for stress in the fluid due to Brownian motion of the individual beads, external forces acting on the beads and intramolecular forces transmitted through the spring connectors. Neglecting external forces, the expression for the stress tensor is

$$\tau_p = -nH\langle QQ \rangle + nkT\delta. \tag{2.23}$$

The same expression can be derived from phase space theory; see Chapter 3. The

52

quantity $\langle \boldsymbol{QQ} \rangle$ is an ensemble average over the distribution function ψ_p. Equation (2.22) for the distribution function ψ_p and Eq. (2.23) for the stress tensor τ_p are a coupled set of equations that can be solved simultaneously with the equation of motion to obtain solutions to any fluid mechanical problem. However, solving for the distribution function is not a trivial task. Since the expression for the stress tensor is related to the distribution function ψ_p only through the average $\langle \boldsymbol{QQ} \rangle$, a considerable simplification is achieved by rewriting Eq. (2.22) in terms of its second-order moment as

$$\langle \boldsymbol{QQ} \rangle_{(1)} = \frac{4kT}{\zeta} \boldsymbol{\delta} - \frac{4H}{\zeta} \langle \boldsymbol{QQ} \rangle. \tag{2.24}$$

Here, the quantity $\langle \boldsymbol{QQ} \rangle_{(1)}$ is the contravariant, codeformational time derivative, which is defined for a general second-rank tensor $\boldsymbol{A}$ as (Bird et al., 1987a)

$$\boldsymbol{A}_{(1)} = \frac{D}{Dt} \boldsymbol{A} - \{ (\boldsymbol{\nabla v})^{\dagger} \cdot \boldsymbol{A} + \boldsymbol{A} \cdot (\boldsymbol{\nabla v}) \} \tag{2.25}$$

where D/Dt is the substantial time derivative.

Eqs. (2.24) and (2.23) form a closed set of equations that can be solved together with the equation of motion. However, following the same procedure with other molecular models, e.g., the rigid dumbbell, gives an analogous equation for the second moment involving the fourth moment, and a closed set of equations is not achieved. Solution of the problem necessitates closure approximations as discussed in Section 2.2.2; the alternative is to solve for the entire distribution function by solving Eq. (2.22).

Combining Eqs. (2.24) and (2.23) yields

$$\tau_p + \lambda_H \tau_{p(1)} = -nkT\lambda_H \boldsymbol{\gamma}_{(1)} \tag{2.26}$$

where $\lambda_H \equiv \zeta/4H$ is the time constant for the Hookean springs. In the absence of solvent contributions, the polymeric contribution to the stress tensor τ_p is set equal to the total deviatoric stress τ in Eq. (2.26). The resultant equation is referred to as the Upper Convected Maxwell (UCM) model and has been widely used in viscoelastic

53

flow calculations because of its simplicity. Adding the Newtonian solvent contribution to the stress tensor $\tau_s = -\eta_s\dot{\gamma}$ to τ_p in Eq. (2.26) gives the Oldroyd-B fluid model as

$$\tau + \lambda_1\tau_{p(1)} = -\eta_0(\gamma_{(1)} + \lambda_2\gamma_{(2)}). \tag{2.27}$$

Here, $\lambda_1 = \lambda_H$ is the relaxation time, $\eta_0 = \eta_s + nkT\lambda_H$ is the zero-shear-rate viscosity and $\lambda_2 = \eta_s/\eta_0\lambda_H$ is the retardation time of the model. Thus, constitutive equations such as the UCM and the Oldroyd-B fluid, originally derived using continuum concepts, can be obtained from kinetic theory using the simple Hookean dumbbell model.

The UCM and Oldroyd-B models incorporate the inherent time-dependent behavior associated with the molecular relaxation process. However, in shear flow, these models predict a constant viscosity η_0 at all shear rates, a constant first normal stress coefficient Ψ_1, and a second normal stress coefficient Ψ_2 that is identically zero. These models also predict an infinite elongational viscosity at finite elongational rates. In using a molecular theory approach in deriving the constitutive equations, the drawbacks and limitations of these equations can be considered in terms of the molecular model used and the assumptions made in the development of the theory. For example, it can be recognized that the infinite elongational viscosity displayed by the UCM model is a result of the infinite extensibility of the Hookean spring in elongational flow. The Hookean spring also is responsible for the constant viscosity behavior of the UCM model in steady shear flows. It is possible to improve these constitutive equations by, for example, replacing the linear spring force law used in the Hookean dumbbell with a nonlinear one that accounts for the finite extensibility of the spring connector, *e.g.,* the *Warner* or the *Finitely Extendible Nonlinear Elastic* (*FENE*) springs (Warner, 1972; Armstrong, 1974a &1974b). A dramatic improvement over the rheological predictions of the UCM model is seen when the FENE springs are used. Thus, in shear flow, models based on FENE dumbbells show a shear-thinning viscosity that compares well with experimental data; in elongational flows, the elongational viscosity is bounded at all elongational rates (Armstrong, 1974a &1974).

Kinetic theory has been very successful in deriving a number of constitutive equations that capture much of the wide range of rheological behavior displayed by polymer solutions and melts. Modelling of the variety of macromolecular systems seen in practice, *e.g.*, branched and linear, flexible and rigid, dilute and concentrated solutions, requires a number of different micromechanical models. A significant advantage of this molecular approach is that since the molecular basis behind the constitutive theory is clearly stated, one can relate the limitations of the theory to the micromechanical model parameters and seek other avenues for improvement in a systematic manner. Thus, the unrealistic material function predictions of the Hookean-dumbbell-based UCM and Oldroyd-B models were corrected by replacing the Hookean spring with a finitely extendible one, leading to the family of FENE models (Warner, 1972; Armstrong, 1974a & 1974b; Bird and DeAguiar, 1983; DeAguiar, 1983; Wedgewood *et al.*, 1991). The Chilcott-Rallison model (Chilcott and Rallison, 1988) that has been used in recent viscoelastic flow calculations, although not rigorously derivable from kinetic theory, is clearly inspired by the idea of FENE-like spring force laws. Other modifications of the UCM and Oldroyd-B models have been attempted, such as the use of an anisotropic drag coefficient to give the Giesekus model (Giesekus, 1982) and incorporating the effect of *hydrodynamic interaction*, *i.e.*, perturbation of the solvent velocity due to the local chain motion (Öttinger, 1985, 1986 & 1987). Multibead generalizations of the Oldroyd-B constitutive theory also have been derived. The simplest of these is based on a N-bead Rouse chain, shown in Fig. 2-6, with each bead connected by a Hookean spring. The resultant model has N modes of relaxation and a different relaxation time constant associated with each mode, and thus accounts for the relaxation spectrum displayed by polymer solutions and melts. The governing equation for each mode is exactly of the form of Eq. (2.26). The use of Hookean springs in the Rouse model leads to unrealistic material functions, and multibead models with nonlinear springs have also been studied (Bird *et al.*, 1980). For concentrated solutions, we have models such as the Doi-Edwards model (Doi and Edwards, 1978a, 1978b, 1978c & 1979) based on ideas of *reptation* first suggested by de Gennes (1971), and the Curtiss-Bird theory (Curtiss and Bird, 1981a & 1981b) that uses anisotropic

mobility and anisotropic Brownian motion to model polymer-polymer interaction.

A common feature shared by the many constitutive theories listed above is that all make the assumption of *spatial homogeneity*. Thus, the distribution function is factored, as given by Eq. (2.21), and the polymer concentration is taken to be uniform over the entire flow domain. The assumption of spatial homogeneity is consistent with the assumption of an *unbounded* system, and the effect of boundaries on the bulk flow is thus ignored. The assumption of spatial homogeneity is also tantamount to assuming no variation in the velocity gradient and stress across the length of the macromolecule and is highly suspect in strongly nonhomogeneous flows, where one intuitively expects a nonhomogeneous distribution of concentration and stress fields with spatial gradients on small length scales. Furthermore, such an assumption is justified *only if* the distribution function is a slowly varying function of r and all spatial variations on the length scale of the macromolecule can be neglected. Strictly speaking, it is not possible to say *a priori* whether the distribution function varies slowly with r or not.

A number of problems are seen in practice, where the system is inherently non-homogeneous, *e.g.*, problems involving sharp gradients in stress and velocity fields such as are seen in flows through abrupt contractions, problems of phase separating systems such as concentrated solutions of molecules with rigid backbones undergoing a transition from a disordered state to an ordered one and problems involving small spatial dimensions where boundary effects play a significant role. The existing theories cannot be applied to the solution of these problems, due to the assumptions of spatial homogeneity. Traditional kinetic theory is generalized in the following chapters to account for the effect of spatial gradients in stress, velocity, concentration and orientation and study the effect on polymer rheology.

Chapter 3

Kinetic Theory of Dilute, Nonhomogeneous Polymer Solutions

The assumption of *spatial homogeneity* is inherent to classical constitutive theories, such as UCM and Oldroyd-B discussed in Section 2.3.3 and makes these models unsuitable to the study of intrinsically nonhomogeneous problem. An extension of these theories to nonhomogeneous systems is developed in this chapter using phase-space kinetic theory, as introduced in Section 2.3.2. The development is carried out using the Hookean dumbbell model for the polymer molecule, but the approach is general and can be extended easily to other micromechanical models.

3.1 Introduction to the Nonhomogeneous Problem

Spatial nonhomogeneities may enter a fluid mechanical problem in a number of ways. The presence of solid boundaries in a problem imposes restrictions on the allowed macromolecular configurations and is thus a source of spatial nonhomogeneity. These wall effects are especially important in flow geometries with small spatial dimensions.

The development of large gradients in stress and velocity fields on length scales comparable to the polymer length is seen in some flow geometries, *e.g.*, flow through an abrupt contraction, discussed in Chapter 1. In such flows, the extended polymer molecule experiences different forces at different points along its length. Such nonhomogeneities on a microstructural length scale can have a large impact on the bulk flow.

In early studies of nonhomogeneous flows, *molecular migration* was speculated as one of the significant effects of such nonhomogeneous stress and velocity fields. Molecular migration here implies that a suspended particle or macromolecule moves or drifts relative to the solvent velocity at its center-of-mass, when its motion is observed on a time scale that is long compared to the time scale of Brownian motion (Aubert *et al.*, 1980). The most unambiguous observation of cross-streamline molecular migration was made by Shaefer *et al.* (1974) in circular Couette flow. In this study, high molecular weight DNA molecules were observed to migrate towards the rotating inner cylinder.

Other speculations of polymer migration in nonhomogeneous flow were based on indirect measurements in the capillary flow of polymer solutions. It was suggested that since molecular migration can produce spatially nonuniform polymer concentrations, it can influence the rheological behavior of the fluid. For example, a number of research groups reported that the viscosity measured in a capillary decreased with decreasing capillary radius and with increasing capillary length (Kozicki *et al.*, 1970; Therien *et al.*, 1970), possibly due to molecular-weight fractionation and molecular migration in the nonhomogeneous flow field. The different results obtained from viscosity measurements of the same macromolecular fluid in homogeneous and nonhomogeneous flow fields at similar values of shear rate were also attributed to molecular migration. It is important to understand the cause of such nonuniformities and assess the importance of their effect on the macroscopic flows of polymer solutions and melts.

Following these observations, a number of theories were propounded in order to explain the origin of molecular migration, and to establish whether or not nonhomoge-

neous stress and velocity fields could lead to nonhomogeneous concentration profiles. One speculation was that in a nonhomogeneous velocity field, a system of macromolecules tends to increase its configurational entropy by diffusing from regions of higher velocity gradients which tend to produce more highly oriented configurations to regions of smaller velocity gradients (Ouano and Biesenberger, 1971). Tirrell and Malone (1977) suggested that gradients of stress drive polymer migration and proposed a phenomenological thermodynamic theory of deformation-induced diffusion. They suggested that the total mass flux j_p was a sum of the Fickian diffusion flux and a new stress-induced flux such that

$$j_p = -(\mathcal{D}\boldsymbol{\nabla} c + \frac{\mathcal{D}}{kT} c \boldsymbol{\nabla} \bar{V})$$ (3.1)

where $\mathcal{D}$ is the translational diffusivity, c is the local macromolecular concentration and $\bar{V}$ is the potential that provides the thermodynamic driving force for migration of the polymer from regions of high stress to regions of lower stress. An expression for the entropic potential $\bar{V}$ was given in terms of the deformation rate $\dot{\gamma}$ as

$$\bar{V} = kT \left[\frac{\lambda^2 \dot{\gamma}^2}{3} - \frac{1}{2} \ln(1 + \frac{2\lambda^2 \dot{\gamma}^2}{3}) \right]$$ (3.2)

Thus, nonuniform deformation rates, and hence nonuniform stress, produce an entropic driving force that forces molecules to regions of lower stress. However, the radial molecular weight fractionation in capillary flow predicted by Tirrell and Malone using this model appears higher than that observed experimentally (Whitlock and Porter, 1972). A similar coupling between stress and concentration fields has also been suggested by Helfand and Frederickson (1989), in a slightly different context. These authors developed a phenomenological theory involving stress-induced diffusion to explain experimental observations of increased turbidity caused by greatly enhanced concentration fluctuations in polymer solutions that begin to phase separate under the influence of shear.

The validity of the phenomenological thermodynamic model of deformation induced diffusion developed by Tirrell and Malone was questioned by Aubert and Tir-

rell (1980) and Aubert *et al.* (1980). They suggested that instead of stress gradients, the real driving force for macromolecular migration was a velocity field that was nonhomogeneous on the length scale of the macromolecule. A similar idea had been proposed earlier by Shaefer *et al.* (1974) to explain their observations of radial migration of DNA molecules in circular Couette flow. Subsequently, Bird (1978) suggested that such a radial migration could be explained within a kinetic theory framework using simple dumbbell models that are suspended in a velocity field with a gradient that shows spatial variation on the length scale of the dumbbell. In this case, the center-of-mass of the dumbbell does not move with the local solvent velocity, and in circular Couette flow, an inward radial migration of macromolecules is predicted.

Aubert and Tirrell (1980) and Aubert *et al.* (1980) extended the ideas of Shaefer *et al.* (1974) and Bird (1978) and confirmed the calculations of these authors that predicted radial migration in circular Couette flow. By studying a number of other problems involving nonhomogeneous velocity fields such as parallel Couette flow, they also showed that molecular migration in this theory is a consequence of curvilinear streamlines. Subsequently, Sekhon *et al.*(1982), Brunn (1983), and Brunn and Chi (1984) showed that macromolecular migration across streamlines could be obtained in rectilinear flows by accounting for hydrodynamic interaction, *i.e.*, the perturbation of the solvent velocity field by finite-sized beads in the dumbbell models. It was established that in unidirectional rectilinear flow, if nonhomogeneous velocity fields alone were responsible for migration, any such migration across streamlines required hydrodynamically interacting beads. However, it was not established whether hydrodynamic interaction, which is a perturbation to the primary flow field, is sufficient to explain the observations of decreased viscosity with decreasing capillary radius, as measured by Kozicki *et al.* (1970) and Thérien *et al.* (1970).

An alternative theory extended to explain the dependence of the viscosity on the capillary radius was that there could be an *apparent* break-down of the *no slip* boundary condition at solid walls in the case of polymer solutions. Historically, the behavior of complex fluids such as polymer solutions and melts near solid boundaries has been the subject of much debate (Schowalter, 1988). Continuum mechanics traditionally

used the *no slip* boundary condition for Newtonian fluids; *i.e.,* there is no motion of the fluid relative to the solid and impenetrable boundary past which the fluid is flowing. However, it is not clear that this is the case even with complex non-Newtonian fluids. Measurements of the flow rate of polymer melts through pipes of varying radius showed that the apparent shear rate depended on capillary radius beyond a certain flow rate, even when the wall shear stress was maintained constant, thus indicating the presence of slip (Denn, 1990). Data collected by Ramamurthy (1986) indicated that changing the material of the die could affect the onset of slip, as indicated by the appearance of a non-zero slope in an apparent-shear-rate *vs.* inverse radius plot, and correlated slip with the onset of melt fracture; see Fig. 1-2. The presence of fluid slip is also thought to have a profound effect on polymer hydrodynamics, leading to specific hydrodynamic instabilities in some cases (Renardy, 1990). It has also been suggested that fluid slip might be necessary in order to develop a self-consistent theory for polymer fluid flow near corners (Lipscomb *et al.,* 1987).

Metzner and coworkers suggested that the *apparent* breakdown of the no-slip boundary condition in polymer solutions and melts is possibly due to the development of a layer free of macromolecules near the wall of the capillary. Their argument suggested that the presence of solid walls in a system invariably introduced some nonhomogeneity that lead to such anomalous behavior. Cohen and Metzner (1982 & 1986) and Metzner *et al.* (1979) used the theory of stress-induced diffusion to explain the formation of such *depletion layers.* They argued that in capillary tube flow, for example, macromolecules will migrate away from the wall region, where they are more ordered and hence at a lower entropic level to the bulk flow region where higher configurational entropies are possible. This diffusion phenomenon could then lead to the depletion of macromolecules in the wall region and consequently to the formation of a low viscosity fluid layer near the tube wall. The remainder of the fluid continuum could appear to *slip* through the tube although the less viscous fluid layer near the wall does not violate the *no slip* boundary condition. As a result, it would be possible to obtain a decrease in viscosity with flow nonhomogeneity. Consequently, considerable flow enhancement may be seen in geometries where wall effects are ex-

pected to be important, such as flow through a narrow capillary or through a porous medium. Extensive studies of such systems (Cohen and Metzner, 1982, 1985 & 1986; Metzner et al., 1979; Chauveteau, 1982) for a variety of macromolecular solutions have revealed such flow enhancement. In these studies, the experimental flow rates at a given level of stress were found to be higher than the viscometric predictions (obtained from cone-and-plate viscometer measurements) by as much as a factor of three. These studies established that the apparent slip phenomenon is not an anomaly, but an important aspect of the flow behavior of polymer solutions in nonhomogeneous stress fields.

Other authors also suggested that apparent slip could result from an interaction of macromolecules with the solid boundary. Brunn (1976) studied the effect of a solid wall on the flow of dilute macromolecular solutions, by taking the interaction between the solute molecules and the wall to be a hard-core repulsion, leading to steric effects on the molecules adjacent to the wall. Here, the wall region was considered separately, and the nonhomogeneous velocity field in this region was interpreted as resulting in an apparent slip velocity. Aubert and Tirrell (1982) also studied the effective viscosities of dilute polymer solutions near confining boundaries, and the related phenomenon of apparent slip by introducing boundaries in the form of a wall potential. By using a kinetic theory approach, they developed a diffusion equation that is valid in the presence of the wall potential. At equilibrium, they showed that the diffusion equation with impenetrable, purely repulsive interfaces results in the development of polymer-depleted layers near the wall. By carrying out a perturbation expansion about this equilibrium solution in the presence of flow, Aubert and Tirrell (1982) also showed that a repulsive wall potential strongly affects fluid viscosity, thereby resulting in apparent slip at the interfaces.

The phenomenon of molecular migration has also been speculated to be related to the so-called "high De problem". There are fundamental difficulties with the existence of solutions and the convergence of numerical methods in the calculation of complex flows of viscoelastic fluids at high De, and this is thought to result from the use of constitutive equations developed for homogeneous flows in solving problems where

nonhomogeneities could play an important role, such as problems with large stress gradients (Keunings, 1986; Lipscomb *et al.*, 1987); see Section 1.1.1. In order to understand this possible cause of the high De problem, it is necessary to understand the cause of molecular migration, and the interplay between the stress, velocity and concentration fields.

These different studies carried out over the last decade have served to establish definitely that nonhomogeneities in stress and velocity fields can lead to the nonuniform distribution of polymer. In addition, experimental evidence suggests that the presence of solid boundaries may be responsible for the apparent slip behavior displayed by polymers and boundaries can thus have a significant impact on the macroscopic flow fields. Walls, in fact, are a source of nonhomogeneities in the system, and thus are closely related to the phenomenon of molecular migration. Until recently, there was no theory that could reconcile all the effects that were observed. More significantly, none of the previous theories considered the interdependence of the stress and velocity fields and the nonuniform concentration profiles. For instance, all the theories discussed above assumed the kinematics *a priori*, and there was no attempt to solve the entire flow problem to establish self-consistent stress, velocity and concentration profiles.

In the last few years, some attempts have been made to remedy these inconsistencies. Nonhomogeneous constitutive theories have been developed using different techniques such as polymer kinetic theory (El-Kareh and Leal, 1989; Bhave *et al.*, 1991), a free-energy-based, Poisson Bracket formulation (Mavrantzas and Beris, 1992a & 1992b) and a continuum body-tensor formalism (Öttinger, 1991 & 1992). In this chapter, the phase-space kinetic theory approach has been used to develop a nonhomogeneous theory by accounting for the interaction between the three field variables, *viz.*, stress, velocity and polymer concentration. The discussion is restricted to dilute solutions in order to keep the theory as simple as possible. A comparison of the dilute solution nonhomogeneous theory developed in this chapter and the other nonhomogeneous theories developed using alternate techniques is presented in Section 3.6.

3.2 Incorporating Spatial Nonhomogeneities

The two main sources of polymer migration are (1) nonhomogeneous stress and velocity fields and (2) polymer interaction with the solid boundary. Molecular migration can potentially result in large scale effects in the macroscopic flow of viscoelastic fluids. Any theory of nonhomogeneities in viscoelastic fluids must account for these elements. In this section, the limitations of classical kinetic theory in studying the nonhomogeneous problem are discussed and the main modifications to the classical kinetic theory that have been made in this thesis are described.

All classical kinetic theories make the assumption of *spatial homogeneity*; see Section 2.3.3. The configurational distribution function Ψ_α for a species α is taken to have no dependence on the location of the center of mass of the molecule and is factored as $\Psi_\alpha(r, Q, t) = n\psi_\alpha(Q, t)$, where the number density n is taken to be constant. Clearly, such theories are inadequate for describing inherently nonhomogeneous phenomena such as molecular migration that can result in nonuniform concentration profiles.

The assumption of spatial nonhomogeneity is consistent with the assumption that the system is infinite and unbounded as well as subject to a homogeneous flow field. As a consequence, the homogeneous theories do not recognize the existence of physical system boundaries. This is clearly a disadvantage since such theories cannot account for the apparent slip phenomena, and cannot prove or disprove speculations on the effect of slip on macroscopic flows. Furthermore, Monte Carlo and molecular dynamics simulations indicate that large deviations from a uniform configurational distribution exist near solid boundaries as a consequence of the steric constraints imposed by the wall on the macromolecular configuration (Theodorou, 1988a & 1988b; Bitsanis and Hadziioanou, 1990; Yethiraj and Hall, 1990). These deviations persist over distances comparable to the radius of gyration of the molecule and may play a significant role in situations where wall effects are important, such as flow in narrow pores (Bitsanis and Hadziioanou, 1990).

No assumptions about the spatial uniformity of the configuration distribution function are made in the development described here. The expression for Ψ_α is not

factored, and the kinetic theory is developed in terms of $\Psi_\alpha = \Psi_\alpha(r, Q, t)$.

The second generalization incorporated here involves explicitly treating the dumb-bells as extended objects in space. This treatment recognizes the fact that a polymer molecule is not a point object, rather it is an extended object with its mass distributed along its length. This distinction is especially important in considering flows where the stress and velocity fields change drastically on the length scale of the polymer extension. The importance of this effect in nonhomogeneous problems has been emphasized by Brunn and Grisafi (1985) and Öttinger (1989a).

For the Hookean dumbbell model that is used here, the mass density of the polymer species p at any point in space is defined as a sum of contributions of the mass of each bead of the dumbbell as

$$\rho_p(r, t) = \sum_\nu m_\nu^p \int \Psi_p(r - R_\nu, Q, t) dQ \tag{3.3}$$

where m_ν^p is the mass of bead ν of polymer species p and R_ν is the relative position of bead ν with respect to the center of mass of the molecule. For the Hookean dumbbell, $R_\nu \equiv (-1)^\nu Q/2$ and $m_\nu^p \equiv m$. Furthermore, the mass density of polymer ρ_p and the number density n are simply related by $\rho_p \equiv 2nm$.

Finally, no assumptions are made about the stress tensor equation. Instead this equation is derived in a way consistent with the treatment of the spatial dependence of the distribution function and the extended nature of the polymer molecules.

In a recent publication, El-Kareh and Leal (1989) also adopted a kinetic theory approach in the development of constitutive equations for nonhomogeneous flows. In this study, the first generalization, viz., a spatially dependent distribution function, was included. However, effects of finite spatial extension of the dumbbell were not considered. The development of El-Kareh and Leal is an extension of the Chilcott-Rallison model (Chilcott and Rallison, 1988), and is based on a dumbbell model with a finitely extendible nonlinear elastic (FENE) spring connector. The nonhomogeneous theory developed in this chapter is compared to the El-Kareh and Leal model at appropriate points in the discussion.

3.3 The Constitutive Equations

3.3.1 Bead-Spring Description of the Physical System

The polymer is modelled as a Hookean dumbbell in order to simplify the development. However, the concepts developed are general and can easily be extended to other molecular models. We consider a volume $\mathcal{V}$ of dilute polymer solution at temperature T, where the macromolecules are modelled as Hookean dumbbells, as shown in Fig. 3-1. The solvent is an incompressible Newtonian fluid of viscosity η_s; the polymer number density is n. The mass of each macromolecule is distributed equally between two mass points or beads, each of mass m, joined by a nonbendable Hookean spring with a spring constant H.

The two beads of the dumbbell are labelled "1" and "2", and have spatial positions described by two position vectors r_1 and r_2, respectively, referenced to an arbitrary, fixed origin in space. The internal configuration of the dumbbell is described by the connector vector $Q = r_2 - r_1$. Since the Hookean dumbbell does not have any constraints, we do not need to use the generalized coordinates discussed in Section 2.3. The center-of-mass location for the dumbbell relative to the fixed origin is written in terms of the bead position vectors as $r_c = \frac{1}{2}(r_1 + r_2)$. The set of vectors (r_1, r_2) or (r_c, Q) is used to describe the configuration of each dumbbell. Similarly, the instantaneous momenta of the beads are given by the momentum vectors p_1 and p_2. The two momentum vectors can be replaced by momenta (p_c, P) associated with the center of mass (p_c) and the internal degrees of freedom (P), respectively.

3.3.2 The Equations of Change

A formal phase-space theory development for general polymeric systems has been presented in Chapters 17 and 18 of Bird *et al.* (1987b). The basic concepts of this approach were introduced in Section 2.3. In the following development the approach given by Bird *et al.* (1987b) is paralleled for a dilute solution of Hookean dumbbells. The theory is developed specifically for nonhomogeneous systems and the differences
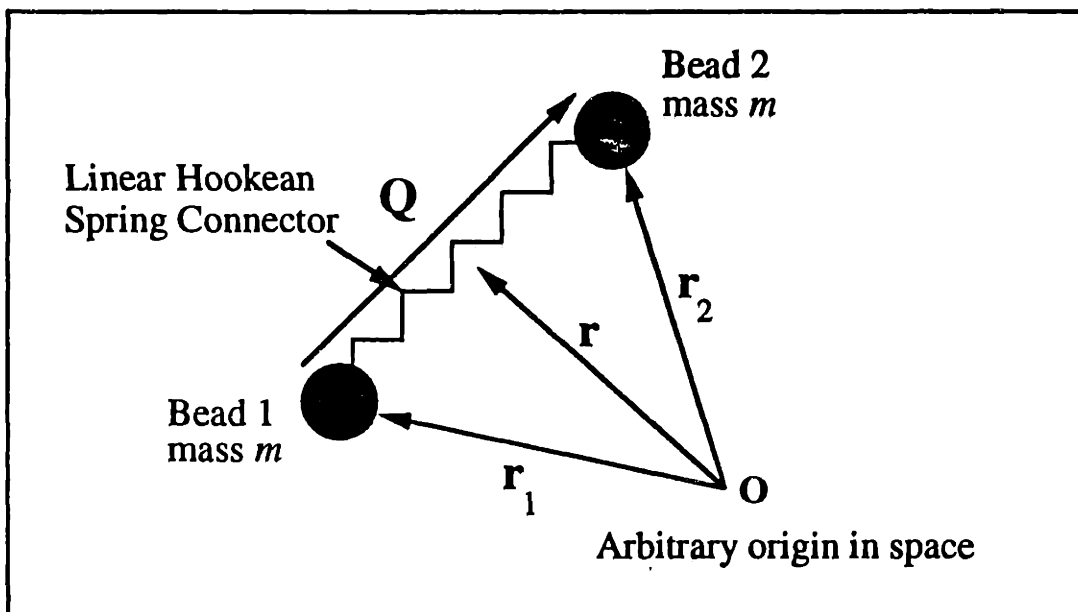
Figure 3-1: The Hookean dumbbell model.

are emphasized between this development and the presentation in Bird *et al.* (1987b).

3.3.2.1 The Species Conservation Equation and the Equation of Motion

The starting point for any development in non-equilibrium statistical mechanics is the *Liouville equation*. For the macromolecular system under consideration, comprising of Hookean dumbbells suspended in a solvent modelled as mass points, the Liouville equation is written as,

$$
\begin{aligned}
\frac{\partial f}{\partial t} &= -\sum_\alpha \sum_i \left(\frac{\partial}{\partial r_c^{\alpha i}} \cdot \dot{r}_c^{\alpha i} f + \frac{\partial}{\partial Q^{\alpha i}} \cdot \dot{Q}^{\alpha i} f + \frac{\partial}{\partial p_c^{\alpha i}} \cdot \dot{p}_c^{\alpha i} f + \frac{\partial}{\partial P^{\alpha i}} \cdot \dot{P}^{\alpha i} f \right) \\
&= -\sum_\alpha \sum_i \left(\frac{1}{m^\alpha} p_c^{\alpha i} \cdot \frac{\partial f}{\partial r_c^{\alpha i}} + \frac{4}{m^\alpha} P^{\alpha i} \cdot \frac{\partial f}{\partial Q^{\alpha i}} + (F^{(e)\alpha i} + F^{\alpha i}) \cdot \frac{\partial f}{\partial p_c^{\alpha i}} \right. \\
&\quad \left. + (\mathcal{F}^{(\phi)\alpha i} + \mathcal{F}^{(e)\alpha i} + \mathcal{F}^{(d)\alpha i}) \cdot \frac{\partial f}{\partial P^{\alpha i}} \right).
\end{aligned}
\tag{3.4}
$$

As discussed in Section 2.3, the independent variables $(r_c^{\alpha i}, Q^{\alpha i}, p_c^{\alpha i}, P^{\alpha i})$ give the instantaneous location of molecule i belonging to species α in the phase-space, and m^α refers to the mass of a molecule of species α. In going from line (1) to line (2) of Eq. (3.4), the time derivatives of the phase-space coordinates $(\dot{r}_c^{\alpha i}, \dot{Q}^{\alpha i}, \dot{p}_c^{\alpha i}, \dot{P}^{\alpha i})$ have been rewritten in terms of the momenta and the various forces acting on a molecule by using Hamilton's equations of motion; see Eq.(2.16). The forces $F^{(e)\alpha i}$ and $F^{\alpha i}$ are the total forces acting on the center of mass of molecule i of species α resulting from the external and intermolecular potentials, respectively. The forces $\mathcal{F}^{(\phi)\alpha i}$, $\mathcal{F}^{(e)\alpha i}$ and $\mathcal{F}^{(d)\alpha i}$ are the relative forces [see Eq. (3.26)] between the beads of molecule i of species α originating from the intramolecular, external and intermolecular potentials, respectively. These forces are discussed at greater length in Section 3.3.2.2. For a system consisting of one polymer species in a solvent, α is either p or s, corresponding to the polymer or solvent species, respectively.

Since in the formal development, the theory is restricted to two-body interactions only, it is unnecessary to deal with the complete phase-space distribution function f. Therefore, lower order distribution functions can be obtained from the full phase-space distribution function, by suitable ensemble averaging; see Section 2.3. Thus, singlet

Dynamical Variable B	Equation of Change
$\sum_{i\nu} m_\nu^\alpha \delta(r_c^{\alpha i} + R_\nu^{\alpha i} - r)$	Species Conservation Equation
$\sum_{i\nu} m_\nu^\alpha \delta(r_c^{\alpha i} + R_\nu^{\alpha i} - r)\delta(Q^{\alpha i} - Q)$	Continuity Equation for $\Psi_\alpha(r - R_\nu, Q, t)$
$\sum_{\alpha i\nu} m_\nu^\alpha(\dot{r}_c^{\alpha i} + \dot{R}_\nu^{\alpha i})\delta(r_c^{\alpha i} + R_\nu^{\alpha i} - r)$	Equation of Motion
$\sum_i \delta(r_c^{\alpha i} - r)\delta(Q^{\alpha i} - Q)\delta(p_c^{\alpha i} - p)\delta(P^{\alpha i} - P)$	Evolution Equation for f_α

Table 3.1: Equations of change for various dynamical variables.

phase-space and configurational distribution functions, f_α and Ψ_α were defined; see Eqs. (2.12) and (2.14). Similarly, pair phase-space and configurational distribution functions $f_{\alpha\beta}$ and $\Psi_{\alpha\beta}$ were also defined; see Eqs. (2.15) and (2.16).

A general equation of change for any dynamical variable B can be obtained by multiplying Eq. (3.4) by B and averaging over the ensemble. Different choice , of the dynamical variable lead to the development of the equations of conservation of species and motion as well as evolution equations for the lower order distribution functions, as illustrated in Table 3.1, and have been described for general systems in Chapter 17 of Bird *et al.* (1987b). The polymer species conservation equation is obtained by choosing the dynamical variable to be

$$B \equiv m \sum_{i\nu} \delta(r_c^{pi} + R_\nu^{pi} - r). \tag{3.5}$$

The mass density of polymer is defined in terms of this choice of B as

$$\rho_P(r, t) \equiv \langle B \rangle. \tag{3.6}$$

This definition of B accounts for the extension of the dumbbell in space and makes explicit the idea that the mass density of polymer at any point r is a sum of contributions from the individual beads. Multiplying Eq. (3.4) by the dynamical variable

B defined in Eq. (3.5) and integrating over the phase-space coordinates yields the species conservation equation

$$\frac{\partial \rho_P}{\partial t} = -m \sum_\nu \frac{\partial}{\partial r} \cdot \left(\int [[\dot{r}]]^P \Psi_p dQ + \frac{(-1)^\nu}{2} \int [[\dot{Q}]]^P \Psi_p dQ \right) \qquad (3.7)$$

where $\Psi_p = \Psi_p(r - R_\nu, Q, t)$ The displaced position argument is a result of the finite extension of the dumbbell in space. The double brackets $[[\ ]]^P$ represent an average over momenta defined as

$$[[B]]^P \equiv \frac{1}{\Psi_p} \int B f_p dp dP. \qquad (3.8)$$

Expression (3.7) is simplified further by expanding the singlet phase-space distribution function f_p in a Taylor series about r up to the first correction, as

$$
\begin{aligned}
& [[\dot{r}]]^P \Psi_p(r - R_\nu, Q, t) \\
= & \int \dot{r} f_p(r - R_\nu, Q, p, P, t) dp dP \\
= & \int \dot{r} f_p(r, Q, p, P, t) dp dP - \frac{\partial}{\partial r} \cdot \int R_\nu \dot{r} f_p(r, Q, p, P, t) dp dP \\
= & [[\dot{r}]]^P \Psi_p(r, Q, t) - R_\nu \cdot \frac{\partial}{\partial r} [[\dot{r}]]^P \Psi_p(r, Q, t)
\end{aligned}
\qquad (3.9)
$$

with a similar result for the integrand involving $[[\dot{Q}]]^P$. Substituting these Taylor expansions into Eq. (3.7) and summing over ν allows expression (3.7) to be written in terms of j_p, the mass flux of polymer relative to the stream velocity v, as

$$\frac{D\rho_P}{Dt} = -\nabla \cdot j_p \qquad (3.10)$$

where

$$j_p = 2m \int [[\dot{r}]]^P \Psi_p dQ - \frac{m}{2} \frac{\partial}{\partial r} \cdot \int Q[[\dot{Q}]]^P \Psi_p dQ - \rho_p v \qquad (3.11)$$

and $\Psi_p = \Psi_p(r, Q, t)$. The stream velocity $v(r, t) = \frac{1}{\rho} \langle \sum_{\alpha i \nu} m_\nu^\alpha (\dot{r}^{\alpha i} + \dot{R}_\nu^{\alpha i}) \, \delta(r^{\alpha i} + R_\nu^{\alpha i} - r) \rangle$ is the mass-average velocity of the fluid, and $D/Dt = \partial/\partial t + v \cdot \nabla$ is the *substantial* (or *material*) derivative, which describes the time rate of change following a fluid particle.

The same process can be repeated with another choice of the dynamical variable B to derive the equation of motion, as described in Chapters 17 and 18 of Bird *et al.* (1987b). For this development, the dynamical variable is taken to be

$$B \equiv m \sum_{\alpha i \nu} (\dot{r}_c^{\alpha i} + \dot{R}_\nu^{\alpha i}) \delta(r_c^{\alpha i} + R_\nu^{\alpha i} - r). \tag{3.12}$$

Note that the particular choice of B again accounts for the finite extension of the molecules. The resultant equation of motion (Eq. 17.4-32 of Bird *et al.*) is

$$\frac{\partial}{\partial t} \rho v = -[\nabla \cdot \rho v v] - [\nabla \cdot \pi] + n \bar{F}^{(e)} \tag{3.13}$$

where the total density of the solution is $\rho = \sum_\alpha \rho_\alpha$. The term $n \bar{F}^{(e)}$ includes all external forces acting on the system, *e.g.*, gravitational forces, and is given as,

$$n \bar{F}^{(e)} = \sum_\alpha \int F^{(e)\alpha} \Psi_\alpha(r, Q, t) dQ. \tag{3.14}$$

The stress tensor π is

$$\pi = \pi^{(k)} + \pi^{(e)} + \pi^{(S)} + \pi^{(D)} \tag{3.15}$$

where the four contributions to the stress tensor are associated with molecular motion, external forces, intramolecular potential, and intermolecular potential, respectively. In the subsequent development, the constitutive theory is first developed by ignoring *all* external forces. The effect of external force fields on the mass conservation equation and on the expression for the stress tensor is presented in Section 3.5.

In the development described in Bird *et al.*, expressions for the contributions to the stress tensor are simplified by expanding the configurational distribution function Ψ_α in a generalized Taylor series about the center of mass of the molecule. In order to be consistent with the truncated Taylor series expansion (3.9) used in the development of the mass flux vector, two terms in the Taylor series are retained for each term. This is a slight extension to the development presented in Chapter 17 of Bird *et al.* (1987b), where only one term is retained in the Taylor series expansion of the kinetic contribution to the stress tensor, $\pi^{(k)}$. The additional terms are identically zero if we
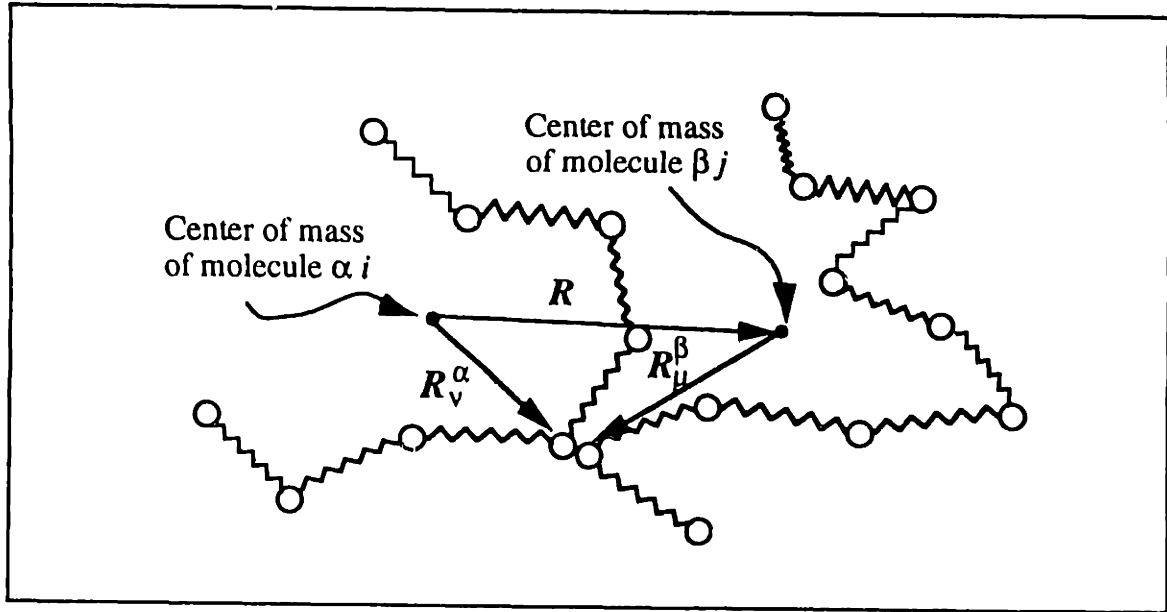
Figure 3-2: Illustration of the short-range force approximation.

make the assumption of equilibration in momentum space and hence this extension leads to no modification of the final expression for the stress tensor for the Hookean dumbbell (or any symmetric dumbbell). All subsequent expressions for the stress tensor are identical to those developed by Bird *et al.*

The intermolecular force is approximated by using a two-body potential and is further simplified with the *short-range force approximation*, which states that non-negligible intermolecular forces result only when beads belonging to two different molecules are in close proximity as shown in Fig. 3-2. The expression for the stress tensor can then be written down as

$$\pi = \pi_k - \sum_{\alpha\beta\nu} \int \int \int R_\nu^\alpha F_\nu^{\alpha\beta} \tilde{\Psi}_{\alpha\beta}(r, R, Q, Q'', t) dQ dQ'' dR \qquad (3.16)$$

where the distribution function $\tilde{\Psi}_{\alpha\beta}$ is a modified pair-distribution function written in terms of the center-of-mass of the pair of molecules αi and βj and the separation between their individual centers-of-mass R. The use of this modified distribution

72

function facilitates application of the short-range force approximation. The quantity π_k is the stress contribution due to the motion of the beads relative to the center of mass of the molecule and $F_\nu^{\alpha\beta} \equiv \sum_\mu F_{\nu\mu}^{\alpha\beta}$ is the force on the center of mass of a molecule of species α due to forces on bead ν arising from interactions with a molecule of species β.

The problem is reduced to the phase-space of a single molecule by treating the intermolecular force as an average hydrodynamic force that is defined as

$$F_\nu^{(h)\alpha} = \frac{1}{\bar{N}\Psi_\alpha} \sum_\beta \int \int F_\nu^{\alpha\beta} \bar{\Psi}_{\alpha\beta}(r, R, Q, Q'', t) dQ'' dR \qquad (3.17)$$

where $\bar{N} = \sum_\alpha x_\alpha N_\alpha$ is the average number of beads per molecule in the solution with species α having mole fraction x_α. For a dilute solution of one polymer species in a solvent, $\bar{N} \simeq 1$.

With these simplifications, the stress tensor expression is (Eq. 18.1-10 of Bird et al.)

$$\pi = \pi_k - \bar{N} \sum_{\alpha\nu} \int R_\nu^\alpha F_\nu^{(h)\alpha} \Psi_\alpha(r, Q, t) dQ. \qquad (3.18)$$

The development of the species conservation equation for the polymer and the hydrodynamic equation of motion for the dilute polymer solution explicitly includes the finite extension of the polymer molecule in space, and hence results in expressions for the polymer mass flux vector j_p and total stress tensor π involving averages with respect to distribution functions with displaced arguments, such as $\Psi_\alpha(r - R_\nu, Q, t)$. The solution of such equations requires an equation of continuity for $\Psi_\alpha(r - R_\nu, Q, t)$, which can be obtained from the Liouville equation with a suitable dynamical variable, as indicated in Table 3.1. Alternatively, with the use of Taylor series expansions, the problem can be reduced to one that requires knowledge of the singlet distribution function $\Psi_\alpha(r, Q, t)$ alone. Thus, after accounting for the finite extension of the molecules, time evolution equations for $\Psi_p(r, Q, t)$ and $\Psi_s(r, t)$ are required for further simplification. Furthermore, as seen in the subsequent development, although we identify certain terms as "solvent" contributions, these are never evaluated explicitly. In effect, the solvent is treated as a continuum. Hence no time evolution equation for

73

Ψ, is derived, although the approach described below could be employed.

3.3.2.2 Equation of Continuity for the Configurational Distribution Function

In order to develop a continuity equation for $\Psi_p(r, Q, t)$, the dynamical variable is chosen as

$$B \equiv \sum_i \delta(r_c^{pi} - r)\delta(Q^{pi} - Q)\delta(p_c^{pi} - p)\delta(P^{pi} - P). \tag{3.19}$$

By following the same procedure as in the previous subsection, the equation of change for the singlet phase-space distribution function is obtained as

$$
\begin{aligned}
\frac{\partial f_p}{\partial t} = & - \frac{\partial}{\partial r} \cdot \dot{r} f_p - \frac{\partial}{\partial Q} \cdot \dot{Q} f_p \\
& - \frac{\partial}{\partial p} \cdot \sum_\beta \int F^{p\beta} f_{p\beta} dr_\beta dQ_\beta dp_\beta dP_\beta \\
& - \frac{\partial}{\partial P} \cdot \left(\mathcal{F}^{(\phi)p} f_p + \sum_\beta \int \mathcal{F}^{p\beta} f_{p\beta} dr_\beta dQ_\beta dp_\beta dP_\beta \right),
\end{aligned}
\tag{3.20}
$$

where $F^{(\cdots)}$ refers to a *total* force acting on the center of mass of a molecule and $\mathcal{F}^{(\cdots)}$ is a *relative* force that is given by a difference of forces acting on the two beads of the dumbbell as defined by Eq. (3.26). Thus, $F^{p\beta}$ is the total force exerted on the center of mass of a polymer molecule by a molecule of species β ($\beta = p$ or s). Similarly, $\mathcal{F}^{p\beta}$ is the relative force on a polymer molecule due to a molecule of species β. The intermolecular forces $F^{p\beta}$ and $\mathcal{F}^{p\beta}$ between the molecule of interest and all other molecules are subsequently approximated by the hydrodynamic forces, $F^{(h)p}$ and $\mathcal{F}^{(h)p}$, respectively. This reduces the problem to the phase-space of a single molecule. Finally, $\mathcal{F}^{(\phi)p}$ is the relative intramolecular force acting on the polymer molecule.

Note that in developing Eq. (3.20) from Eq. (3.4), all external force contributions have been dropped. The theory is first developed in the absence of external forces, for the sake of simplicity. In Section 3.5, the effect of external forces is incorporated back into the equations and the importance of these terms is discussed.

74

Integrating over all momenta and noting that the distribution function tends to zero as $p \rightarrow \infty$ and $P \rightarrow \infty$ gives the equation of change for the singlet configurational distribution function as

$$\frac{\partial \Psi_P}{\partial t} = -\frac{\partial}{\partial r} \cdot ([[\dot{r}]]^P \Psi_P) - \frac{\partial}{\partial Q} \cdot ([[\dot{Q}]]^P \Psi_P). \tag{3.21}$$

Equation (3.21) is the same as Eq. 13.2-11 of Bird *et al.* that was derived in a mean field approximation starting directly from a reduced singlet configurational distribution function.

In order to obtain a more useful form of Eq. (3.21), it is necessary to know the rate-of-change of the center of mass location and the internal configuration of the polymer, *i.e.*, to derive expressions for the momentum space averages $[[\dot{r}]]^P$ and $[[\dot{Q}]]^P$. This is accomplished by realizing that the total forces F govern the motion of the center of mass. Similarly, the relative forces $\mathcal{F}$ determine the evolution of the internal configuration.

Multiplying Eq. (3.20) by p and averaging over all momenta yields the equation of motion for the center-of-mass vector r as

$$m^P \left[\frac{\partial}{\partial t} (v \Psi_P) + \nabla \cdot (v v \Psi_P) \right] + \frac{\partial}{\partial t} ([[p - m^P v]]^P \Psi_P) + \nabla \cdot (v [[p - m^P v]]^P \Psi_P)$$
$$+ \nabla \cdot ([[p - m^P v]]^P v \Psi_P) = (\bar{N} F^{(h)p} + F^{(b)p}) \Psi_P. \tag{3.22}$$

Neglecting the acceleration terms in the square-bracket on the left corresponds to neglecting the inertia of the beads and it is shown to be a reasonable assumption as explained in Section 3.5. All other terms on the left involve the momentum space averages $[[p - m^P v]]^P$. These terms are identically zero if one makes the assumption of equilibration in momentum space, since at equilibrium f_p is an even function of p. Thus, the total force balance is written as

$$\bar{N} F^{(h)p} + F^{(b)p} = 0 \tag{3.23}$$

where the superscripts (h) and (b) refer to hydrodynamic and Brownian forces, re-

spectively. For a dilute polymer solution, $\bar{N} \simeq 1$. The total force on a molecule is related to the force on an individual bead by

$$F^{(\cdots)p} = \sum_\nu F_\nu^{(\cdots)p} \tag{3.24}$$

where the superscript $(\ldots)$ refers to either of the above forces.

Similarly, multiplying Eq. (3.20) by P and integrating over momenta gives the equation of motion for the internal coordinates of the molecule. Neglecting acceleration terms gives a relative force balance

$$\mathcal{F}^{(h)p} + \mathcal{F}^{(b)p} + \mathcal{F}^{(\phi)p} = 0 \tag{3.25}$$

in which the superscripts (h), (b) and (ϕ) refer to the relative hydrodynamic, Brownian and intramolecular forces, respectively. The relative force between the beads of the dumbbell is related to the force on an individual bead by

$$\mathcal{F}^{(\cdots)p} = \frac{1}{2} \sum_\nu (-1)^\nu F_\nu^{(\cdots)p} \tag{3.26}$$

The expressions for the different total and relative forces that are obtained from the equations of motion for the center of-mass and internal coordinates are simplified further below. The simplifications used also have been discussed in Sections 18.2 and 18.3 of Bird *et al.* (1987b).

1. *Hydrodynamic Drag Force.* The drag experienced by each bead as it moves through the solution is approximated by a generalized Stokes' relation

$$F_\nu^{(h)p} = -\zeta \cdot ([[\dot{r}_\nu]]^p - v_\nu) \tag{3.27}$$

where v_ν is the solution velocity at the position of bead ν and is related to the velocity at the center of mass by

$$v_\nu = v(r) + (-1)^\nu \frac{Q}{2} \cdot \frac{\partial}{\partial r} v(r). \tag{3.28}$$

76

Equation (3.28) is obtained by expanding the velocity field v_ν in a Taylor series about the center-of-mass location r. Note that in this development the gradient-of-velocity tensor $\kappa \equiv \nabla v^\dagger$ is taken to be spatially-dependent, unlike the homogeneous theories where κ is taken to be a constant; see Section 2.3.3. Perturbations of the velocity field due to hydrodynamic interaction are not considered.

In this development, the friction tensor ζ is assumed to be isotropic, i.e., $\zeta = \zeta \delta$ where ζ is a scalar drag coefficient and δ is the unit tensor. Generalizations of the friction tensor that account for anisotropic effects of extended molecules could also be used. In the case of homogeneous theories, anisotropic drag results in the Giesekus model (Giesekus, 1982; Bird et al., 1987a & 1987b). The incorporation such anisotropies into the friction tensor could be important in studying the molecular dynamics close to solid walls. Monte Carlo simulations by Mansfield and Theodorou (1989) indicate that such anisotropies in the diffusive motion of chains are inherent near a solid surface.

Expressions for the total and relative hydrodynamic forces are obtained from Eq. (3.27) by using Eqs. (3.24) and (3.26) as

$$F^{(h)p} = -2\zeta([[\dot{r}]]^p - v) \tag{3.29}$$

and

$$\mathcal{F}^{(h)p} = -\frac{1}{2}\zeta([[\dot{Q}]]^p - \kappa \cdot Q). \tag{3.30}$$

2. *Brownian Force.* An assumption of *equilibration in momentum space* is made in order to approximate the total and relative Brownian forces on each polymer molecule, i.e., the velocity distribution is taken to be *Maxwellian*. Then, the total Brownian force on the center of mass of the polymer molecule is (Bird et al., 1987b)

$$F^{(b)p} = -kT\frac{\partial \ln \Psi_p}{\partial r} \tag{3.31}$$

and the relative Brownian force between the two beads of the dumbbell is

$$\mathcal{F}^{(b)p} = -kT\frac{\partial \ln \Psi_p}{\partial Q}. \tag{3.32}$$

3. *Intramolecular Force.* The spring in the Hookean dumbbell is modelled by an intramolecular potential $\phi^p(Q) = \frac{1}{2}HQ^2$. Thus, the relative intramolecular force is

$$\mathcal{F}^{(\phi)p} = -\frac{\partial}{\partial Q}\phi^p = -HQ. \tag{3.33}$$

Substituting expressions (3.29) - (3.33) for the total and relative forces into Eqs. (3.23) and (3.25) gives relations for $[[\dot{r}]]^p$ and $[[\dot{Q}]]^p$ as

$$[[\dot{r}]]^p = v(r) - \frac{kT}{2\zeta}\frac{\partial \ln \Psi_p}{\partial r} \tag{3.34}$$

and

$$[[\dot{Q}]]^p = Q \cdot \frac{\partial v}{\partial r} - \frac{2kT}{\zeta}\frac{\partial \ln \Psi_p}{\partial Q} - \frac{2H}{\zeta}Q. \tag{3.35}$$

Then combining Eqs. (3.21), (3.34) and (3.35) gives the diffusion equation for a non-homogeneous, dilute solution of Hookean dumbbells as

$$\begin{aligned}
\frac{\partial \Psi_p}{\partial t} = \ & -\frac{\partial}{\partial r} \cdot \left[\left(v(r) - \frac{kT}{2\zeta}\frac{\partial \ln \Psi_p}{\partial r} \right) \Psi_p \right] \\
& -\frac{\partial}{\partial Q} \cdot \left[\left(Q \cdot \frac{\partial v}{\partial r} - \frac{2kT}{\zeta}\frac{\partial \ln \Psi_p}{\partial Q} - \frac{2H}{\zeta}Q \right) \Psi_p \right].
\end{aligned} \tag{3.36}$$

3.3.2.3 The Mass Flux Vector and the Stress Tensor

The expression for the mass flux vector (3.11) is simplified further by using Eqs. (3.34) and (3.35) to yield

$$j_p = -\frac{kT}{\zeta}\nabla \rho_p - \frac{m}{2}\nabla \cdot \{QQ\} \cdot \nabla v + \frac{mH}{\zeta}\nabla \cdot \{QQ\}. \tag{3.37}$$

78

Here, the new symbol { } refers to an integral over all momentum and internal coordinates and is defined for a dynamical variable $B(r, Q)$ as

$$\{B\} \equiv \int B\Psi_p(r, Q, t)dQ. \tag{3.38}$$

Note that B is a function of r and Q alone and that $\{B\}$ is a function of r and t only. We call the quantity $\{QQ\}$ the *structure tensor* as it describes the probable shape of the polymer in solution.

The expression for the stress tensor (3.18) is also simplified further. The relative force balance (3.25) along with Eq. (3.26) is used to rewrite Eq. (3.18) in terms of Brownian and intramolecular forces. Then, substituting for the different forces, separating the polymer and solvent contribution and using Eqs. (3.34) and (3.35) yields the following expression for the stress tensor

$$\pi = \pi_s - H\{QQ\} + 2nkT\delta \tag{3.39}$$

where π_s is the solvent contribution to the total stress tensor and the remainder of the right side of Eq. (3.39) is the polymer contribution π_p.

Equation (3.39) is written in terms of the deviatoric stress τ by subtracting the corresponding equation at equilibrium, in the absence of any confining walls. By using an explicit expression for the Newtonian solvent contribution, we obtain the *Kramers form* of the stress tensor

$$\tau = \tau_s + \tau_p \tag{3.40}$$

where the solvent contribution to the stress is

$$\tau_s = -\eta_s \dot{\gamma} \tag{3.41}$$

and the polymeric contribution to the stress is given by

$$\tau_p = -H\{QQ\} + nkT\delta. \tag{3.42}$$

In Eq. (3.41), $\dot{\gamma} \equiv \nabla v + \nabla v^\dagger$ is the rate-of-strain tensor. The earliest derivation of Eq. (3.42) for the stress was given by Kramers (1944) using elementary physical arguments and includes contributions to the state of stress from the different forces identified in the previous subsection. Equations (3.40), (3.41) and (3.42) differ slightly from the Kramers equation given in Table 13.3-1 of Bird *et al.* (1987b) in that the configurational distribution function has not been factored here.

3.3.2.4 Equations for the Mass Flux and Stress

In the previous subsection, the mass flux vector and the stress tensor have been expressed in terms of the structure tensor $\{QQ\}$. A governing equation for $\{QQ\}$ is obtained from the diffusion equation (3.36) by taking the second moment with respect to Q. This operation yields

$$\begin{aligned}
\frac{\partial\{QQ\}}{\partial t} &= -v \cdot \nabla\{QQ\} + (\nabla v)^\dagger \cdot \{QQ\} + \{QQ\} \cdot \nabla v \\
&+ \frac{kT}{2\zeta}\nabla^2\{QQ\} + \frac{4nkT}{\zeta}\delta - \frac{4H}{\zeta}\{QQ\}.
\end{aligned} \tag{3.43}$$

We identify the contravariant convected derivative of $\{QQ\}$ (see Section 2.2, Eq. (2.25)) as

$$\{QQ\}_{(1)} = \frac{\partial\{QQ\}}{\partial t} + v \cdot \nabla\{QQ\} - ((\nabla v)^\dagger \cdot \{QQ\} + \{QQ\} \cdot \nabla v). \tag{3.44}$$

Combining Eqs. (3.43) and (3.44) gives

$$\{QQ\}_{(1)} = \frac{kT}{2\zeta}\nabla^2\{QQ\} + \frac{4nkT}{\zeta}\delta - \frac{4H}{\zeta}\{QQ\}. \tag{3.45}$$

Equation (3.45) governs the structure tensor $\{QQ\}$ and describes the evolution of the average orientation and extension of the dumbbells with the flow field. Equations

(3.37), (3.40), (3.41), (3.42) and (3.45), in conjunction with the species conservation equation (3.10) and the equation of motion (3.13), form a complete set of equations required to solve a general fluid mechanics problem.

Note that the equation for the structure tensor developed for a Hookean dumbbell model is a rare example that does not require a *closure approximation* in order to obtain a closed set of equations; see Sections 2.3 and 5.4. For Hookean dumbbells, it is possible to eliminate the structure tensor in terms of the polymeric contribution to the stress tensor given by Eq. (3.42). Thus, substituting Eq. (3.42) into Eq. (3.37) yields

$$
\begin{aligned}
\boldsymbol{j}_p = {}& -D_{tr}\boldsymbol{\nabla}\rho_p + \frac{4mD_{tr}\lambda_H}{kT}\boldsymbol{\nabla}\cdot(\boldsymbol{\tau}_p\cdot\boldsymbol{\nabla}\boldsymbol{v}) - 2D_{tr}\lambda_H\boldsymbol{\nabla}\cdot(\rho_p\boldsymbol{\nabla}\boldsymbol{v}) \\
& -\frac{2mD_{tr}}{kT}\boldsymbol{\nabla}\cdot\boldsymbol{\tau}_p
\end{aligned}
\tag{3.46}
$$

where $\lambda_H = \zeta/4H$ is the relaxation time constant of the dumbbells and $D_{tr} = kT/2\zeta$ is the translational diffusivity of the dumbbells in solution, as given by the Nernst-Einstein equation in the absence of hydrodynamic interaction (*cf.* Eq. 18.4-31 of Bird *et al.*). The different contributions to the mass flux vector can be identified as

$$
\boldsymbol{j}_p \equiv \boldsymbol{j}_{\text{diff},p} + \boldsymbol{j}_{\text{vel},p} + \boldsymbol{j}_{\text{stress},p}
\tag{3.47}
$$

where

$$
\boldsymbol{j}_{\text{diff},p} \equiv -D_{tr}\boldsymbol{\nabla}\rho_p,
\tag{3.48}
$$

$$
\boldsymbol{j}_{\text{vel},p} \equiv \frac{4mD_{tr}\lambda_H}{kT}\boldsymbol{\nabla}\cdot(\boldsymbol{\tau}_p\cdot\boldsymbol{\nabla}\boldsymbol{v}) - 2D_{tr}\lambda_H\boldsymbol{\nabla}\cdot(\rho_p\boldsymbol{\nabla}\boldsymbol{v}),
\tag{3.49}
$$

$$
\boldsymbol{j}_{\text{stress},p} \equiv -\frac{2mD_{tr}}{kT}\boldsymbol{\nabla}\cdot\boldsymbol{\tau}_p.
\tag{3.50}
$$

The first contribution to the total flux is the standard diffusive flux. The forms of the two new contributions (3.49) and (3.50) have only been speculated on in previous work (Tirrell and Malone, 1977; Aubert and Tirrell, 1980; Aubert *et al.*, 1980). Nonhomogeneous velocity gradients lead to a flux of macromolecules defined as $\boldsymbol{j}_{\text{vel},p}$.

In rectilinear flows, the velocity is given by a single Cartesian component and all gradients are in directions orthogonal to the direction of velocity. By examining Eq. (3.49), the contraction of the tensors is such that $\nabla \cdot j_{vel,p}$ is identically zero in such rectilinear flows, and hence this flux contribution has no effect on migration. Macromolecular migration can result only from $j_{stress,p}$ in such flows. However, in curvilinear flows, the velocity must be described by at least two Cartesian components, with gradients in the same direction. Hence, $\nabla \cdot j_{vel,p}$ can be nonzero, and thus contribute to macromolecular migration. This conclusion is supported by the work of Aubert and Tirrell (1980) and Sekhon et al. (1982). Stress gradients also provide a driving force for molecular migration, and the corresponding flux is represented by $j_{stress,p}$. Coincidentally, the phenomenological theory of Helfand and Frederickson (1989) that was proposed to explain enhanced concentration fluctuations in shear flow assumes an identical expression for $j_{stress,p}$.

Similarly, rewriting Eq. (3.45) in terms of the polymer contribution to the stress tensor gives

$$\tau_p + \lambda_H \tau_{p(1)} - D_{tr}\lambda_H \nabla^2 \tau_p - kT\lambda_H [\frac{Dn}{Dt} - D_{tr}\nabla^2 n]\delta = -nkT\lambda_H \dot{\gamma}. \qquad (3.51)$$

Equations (3.46) and (3.51) are the constitutive equations for the mass flux vector and the polymeric contribution to the stress tensor in a dilute, nonhomogeneous, polymer solution. These equations constitute the main result of this chapter. Note that the Eqs. (3.46) and (3.51) are coupled: the mass density distribution depends on the gradients of stress, and the stress is a function of the local density and its spatial derivatives. In the limit $D_{tr} = 0$, the constitutive equation reduces to the Oldroyd-B model, i.e., $Dn/Dt = 0$ or $n = $ constant and $\tau_p + \lambda_H \tau_{p(1)} = -nkT\lambda_H\dot{\gamma}$.

For the solution of fluid mechanics problems, it is more convenient to write the species conservation equation (3.10) in terms of the number density n, as

$$\frac{Dn}{Dt} = D_{tr}\nabla^2 n - 2\frac{D_{tr}\lambda_H}{kT}\nabla\nabla:(\tau_p \cdot \nabla v) + 2D_{tr}\lambda_H\nabla\nabla:(n\nabla v) + \frac{D_{tr}}{kT}\nabla\nabla:\tau_p. \qquad (3.52)$$

Combining Eqs. (3.51) and (3.52) gives the following useful form for the constitutive

equation

$$\tau_p + \lambda_H \tau_{p(1)} - D_{tr}\lambda_H \nabla^2 \tau_p + 2D_{tr}\lambda_H^2 \nabla\nabla : (\tau_p \cdot \nabla v)\delta$$

$$-2D_{tr}\lambda_H^2 kT\nabla\nabla : (n\nabla v)\delta - D_{tr}\lambda_H \nabla\nabla : \tau_p\delta = -nkT\lambda_H\dot{\gamma}. \qquad (3.53)$$

Equations (3.40), (3.41), (3.52) and (3.53) together with the equation of motion complete the set of equations required to solve a general fluid mechanical problem, and their use is illustrated in Section 3.4.

3.3.3 Comparison with the Oldroyd-B Model

The consideration of nonhomogeneities results in significant changes in the constitutive equation for stress in a homogeneous, dilute solution of Hookean dumbbells. To appreciate these differences the constitutive equation is written in dimensionless form with characteristic scales that are appropriate to the macroscopic flow. Dimensionless position $\bar{r} = r/L$, time $\bar{t} = t/\frac{L}{V}$, velocity $\bar{v} = v/V$, and stress $\bar{\tau} = \tau/n_{av}kT\lambda_H\frac{V}{L}$ are scaled with characteristic length L, velocity V and a viscous stress due to the polymer. The viscous stress in the last scaling involves the average polymer contribution to the viscosity $\eta_{p,av} = n_{av}kT\lambda_H$, which is given in terms of the average number density n_{av}. The number density n is also scaled with the average number density as $\bar{n} = n/n_{av}$, where

$$n_{av} \equiv \frac{1}{\mathcal{V}}\int_\mathcal{V} n d\mathcal{V}. \qquad (3.54)$$

Since no chemical reactions are considered, the average number density $n_a v$ is a constant.

All subsequent equations are written in terms of dimensionless variables, and the overbars are omitted for convenience. In terms of these dimensionless variables, Eqs. (3.52) and (3.53) are

$$\frac{Dn}{Dt} = \frac{1}{Pe}\nabla^2 n - 2\frac{De^2}{Pe}\nabla\nabla : (\tau_p \cdot \nabla v) + 2\frac{De}{Pe}\nabla\nabla : (n\nabla v) + \frac{De}{Pe}\nabla\nabla : \tau_p \qquad (3.55)$$

83

and

$$\tau_p + \mathrm{De}\tau_{p(1)} - \frac{\mathrm{De}}{\mathrm{Pe}}\nabla^2\tau_p + 2\frac{\mathrm{De}^2}{\mathrm{Pe}}\nabla\nabla : (\tau_p \cdot \nabla v)\delta$$

$$-2\frac{\mathrm{De}}{\mathrm{Pe}}\nabla\nabla : (n\nabla v)\delta - \frac{\mathrm{De}}{\mathrm{Pe}}(\nabla\nabla : \tau_p)\delta = -n\dot{\gamma}. \qquad (3.56)$$

The two dimensionless groups that appear in Eqs. (3.55) and (3.56) are the Deborah number $\mathrm{De} \equiv \lambda_H V/L$ and the Peclet number $\mathrm{Pe} \equiv LV/D_{tr}$. The Deborah number is the ratio of the fluid relaxation time to a characteristic time for the macroscopic flow and its relevance in viscoelastic fluid mechanics was discussed in Section 2.1; the Peclet number is the ratio of the convective to diffusive fluxes of the macromolecules.

The ratio $\mathrm{De}/\mathrm{Pe} = \lambda_H D_{tr}/L^2$ that appears in Eqs. (3.55) and (3.56) is particularly important in understanding nonhomogeneous effects and is interpreted as the ratio of a diffusive length scale to a length scale of the macroscopic flow. The diffusive length used here is that distance $(\lambda_H D_{tr})^{1/2}$ the polymer molecule diffuses in a relaxation time. Thus, a polymer molecule can retain its average internal configuration as it diffuses over this distance; and provided that the kinematics change over a similar length scale, stress diffusion will be observed. Consequently, the stresses in neighboring fluid elements with differing particle paths are no longer independent, and the fluid may be termed *nonsimple*. This contrasts *simple* fluid theories (Oldroyd, 1950 & 1984) where the stress in a fluid element is assumed independent of the rheological history of the neighboring fluid elements.

Typically, the ratio De/Pe is very small. Translational diffusivities D_{tr} for dilute solutions of polymers are approximately 10^{-7} cm^2/s, (*CRC Polymer Handbook*, 1975) and typical relaxation times for polymer solutions are reported to be $10^{-2} \leq \lambda \leq 1$ s (Bird *et al.*, 1987a). Thus, for a physical length scale of about 1 cm, the parameter De/Pe is in the range $10^{-7} - 10^{-9}$, and stress diffusion is not expected to be important except over length scales of $10^{-3} - 10^{-5}$ cm. As the length scale of the problem decreases, as is true for flow in narrow channels, the importance of stress diffusion increases.

The small parameter De/Pe multiplying the diffusive terms in the constitutive

equations leads to the formation of boundary layers that connect the bulk fluid region, where polymer migration is unimportant, to boundary regions where the polymer configuration, stress, and number density differ from their bulk values. Such layers are expected next to solid boundaries where the available molecular configurations are severely restricted because of steric interactions with the wall. This point is discussed further in Sections 3.3.4 and 3.4.2.

The presence of the diffusive terms has other important mathematical implications; these are most easily seen by considering the reduced model derived by El-Kareh and Leal (1989) which is obtained by incorporating the spatial dependence of the configurational distribution function and neglecting effects due to the spatial extension of the polymer molecule. Note that in order to be consistent with the development in this chapter, the FENE springs used by El-Kareh and Leal are replaced by a simple Hookean spring. With these assumptions, the governing structure tensor equation is the same as Eq. (3.45), but the expression for the number density is considerably simpler than Eq. (3.52). The resulting equations are

$$\frac{Dn}{Dt} = \frac{1}{\text{Pe}} \nabla^2 n \tag{3.57}$$

and

$$\tau_p + \text{De}\tau_{p(1)} - \frac{\text{De}}{\text{Pe}} \nabla^2 \tau_p = -n\dot{\gamma}. \tag{3.58}$$

For flows in systems with inert, solid boundaries, Eq. (3.57) predicts a uniform concentration $n = 1$. Thus, the only modification to the Oldroyd-B model is the stress diffusion term $\nabla^2 \tau_p$ in Eq. (3.58). This term has a profound effect on the mathematics of the constitutive equation. Foremost, it converts Eq. (3.58) from a hyperbolic equation with streamwise characteristics to a formally parabolic equation. Introducing stress diffusion removes the discontinuities in τ_p that are admissible in a hyperbolic constitutive equation. El-Kareh and Leal (1989) have demonstrated other important consequences of stress diffusion by proving the existence of smooth and bounded solutions to the creeping flow equation of motion for arbitrary values of De. This proof relies on bounds on the smoothness of τ_p that result because of the regularization of

the constitutive equation caused by stress diffusion. Another important consequence of the diffusive term in Eq. (3.58) is that specification of τ_p or normal derivatives of τ_p is required on *all* boundaries for all time. In contrast, the Oldroyd-B model (De/Pe $= 0$) requires data on only the normal components of τ_p at inflow boundaries (Renardy *et al.*, 1987). Setting the stress level on boundaries is aphysical. The general theory described here circumvents this difficulty by allowing the density to vary, so that setting polymer orientation does not set the stress.

3.3.4 Boundary Conditions

The polymer species conservation equation (3.55) and the stress constitutive equation (3.56) are both parabolic and require boundary conditions on all boundaries of the flow. The discussion here focuses on the boundary conditions at smooth, inert, solid walls that are oriented with unit normal δ_n and unit tangent vectors δ_{t_1} and δ_{t_2}. If the boundary is impenetrable, no material flux is allowed normal to its surface and

$$\delta_n \cdot j = 0 \qquad (3.59)$$

The average concentration n_{av} is set by adding the integral constraint (3.54) to the equation set.

Prescribing the polymer contribution to the stress field at the boundary requires knowledge of the distribution of molecular configurations there. A number of recent Monte Carlo simulations of equilibrium and nonequilibrium configuration distributions of polymer solutions and melts confined between parallel plates have focussed on this problem (Theodorou, 1988a & 1988b; Bitsanis and Hadziioanou, 1990; Yethiraj and Hall, 1990). These studies indicate that the presence of a solid impenetrable wall affects configurations of the polymer molecules in a narrow interfacial region next to the wall, of thickness comparable to the mean radius of gyration of the polymer molecules. Furthermore, the presence of a wall affects only those polymers that are close enough to have at least a part of their chain length within the interface. The portions of the polymer chain that are within the interfacial region are shown to be

aligned parallel to the wall, such that the radius of gyration in the direction parallel to the wall is greater than the radius of gyration perpendicular to the wall. These studies also indicate that in the case of dilute solutions, the presence of the wall causes a depletion of polymer in the interfacial region due to an entropic driving force that results from the constrained configurations of the polymer molecules next to the wall. The authors suggest that the local ordering of the macromolecules next to the wall leads to decreased entropy and molecules migrate into the bulk fluid where all configurations are possible. These interfacial depletion layers have been observed experimentally using the technique of Evanescent Wave-Induced Fluorescence (EWIF) both in static polymer solutions (Rondelez *et al.*, 1987) and in the presence of flow (Ausserre *et al.*, 1991). We attempt to incorporate some of the physics that is responsible for the formation of these depletion layers into the boundary conditions for stress.

The Hookean dumbbell model for macromolecules cannot reproduce all the complexity of the configurational restrictions on macromolecules near solid boundaries. In keeping with the simplicity of the molecular model, simplified boundary conditions that try to capture the essence of the distribution of configurations near a wall are employed. We simply require the dumbbells to be parallel to the wall as a boundary condition as shown in Fig. 3-3. This boundary condition is consistent with the Monte Carlo simulations of macromolecular configurations adjacent to a solid wall and states that *if* the dumbbell center-of-mass is on the wall, the dumbbell must be parallel to it. It would be reasonable to assume that, at equilibrium, molecules close to the wall are oriented *randomly* in a plane parallel to the wall. This distribution should show some dependence on the applied wall shear rate, and at high shear rates, the molecules should tend to align in the flow direction. However, to simplify the boundary condition, we assume that the molecules are always aligned in the direction of flow. As a further simplification, the length of each dumbbell adjacent to the wall is set to its equilibrium length. Thus, for a problem of rectilinear shear flow in the x-direction, the corresponding boundary condition on the macromolecules would be $Q = Q_o \delta_x$, where Q_o is the equilibrium dumbbell length. This is a reasonable as-
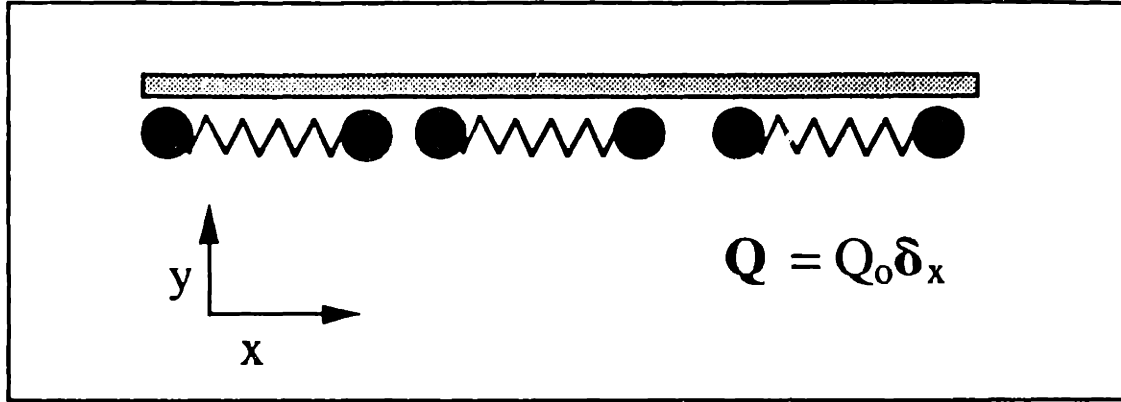
Figure 3-3: Macromolecular configuration at the wall.

sumption at equilibrium (Bitsanis and Hadziioanou, 1990), but does not account for possible stretching caused by the local flow.

By setting the macromolecular configuration at the wall, a boundary condition for the stress τ_p is specified using Eq. (3.42) as

$$\tau_{p,w} = -n_w H Q_o^2 \delta_x \delta_x + n_w kT \delta. \tag{3.60}$$

Note that the specification of stress at the wall $\tau_{p,w}$ also requires the specification of the polymer concentration at the wall n_w that is determined by solving the species conservation equation simultaneously with the stress constitutive relation. The numerical value of τ_p is thus determined from n_w as a part of the solution to any problem.

3.4 Rectilinear Shear Flow

3.4.1 Analysis

As an example of the use of equations (3.52) and (3.53) for species conservation and stress, a simple shear flow in which the boundaries are included is considered in this

section. Consider the rectilinear shear flow of a dilute polymer solution between parallel plates, $v_x = v_x(y), v_y = v_z = 0$. The bottom plate $y = 0$ is held stationary, and the upper plate $y = 1$ is moved with constant velocity 1. The characteristic length and velocity scales are chosen as the dimensional gap width L and the dimensional velocity of the upper plate V, respectively. The flow is assumed to be steady and one-dimensional. For this flow $\tau = \tau(y)$ and $n = n(y)$. Furthermore, the two transverse components of shear stress are zero, i.e., $\tau_{xz} = \tau_{yz} = 0$ because the flow does not vary in the z-direction. With these assumptions, the continuity equation is automatically satisfied, and the equation of motion yields

$$\frac{d\tau_{xy}}{dy} = 0 \tag{3.61}$$

$$\frac{d\tau_{yy}}{dy} + \frac{dp}{dy} = 0 \tag{3.62}$$

where p is the pressure. The conservation equation for the macromolecules is

$$\frac{d^2 n}{dy^2} + \mathrm{De}\frac{d^2 \tau_{yy}}{dy^2} = 0. \tag{3.63}$$

There are no contributions from the nonhomogeneous velocity gradient flux ($j_{\mathrm{vel},p}$) because the flow is rectilinear. The constitutive equation is written in component form as

$$\tau_{xx} - 2\mathrm{De}\left[\tau_{xy} + \frac{\eta_s}{\eta_{p,av}}\frac{dv_x}{dy}\right]\frac{dv_x}{dy} - \frac{\mathrm{De}}{\mathrm{Pe}}\frac{d^2 \tau_{xx}}{dy^2} - \frac{\mathrm{De}}{\mathrm{Pe}}\frac{d^2 \tau_{yy}}{dy^2} = 0 \tag{3.64}$$

$$\tau_{yy} - 2\frac{\mathrm{De}}{\mathrm{Pe}}\frac{d^2 \tau_{yy}}{dy^2} = 0 \tag{3.65}$$

$$\tau_{zz} - \frac{\mathrm{De}}{\mathrm{Pe}}\frac{d^2 \tau_{zz}}{dy^2} - \frac{\mathrm{De}}{\mathrm{Pe}}\frac{d^2 \tau_{yy}}{dy^2} = 0 \tag{3.66}$$

$$\tau_{xy} - \mathrm{De}\tau_{yy}\frac{dv_x}{dy} - \frac{\mathrm{De}}{\mathrm{Pe}}\frac{\eta_s}{\eta_{p,av}}\frac{d^2}{dy^2}\left[\frac{dv_x}{dy}\right] + \left[n + \frac{\eta_s}{\eta_{p,av}}\right]\frac{dv_x}{dy} = 0 \tag{3.67}$$

where Eq. (3.61) has been used to simplify Eq. (3.67). The highest derivative terms in the Eqs. (3.64)-(3.67) are all multiplied by the ratio De/Pe. Thus, in the limit De/Pe = 0, Eqs. (3.63)-(3.67) are singular. For typical values of De/Pe $\ll$ 1, the equations lead to the development of boundary layers. By using scaling arguments, it can be shown that the boundary layer thickness scales as $(De/Pe)^{1/2}$. In the limit De/Pe $\rightarrow$ 0, the thickness of the boundary layer becomes vanishingly small and the solution reduces to the result for the Oldroyd-B constitutive model at all points except at the wall.

The governing equations are solved by using the boundary conditions described in Section 3.3.4. The *no flux* boundary condition (3.59) reduces to

$$\frac{dn}{dy} + \text{De}\frac{d\tau_{yy}}{dy} = 0. \tag{3.68}$$

The stress at the solid boundaries is determined by specifying that the dumbbells are aligned parallel to the wall as

$$\boldsymbol{Q} = Q_o \boldsymbol{\delta}_x, \quad \text{at } y = 0 \text{ and } y = L \tag{3.69}$$

where $\boldsymbol{\delta}_x$ is the unit vector in the x-direction and Q_o is the equilibrium length of each dumbbell.

Using the polymeric contribution to the Kramers stress tensor (3.42) and Eq. (3.69) gives the polymer contribution to the deviatoric stress at the wall, in dimensional form, as

$$\tau_{p,w} = -n_w H Q_o^2 \boldsymbol{\delta}_x \boldsymbol{\delta}_x + n_w kT \boldsymbol{\delta} \tag{3.70}$$

where n_w is the polymer number density at the wall. Since n_w is determined as part of the solution, the stress at the wall is not set *a priori*, but is determined as part of the solution to the boundary-value problem. Adding the solvent contribution to the

stress and writing the components in dimensionless form gives

$$
\tau_w = \begin{pmatrix} \frac{n_w}{De}\left(1 - \frac{HQ_a^2}{kT}\right) & -\frac{\eta_s}{\eta_{p,av}}\left(\frac{\partial v_x}{\partial y}\right)_{wall} & 0 \\ -\frac{\eta_s}{\eta_{p,av}}\left(\frac{\partial v_x}{\partial y}\right)_{wall} & \frac{n_w}{De} & 0 \\ 0 & 0 & \frac{n_w}{De} \end{pmatrix}.
\tag{3.71}
$$

The velocity field is assumed to satisfy *no slip* boundary conditions.

The governing equations (3.61)-(3.67) and boundary conditions are solved numerically by using a centered finite difference scheme. The calculations were performed with a uniform grid of between 500 and 1000 points across the gap $0 \leq y \leq 1$. The development of steep boundary layers near the solid walls restricts calculations with these mesh sizes to values of De/Pe above 10^{-5}, which are realistic only in small geometries with a characteristic length scale of 0.1 mm or smaller.

3.4.2 Results

3.4.2.1 Equilibrium Solution

Before proceeding with a description of results in simple shear flow, it is worthwhile to examine the predictions of the nonhomogeneous constitutive theory developed in Section 3.3.2.4 in the absence of flow. In this no-flow situation, the characteristic scales that were introduced in Section 3.3.3 can no longer be used since there is no characteristic velocity in the system. A dimensionless form of the equations at equilibrium is obtained by setting the dimensionless stress as $\bar{\tau} \equiv \tau/n_{av}kT$. The characteristic scales for number density n and position r are unchanged. The overbars in the subsequent equations are dropped for convenience and all variables refer to the dimensionless quantities. Thus, at steady state, the species conservation equation reads

$$
\nabla^2 n + \nabla\nabla : \tau_p = 0
\tag{3.72}
$$

and the stress constitutive equation reads

$$
\tau_p - \frac{De}{Pe}\nabla^2 \tau_p - \frac{De}{Pe}\nabla\nabla : \tau_p \delta = 0
\tag{3.73}
$$

91

where $De/Pe \equiv D_{tr}\lambda_H/L^2$ and is independent of the upper-plate velocity V. The governing equations for n and τ_{yy} for the one-dimensional case are of particular interest and are coupled as

$$\frac{d^2n}{dy^2} + \frac{d^2\tau_{yy}}{dy^2} = 0$$

$$\tau_{yy} - 2\frac{De}{Pe}\frac{d^2\tau_{yy}}{dy^2} = 0 \qquad (3.74)$$

A solution to this coupled set of equations is obtained by using the no flux boundary condition at the wall

$$\frac{dn}{dy} + \frac{d\tau_{yy}}{dy} = 0 \qquad (3.75)$$

and by setting $\tau_{yy} = n_w$ at the solid wall. The latter condition is a consequence of imposing parallel orientation on the dumbbells that are adjacent to the wall. Note that the polymer concentration at the wall n_w is determined as part of the solution and hence this condition does not set the stress at the wall to any fixed value.

The resulting concentration profile is plotted in Fig. 3-4 for values of $De/Pe = 10^{-2}$, 10^{-3} and 10^{-4}. The formation of a polymer depleted layer is clearly seen. The thickness of this depletion layer scales as $De/Pe^{1/2} \equiv \sqrt{kT/8H}$ that is proportional to the radius of gyration of the dumbbells, $r_g \equiv \sqrt{3kT/H}$.

3.4.2.2 Solutions in Presence of Flow

Solution profiles for the normal stresses, velocity, and the number density are shown in Figs. 3-5-3-7, as computed for $De = 1$, $\eta_s/\eta_{p,av} = 0.0241$ and values of the Peclet number in the range $10^2 \leq Pe \leq 10^4$. The ratio $\eta_s/\eta_{p,av} = 0.0241$ is based on a solvent viscosity of 1 mPa·s, average number density of dumbbells equal to 10^{14} molecules/cm^3, temperature $T = 300$ K, and a relaxation time of 0.1 sec. These results illustrate the effect of changing the diffusivity of the polymer D_{tr} while holding all other parameters constant. The corresponding solutions for the Oldroyd-B model ($Pe \rightarrow \infty$) are also shown. The development of the boundary layers adjacent to the solid walls is clearly seen. The thickness of these layers shrinks with decreasing
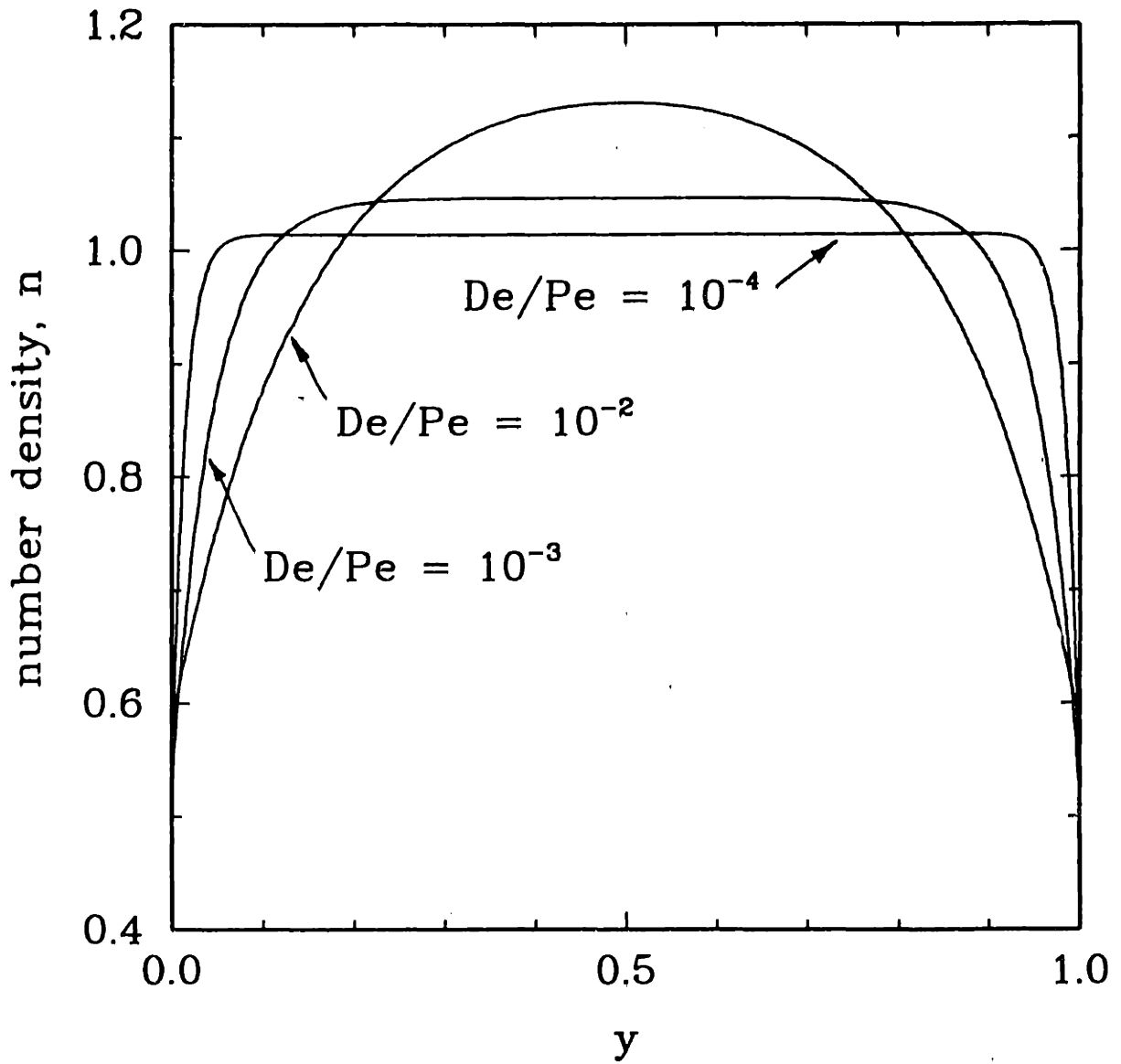
Figure 3-4: Concentration profile at equilibrium.
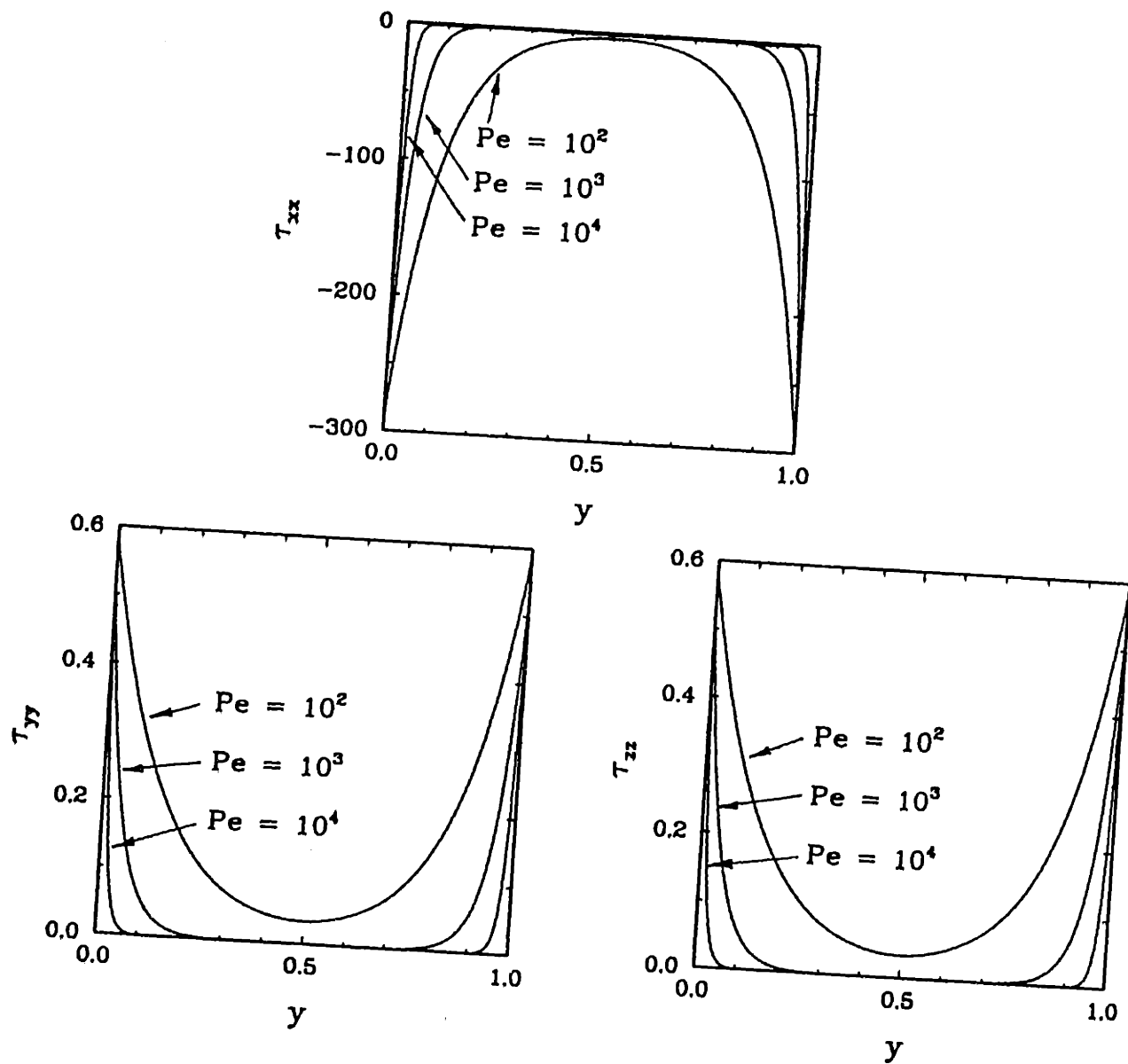
Figure 3-5: Normal stresses in rectilinear shear flow for $De = 1$ and $Pe = 10^2, 10^3$ and 10^4. In the high Peclet number limit, the values tend to the Oldroyd-B results of $\tau_{xx} = -2$, $\tau_{yy} = \tau_{zz} = 0$, though these are difficult to see with the scales used in the plots.
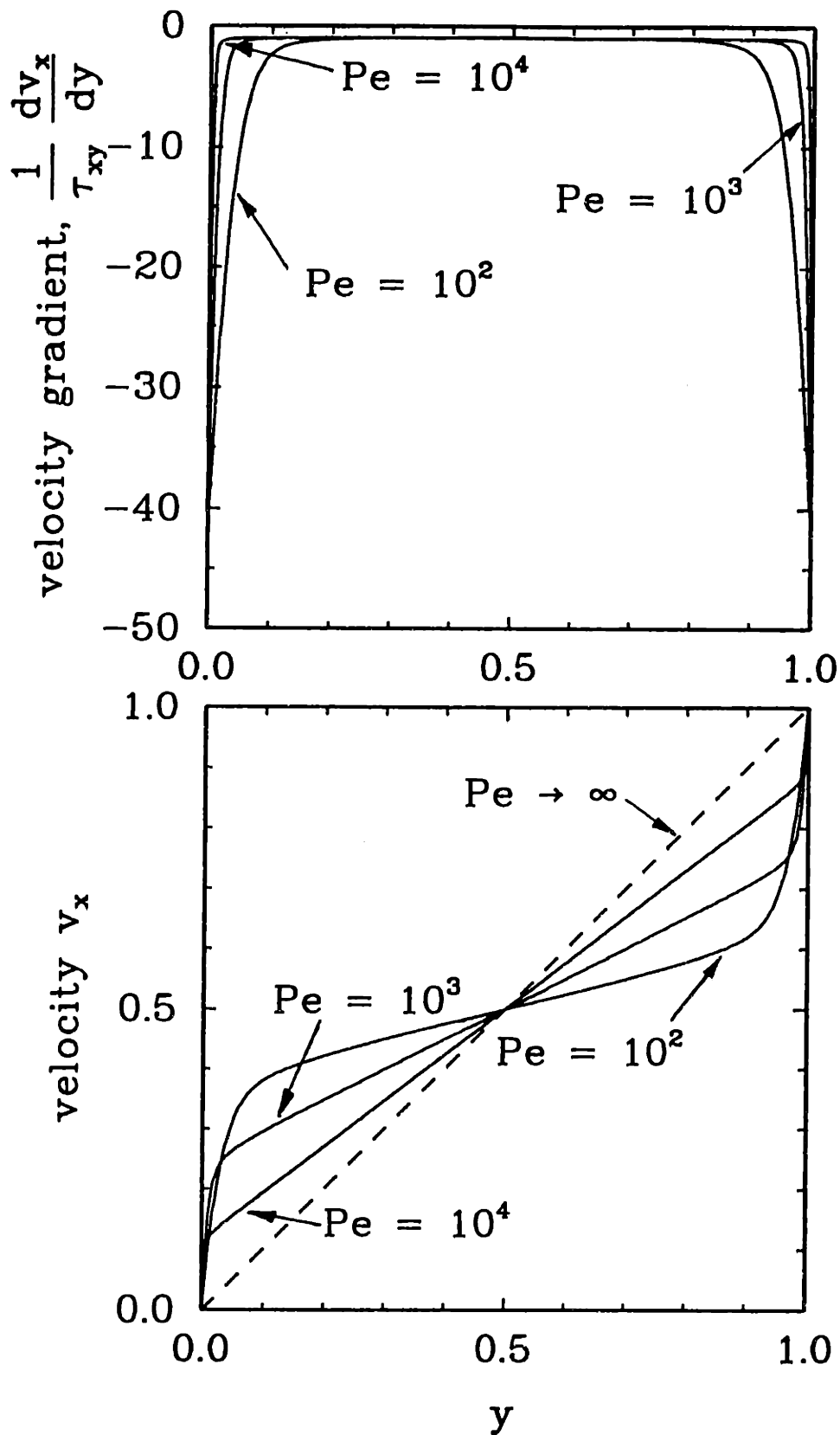
Figure 3-6: Velocity gradient and velocity in rectilinear shear flow for De $= 1$ and Pe $= 10^2, 10^3$ and 10^4. In the high Peclet number limit, the velocity gradient and velocity field tend to the results for the Oldroyd-B model.
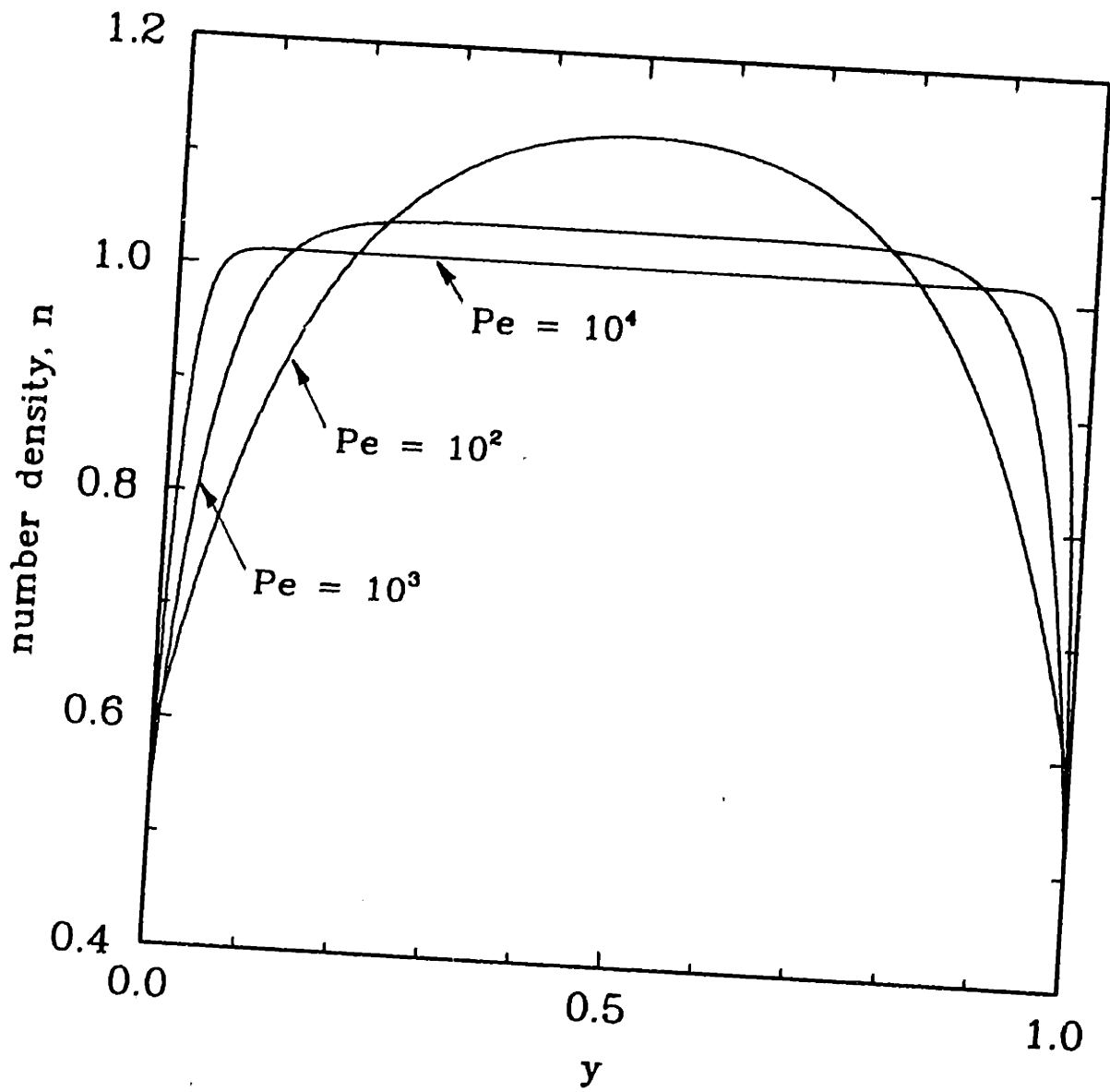
Figure 3-7: Concentration profile in rectilinear shear flow for De = 1 and Pe = $10^2, 10^3$ and 10^4. In the high Peclet number limit, the number density tends to the Oldroyd-B value of n=1.

De/Pe, and the profiles in the bulk flow tend to the results for the Oldroyd-B model with increasing Pe.

As seen in Fig. 3-6, the velocity gradient dv_x/dy is constant throughout the bulk flow, but increases rapidly near the wall. This increase is a consequence of modelling the beads as point masses and of constraining the orientation to be parallel to the wall. Under these assumptions, the dumbbells adjacent to the wall are invisible to the flow and do not contribute to the solution viscosity. Furthermore, the number density of the polymer is also smaller in the wall region than in the bulk. Thus, a low viscosity layer forms adjacent to the wall, and a higher velocity gradient is developed to maintain the constant shear stress.

The prediction of a low viscosity wall layer agrees with the concept of *apparent slip* of polymer solutions near boundaries (Cohen and Metzner, 1982, 1985 & 1986; Brunn, 1976). The development of an apparent slip velocity v_s is clearly seen in Fig. 3-6(b). The magnitude of v_s is computed by extrapolating the velocity profile in the bulk to the walls. A slip coefficient β is obtained from the *Navier slip law* as

$$(v_s \cdot \delta_t) = \beta(\tau : \delta_t \delta_n) \tag{3.76}$$

where $v_s = v_{\text{wall}} - v_{\text{fluid}}$, δ_n is the unit normal pointing into the fluid and δ_t is the unit tangent in the direction of flow. In the high Pe number limit, the slip coefficient scales as $(\text{De/Pe})^{1/2}$, as seen in Fig. 3-8. This implies $(v_s \cdot \delta_t) = \beta_o(\text{De/Pe})^{1/2}(\tau : \delta_t \delta_n)$.

The constant shear stress across the gap is tabulated in Table 3.2 for a range $100 \leq \text{Pe} < \infty$. At the highest value of Pe, τ_{xy} is still 20 percent below the value for the Oldroyd-B model (Pe $\rightarrow \infty$). This difference should decrease further with increasing Pe until at Pe $\sim O(10^7)$ the presence of the wall layer should have no effect on the measurement of viscosity. Note that the Oldroyd-B value must be attained if wall shear stress measurements are to reflect the bulk behavior of the liquid as is typically assumed in rheometry. Following the approach of Brunn (1976) to obtain an estimate
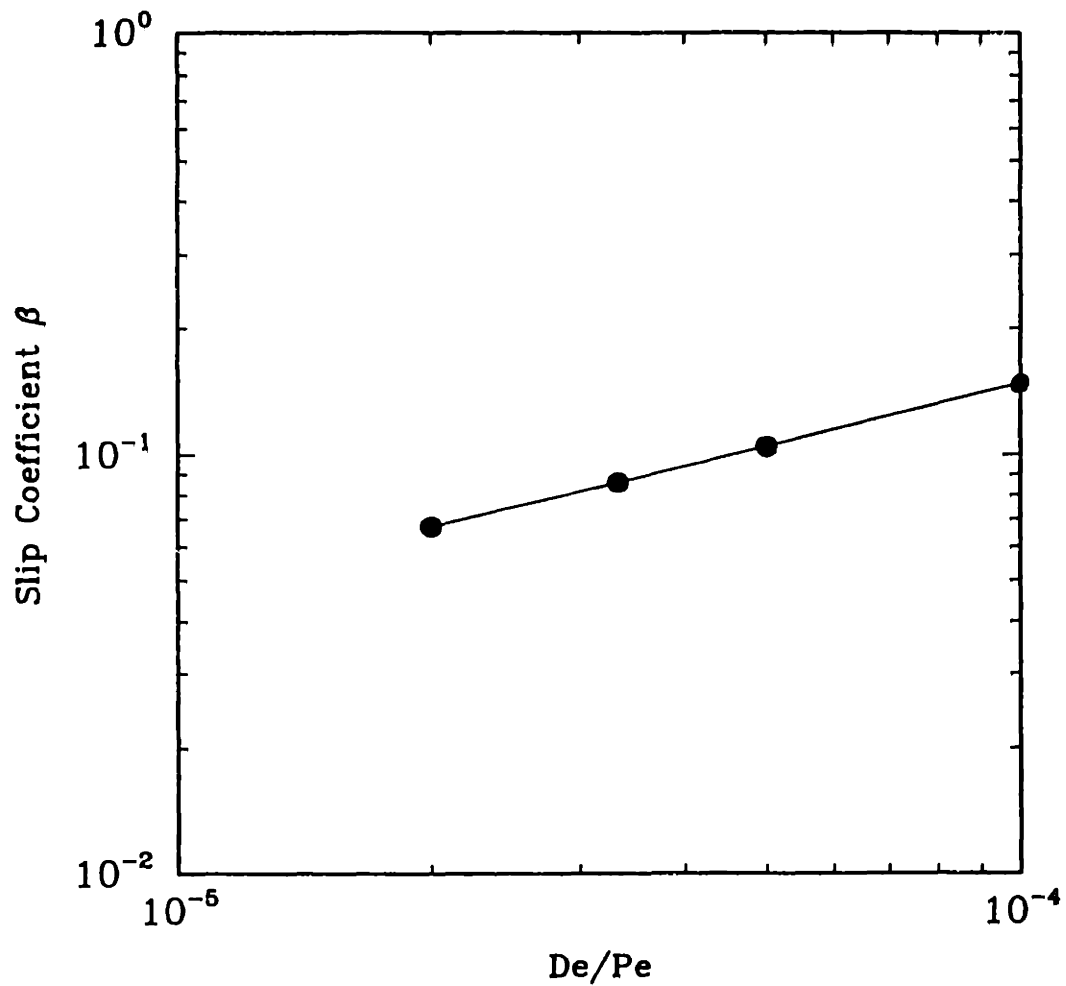
Figure 3-8: Slip coefficient β plotted as a function of De/Pe. The coefficient β is obtained from the Navier slip law (Eq. (3.76)) and the magnitude of v_s is obtained by extrapolating the velocity profile given in Fig. 3-6(b) in the bulk to the walls. The data approximately satisfy the relation $\beta \propto (\mathrm{De/Pe})^{1/2}$.

Pe	τ_{xy}
10^2	-0.2751
10^3	-0.5396
10^4	-0.7951
∞ (Oldroyd-B model)	-1.0241

Table 3.2: Shear stress in rectilinear shear flow for De = 1 and different Peclet numbers.

of error in the measured viscosity in terms of the slip velocity, we have

$$\eta_{measured} = \eta_{actual}(1 - 2|v_s|) \tag{3.77}$$

Thus, for a gap of 1 mm typically used in parallel-plate rheometers, for a fluid with a D_{tr} of 10^{-7} cm^2/sec and a λ_H of 0.1 sec, the error in measured viscosity is about 1.0 %.

The flux $j_{vel,p}$ vanishes for rectilinear flows and does not contribute to migration of polymer away from the wall. However, the imposition of constrained orientation near the wall sets up gradients of stress that provide the necessary driving force for migration. This cross-streamline migration leads to the development of a concentration gradient in which Fickian diffusion exactly balances stress-driven diffusion. The polymer migrates away from the wall region into the bulk and results in the formation of a polymer-depleted layer adjacent to the wall; see Fig. 3-7. The thickness of the depletion layer scales as $(De/Pe)^{1/2}$ and is directly proportional to the equilibrium length of the polymer molecule $3kT/H$.

The experimental observations of the depletion layer using Evanescent Wave-Induced Fluorescence (EWIF) by Rondelez et al. (1987) and Ausserre et al. (1991) offer an important point for comparison with the predictions of this model. The

EWIF optical technique was used by these authors to measure the overall thickness of the depletion layer in stiff xanthan solutions and monomer concentration profiles within the depletion layer. The variation of the angle of incidence θ of the laser beam ($\lambda_o = 488$ nm) allows the penetration of the evanescent wave to be tuned between ∞ and values as low as 70 nm. The polymer concentration profile close to the wall can thus be probed with great accuracy. The observations of Rondelez *et al* (1987) at equilibrium indicate that the depletion layer is on the order of the radius-of-gyration of the polymer molecule. This observation is in agreement with our predictions at equilibrium; see Section 3.4.2.1. In the presence of shear, however, Ausserre *et al.* (1991) report a thickening of the depletion layer with increase in bulk shear rate in dilute xanthan solutions. In this study, the flow in the visualization cell is imposed with suction from a motor-driven syringe. The local shear rate in the area of observation is taken to be constant and is calculated using a laminar flow model. The laminar flow model does not account for changes in shear rate near the wall due to molecular ordering and the shear rate values used by the authors are questionable. However, the difference between the depletion layer thickness in static solutions and in the presence of flow is significantly different and the overall conclusion of thickening of the depletion layer in the presence of flow is accurate.

We studied the effect of changing the bulk shear rate in two ways. First, the wall velocity V was changed while holding the gap width L constant. Since the ratio De/Pe is independent of the velocity scale V, these calculations were carried out at different values of De (De = 1, 10, 100), but at a constant De/Pe = 10^{-3}. The concentration profile was unchanged. Second, the gap width L was decreased while holding the wall velocity constant. The concentration profile was modified, as a consequence of changing the ratio De/Pe. The depletion layer appears thicker, because $(\text{De/Pe})^{1/2}$ increases with decreasing L. However, on an absolute length scale, the thickness of the depletion layer near the wall is virtually unchanged, as seen from Fig. 3-9 for the two gap widths L and $L/2$.

Thus, our results indicate that shear rate has no effect on the thickness of the concentration boundary layer. This should be clear from the governing equations also,
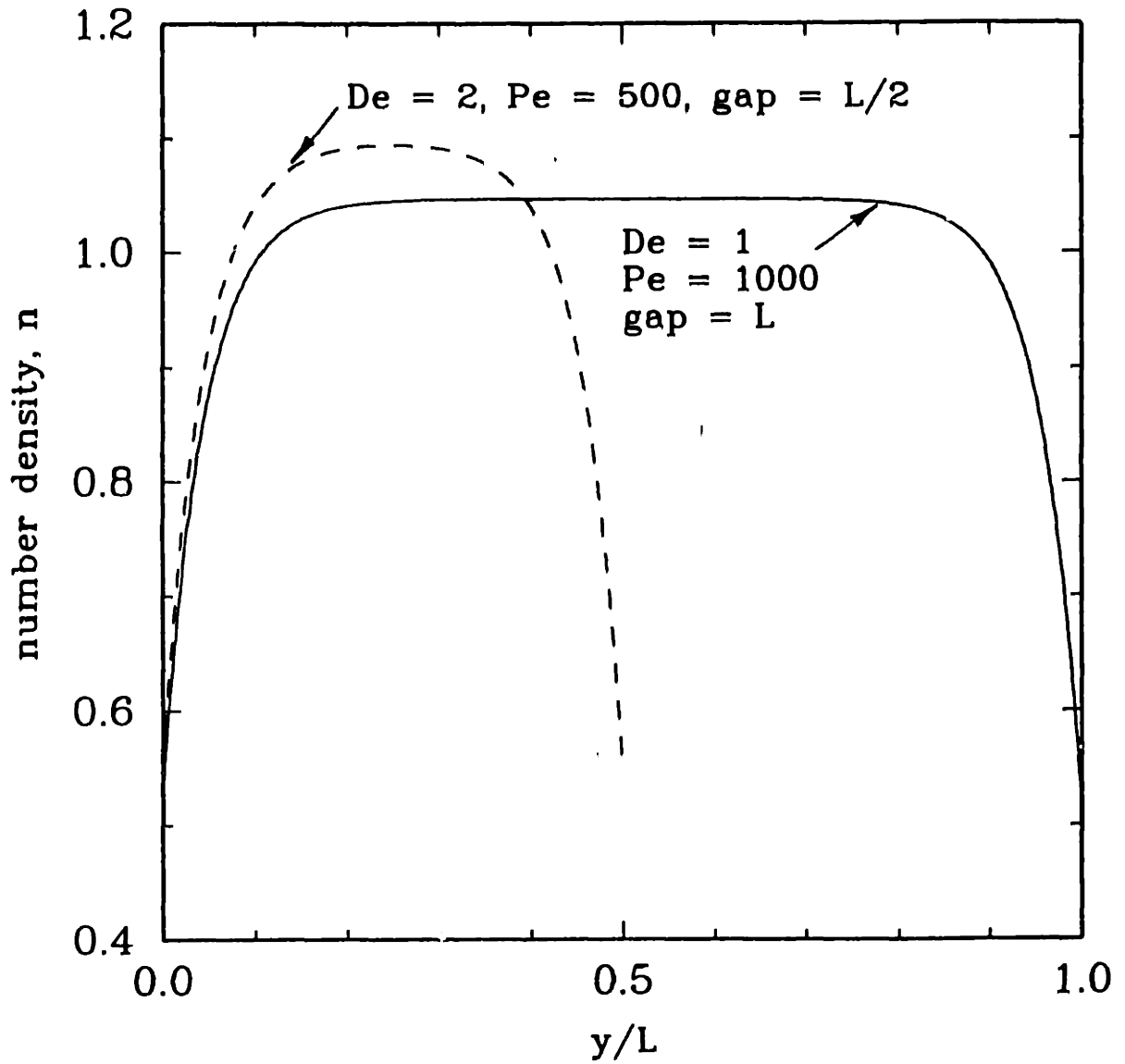
Figure 3-9: Calculations of effect of decreasing plate separation on concentration profile. Results for De=2 and Pe=500 correspond to a gap width half that for De=1 and Pe=1000.

since only n and τ_{yy} are coupled together, and neither depends on the dimensionless shear rate. This conclusion disagrees with the experimental data of Ausserre *et al.* (1991) which shows a thickening of the depletion layer with shear rate. It is interesting that a variation in the layer thickness with increasing shear rate will be predicted by our analysis only if the molecular orientation *at* the wall is allowed to change with shear rate. It may also be necessary to allow for coupling between the normal stress components τ_{yy} and τ_{xx} in the vicinity of the wall, that could result from only part of the polymer chain being flattened at the wall while the remainder penetrates into the bulk. Such a coupling cannot be incorporated using a simple dumbbell model; it is conceivable, though, that multibead models could allow this coupling.

There is some controversy surrounding the effect of local hydrodynamics on the thickness of the depletion layer in flexible and rod-like polymers. Duering and Rabin (1990) used dynamic Monte Carlo techniques to study dilute solutions of flexible polymer chains in the vicinity of a hard wall. The polymer was modelled as consisting of N monomer units, where the monomers were free to move subject to constraints on maximum distance between nearest neighbors and on minimum distance between any two monomer units. The constraints thus accounted for maximum extension of the "chain" of monomers and excluded volume interactions between parts of the chain. Their calculations indicate that for dilute solutions of flexible polymer chains, the thickness of the depletion layer *decreases* with increasing shear rate. Duering and Rabin (1990) attribute the discrepancy between their result and the experimental results of Ausserre *et al.* (1991) to the stiff rod-like nature of the xanthan polymers used in the experiments.

In order to resolve the controversy, de Pablo *et al.* (1992) studied the effect of shear on depletion layers in dilute solutions of rod-like polymers using a stochastic method to study the time evolution of the configurational distribution function. The polymer molecule was modelled using both the rigid dumbbell and the multibead-rod models. De Pablo *et al.* showed that the depletion layer thickness decreases at low shear rates and again increases at higher shear rates. It should be noted, though, that both Duering and Rabin (1990) and de Pablo *et al.* (1992) fail to account for the large

velocity gradients developed near the wall as a consequence of molecular ordering (see Fig. 3-6); in fact, both groups assume the velocity profile to be the same as in simple shear flow. It is difficult to assess the importance of the local velocity profile on the conclusions drawn by de Pablo *et al.* and by Duering and Rabin, without solving the entire equation set for stress, velocity and concentration in a self-consistent manner. The analysis in this section is the first attempt at such a description.

3.5 Incorporating Bead Inertia and External Forces

The nonhomogeneous development of Section 3.3 neglected the effects of bead inertia by dropping all the acceleration terms in the force balance. Furthermore, external forces were also neglected for the sake of simplicity. These omissions are remedied in the present section, and a consistent method of incorporating bead inertia is developed. The treatment here differs from that in Chapters 17 and 18 of Bird *et al.* (1987b) in that inertial effects are not considered by these authors. The differences are highlighted at suitable points in the discussion.

In order to incorporate effects of bead inertia, we follow the procedure used in deriving the generalized flux equations for point particles (Bird *et al.*, 1960; deGroot and Mazur, 1984). As discussed in Section 3.3.2, the equation of motion for the center-of-mass vector r is obtained by multiplying Eq. (3.20) by p and averaging over all momenta. After a little mathematical manipulation, this yields

$$m^p \left[\frac{\partial}{\partial t}(v\Psi_p) + \nabla \cdot (vv\Psi_p) \right] + \frac{\partial}{\partial t}(\, [[p - m^p v]]^p \Psi_p) + \nabla \cdot (v[[p - m^p v]]^p \Psi_p)$$
$$+ \nabla \cdot (\, [[p - m^p v]]^p v \Psi_p) = (\bar{N} F^{(h)p} + F^{(b)p} + F^{(e)p})\Psi_p. \qquad (3.78)$$

The term enclosed in the square brackets [ ] can be further simplified by using the equation of motion (3.13) and the evolution equation for Ψ_p (3.21) as

$$\frac{\partial}{\partial t}(v\Psi_p) \quad + \quad \nabla \cdot (vv\Psi_p) = \frac{\Psi_p}{\rho}(-\nabla \cdot \pi + n\bar{F}^{(e)})$$
$$- \left(\frac{1}{m^p}\nabla \cdot (\, [[p - m^p v]]^p \Psi_p) + \frac{\partial}{\partial Q} \cdot (\, [[\dot{Q}]]^p \Psi_p) \right) v. \qquad (3.79)$$

103

The terms on the left side of Eq. (3.78) are all acceleration terms and are now simplified by replacing them with the corresponding equilibrium values. Since f_p is an even function of $(p - m^p v)$ at equilibrium, all terms involving the momentum space average $[[p - m^p v]]^P$ are zero. Also, at equilibrium, $\nabla \cdot \pi = \nabla p$. Making these substitutions and combining Eqs. (3.78), (3.14) and (3.79) yields the total force balance as

$$\bar{N} F^{(h)p} + F^{(b)p} + \left(F^{(e)p} - \frac{m^p}{\rho} \sum_\alpha \int F^{(e)\alpha} \Psi_\alpha dQ \right)$$
$$+ \frac{m^p}{\rho} \nabla p + \frac{m^p}{\Psi_p} \frac{\partial}{\partial Q} \cdot ([[\dot{Q}]]^p \Psi_p) v = 0. \tag{3.80}$$

For a dilute solution $\bar{N} \simeq 1$, as in Section 3.3.2. In order to specify completely the force balance and hence to obtain an expression for $[[\dot{r}]]^p$, an expression for the rate of change of the internal configuration of the polymer , $i.e.$, $[[\dot{Q}]]^p$, is also needed.

An equation of motion for the internal coordinates is obtained by multiplying Eq. (3.20) by P and averaging over all momenta to yield

$$\frac{\partial}{\partial t}([[P]]^p \Psi_p) + \frac{1}{m^p} \nabla \cdot ([[pP]]^p \Psi_p) = (\mathcal{F}^{(h)p} + \mathcal{F}^{(b)p} + \mathcal{F}^{(\phi)p} + \mathcal{F}^{(e)p}) \Psi_p. \tag{3.81}$$

The acceleration terms are again replaced by the corresponding equilibrium value. Since f_p is an even function of P at equilibrium, all acceleration terms are identically zero and the relative force balance is simply given as

$$\mathcal{F}^{(h)p} + \mathcal{F}^{(b)p} + \mathcal{F}^{(\phi)p} + \mathcal{F}^{(e)p} = 0. \tag{3.82}$$

This expression is analogous to assuming that the acceleration of both beads is equal. The required expression for $[[\dot{Q}]]^p$ can be obtained from Eq. (3.82) analogous to the development in Section 3.3.2.2.

The hydrodynamic forces in Eqs. (3.80) and (3.82) are again approximated by a generalized Stokes' relation; see Eq. (3.27). The total and relative Brownian forces are given by Eqs. (3.31) and (3.32) after making the approximation of *equilibration in momentum space*. The equilibration in momentum space approximation has also

been used to simplify the acceleration terms in the force balance. This assumption has been questioned by Schieber and Öttinger (1988). However, as we show in this section, it has little effect on the overall predictions. The equation governing the center-of-mass motion of the dumbbell in the presence of external forces is then

$$
\begin{aligned}
[[\dot{r}]]^p &= v(r) - \frac{kT}{2\zeta}\frac{\partial \ln \Psi_p}{\partial r} + \frac{1}{2\zeta}\left(F^{(e)p} - \frac{m^p}{\rho}\sum_\alpha \int F^{(e)\alpha}\Psi_\alpha dQ\right) \\
&+ \frac{m^p}{2\zeta}\frac{1}{\rho}\nabla p + \frac{m^p}{2\zeta}\frac{1}{\Psi_p}\frac{\partial}{\partial Q}\cdot([[\dot{Q}]]^p\Psi_p)v.
\end{aligned}
\tag{3.83}
$$

The equation for the rate of change of the internal configuration of the dumbbell is found to be

$$
[[\dot{Q}]]^p = Q\cdot\frac{\partial v}{\partial r} - \frac{2kT}{\zeta}\frac{\partial \ln \Psi_p}{\partial Q} - \frac{2H}{\zeta}Q + \frac{1}{\zeta}[F_2^{(e)} - F_1^{(e)}].
\tag{3.84}
$$

If the external force on both the beads is identical, there is no net contribution of the external force to the equation of motion of the connector vector Q.

Following the same procedure as in Section 3.3.2, expressions for the mass flux vector and the stress tensor can be obtained. Thus, substituting Eqs. (3.83) and (3.84) into Eq. (3.11) gives the mass flux vector as

$$
\begin{aligned}
j_p &= -\frac{kT}{\zeta}\nabla\rho_p + \frac{\rho_p}{2\zeta}\left(F^{(e)p} - \frac{m^p}{\rho}\sum_\alpha \int F^{(e)\alpha}\Psi_\alpha dQ\right) + \frac{m}{\zeta}\frac{\rho_p}{\rho}\nabla p \\
&- \frac{m}{2}\nabla\cdot\{QQ\}\cdot\nabla v + \frac{mH}{\zeta}\nabla\cdot\{QQ\} - \frac{m}{2\zeta}\nabla\cdot\{Q[F_2^{(e)} - F_1^{(e)}]\}.
\end{aligned}
\tag{3.85}
$$

The first term on the right side of Eq. (3.85) is the usual concentration diffusion term, the second term corresponds to *forced diffusion*, and the third term is the *pressure diffusion* term. The forced diffusion and pressure diffusion terms result from a consistent treatment of bead inertia and are seen in the generalized mass flux expression for solutions of point particles; see Eq. 18.4-15 of Bird *et al.* (1960). If the only external force acting on the system is that due to gravity (*i.e.*, $\bar{F}^{(e)p} = m^p g$),

105

the forced diffusion term reduces to zero because

$$m^p g - \frac{m^p}{\rho} \sum m^\alpha n^\alpha g = 0 \quad \text{since} \sum m^\alpha n^\alpha = \rho. \qquad (3.86)$$

The treatment in Bird *et al.* (1987b) neglects the effects of bead inertia and the finite spatial extension of the dumbbell to give the expression for the mass flux vector as

$$\boldsymbol{j}_p = -D_{tr} \left(\boldsymbol{\nabla}\rho_p - \frac{\rho_p}{kT} \bar{\boldsymbol{F}}^{(e)p} \right). \qquad (3.87)$$

Effects of pressure diffusion, stress induced diffusion and diffusion due to nonhomogeneous velocity gradients are not accounted for by Eq. (3.87).

Both the flux expressions (3.85) and (3.87) suffer from a common drawback in that buoyancy effects are not taken into account. This is a consequence of treating the beads on the dumbbell as *point particles*, occupying no volume. This can be seen more clearly from Eq. (3.87). For instance, if the only external force is due to gravitational acceleration with $\bar{\boldsymbol{F}}^{(e)p} = m^p g$, where $m^p = 2m$, there is a constant gravitational pull acting on the polymer molecules causing polymer migration to the bottom of the container, a process that is termed *sedimentation*. Such migration of polymer molecules in a solution due to gravitational pull is never observed in reality.

The expression for the stress tensor can be obtained in a manner analogous to obtaining the mass flux vector. Using the relative force balance (3.82) along with Eq. (3.26) in Eq. (3.18), and subtracting the equilibrium contribution corresponding to $\kappa = 0$ and $\boldsymbol{F}_\nu^{(e)} = 0$ yields the expression for the stress as

$$\boldsymbol{\tau} = \boldsymbol{\tau}_s - H\{\boldsymbol{QQ}\} + nkT\boldsymbol{\delta} + \frac{1}{2}\{\boldsymbol{Q}[\boldsymbol{F}_2^{(e)} - \boldsymbol{F}_1^{(e)}]\}. \qquad (3.88)$$

Thus, if the same external force acts on both the beads, the expression for the stress tensor is the same as Eqs. (3.40)-(3.42). The diffusion equation for Ψ_p and the equation for the second moment $\{\boldsymbol{QQ}\}$ can be similarly obtained.

By making the assumption that $\boldsymbol{F}_2^{(e)} = \boldsymbol{F}_1^{(e)}$ as in the case of simple gravitational force, the expression for the stress tensor (3.42) is used to eliminate the structure

tensor, as in Section 3.2.2. Coupled equations are obtained for n and τ_p. Thus, the species conservation equation in terms of the number density is given as

$$
\begin{aligned}
\frac{Dn}{Dt} &= D_{tr}\nabla^2 n - \frac{D_{tr}}{kT}\nabla \cdot \left[n \left(F^{(e)p} - \frac{m^p}{\rho}\sum_\alpha F^{(e)\alpha}n^\alpha \right) \right] - \frac{D_{tr}}{kT}\nabla \cdot \left(\frac{\rho_p}{\rho}\nabla p \right) \\
&\quad - 2\frac{D_{tr}\lambda_H}{kT}\nabla\nabla : (\tau_p \cdot \nabla v) + 2D_{tr}\lambda_H \nabla\nabla : (n\nabla v) + \frac{D_{tr}}{kT}\nabla\nabla : \tau_p \quad (3.89)
\end{aligned}
$$

and the stress constitutive equation is

$$
\begin{aligned}
&\tau_p + \lambda_H \tau_{p(1)} - D_{tr}\lambda_H \nabla^2 \tau_p + 2D_{tr}\lambda_H^2 \nabla\nabla : (\tau_p \cdot \nabla v)\delta \\
&-2D_{tr}\lambda_H^2 kT\nabla\nabla : (n\nabla v)\delta - D_{tr}\lambda_H \nabla\nabla : \tau_p\delta \\
&+\frac{D_{tr}\lambda_H}{kT}\nabla \cdot \left[\left(F^{(e)p} - \frac{m^p}{\rho}\sum_\alpha F^{(e)\alpha}n^\alpha \right) \tau_p \right] + \frac{m}{\zeta}\frac{\lambda_H}{\rho}\nabla \cdot (\nabla p \tau_p) \\
&-\frac{m}{\zeta}\lambda_H v \cdot \nabla[(\nabla v)^\dagger \cdot \tau_p + \tau_p \cdot \nabla v - nkT\dot\gamma - \frac{1}{\lambda_H}\tau_p] \\
&= -nkT\lambda_H\dot\gamma. \quad (3.90)
\end{aligned}
$$

By comparing Eqs. (3.53) and (3.90) all the additional terms are seen to be scaled with the factor m/ζ with units of time. Thus, in addition to the relaxation time of the polymer molecule, we have an additional time constant which may also have to be considered. This additional time constant appears as a consequence of incorporating the acceleration terms in the equation of motion, and hence is referred to as $t_{inertial} \equiv m/\zeta$. For typical molecular weights of 10^5 gm/mol and $D_{tr} = 10^{-7}$, $t_{inertial} \sim 10^{-13}$ s (Fixman, 1965). Thus, the additional terms in the species conservation equation and the stress constitutive equation will have very little effect on the overall predictions in most applications.

Large inertial forces are seen in applications such as ultracentrifugation, where rotational speeds Ω of the ultracentrifuge are as high as 10^5 s^{-1} and the inertial terms introduced in this theory could be potentially important. The inertial constitutive theory was therefore used to study this application, with the external force on bead ν given as $F_\nu^{(e)} = m\Omega^2 r_\nu$. Note that the forces on the two beads are significantly different and Eqs. (3.89) and (3.90) must be modified to account for this factor.

Scaling analysis of the resultant equations showed that in the stress constitutive equation, only those terms corresponding to the Upper Convected Maxwell model are important. In the species conservation equation, under the assumption of rigid rotation, the Fickian and pressure diffusion terms balance, as in the case of models for point particles and no new effects are seen due to polymer extension. It is also worthwhile to examine the extension of the dumbbell in such high centrifugal fields. For rigid rotation, $\tau_p = 0$. Hence, from Eq. (3.88)

$$\{QQ\} = \frac{4nkT}{\zeta} \frac{1}{(\frac{1}{\lambda_H} - t_{inertial}\Omega^2)}\delta. \tag{3.91}$$

For typical values of $\lambda_H \sim 0.1 - 0.01$ s, $t_{inertial} \sim 10^{-13}$ s and $\Omega \sim 10^5$ s^{-1}, the inverse polymer relaxation time $1/\lambda_H$ is four to five orders of magnitude higher than $t_{inertial}\Omega^2$, and hence high rotational speeds do not result in large extension. Thus, neglecting bead inertia in the previous development is justifiable. Similar conclusions have also been drawn by Schieber and Öttinger (1988).

3.6 Summary and Discussion

A general framework for incorporating spatial nonhomogeneities into micromechanical-model-based constitutive theories for dilute polymer solutions has been developed by using a phase space kinetic theory. The behavior of polymer solutions in highly nonhomogene us flows is shown to be potentially influenced by molecular migration caused by concentration, stress, and velocity gradients. The constitutive theory presented here accounts for these effects by including spatial dependence of the configurational distribution function and finite extension of the macromolecules in the kinetic theory. The resulting constitutive equations describe a nonsimple viscoelastic fluid with a spatially nonhomogeneous composition field caused by macromolecular migration. The importance of this migration and its effect on stress scales with the ratio De/Pe $= \lambda_H D_{tr}/L^2$, which is interpreted as a ratio of the distance a polymer molecule can diffuse in one relaxation time to a physical length scale characteristic of

the macroscopic flow. Typically, the length scale for diffusion is small ($\mathcal{O}(100\mu m)$) and the importance of macromolecular migration is confined to very small-scale systems, such as narrow pores and channels, to thin boundary layers near solid walls, and to regions of very high stress gradients.

Solution of this model for a flow problem requires information about the polymer configuration near boundaries as is discussed in Section 3.2.3 for the case where the dumbbells are all aligned parallel to a wall and in the flow direction. Boundary layers in stress and concentration are predicted and scale as $(\text{De/Pe})^{1/2}$, independent of the flow velocity. This leads to the prediction of apparent fluid slip near the wall due to the decreased fluid viscosity in the boundary layer caused by molecular orientation. The apparent slip coefficient β computed from this theory scales as $(\text{De/Pe})^{1/2}$.

The presence of fluid slip may have a profound effect on polymer hydrodynamics. Renardy (1990) has studied the Upper Convected Maxwell model using a slight modification of the Navier slip law by assuming the slip velocity to be a function of the history of the shear stress at the wall. He shows that short wave instabilities that are confined to boundary regions occur and could provide a possible explanation for the melt fracture phenomenon. Fluid slip and macromolecular migration also may be necessary to develop a self-consistent theory for polymer fluid flow near corners such as in flow through an abrupt contraction where very large, mathematically infinite stress gradients are predicted. However the analysis presented here suggests slip associated with molecular migration and a depletion layer next to a solid wall will be unimportant in the measurement of rheological properties. For instance, for a gap of 1 mm and typical values of the translational diffusivity and relaxation time, the error in measured viscosity is only about 0.1-1 %.

Similar ideas on the importance of polymer diffusion in resolving problems of convergence at high De and in the presence of large stress gradients have motivated the development of the so-called "multiparticle constitutive equations" (Öttinger, 1991) within the body tensor formalism developed by Lodge (1974). By using this formalism, equations for the polymer mass density and stress tensor have been developed from a continuum mechanics point of view (Öttinger, 1992). These equations were

translated by Öttinger (1992) into the Cartesian space tensor formalism for the purpose of comparing them with the kinetic theory equations derived in Section 3.3.2.3. The equation for polymer number density is

$$\frac{Dr}{Dt} + \boldsymbol{\nabla} \cdot (\boldsymbol{b}n) - \boldsymbol{\nabla}\boldsymbol{\nabla}{:}(\boldsymbol{D}n) = 0 \qquad (3.92)$$

where $\boldsymbol{b}$ is the migration velocity and $\boldsymbol{D}$ is the diffusion tensor. The constitutive equation for the polymeric contribution to the stress tensor is

$$\boldsymbol{\tau}_p + \lambda_H \boldsymbol{\tau}_{p(1)} + \lambda_H \boldsymbol{\nabla} \cdot (\boldsymbol{b}\boldsymbol{\tau}_p) - \lambda_H \boldsymbol{\nabla}\boldsymbol{\nabla}{:}(\boldsymbol{D}\boldsymbol{\tau}_p) = -nkT\lambda_H \dot{\boldsymbol{\gamma}}. \qquad (3.93)$$

These equations have been written in the notation adopted in the kinetic theory development of this chapter for ease of comparison. Constitutive equations for the migration velocity and the diffusion tensor are required in order to obtain a closed set of equations. For Hookean dumbbell models without hydrodynamic interaction, Öttinger (1992) gives

$$\begin{aligned} \boldsymbol{b} &= 0 \\ \boldsymbol{D} &= D_{tr}(\boldsymbol{\delta} + \frac{\boldsymbol{\tau}_p}{nkT}) \end{aligned} \qquad (3.94)$$

Substituting these expressions for $\boldsymbol{b}$ and $\boldsymbol{D}$ into Eqs. (3.92) and (3.93) gives

$$\frac{Dn}{Dt} = D_{tr}\boldsymbol{\nabla}^2 n + \frac{D_{tr}}{kT}\boldsymbol{\nabla}\boldsymbol{\nabla}{:}\boldsymbol{\tau}_p \qquad (3.95)$$

and

$$\boldsymbol{\tau}_p + \lambda_H \boldsymbol{\tau}_{p(1)} - \lambda_H D_{tr}\boldsymbol{\nabla}^2\boldsymbol{\tau}_p - \frac{\lambda_H D_{tr}}{kT}\boldsymbol{\nabla}\boldsymbol{\nabla}{:}(\frac{1}{n}\boldsymbol{\tau}_p\boldsymbol{\tau}_p) = -nkT\lambda_H \dot{\boldsymbol{\gamma}}. \qquad (3.96)$$

On comparing Eq. (3.95) with Eq. (3.52), the terms corresponding to the flux due to the nonhomogeneous velocity gradients are missing from the continuum mechanics equation for number density. Moreover, suppose the translational diffusivity D_{tr} is

110

taken to be isotropic in Eqs. (3.92) and (3.93), the reduced model of El-Kareh and Leal (1989) that was discussed in Section 3.3.3 is obtained. It therefore appears that the stress diffusion terms in the continuum mechanics development of Öttinger (1992) is a consequence of treating the diffusivity to be anisotropic, rather than a consequence of finite spatial extent of the dumbbell as in the case of the kinetic theory development. The two treatments also differ in the contraction of the diffusivity tensor and hence the use of a anisotropic diffusivity in the kinetic theory development does not result in the equations derived by Öttinger (1992). Note also that the stress constitutive equation derived by Öttinger involves a nonlinear quadratic term in stress, the effect of which in the rectilinear shear flow problem has not been assessed.

Recently, another theory of nonhomogeneous systems has been developed (Mavrantzas and Beris, 1992a & 1992b). The theory uses a Helmholtz free energy approach and has been developed using the generalized Poisson bracket formulation of transport processes (Beris and Edwards, 1990). The transport equations that are obtained using this formulation are expressed in terms of the Hamiltonian H of the entire polymer solution. The equation for the stress tensor developed by Mavrantzas and Beris (1992a) is

$$\tau_{\alpha\beta} = 2C'_{\beta\gamma}\frac{\delta H}{\delta C_{\gamma\alpha}} + \eta_s \left[\frac{\partial u_\beta}{\partial r_\alpha} + \frac{\partial u_\alpha}{\partial r_\beta} \right] \tag{3.97}$$

where $C \equiv \{QQ\}$. The evolution equation for C is

$$\begin{aligned}
\frac{\partial C_{\alpha\beta}}{\partial t} &+ \nabla_\gamma(u_\gamma C_{\alpha\beta}) - C_{\gamma\beta}\nabla_\gamma u_\alpha - C_{\alpha\gamma}\nabla_\gamma u_\beta \\
&= -\Lambda_{\alpha\beta\gamma\epsilon}\frac{\delta H}{\delta C_{\gamma\epsilon}} + \nabla_\gamma \left[B_{\alpha\beta\gamma\epsilon\zeta\eta}\nabla_\eta \left(\frac{\delta H}{\delta C_{\epsilon\zeta}} \right) \right]
\end{aligned} \tag{3.98}$$

where the fourth order tensor Λ is inversely proportional to the polymer relaxation time λ and the sixth order tensor B governs the anisotropic diffusion of the structure tensor C. This latter term is missing from the kinetic theory development presented in this chapter and is responsible for predicting the onset of spinodal decomposition in binary polymer blends (Mavrantzas and Beris, 1992b). Finally, the species

conservation equation is

$$\frac{\partial n}{\partial t} = -\nabla_\alpha(u_\alpha n) + \nabla_\gamma(\sum_{k=1}^{2}(a_{1k}\nabla_\gamma\frac{\delta H}{\delta\rho_k}))$$ (3.99)

where the coefficients a_{1k} satisfy the condition $a_{11} + a_{12} = 0$ and $\delta H/\delta\rho_k$ is the generalized chemical potential. Expressions for the Hamiltonian H are obtained from nonequilibrium thermodynamics to give a closed set of equations. The expressions are modified in situations where the effect of a solid boundary is to be considered. In this situation, the loss of available conformations in the presence of a solid barrier and the corresponding reduction in entropy is calculated. A two-dimensional random walk problem is set up and the probability W of finding the chain end at a point (x, y) without ever having crossed the wall is first estimated by setting up a boundary value problem. An excess partition function Z and the loss of entropy ΔS that characterizes the chains in the interfacial region due to the excluded conformations are then calculated from W. The Hamiltonian of the polymer solution is modified to account for the conformational loss near the boundary. The final forms of the transport equations are then derived by substituting this expression for the Hamiltonian into Eqs. (3.97)-(3.99).

Concentration and velocity profiles in simple shear flow are estimated by solving these equations with boundary conditions. The results for the velocity profile agree with those shown in Fig. 3-6(b); calculations of apparent slip velocity also appear to validate the linear Navier slip law, in agreement with the results presented in Section 3.4.2. However, a significant difference is seen in the concentration profile. By excluding all polymer conformations adjacent to the wall in calculating the probability function W, Mavrantzas and Beris (1992a) predict $n = 0$ at the wall for all flow rates. However, the molecular model used in the development does not account for finite bead sizes, and as such should at least allow the configuration described in Section 3.3.4. Mavrantzas and Beris also report an increase in the polymer chain concentration at the wall relative to equilibrium with increase in shear rate, and an effective thinning of the depletion layer. This *disagrees* with the data of Ausserre *et*

al. (1991), but appears to be in agreement with the Brownian dynamics simulation of Duering and Rabin (1990); the discrepancy is assumed by Mavrantzas and Beris (1992a) to be a result of the rigid-rod-like xanthan solutions used in the experiments. Note, however, that the results of Duering and Rabin (1990) do not account for the local changes in the velocity field in the vicinity of the wall and hence are not a suitable basis for comparison.

The development that is presented in this chapter serves to illustrate that even with a simplistic model such as the Hookean dumbbell a number of different ideas and hypotheses such as polymer depletion and apparent slip relating to the nonhomogeneous problem can be resolved. Since the ideas presented in this development are general, a rigorous approach can again be used in extending the same theory to more realistic molecular models. It is also interesting to study the impact of such a nonhomogeneous theory in predicting the behavior of concentrated systems. Towards this end, the theory presented in this chapter is extended to concentrated systems of rigid rods that form liquid crystalline phases in Chapter 4. The governing equations derived in Chapter 4 that are applicable to concentrated systems can be easily reduced to dilute solutions of rigid rods by neglecting all terms involving intermolecular interactions by virtue of high concentration. The resultant equation can be expected to be slightly more complex than the ones presented in this chapter, due to the presence of a constraint in the molecular model. However, the significant conclusions of polymer depletion and apparent slip due to stress-induced molecular migration will be essentially the same.

Chapter 4

A Constitutive Equation for Nonhomogeneous Liquid Crystalline Polymer Solutions

4.1 Introduction

The microscopic structural order present in liquid-crystalline systems is responsible for some unique optical and mechanical properties. These properties have been exploited industrially over the last decade to produce specialty polymers that are used to make composites with ultra-high modulus and high chemical resistance, polymer dispersed films for light control applications, and for optical information processing and display devices (Ciferri, 1982). A common example is the aromatic polyamide fiber *Kevlar* that has the same tensile strength as steel with one-fifth the density. The development of *uniform* orientational order is key to exploiting the unique properties of these materials.

Developing a constitutive equation for liquid crystal polymers that provides an understanding of structure development and the formation of spatial nonhomogeneities in these systems with increasing concentration, together with an understanding of the effects of flow fields on the microstructure has posed a considerable challenge to kinetic theorists and rheologists. The nonhomogeneous kinetic theory for polymer

solutions presented in Chapter 3 provides a natural framework for developing such a constitutive equation. Concentrated systems of rigid-rod-like polymers that undergo a transition from a disordered phase to an ordered liquid crystalline phase or *mesophase* with increasing concentration are the subject of study in this chapter.

The liquid crystalline phase is intermediate between the ordinary fluid phase which has only short-range order and a solid crystalline phase which has perfect positional and orientational order in the absence of defects. It is generally observed in substances with rigid molecular structure, either rod-like or disk-like. Systems that form mesophases with increase in concentration are termed *lyotropic* systems, whereas systems that are transformed from an isotropic liquid state to a mesophase by simply decreasing temperature are called *thermotropic*. These mesophases are further classified depending on the kind of molecular ordering present, whether positional, orientational or both (Wissbrun, 1981). A mesophase with long-range orientational order and no positional order is termed *nematic*. In the nematic phase, there is a tendency for the individual molecules to lie along a preferred direction identified by a *director vector n*. Generally, the orientational ordering is not perfect and is characterized by a spread of angles about the director; see Fig. 4-1(a). The degree of ordering is described by an *order parameter S*; see Eqs. (4.25) and (4.26). Closely related to the nematic mesophases are the *cholesteric* mesophases, named after the cholesterol esters in which they were first observed. Cholesterics are characterized by a director vector that varies helically in space, in addition to displaying long-range orientational order; see Fig. 4-1(b). In common with nematic liquid crystals, cholesteric phases also possess no positional order. The most ordered liquid crystals are the *smectic* mesophases, in which the molecules are arranged in well-defined layers, as shown in Fig. 4-1(c). There is positional order in smectic phases in the direction perpendicular to the layers. Within the layers different types of orientational order are seen, allowing classification of the smectic mesophases into types A, C, etc. The nematic, cholesteric and smectic mesophases are observed in both rod-like and disk-like systems. In addition, systems of disk-like molecules also exhibit a *columnar* phase; see Fig. 4-1(d). In this thesis, only lyotropic nematic mesophases are considered.
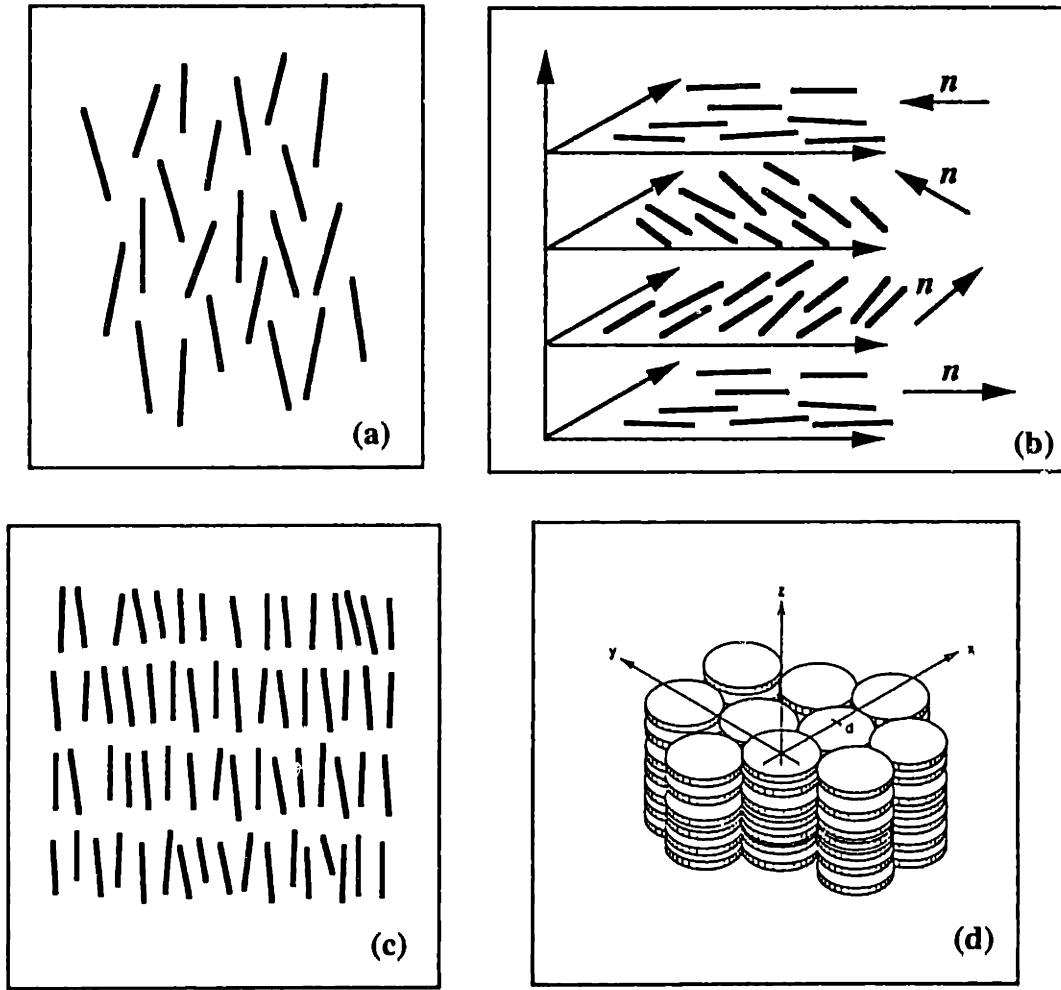
Figure 4-1: Different forms of orientational order seen in liquid crystals: (a) nematic (b) cholesteric (c) smectic (d) columnar phases are displayed.

In common with crystalline solids, perfect ordering in different mesophases is disturbed by the presence of defects and distortions. Distortions in the molecular ordering as described by the local orientation of the director vector often arise due to incompatibility between the orientations set by bounding surfaces and external orienting fields (de Gennes, 1974). Consequently, the director vector $n(r)$ varies continuously in space. The three basic modes of distortions are termed *bend*, *splay* and *twist*, and are illustrated in Fig. 4-2(a). Most distortions seen experimentally are combinations of these three basic modes. The director vector n sometimes undergoes almost discontinuous changes in orientation; these discontinuities are termed *disclinations* and can be located at points, on lines or on surfaces, and result in *defects* in the perfect mesophases. The persistent presence of such disclinations is associated with a *polydomain texture* in liquid crystalline polymers, as schematically shown in Fig. 4-2(b). The *domain* is viewed as a region of local order bounded by surface disclinations and is seen in a polarizing microscope as a light region between extinction bands; it constitutes the smallest unit of the texture observed in liquid crystalline polymers. The average size of the domain is set by the defect density, and is taken to be the average distance between neighboring disclinations. Typical domain sizes in polymeric nematics are $\mathcal{O}(1)$ μm (Marrucci, 1984). De Gennes (1974) argues that surface or sheet disclinations that form domain boundaries are energetically unstable, and decay to give point or line disclinations. However, this view of domains is still commonly accepted as a convenient way to explain the optical observations (Larson and Doi, 1991).

The imposed flow field and the supramolecular ordered structure present in liquid crystal polymers are closely related and result in complex rheology. The presence of the so-called "polydomains" complicates the situation further, and makes modelling of liquid crystal rheology a challenging task. To illustrate the complexity, it is worthwhile to compare the rheology of isotropic and liquid crystal polymers (LCPs). Unlike isotropic polymers, where the viscosity increases monotonically with concentration, the viscosity-concentration plot for a lyotropic liquid crystal at low shear rates displays a sharp maximum, followed by a continuous decrease in the viscosity. This viscosity
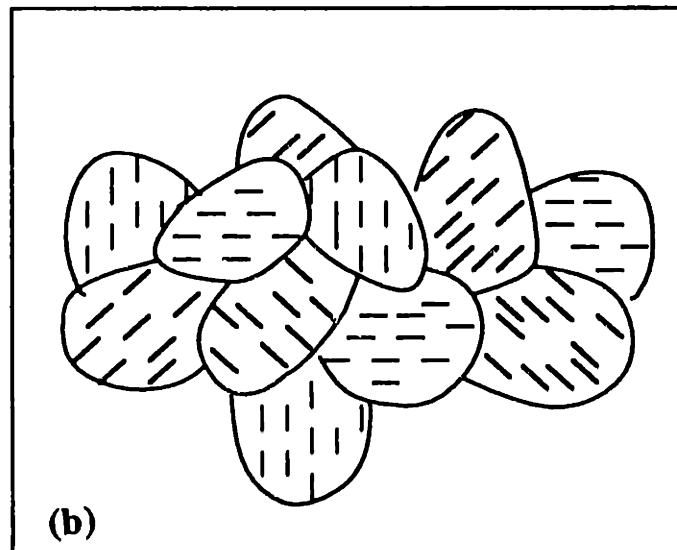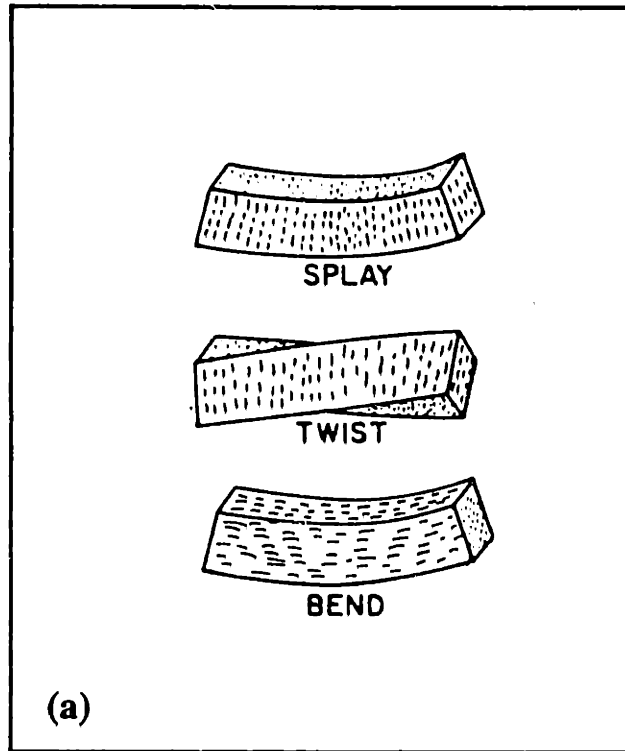
Figure 4-2: (a) Bend, splay and twist type of distortions (*reproduced from* Stephen and Straley, 1974) (b) Polydomain structure in liquid crystals.

decrease is a result of the phase transition from an isotropic to a nematic state. For an isotropic polymer, the viscosity-shear-rate curve displays a constant viscosity plateau at low shear rates, and shear-thinning behavior at high shear rates, as described in Section 2.1. In addition, LCPs sometimes also display shear-thinning at very low shear rates. The three regions are often referred to as Region I, Region II and Region III; see Fig. 4-3(a). Onogi and Asada (1980) have suggested that the Region I behavior is related to the polydomain structure prevalent in LCPs. They argue that the evolution of the liquid crystal from a polydomain to a monodomain under the influence of flow leads to the transition from Region I to Region II on the viscosity-shear-rate curve. A schematic representation of this transition is shown in Fig. 4-3(b). Optical observations of the polydomain texture in LCPs indicate that the domains tend to get distorted in the presence of flow and the average domain size decreases (Larson, 1992; Gleeson et al., 1991). However, it has not been possible as yet to definitively relate these observations to the Region I behavior seen in the LCPs. The Region III behavior of an LCP is similar to that of an isotropic polymer.

Typical behavior for Ψ_1 for isotropic polymers, as illustrated in Fig. 2-2, shows that the first normal stress difference varies as $\dot{\gamma}^2$ at low shear rates. However, experimental observations in liquid crystals indicate that the normal stress difference for LCPs varies as $\dot{\gamma}$ as a consequence of anisotropic ordering in the system. In addition, negative first normal stress coefficients also have been observed for LCPs (Kiss and Porter, 1978); see Fig. 4-4. The incidence of negative first normal stress differences is accompanied by a large second normal stress difference (Magda et al., 1991). Recent theories for liquid crystals suggest that this unusual behavior of the normal stress differences is a consequence of an en masse molecular tumbling; this is discussed in Chapter 5 in greater detail.

Other rheological observations that are quite different from those seen in isotropic polymers also have been attributed to the presence of a defect texture in the LCP; these observations include multiple damped oscillations in stress in transient experiments such as step increase in shear flow and flow reversal (Moldenaers and Mewis, 1988; Burghardt and Fuller, 1991) and slow elastic strain recovery after removal of
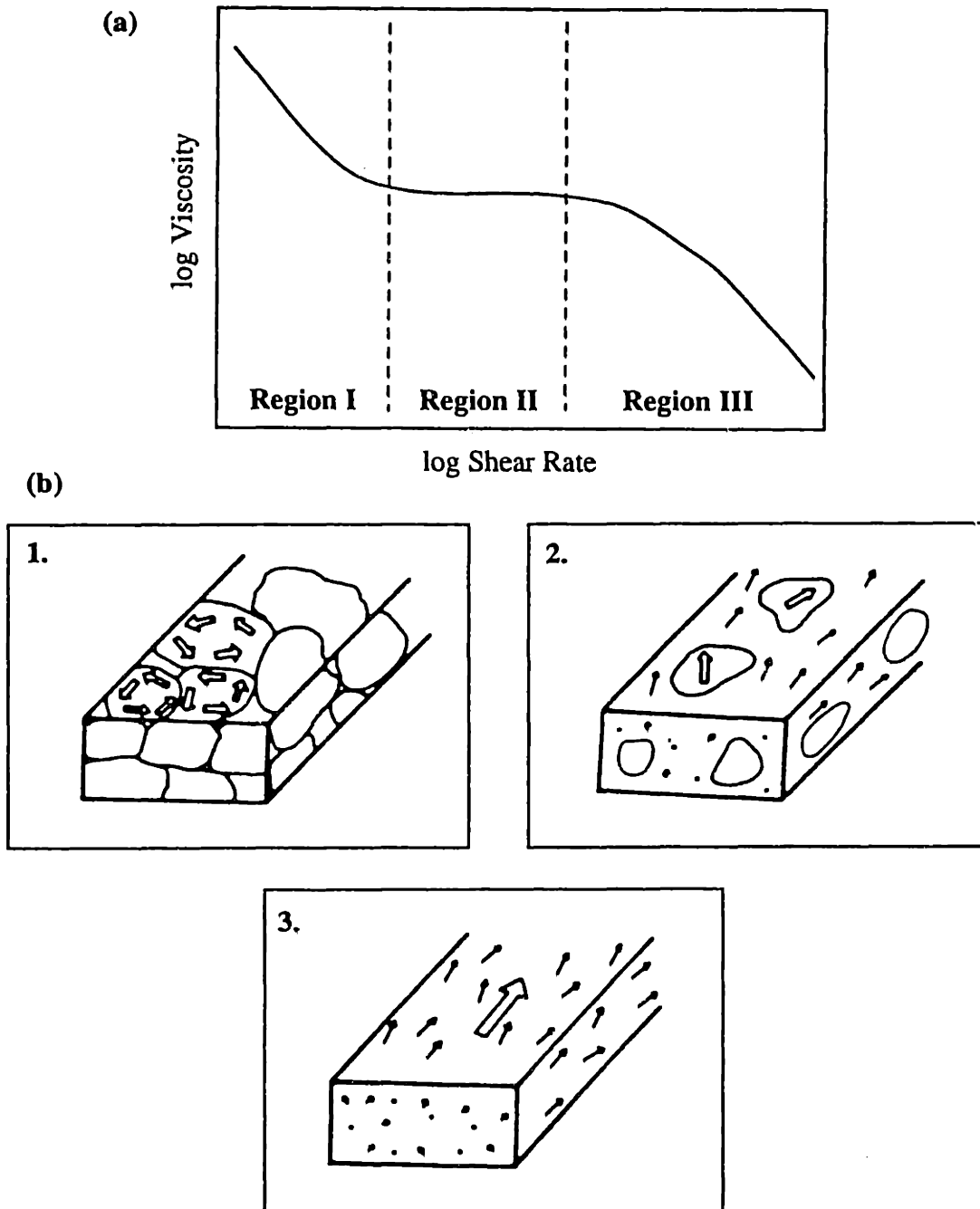
Figure 4-3: (a) Typical viscosity-shear-rate curve for an LCP. (b) Schematic represen-
tation of the break-up of a polydomain structure: 1. Piled polydomain, 2. dispersed
polydomain and 3. monodomain (*reproduced from* Onogi and Asada, 1980).

120
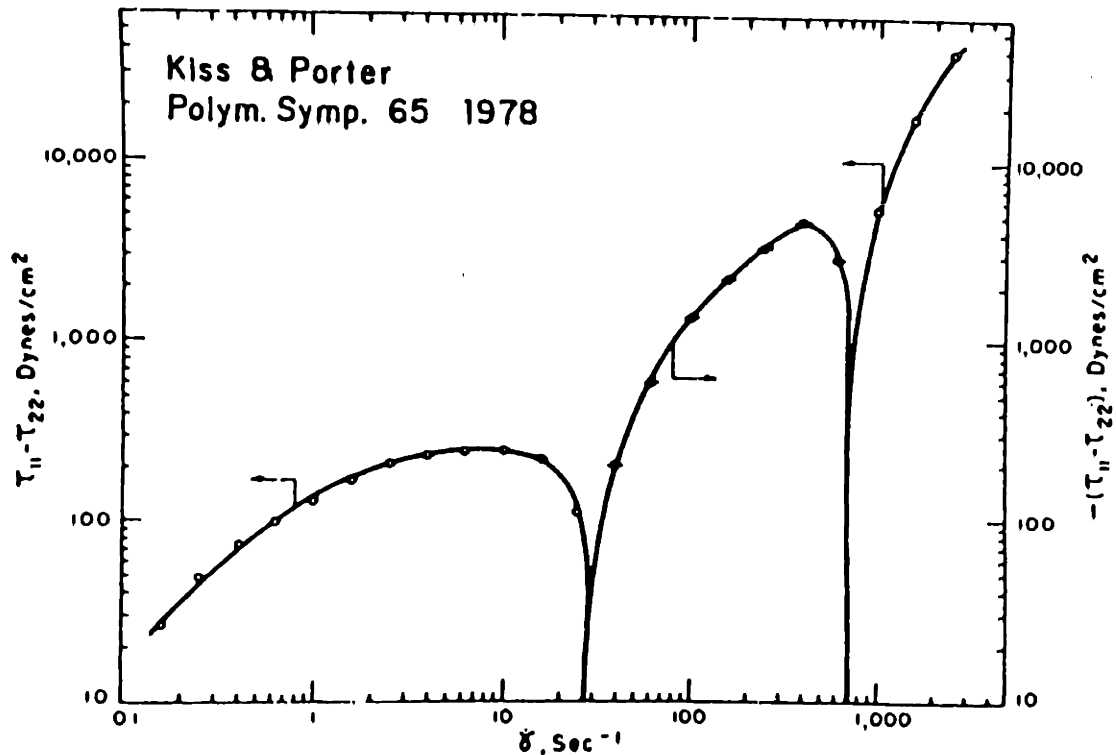
Figure 4-4: Steady-state first normal stress difference as a function of shear rate for a liquid crystalline solution of PBG (*reproduced from* Kiss and Porter, 1978).

the shear stress (Larson and Doi, 1991). In a number of these observations, the transient data scale very well with *strain*; *i.e.*, when the time coordinate is scaled with the reciprocal strain-rate rather than with a characteristic molecular relaxation time. This scaling also is taken to indicate the presence of a texture in LCPs (Larson and Doi, 1991), although the same behavior is displayed by other concentrated melts that are not necessarily liquid crystalline in nature (Bird *et al.*, 1987a).

Orientation imposed by boundaries has a significant effect on the orientational order seen in the bulk of the system in LCPs (Srinivasrao and Berry, 1991). As in the case of low-molecular-weight nematics, the incompatibility between the orientation imposed by the boundary conditions and that imposed by the flow field can conceivably cause development of texture and thus can affect the rheological behavior displayed by the LCP.

Constitutive theories for concentrated systems that can form liquid crystalline phases must be capable of describing the anisotropic microstructure that leads to rhe-

ological behavior very different from that seen in isotropic polymer solutions. These theories also must be capable of addressing the issue of nonhomogeneities, whether imposed due to boundary constraints or intrinsically present in the form of defects or polydomains. The two main theories that have been proposed for liquid crystals are the Leslie-Ericksen-Parodi theory and the Doi theory. Neither theory possesses all the necessary features; these theories are discussed at length in Section 4.2. The Leslie-Ericksen-Parodi theory is a nonhomogeneous continuum theory that applies to low-molecular-weight nematics. It accounts for the effects of director distortion, but does not account for the nonlinear rheology displayed by polymeric nematics. The Doi theory is a homogeneous molecular theory that is capable of predicting the isotropic-nematic (I-N) phase transition in LCPs. The assumption of spatial homogeneity intrinsic to the development of this theory makes it unsuitable for the study of boundary effects or polydomain structures. The nonhomogeneous theory presented in Chapter 3 presents a viable means of extending the Doi theory to nonhomogeneous systems.

By using phase-space kinetic theory, a nonhomogeneous theory for liquid crystalline systems is developed in Section 4.3. Frequent reference is made to the analogous development of Section 3.2, to avoid unnecessary repetition. The rigid dumbbell model is used to describe the backbone rigidity of the macromolecules that form mesophases; the model is introduced in Section 4.3.1 with other relevant notation. The excluded volume interaction between the rigid macromolecules is responsible for the development of long-range order, and a proper description of this interaction is crucial to the development of a model for liquid crystalline materials. The pairwise excluded volume potential first used by Onsager (1949), and its mean-field version originally developed by Maier and Saupe (1958 & 1959) have been used to study the isotropic-nematic phase transition in homogeneous systems. A generalization of these potentials to nonhomogeneous systems must account for the extended nature of the interacting molecules that results in a finite range of interaction. Different generalizations of the interaction potential, each based on different ranges of interaction, are presented in Section 4.3.2. The nonhomogeneous constitutive theory is finally derived

in Section 4.3.3, for an unspecified form of the intermolecular potential. An extension of these equations to any specific form of the potential discussed in Section 4.3.2 is fairly straightforward. The relevant equations derived in this section are the diffusion equation for the distribution function and expressions for the stress tensor and mass flux vector. The theory presented here is an extension of Doi's molecular theory that accounts for spatial nonhomogeneities. The predictions of the constitutive model are studied in greater detail in Chapter 5 under conditions of spatial uniformity, and in Chapter 6 to develop an understanding of spatial structure that is formed at the I-N transition point.

4.2 Review of Existing Theories for Liquid Crystalline Materials

4.2.1 The Continuum Theory of Leslie, Ericksen and Parodi

The earliest attempts to develop a constitutive equation for liquid crystalline materials were made by Ericksen (1960 &1961), Leslie (1966 & 1968) and Parodi (1970). The Leslie-Ericksen-Parodi (LEP) model extends Frank's continuum theory of curvature elasticity (Frank, 1958) developed for liquid crystals at rest to model flow behavior of nematic liquid crystals. The total stress tensor in the LEP theory is expressed as the sum of an isotropic contribution due to pressure, an elastic contribution due to spatial variations of the director that is obtained from Frank's elasticity theory and a viscous contribution due to the effects of flow as

$$\pi = p\delta + \tau^e + \tau^v. \tag{4.1}$$

Frank's expression for the elastic free energy is based on the assumption that the torque stresses in a liquid crystal subjected to deformation are proportional to the curvature strains. The state of local order in the nematic is associated with a director $n(r)$ that varies continuously in space and that is capable of describing the distorted

state of the system. By recognizing that n and $-n$ are indistinguishable in the nematic phase, the free energy per unit volume of the deformed nematic liquid crystal relative to that in the state of uniform orientation is written compactly as (de Gennes, 1974)

$$F_D = \frac{1}{2}K_{11}(\nabla \cdot n)^2 + \frac{1}{2}K_{22}(n \cdot \nabla \times n)^2 + \frac{1}{2}K_{33}(n \times \nabla \times n)^2 \qquad (4.2)$$

where the three elastic constants K_{11}, K_{22} and K_{33} are associated with the curvature strains of splay, twist and bend, respectively; see Fig. 4-2(a). These constants are generally unequal and ordered such that $K_{22} < K_{11} \ll K_{33}$. Sometimes, though, for the sake of simplicity, all three constants are taken to be equal in the so-called "one-constant approximation". In terms of the distortional free energy, the elastic contribution to the total stress τ^e, or the *Ericksen stress*, is

$$\tau^e = -\frac{\delta F_D}{\delta \nabla n} \cdot (\nabla n)^{\dagger}. \qquad (4.3)$$

The viscous stress contribution τ^v is assumed to be a linear function of n, N and $\dot{\gamma}$ and is written as

$$\tau^v = -\frac{1}{2}\left[\alpha_1 nnnn{:}\dot{\gamma} + 2\alpha_2 nN + 2\alpha_3 Nn + \alpha_4\dot{\gamma} + \alpha_5 nn \cdot \dot{\gamma} + \alpha_6\dot{\gamma} \cdot nn\right] \qquad (4.4)$$

where

$$N = \frac{Dn}{Dt} - \frac{1}{2}\omega \cdot n. \qquad (4.5)$$

Here, $\dot{\gamma} = \nabla v + \nabla v^{\dagger}$ is the rate-of-strain tensor, $\omega = \nabla v - \nabla v^{\dagger}$ is the vorticity tensor, and D/Dt is the material time derivative. Of the six Leslie coefficients α_i ($i = 1\ldots 6$), only five are independent according to *Parodi's relation* (Parodi, 1970)

$$\alpha_2 + \alpha_3 = \alpha_6 - \alpha_5. \qquad (4.6)$$

It follows from Eqs. (4.2)-(4.4) that the total stress π is generally asymmetric, even in the absence of external fields. It is known to be symmetric only under the one constant approximation that equates all three Frank's elasticity constants. The set of

governing equations is completed by writing Oseen's equation for the director vector n as (Chandrasekhar, 1977)

$$\hat{\rho}\frac{D^2n}{Dt^2} = G + g - \nabla \cdot \pi^s \qquad (4.7)$$

where $\hat{\rho}$ is a material constant with units of moment of inertia per unit volume, G is the external director body force, g is the intrinsic director body force, and π^s is the director surface stress. The intrinsic director body force g is written as a sum of elastic and viscous contributions as

$$g = g^e + g^v \qquad (4.8)$$

where

$$g^e = \gamma n - \beta \cdot \nabla n - \frac{\delta F_D}{\delta n} \qquad (4.9)$$

and

$$g^v = \lambda_1 N + \frac{\lambda_2}{2}n \cdot \dot{\gamma}. \qquad (4.10)$$

In the above equations, the constants γ and β are arbitrary, $\lambda_1 = \alpha_2 - \alpha_3$, $\lambda_2 = \alpha_5 - \alpha_6$ and F_D refers to Frank's distortional free energy as given by Eq. (4.2). The director surface stress is given by

$$\pi^s = -\beta n - \frac{\delta F_D}{\delta \nabla n}. \qquad (4.11)$$

The arbitrary constants γ and β represent the arbitrariness in determining the director, analogous to the indeterminacy of pressure up to an arbitrary constant. This problem is often overcome by taking the cross-product of Eq. (4.7) with n, and rewriting the result in the form of a torque balance as (Larson, 1988)

$$n \times \left(\nabla \cdot \frac{\delta F_D}{\delta \nabla n} - \frac{\delta F_D}{\delta n} + \lambda_1 N + \frac{\lambda_2}{2}n \cdot \dot{\gamma} \right) = 0 \qquad (4.12)$$

Equations (4.1)-(4.12) complete the Leslie-Ericksen-Parodi model for nematic liquid crystals and can be used in conjunction with the equations of motion and continuity to determine the pressure p, velocity v and director n.

The LEP theory directly incorporates Frank's distortional free energy and is ideally suited for the study of distortions, defects and domains in liquid crystals. Boundary effects are also easily considered, by using the *strong anchoring condition* and specifying the director vector at walls. This is reminiscent of the setting of dumbbell orientation in Chapter 3. Since it was the earliest theory developed for liquid crystals, the LEP model has been used extensively for interpretation of experimental data, especially for low-molecular-weight nematics (de Gennes, 1974). However, its applicability to liquid crystalline polymers is limited. The assumption of linear dependence of τ^v on shear rate in the development of the LEP theory restricts it to low deformation rates; consequently, the model cannot describe nonlinear rheological properties, such as shear-thinning of the viscosity and normal stresses which are observed in liquid crystalline polymers (Wissbrun, 1981). The LEP model presupposes the presence of a director vector n and assumes a uniform degree of ordering throughout the system. Thus, it does not allow for phase transitions to the ordered phase that occur with increasing polymer concentration; development of orientational order in the presence of flow is also not considered. While these assumptions are suitable for low-molecular-weight nematics, they cannot be justified in the study of LCPs. Moreover, even the model as described by Eqs. (4.1)-(4.12) involves five adjustable parameters in the expression for τ^v and three elasticity constants in Eq. (4.2) for F_D all of which must be determined experimentally. The LEP model thus provides little insight into the interaction of flow and microstructure, and molecular theories are preferable for the study of LCPs. However, the extensive work done using the LEP theory to interpret experimental data has led to some effort in determining the different constants from molecular theories (Marrucci, 1982; Kuzuu and Doi, 1983 & 1984).

4.2.2 The Doi Molecular Theory

Doi (1980 & 1981) made the first attempt at developing a molecular theory for liquid-crystalline polymers. Doi's model overcomes a number of drawbacks present in the LEP theory; primarily it accounts for the isotropic-nematic phase transition, and also

predicts some of the nonlinear rheological properties exhibited by LCPs. However, since the theory makes the assumption of spatial homogeneity, it is restricted to homogeneous systems alone. The concepts laid down in Chapter 3 are used to extend some of Doi's ideas to a nonhomogeneous theory in Section 4.3. In order to avoid repetition, the detailed development of Doi's theory is not discussed here. Instead, only the final equations and some significant results are presented. In the subsequent development of the nonhomogeneous theory, references to Doi's theory are made where relevant.

Doi's model is based on Onsager's expression for the free energy of a concentrated solution containing rod-like polymeric molecules (Onsager, 1949) and uses the Maier-Saupe approximation to the polymer-polymer interaction potential (Maier and Saupe, 1958 & 1959). An equation for the orientational distribution function is first developed by starting from the theory of Kirkwood and Auer (1951). Next, Doi develops an expression for the stress tensor based on the procedure used by Doi and Edwards (1978a, 19878b, 1978c & 1979) in their theory for dilute and semidilute solutions of rigid, rod-like polymers. Essentially, the expression for the stress tensor τ is comprised of two separate contributions. The first contribution, termed as *elastic stress*, is obtained by calculating the change in free energy caused by a small virtual deformation. The second contribution is the *viscous stress* that is associated with hydrodynamic energy dissipation. Following Doi and Edwards (1978a, 1978b, 1978c & 1979), Doi (1981) ignores the contribution of this viscous stress. Doi and coworkers argue that the contribution of the viscous stress term is small compared to the elastic stress, especially in the semi-dilute and concentrated regimes, and hence need not be considered. Although this is true at low rates of deformation, the contribution of the viscous stresses at higher deformation rates is significant and the validity of the assumptions under such conditions is questionable.

A closed set of governing equations is finally obtained after making some closure approximations (see Chapter 5) and can be written as

$$S_{(1)} = F(S) + G(S, \kappa) \tag{4.13}$$

127

where

$$F(S) = -6\bar{D}_r \left[(1 - \frac{U}{3})S - U(S \cdot S) + U(S{:}S)(S + \frac{1}{3}\delta) \right] \qquad (4.14)$$

and

$$G(S, \kappa) = \frac{1}{3}\dot{\gamma} - 2(\kappa{:}S)(S + \frac{1}{3}\delta). \qquad (4.15)$$

Here, S is a *spatially independent* structure tensor that describes the orientation and degree of ordering in the nematic phase; see Eq. (5.5). The dimensionless constant U is a measure of polymer concentration and $S_{(1)}$ is the upper-convected derivative; see Eq. (2.25). The term $\bar{D}_r$ is an average rotational diffusivity that accounts for the constraints on the rotation of an individual rod due to the presence of surrounding rods and is approximated as

$$\bar{D}_r = \frac{c_1 D_{r0}(nL^3)^{-2}}{(1 - 3/2S{:}S)^2} \qquad (4.16)$$

where c_1 is an arbitrary constant, n is the number density, L is the length of the rigid rod and D_{r0} is the rotational diffusivity in the limit of infinite dilution. The stress tensor that is obtained from Onsager's equilibrium free energy expression is given as

$$\tau = -\frac{nkT}{2\bar{D}_r}F(S). \qquad (4.17)$$

These equations can be solved in conjunction with the equations of motion and continuity to determine the microstructure in the presence of flow and the associated material functions.

Doi's model provides a quantitative description of the isotropic-nematic phase transition that occurs as the concentration of polymer is increased in a solution at rest, and correctly predicts the maximum in the zero-shear-rate viscosity that has been experimentally observed; see Section 4.1. At low shear rates, the Doi model predicts the linear dependence of normal stress differences on shear rate and the constant viscosity plateau. Shear-thinning at higher shear rates is also predicted. However, neglect of the viscous stress term in calculating the stress tensor results in aphysical predictions of material functions at high shear rates. For instance, in the limit of

128

high shear rate, the viscosity decreases more rapidly than $\dot{\gamma}^{-1}$, which corresponds to a maximum in the shear stress as a function of shear rate. This behavior is physically impossible and limits the range of applicability of Doi's model. A similar problem is encountered in the Doi-Edwards theory for the dilute and semi-dilute solutions.

Jain and Cohen (1981) have shown that including the viscous stress term changes the predictions of the Doi-Edwards theory for steady shear flow material functions, especially at high shear rates. The viscosity predicted by the extended model of Jain and Cohen does not show the excessive shear thinning inherent to the theories of both Doi-Edwards and Doi, and fits experimental data very well in the semi-dilute region. The effect of adding the viscous stress term was investigated by Dahler *et al.* (1983) for elongational flows, and a similar conclusion was reached about its importance at high elongation rates.

In this chapter, the expression for the stress tensor is derived from phase-space kinetic theory following the procedure described by Bird *et al.* (1987b). A consistent treatment of the hydrodynamic forces acting on the system automatically results in the viscous stress contribution, and the aphysical behavior of Doi's theory is thus avoided.

It is apparent from the above discussion that the Doi model does not predict the Region I shear-thinning behavior reported by Onogi and Asada (1980), possibly because it is a homogeneous theory. However, it has not been shown conclusively that the Region I behavior is indeed due to a polydomain texture in the LCP. The Doi model also cannot predict the negative first normal stress coefficient Ψ_1 that has been reported; see Section 4.1. Recently, it has been shown that negative values of Ψ_1 result from a periodic *tumbling* of the molecules (Marrucci and Maffettone, 1989; Larson, 1990; Larson and Öttinger, 1991). It is surmised here that the Doi model fails to predict this behavior as a result of the closure approximation made in the development of the theory; this point is elaborated further in Chapter 5.

The development of the Doi molecular theory has given a large impetus to the study of rheology of liquid crystalline systems. In the last decade, since the development of the Doi model, a number of studies have investigated the effects of both
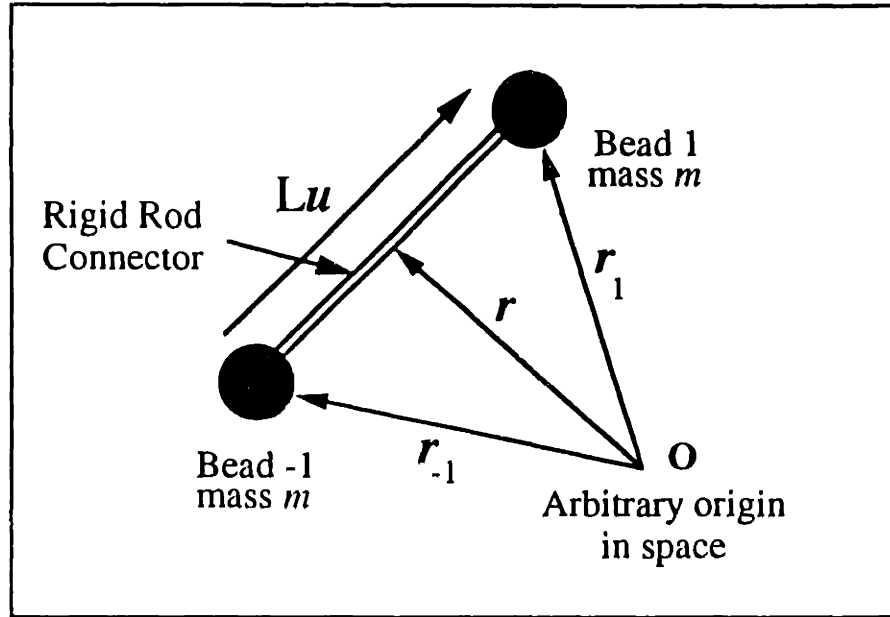
Figure 4-5: The rigid dumbbell model.

shear and shearfree flows on the isotropic-nematic transition, as predicted by the Doi model (See *et al.*, 1990; Hu and Ryskin, 1991). However, the picture of the coexisting phases that is presented is often over-simplified. In fact, the Doi model admits a very rich and complex solution structure that has never been fully investigated. The complete solution structure in shear and shearfree flows is presented in Chapter 5, before the study of nonhomogeneous effects is described.

4.3 Development of the Constitutive Equation

4.3.1 Description of the Molecular Model

The solution of rod-like polymers is modelled as an ensemble of rigid dumbbells suspended in a Newtonian solvent of viscosity η_s; see Fig. 4-5. The polymer number density is n. This model accounts for the ability of the polymer molecules to orient in the flow and ignores the stretching and bending motions that are of minor importance

$uu + ss + tt = \delta$
$\frac{\partial}{\partial u} = s\frac{\partial}{\partial \theta} + t\frac{1}{\sin\theta}\frac{\partial}{\partial \phi}$
$\int uu\,du = \frac{4\pi}{3}\delta$
$\int uuuu\,du = \frac{4\pi}{15}(\delta\delta + I + I^\dagger)$

Table 4.1: Some relations between unit vectors in spherical coordinates.

in determining the rheological properties of such solutions. Each dumbbell consists of two point beads of equal mass m, labelled as $\nu = +1$ and $\nu = -1$, connected by a massless rod of length L. The interaction with the solvent is assumed to take place only at the beads. The location of bead ν with respect to an arbitrary origin is given by position vector r_ν and the location of the center of mass of the dumbbell is r_c. The relative position of bead ν with respect to the center of mass is given by $R_\nu \equiv r_\nu - r_c$. The presence of a constraint in the molecular model, *viz.*, the rigid rod connector makes it convenient to use generalized coordinates Q_s to describe the internal configuration of the molecule. For a rigid rod model, the generalized coordinates of choice are the polar angles (θ, ϕ), or equivalently, the unit vector u oriented along the axis of the dumbbell as shown in Fig. 4-5. The unit vector u is related to the polar angles (θ, ϕ) through the spherical unit vectors s and t in the θ and ϕ directions, respectively. Some of the important relations between the unit vectors in spherical coordinates are summarized in Table 4.1. Additional relations that have been used are given in Appendix E of Bird *et al.* (1987b). The relative bead position vector is $R_\nu \equiv (L\nu/2)u$.

The configuration of each dumbbell is set by either (r_c, u) or (r_c, Q), where Q collectively denotes the polar angles (θ, ϕ). The center-of-mass momentum is given as $p_c = m_p\dot{r}_c$, where $\dot{r}_c$ is the center-of-mass velocity. Similarly, the generalized momenta for the internal degrees of freedom of the rigid dumbbell are given as $P_s = \sum_t g_{st}\dot{Q}_t$. Here, we have introduced the components of the *metric matrix* $\{g_{st}\}$ given

as

$$g_{st} = \sum_{\nu}(b_{\nu s} \cdot b_{\nu t}) \tag{4.18}$$

where $\{b_{\nu s}\}$ are the *base vectors* defined as

$$b_{\nu s} \equiv \sqrt{m_\nu}\frac{\partial}{\partial Q_s}R_\nu. \tag{4.19}$$

The components of the matrix inverse to the (g_{st})-matrix are denoted by G_{st}. For the rigid dumbbell model described above, the base vectors are compactly written as

$$b_{\nu s} = \frac{L\nu}{2}\sqrt{m}c_s, \quad s \equiv \theta, \phi \tag{4.20}$$

where the *unit sphere base vectors* c_s are given as $c_\theta = s$ and $c_\phi = \sin\theta\ t$. The components of the metric matrix and its inverse are

$$g_{st} = \frac{L^2}{4}m_p c_{ss}\delta_{st}; \quad G_{st} = \frac{4}{L^2}\frac{1}{m_p c_{ss}}\delta_{st}. \tag{4.21}$$

The independent variables (r_c, Q, p_c, P) define the instantaneous location in phase space of the dumbbell and $(\dot{r}_c, \dot{Q}, \dot{p}_c, \dot{P})$ are the time derivatives of the phase-space coordinates that are given by Hamilton's equations of motion; see Eq.(4.48).

Following the development in Chapter 3, the constitutive equation is derived by starting from the full phase-space distribution function f. By restricting the theory to two-body interactions and by taking the normalized velocity distribution to be Maxwellian about the mass-average velocity v at the center of mass of the dumbbell, the final equations are given in terms of averages involving just the lower order configurational space distribution functions. As in Chapter 3, the singlet configurational space distribution function $\Psi_p(r, \theta, \phi, t)$ is of particular interest and is defined such that $\Psi_p(r, \theta, \phi, t)drd\theta d\phi$ represents the fraction of dumbbells with center of mass in the region dr about r and with orientation in the range (θ, ϕ) to $(\theta + d\theta, \phi + d\phi)$. An alternative configurational distribution function $f_p(r, u, t)$ also can be defined in which $f_p(r, u, t) \equiv (1/\sin\theta)\Psi_p(r, \theta, \phi, t)$. The distribution function $f_p(r, u, t)$ should not be confused with the singlet phase-space distribution function of Chapter 3. When

the dumbbells are randomly distributed and all orientations are equally probable, the equilibrium configurational distribution function is

$$\Psi_{p,\text{eq}} \equiv n_{av}\frac{\sin\theta}{4\pi} \text{ or } f_{p,\text{eq}} \equiv \frac{n_{av}}{4\pi} \tag{4.22}$$

where n_{av} is the average number density of polymer. The local number density $n(r,t)$ is defined as

$$\iint \Psi_p(r,\theta,\phi,t)d\theta d\phi = n \text{ or } \int f_p(r,u,t)du = n \tag{4.23}$$

where both integrals denote integration over the surface of the unit sphere and are equivalent.

Average properties for the system are defined in terms of these distribution functions. A particularly useful average property for rigid rod-like polymers is the orientational order tensor or the structure tensor S, which is defined as

$$S \equiv \frac{1}{n}\{uu - \frac{1}{3}\delta\} \equiv \frac{1}{n}\int(uu - \frac{1}{3}\delta)f_p(r,u,t)du \tag{4.24}$$

where { } is an integral over all internal coordinates, as defined in Chapter 3. The structure tensor S defined in Eq. (4.24) is the nonhomogeneous analogue of the structure tensor used in Doi's theory; see Section 4.2.2.

In a nematic liquid-crystalline phase at rest, uniaxial symmetry about a director vector n is seen and the structure tensor defined by Eq. (4.24) takes a special form. Uniaxial symmetry implies that two eigenvalues of the structure tensor are equal and n is the eigenvector corresponding to the distinct eigenvalue, so that the structure tensor S is written as (Ericksen, 1984)

$$S = S(nn - \frac{1}{3}\delta) \tag{4.25}$$

where the scalar structural order parameter S is given by (Tsvetkov, 1942)

$$S = \frac{3}{2}\langle(u \cdot n)^2\rangle - \frac{1}{2}. \tag{4.26}$$

133

The parameter S falls in the range $-1/2 \leq S \leq 1$ and is a measure of the degree of order in the system. A state of random order corresponds to $S = 0$; this is clear by substituting Eq. (4.22) for f_p in Eq. (4.24), and evaluating the orientational averages. If S is positive, the largest eigenvalue of S is not degenerate and the system exhibits prolate uniaxial symmetry. In this state, the molecular axes are aligned about the director axis; perfect alignment is achieved in the limit $S = 1$. When S is negative, the system exhibits oblate uniaxial symmetry with the molecular axes approximately lying in planes orthogonal to the director axis. The limit $S = -1/2$ corresponds to having all molecules lying perfectly in planes orthogonal to the director axis with random in-planar orientation. From Eqs. (4.25) and (4.26), the order parameter S is given by either

$$|S| = [(3/2)S{:}S]^{1/2} \tag{4.27}$$

or

$$S = [(9/2)(S \cdot S){:}S]^{1/3}. \tag{4.28}$$

The second form of the scalar order parameter removes the ambiguity of sign associated with the first definition, and is helpful in determining whether a prolate or an oblate symmetry is observed.

4.3.2 The Intermolecular Potential

The development of orientational order with increasing concentration in liquid crystalline systems consisting of molecules with rigid backbones is a consequence of the excluded volume interaction between these molecules. A proper description of these intermolecular forces is crucial to the development of any model for the liquid crystalline material.

The earliest theory of this phase transition was that by Onsager (1949) based on the Mayer cluster expansion and has been described in Doi and Edwards (1986). Based on Onsager's development, Doi and Edwards (1986) expressed the free energy

per unit volume of a concentrated solution of rigid rods as

$$\mathcal{A} = nkT \left[\ln n - 1 + \int f_p(u, t) \ln f_p(u, t) du + \frac{1}{2} n \int\int \beta(u, u') f_p(u, t) f_p(u', t) du du' \right]$$
(4.29)

where n is the number density and f_p is the distribution function, which equals $1/4\pi$ in the isotropic equilibrium state. The first integral term in Eq. (4.29) is an entropic contribution that also appears in dilute solution theories. The second integral term results from pairwise *excluded volume* effects. In this expression, $\beta(u, u')$ is the excluded volume per rod and is given by

$$\beta(u, u') = 2L^2 b |u \times u'|$$
(4.30)

where L and b are the length and radius of the rigid rod, respectively. The origin of Eq. (4.30) is clear from Fig. 4-6. The excluded volume effects become increasingly important with increasing concentration and result in a transition from a disordered to an ordered phase; see Fig. 4-7. Equation (4.29) assumes a hard-body interaction between the rods that does not allow interpenetration of the rods and neglects three-body and higher-order interactions. The equilibrium distribution function f_p is then determined by minimizing $\mathcal{A}$ for all variations of f_p, which gives

$$f(u, t) = c \exp[-V(u)/kT]$$
(4.31)

where c is the normalization constant and $V(u)$ is the mean-field potential that acts on the test rod with orientation u due to all other surrounding rods with orientation u' defined by

$$V(u) = nkT \int \beta(u, u') f_p(u', t) du'.$$
(4.32)

This discussion implicitly assumes a constant number density and a spatially independent distribution function $f_p(u, t)$, and cannot be used, as such, in the development of a nonhomogeneous liquid crystalline theory. However, based on the hard-rod potential that was used by Onsager (1949), a generalization of the above mean-field
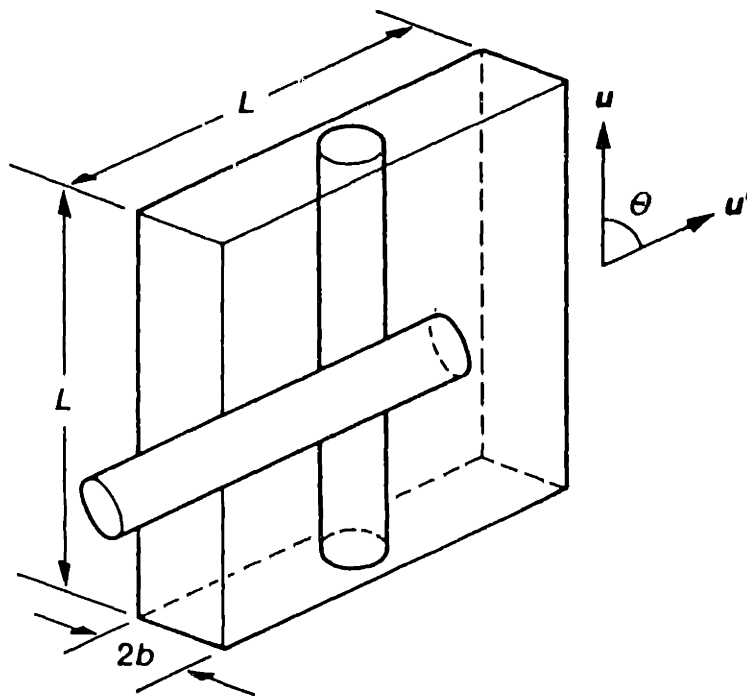
Figure 4-6: Excluded volume between two rods with orientations u and u' (*reproduced from* Doi and Edwards, 1986). For a given position of the rod in the direction u, the center of mass of the other rod is not allowed in the parallelepiped region shown in the figure.

(a) DILUTE   (b) ISOTROPIC CONCENTRATED   (c) NEMATIC
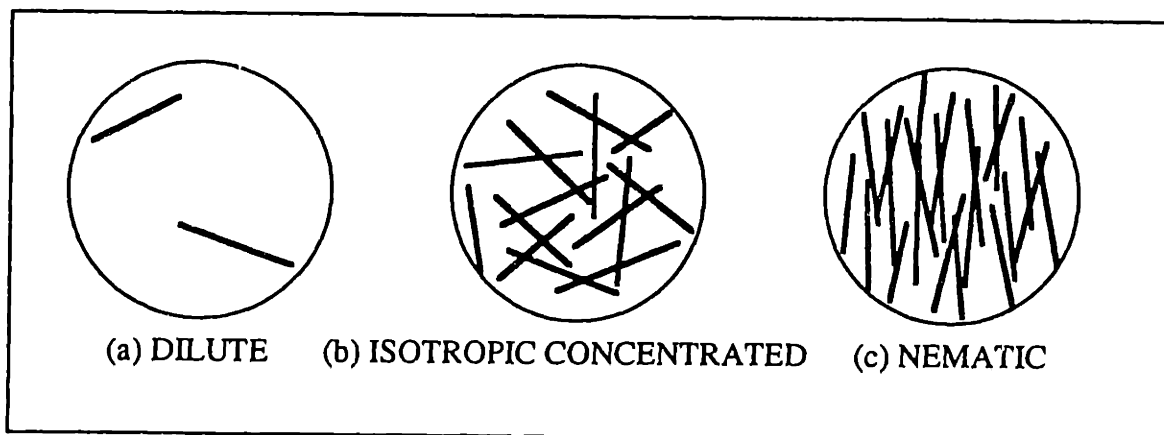
Figure 4-7: Three concentration regimes of rod-like polymers: (a) dilute solution, (b) isotropic concentrated solution, and (c) liquid crystalline solution.

potential is obtained and is discussed next.

Let $\Phi_{12}(r - r', u, u')$ be the interaction potential between two rigid rods 1 and 2 with configurations (r, u) and (r', u'), respectively. Note that the interaction potential depends only on the separation $r - r'$ of the two rigid rods, and not the exact location. In the mean-field approximation, the net molecular field that acts on the test rod (r, u) due to all other rods (r', u') is

$$\Phi^{(p)} = kT \int \Phi_{12}(r - r', u, u') f_p(r', u', t) dr' du'. \tag{4.33}$$

By following Onsager (1949), the interaction potential Φ_{12} is taken to be a hard-body interaction that does not permit interpenetration of the rods, and is written as (Doi et al., 1988)

$$\Phi_{12}(r - r', u, u') = \begin{cases} 1, & \text{if the rods } (r, u) \text{ and } (r', u') \text{ overlap,} \\ \\ 0, & \text{otherwise.} \end{cases} \tag{4.34}$$

According to Straley (1973), the distance $r - r'$ between the rigid rods can be expressed in terms of the oblique coordinates (ξ, η, ζ) along the molecule as

$$r' - r = u\xi + u'\eta + \frac{u \times u'}{|u \times u'|}\zeta \tag{4.35}$$

and $dr' = |u \times u'| d\xi d\eta d\zeta$; see Fig. 4-8. With reference to Fig. 4-8, the two rods overlap if $|\xi| < L/2$, $|\eta| < L/2$ and $|\zeta| < b$. Combining Straley's oblique coordinates (4.35) with Eqs. (4.33) and (4.34), it is clear that the only nonzero contribution to the mean field excluded volume potential is

$$\Phi^{(p)} = kT \int \int_{\xi=-L/2}^{L/2} \int_{\eta=-L/2}^{L/2} \int_{\zeta=-b}^{b} f_p(r + u\xi + u'\eta + \frac{u \times u'}{|u \times u'|}\zeta, u', t) |u \times u'| d\xi d\eta d\zeta du'. \tag{4.36}$$

Expanding the distribution function f_p in Eq. (4.36) in a Taylor series about r and
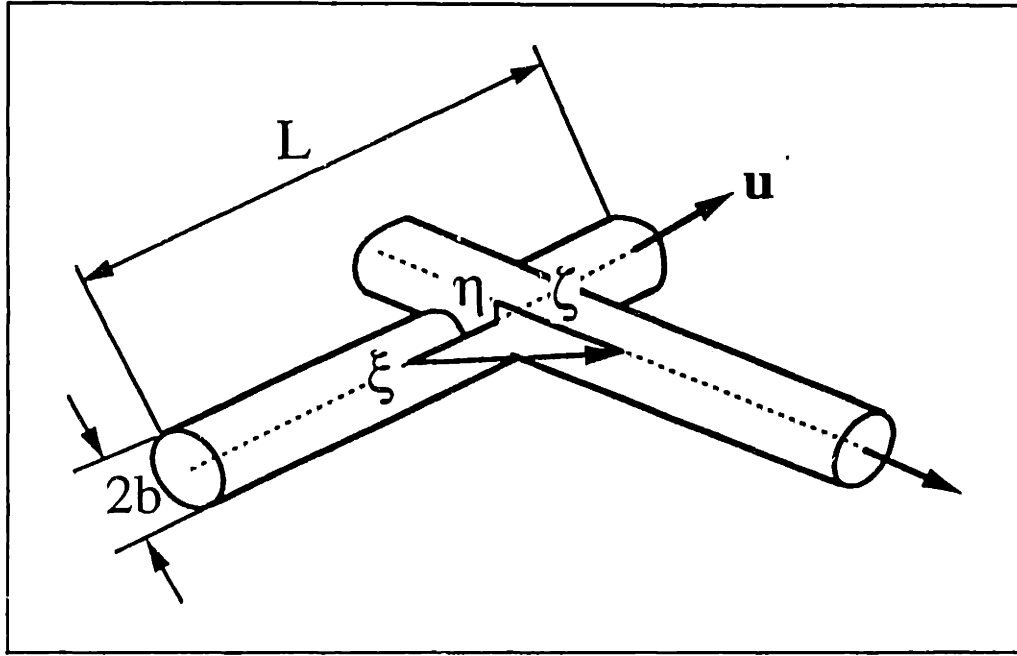
Figure 4-8: Geometry of two intersecting rods (*reproduced from* Straley, 1973).

retaining only the first term yields on simplification

$$\Phi^{(p)} = 2bL^2kT \int |u \times u'| f_p(r, u', t) du'. \tag{4.37}$$

Equation (4.37) is the nonhomogeneous version of the mean-field potential given in Eq. (4.32). Expanding $|u \times u'| = \sin(u, u')$ in terms of irreducible tensors that are equivalent to the surface spherical harmonics, as suggested by Doi (1981), gives

$$\sin(u, u') = \frac{\pi}{4} \left[1 - \frac{15}{16}(uu - \frac{1}{3}\delta){:}(u'u' - \frac{1}{3}\delta) + \ldots \right]. \tag{4.38}$$

Substituting Eq. (4.38) into Eq. (4.37) and neglecting tensors of fourth-rank and higher order, as well as the constant first term, gives the mean-field excluded volume potential as

$$\Phi^{(p)M-S} = -\frac{3}{2}NkT(uu - \frac{1}{3}\delta){:}\{uu - \frac{1}{3}\delta\} \tag{4.39}$$

or by substituting for the structure tensor S from Eq. (4.24), as

$$\Phi^{(p)\text{M}-\text{S}} = -\frac{3}{2}\mathcal{N}kT(\boldsymbol{uu} - \frac{1}{3}\boldsymbol{\delta}):S \tag{4.40}$$

where $N \equiv 2cbL^2$, $\mathcal{N} \equiv nN$ and c is a numerical factor of $\mathcal{O}(1)$. This potential is referred to as the *Maier-Saupe potential* in subsequent discussion since a form similar to the homogeneous version of this potential was used by Maier and Saupe (1958 & 1959) in their theory for low-molecular-weight nematics and leads to the formation of liquid crystalline phases at sufficiently high concentrations.

The nonhomogeneous Maier-Saupe potential given by Eq. (4.39) corresponds to the contribution to the excluded volume potential from an interaction between two rods with coincident centers-of-mass, *i.e.*, $\boldsymbol{r} = \boldsymbol{r}'$. However, due to their extended nature, two rigid rods may interact even when their centers-of-mass are separated by a finite distance as shown in Fig. 4-8. The contributions of these interactions to the mean-field potential are significant; their neglect leads to aphysical predictions as discussed in Chapter 6.

The finite separation between the test rod $(\boldsymbol{r}, \boldsymbol{u})$ and any other rod $(\boldsymbol{r}', \boldsymbol{u}')$ is taken into account by retaining more terms in the Taylor series expansion for f_p in Eq. (4.36) as

$$
\begin{aligned}
&f_p(\boldsymbol{r} + \boldsymbol{u}\xi + \boldsymbol{u}'\eta + \frac{\boldsymbol{u} \times \boldsymbol{u}'}{|\boldsymbol{u} \times \boldsymbol{u}'|}\zeta, \boldsymbol{u}', t) \\
\simeq\ &f_p(\boldsymbol{r} + \boldsymbol{u}\xi + \boldsymbol{u}'\eta, \boldsymbol{u}', t) \\
=\ &f_p(\boldsymbol{r}, \boldsymbol{u}', t) + (\boldsymbol{u}\xi + \boldsymbol{u}'\eta) \cdot \frac{\partial}{\partial \boldsymbol{r}}f_p(\boldsymbol{r}, \boldsymbol{u}', t) \\
&+ \frac{1}{2}(\boldsymbol{u}\xi + \boldsymbol{u}'\eta)(\boldsymbol{u}\xi + \boldsymbol{u}'\eta):\frac{\partial}{\partial \boldsymbol{r}}\frac{\partial}{\partial \boldsymbol{r}}f_p(\boldsymbol{r}, \boldsymbol{u}', t).
\end{aligned}
\tag{4.41}
$$

Note that the variation of the distribution function in the ζ direction is small and therefore neglected in the first line of Eq. (4.41). Furthermore, the Taylor series inherently presupposes a gradual variation in the distribution function about the position vector $\boldsymbol{r}$. Substituting the Taylor series expansion (4.41) into Eq. (4.36)

yields on simplification

$$\Phi^{(p)h-r} = 2bL^2kT \int |u \times u'| f_p(r, u', t) du'$$

$$+ \frac{1}{12} bL^4 kT \int (uu + u'u') : \frac{\partial}{\partial r} \frac{\partial}{\partial r} f_p(r, u', t) |u \times u'| du' \qquad (4.42)$$

where the superscript "h-r" refers to the hard-rod nature of the potential. This potential is referred to as the hard-rod potential in subsequent discussion. Rewriting $|u \times u'|$ in terms of irreducible tensors, analogous to the development of Eq. (4.39) gives the mean-field excluded volume potential as

$$\Phi^{(p)h-r} = -\frac{3}{2} NkT (uu - \frac{1}{3}\delta) : \{uu - \frac{1}{3}\delta\} - \frac{1}{16} NkT L^2 \nabla\nabla : (uuuu) : \{uu - \frac{1}{3}\delta\}$$

$$-\frac{1}{16} NkT L^2 \nabla\nabla : \{uuuu\} : (uu - \frac{1}{3}\delta). \qquad (4.43)$$

The gradient terms in Eq. (4.43) account for the finite separation between two intersecting rigid rods and define a range of interaction about the test rod (r, u) that is roughly $\mathcal{O}(L)$. In the absence of spatial gradients, i.e., under conditions of spatial homogeneity, the extended hard-rod potential reduces to the Maier-Saupe potential.

Another extension of the Maier-Saupe potential has been recently suggested by Marrucci and Greco (1991) and Greco and Marrucci (1992a & 1992b). These authors introduce a finite range of interaction ℓ about a rigid rod, as illustrated in Fig. 4-9. In this interpretation, all rods within this finite capsule-like domain are taken to interact equally with the test rod (r, u), while all rods out of this region contribute nothing to the hard rod potential. The parameter ℓ is completely arbitrary and can be chosen such that either $\ell \sim L$ or $\ell \gg L$. Following Greco and Marrucci (1992a), the mean field intermolecular potential is written as

$$\Phi^{(p)Mar}(r, u) = -\frac{3}{2} \frac{NkT}{LV} (uu - \frac{\delta}{3}) : \int \int_{-L/2}^{L/2} \int_{dV} (u'u' - \frac{\delta}{3}) f_p(r + su + R, u', t) du' ds dV. \qquad (4.44)$$

The form of the potential and the range of interaction for $\ell \sim L$ is similar to $\Phi^{(p)h-r}$, and in this case, no advantage is seen in adopting the form suggested by Greco and
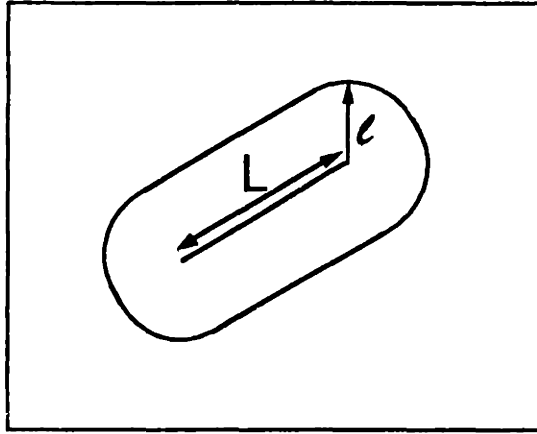
Figure 4-9: Finite range of interaction about the rigid rod.

Marrucci (1992a). Therefore, we choose $\ell \gg L$ and neglect the variation of the distribution function over the coordinate s spanning the length of the test rod (r, u). Expanding the distribution function f_p in Eq. (4.44) in a Taylor series about r yields on simplification

$$\Phi^{(p)\text{Mar}} = -\frac{3}{2}NkT(uu - \frac{1}{3}\delta):\{uu - \frac{1}{3}\delta\} - \frac{1}{16}NkT\ell^2\nabla^2(uu - \frac{1}{3}\delta):\{uu - \frac{1}{3}\delta\}. \quad (4.45)$$

The potential in Eq. (4.45), although considerably simpler than the hard-rod potential $\Phi^{(p)\text{h-r}}$ given in Eq. (4.43), retains the gradient terms, the importance of which is discussed at length in Chapter 6. The primary difference between these two alternate forms of the potential is the domain of interaction between the molecules and is of great significance in studying the nonhomogeneous aspects of the isotropic-nematic phase transition.

Comparing the three forms of the intermolecular potential listed in Table 4.2 shows that they differ in details of the nonhomogeneous terms. However, since gradient terms vanish under conditions of spatial homogeneity, all three forms are identical and reduce to the homogeneous Maier-Saupe potential. Thus, the question of choice of potential under conditions of spatial uniformity does not arise. The same is not

$\Phi^{(p)h-r}$	$-\frac{3}{2}NkT(uu - \frac{1}{3}\delta){:}\{uu - \frac{1}{3}\delta\} - \frac{1}{16}NkTL^2\nabla\nabla{:}(uuuu){:}\{uu - \frac{1}{3}\delta\}$ $-\frac{1}{16}NkTL^2\nabla\nabla{:}\{uuuu\}{:}(uu - \frac{1}{3}\delta)$
$\Phi^{(p)Mar}$	$-\frac{3}{2}NkT(uu - \frac{1}{3}\delta){:}\{uu - \frac{1}{3}\delta\} - \frac{1}{16}NkT\ell^2\nabla^2(uu - \frac{1}{3}\delta){:}\{uu - \frac{1}{3}\delta\}$
$\Phi^{(p)M-S}$	$-\frac{3}{2}NkT(uu - \frac{1}{3}\delta){:}\{uu - \frac{1}{3}\delta\}$

Table 4.2: Alternate forms of the mean-field intermolecular potential.

true in the study of nonhomogeneous systems, and the point is elaborated further in Chapter 6. In the remainder of this chapter, the equations of change are developed for an unspecified potential $\Phi^{(p)}$. Expressions for any particular choice of $\Phi^{(p)}$ can be obtained from these general equations.

4.3.3 The Equations of Change

The development in Chapter 3 is followed and a nonhomogeneous constitutive equation for the system of rigid rods is developed by taking the intermolecular forces into account with an unspecified form of the excluded volume potential.

4.3.3.1 The Species Conservation Equation and the Equation of Motion

The Hamiltonian of the entire system consisting of all the solvent and polymer molecules is written as (see Eq. (2.10))

$$\mathcal{H}^{(T)} \equiv \sum_\alpha \sum_i \left[\frac{1}{2m^\alpha}(p_c^{\alpha i})^2 + \mathcal{K}_{int} + \phi^{(e)\alpha i} + \Phi^{(p)\alpha i} \right] + \Phi \qquad (4.46)$$

where the superscript αi refers to a molecule i of species α ($\alpha = p$ or s) and

$$\mathcal{K}_{int} \equiv \frac{1}{2}\sum_{st} g_{st}\dot{Q}_s\dot{Q}_t. \qquad (4.47)$$

Note that Eq. (4.46) contains no intramolecular potential term since the polymer is modelled as a rigid rod. Also note that the excluded volume part of the intermolecular potential is approximated by a separate mean field potential $\Phi^{(p)\alpha i}$. The other

intermolecular potential term Φ is treated as before, by approximating it as a sum of two-body potentials, and is taken to result in a net hydrodynamic force exerted by the solution on the molecule of interest. From Eq. (4.46) and Eq. (2.9), Hamilton's equations of motion are written as

$$\dot{r}_c^{\alpha i} = \frac{\partial \mathcal{H}^{(T)}}{\partial p_c^{\alpha i}} = \frac{1}{m^\alpha} p_c^{\alpha i}$$

$$\dot{Q}_s^{\alpha i} = \frac{\partial \mathcal{H}^{(T)}}{\partial P_s^{\alpha i}} = \sum_t G_{st}^{\alpha i} P_{,t}^{\alpha i} = \frac{4}{L^2} \frac{1}{m_p c_{ss}} \cdot P_s$$

$$\dot{p}_c^{\alpha i} = -\frac{\partial \mathcal{H}^{(T)}}{\partial r_c^{\alpha i}} = F^{(e)\alpha i} + F^{\alpha i} + F^{(p)\alpha i}$$

$$\dot{P}_s^{\alpha i} = -\frac{\partial \mathcal{H}^{(T)}}{\partial Q_s^{\alpha i}} = \mathcal{F}_s^{(k)\alpha i} + \mathcal{F}_s^{(e)\alpha i} + \mathcal{F}_s^{(d)\alpha i} + \mathcal{F}_s^{(p)\alpha i}. \tag{4.48}$$

The forces $F^{(e)\alpha i}$ and $F^{\alpha i}$ are the total forces acting on the center of mass of molecule i of species α resulting from the external and intermolecular potentials, respectively, and also appeared in the development for Hookean dumbbells in Chapter 3; see Eq. (3.4). In addition, we now have a force $F^{(p)\alpha i}$ on the center of mass due to the excluded volume potential $\Phi^{(p)\alpha i}$. The forces ($\mathcal{F}_s^{(k)\alpha i}$, $\mathcal{F}_s^{(e)\alpha i}$, $\mathcal{F}_s^{(d)\alpha i}$, $\mathcal{F}_s^{(p)\alpha i}$) are the generalized forces on molecule αi associated with the generalized coordinates Q_s. The generalized force $\mathcal{F}_s^{(k)\alpha i}$ arises from the use of non-Cartesian coordinates, and the others originate from the external, intermolecular and excluded volume potentials, respectively. Note that $\dot{Q}_s^{\alpha i}$ in Eq. (4.48) refers only to the polymer species, and hence Eq. (4.21) has been used to simplify this term.

By using Hamilton's equations of motion as given by Eq. (4.48), the Liouville equation (3.4) for this system is written as

$$\begin{aligned}
\frac{\partial f}{\partial t} = & -\sum_\alpha \sum_i \left\{ \frac{1}{m^\alpha} p_c^{\alpha i} \cdot \frac{\partial f}{\partial r_c^{\alpha i}} + \sum_{st} G_{st}^{\alpha i} P_t^{\alpha i} \frac{\partial f}{\partial Q_s^{\alpha i}} \right. \\
& \left. + (F^{(e)\alpha i} + F^{\alpha i} + F^{(p)\alpha i}) \cdot \frac{\partial f}{\partial p_c^{\alpha i}} + \sum_s \mathcal{F}_s^{\alpha i} \frac{\partial f}{\partial P_s^{\alpha i}} \right\}
\end{aligned} \tag{4.49}$$

where $\mathcal{F}_s^{\alpha i}$ is the sum of the different generalized forces. The Liouville equation is the starting point for the further development of the constitutive equations, and the

143

different manipulations and approximations described in Section 3.3.2 are used here to derive the different equations of change.

Thus, choosing the dynamic variable given by Eq. (3.5), the polymer species conservation equation is obtained as

$$\frac{D\rho_p}{Dt} = -\nabla \cdot j_p \tag{4.50}$$

where

$$j_p = m^P \int [[\dot{r}]]^P \Psi_p dQ_s - \frac{L^2 m^P}{4} \frac{\partial}{\partial r} \cdot \int u[[\dot{u}]]^P \Psi_p dQ_s - \rho_p v \tag{4.51}$$

and $\Psi_p = \Psi_p(r, Q, t)$. The stream velocity $v(r, t)$ is the mass-average velocity.

Similarly, choosing the dynamical variable given by Eq. (3.12) and following the development in Chapter 17 of Bird $et\ al.$ (1987b) leads to the equation of motion

$$\frac{\partial}{\partial t} \rho v = -[\nabla \cdot \rho v v] - [\nabla \cdot \pi] + n\bar{F}^{(e)} - \{\nabla \Phi^{(p)}\} \tag{4.52}$$

where $n\bar{F}^{(e)}$ is defined by Eq. (3.14) and $\{\nabla \Phi^{(p)}\}$ is

$$\{\nabla \Phi^{(p)}\} = \int \nabla \Phi^{(p)} \Psi_p(r, Q, t) dQ. \tag{4.53}$$

The stress tensor π is

$$\pi = \pi^{(k)} + \pi^{(e)} + \pi^{(S)} + \pi^{(D)} + \pi^{(p)} \tag{4.54}$$

where the different contributions to the stress tensor are associated with molecular motion ($\pi^{(k)}$), external forces ($\pi^{(e)}$), use of generalized non-Cartesian coordinates ($\pi^{(S)}$), the intermolecular potential Φ ($\pi^{(D)}$) and the excluded volume potential $\Phi^{(p)}$ ($\pi^{(p)}$), respectively. In the subsequent development, external forces are not considered.

By following the development in Section 3.3.2 and Chapters 17 and 18 of Bird et

al. (1987b), the expression for the stress tensor is simplified to yield Eq. (3.18) as

$$\pi = \pi_k - \bar{N} \sum_{\alpha\nu} \int R_\nu^\alpha F_\nu^{(h)\alpha} \Psi_\alpha(r, Q, t) dQ \qquad (4.55)$$

where π_k is the stress contribution due to the motion of the beads relative to the center of mass of the molecule, $F_\nu^{(h)\alpha}$ is the hydrodynamic force acting on bead ν of a molecule of species α and $\bar{N} = \sum_\alpha x_\alpha N_\alpha$ is the average number of beads per molecule in the solution with species α having mole fraction x_α.

As in Chapter 3, further simplification of the expressions for the mass flux and stress tensor requires evaluation of averages with respect to the singlet configurational distribution functions Ψ_α for the solvent and polymer species. The solvent is treated as a continuum and the distribution function Ψ_s is not explicitly evaluated. However, a time evolution equation for Ψ_p is required along with expressions for the momentum space averages $[[\dot{r}]]$ and $[[\dot{u}]]$, and these are derived next.

4.3.3.2 Equation of Continuity for Configurational Distribution Function and Relevant Force Balances

In order to develop a continuity equation for $\Psi_p(r, Q, t)$, the dynamical variable is chosen as

$$B \equiv \sum_i \delta(r_c^{p^i} - r)\delta(Q^{p^i} - Q)\delta(p_c^{p^i} - p)\delta(P^{p^i} - P). \qquad (4.56)$$

Multiplying the Liouville equation (4.49) by B, and integrating over all phase space coordinates yields an expression for the singlet phase-space distribution equation. Further integrating over all momenta yields the equation of change for the singlet configurational distribution function as

$$\frac{\partial \Psi_p}{\partial t} = -\frac{\partial}{\partial r} \cdot ([[\dot{r}]]^p \Psi_p) - \frac{\partial}{\partial \theta}([[\dot{\theta}]]^p \Psi_p) - \frac{\partial}{\partial \phi}([[\dot{\phi}]]^p \Psi_p) \qquad (4.57)$$

or in terms of f_p as

$$\frac{\partial f_p}{\partial t} = -\frac{\partial}{\partial r} \cdot ([[\dot{r}]]^p f_p) - \frac{\partial}{\partial u} \cdot ([[\dot{u}]]^p f_p). \qquad (4.58)$$

145

Expressions for the rate of change of the center of mass and the internal configuration of the polymer are required to obtain more useful forms of Eqs. (4.57) and (4.58). As described in Chapter 3, these expressions can be obtained from the total and generalized force balances. Thus, multiplying the evolution equation for the singlet phase-space distribution equation by p and averaging over all momenta yields a total force balance as

$$\bar{N} F^{(h)p} + F^{(b)p} + F^{(p)p} = 0. \tag{4.59}$$

The acceleration terms have been dropped in writing Eq. (4.59). The total hydrodynamic force $F^{(h)p}$ is an approximation to the intermolecular force $F^{p\beta}$ between the molecule of interest and all other molecules. In developing Eq. (4.59), terms involving the divergence of a momentum flux with respect to the solution velocity v at the center of mass are identified as the Brownian motion contribution $F^{(b)p}$; see Chapter 17 of Bird $et\ al.$ (1987b) for more details. Note that external forces have been dropped in Eq. (4.59).

Next, multiplying the evolution equation for the singlet phase-space distribution equation by P_s and averaging over all momenta yields a generalized force balance as

$$\mathcal{F}_s^{(h)p} + \mathcal{F}_s^{(b)p} + \mathcal{F}_s^{(p)p} = 0. \tag{4.60}$$

As in the development of the total force balance, the acceleration terms have been neglected, as well as the external force terms. The generalized hydrodynamic force is again an approximation to the generalized intermolecular force $\mathcal{F}_s^{p\beta}$, and terms involving the derivative of a momentum flux with respect to the generalized coordinates are identified as the generalized Brownian force $\mathcal{F}_s^{(b)p}$.

The scalar generalized force balance of Eq. (4.60) can be rewritten as a vector force balance in terms of effective forces, as

$$\mathcal{F}_\nu^{(h)p} + \mathcal{F}_\nu^{(b)p} + \mathcal{F}_\nu^{(p)p} = 0 \tag{4.61}$$

146

where the effective forces $\mathcal{F}_\nu^{(\cdots)p}$ are given by

$$
\begin{aligned}
\mathcal{F}_\nu^{(\cdots)p} &= \sqrt{m}\sum_{st}\mathcal{F}_s^{(\cdots)p}G_{st}b_{\nu t}\\
&= \frac{2}{L^2}\frac{m}{m^p}L\nu\sum_s\mathcal{F}_s^{(\cdots)p}\frac{1}{c_{ss}}c_s.
\end{aligned}
\tag{4.62}
$$

The expressions for the different total and effective forces that are obtained from the equations of motion for the center-of-mass and internal coordinates are simplified further, by using approximations similar to those described in Chapter 3, and have been described below.

1. *The Hydrodynamic Drag Force.* The hydrodynamic drag force experienced by each bead as it moves through the solution is again given by Eq. (3.27) as

$$
F_\nu^{(h)p} = -\zeta \cdot \left([[\dot{r}_\nu]]^p - v_\nu\right)
\tag{4.63}
$$

where v_ν is the solution velocity at the position of bead ν and is related to the velocity at the center of mass by

$$
v_\nu = v(r) + \kappa \cdot R_\nu = v(r) + \frac{L\nu}{2}\kappa \cdot u
\tag{4.64}
$$

where $\kappa = (\nabla v)^\dagger$. Hydrodynamic interaction is again neglected. Unlike Chapter 3, in the present development the tensorial friction coefficient ζ is not assumed to be isotropic. In a solution of rigid dumbbells with some degree of orientational order, the resistance to motion in the direction perpendicular to the dumbbell axis is expected to be somewhat higher than that encountered along its axis; therefore, the model for the friction tensor should give friction coefficients that are different in the directions of dumbbell rotation and axial translation. By following Bird and DeAguiar (1983), the empiricism for ζ used in this chapter is

$$
\zeta = \zeta\left[uu + \frac{1}{\sigma}(\delta - uu)\right]
\tag{4.65}
$$

where the anisotropic drag parameter σ lies in the range $0 < \sigma \le 1$ and ζ is a

147

scalar friction coefficient. The expression for ζ can be easily inverted to give

$$\zeta^{-1} = \frac{1}{\zeta}Z = \frac{1}{\zeta}[\sigma\boldsymbol{\delta} + (1 - \sigma)\boldsymbol{uu}]. \tag{4.66}$$

When $\sigma = 1$, the friction tensor is isotropic with $\zeta = \zeta\boldsymbol{\delta}$ and $Z = \boldsymbol{\delta}$. Decreasing the value of σ corresponds to increasing the ratio of resistance encountered perpendicular to the dumbbell to that encountered along the axis. Even in dilute solutions of rigid rods, where unhindered motion is possible, exact calculations of drag around a single rod-like particle indicate that $\sigma = 0.5$ (Doi and Edwards, 1986).

The drag experienced by a rigid rod in a concentrated isotropic solution and an ordered solution with prolate symmetry can be expected to be different. In an approach such as this, where the entire effect of the surrounding medium on the anisotropic drag is described by means of a single parameter, the dependence of σ on the state of order in the surrounding medium must be considered. Moreover, in the context of a liquid crystalline system, where a transition from a disordered state to an ordered one is seen with increasing concentration, it is also necessary to include the dependence of σ on concentration. Adapting the empiricism suggested by Doi and Edwards (1986) for the rotational diffusivity, a suitable form for σ is

$$\sigma = \sigma_0 \frac{\mathcal{F}(\mathcal{N})}{(1 - (3/2)\boldsymbol{S}{:}\boldsymbol{S})^2} \tag{4.67}$$

where

$$\mathcal{F}(\mathcal{N}) = (1 + \frac{1}{\beta}\left(\frac{L}{d}\right)^2 \mathcal{N}^2)^{-1}. \tag{4.68}$$

The parameter β is theoretically estimated to be $\mathcal{O}(10)$, although experimental measurements of the rotational diffusivity indicate that the value may be as high as $10^3 - 10^4$ (Pecora, 1985). The ratio L/d is the ratio of the length to diameter of the rigid rod. Rather than consider such a complex dependence on $\boldsymbol{S}$ and $\mathcal{N}$, the parameter σ is often taken to be a constant, for the sake of simplicity.

From Eq. (3.24), the total hydrodynamic force is obtained as

$$F^{(h)p} = -2\zeta \cdot ([[\dot{r}]] - v).$$ (4.69)

The generalized hydrodynamic drag force $\mathcal{F}_s^{(h)p}$ is related to the total drag force on the bead $F_\nu^{(h)p}$ by (see Eq. 18.1-13 of Bird *et al.* (1987b))

$$\mathcal{F}_s^{(h)p} = \bar{N} \sum_\nu \frac{1}{\sqrt{m}} (b_{\nu s} \cdot F_\nu^{(h)p}).$$ (4.70)

By using Eq. (4.20) and Eq. (4.63), the above equation can be simplified to give the generalized hydrodynamic drag force as

$$\mathcal{F}_s^{(h)p} = -\bar{N} \frac{L^2}{2} c_s \cdot [\zeta \cdot ([[\dot{u}]] - \kappa \cdot u)].$$ (4.71)

The effective hydrodynamic force $\mathcal{F}_\nu^{(h)p}$ can then be written from Eq. (4.62) as

$$\mathcal{F}_\nu^{(h)p} = -\bar{N} L \nu \frac{m}{m^p} \sum_s c_s \cdot [\zeta \cdot ([[\dot{u}]] - \kappa \cdot u)] \frac{1}{c_{sn}} c_s.$$ (4.72)

2. *The Brownian Force.* The expressions for the total and generalized Brownian forces involve momentum space averages such as $[[P_t P_s]]^p$, $[[(p - m^p v)(p - m^p v)]]^p$, etc. In order to simplify these averages, an assumption of *equilibration in momentum space* is made, *i.e.*, the velocity distribution is taken to be Maxwellian about the mass average velocity v at the center of mass of the dumbbell. Then, the total Brownian force on the center of mass of the polymer is

$$F^{(b)p} = -kT \nabla \ln \Psi_p$$ (4.73)

and the generalized Brownian force $\mathcal{F}_s^{(b)p}$ is

$$\mathcal{F}_s^{(b)p} = -kT \frac{\partial}{\partial Q_s} \ln \left(\frac{\Psi_p}{\sqrt{g}} \right).$$ (4.74)

In the above expression, $g = \det(g_{st})$ and equals $L^2 m^p \sin^2 \theta / 2$. Thus, $\mathcal{F}_s^{(b)p}$ also

149

is written as

$$\mathcal{F}_s^{(b)p} = -kT\frac{\partial}{\partial Q_s}\ln f_p.$$ (4.75)

An expression for the effective Brownian force $\mathcal{F}_\nu^{(b)p}$ is obtained from Eq. (4.62). Instead of making the equilibration in momentum space assumption, Menon (1990) suggested using an anisotropic velocity distribution. By following Bird and DeAguiar (1983), the time average of the rapidly fluctuating Brownian force on bead ν was expressed in terms of the distribution function as

$$\boldsymbol{F}_\nu^{(b)} = -\nu\frac{kT}{Lf_p}\frac{\partial}{\partial u}\cdot[\boldsymbol{\xi}^{-1}f_p] \quad (\nu\pm 1)$$ (4.76)

where $\boldsymbol{\xi}^{-1}$ was taken to be a measure of the skewness in the velocity distribution, and therefore, of the anisotropy in the Brownian motion. It is likely that the Brownian force caused by bombardment and jostling of dumbbells by solvent molecules is anisotropic, due to the structural order present in concentrated or liquid-crystalline polymer solutions. However, the form given by Menon (1990) is rigorously derivable from phase-space theory only for models with no constraints, and was used by Bird and DeAguiar (1983) for solutions of flexible dumbbells. Its applicability to models with constraints such as the rigid dumbbell is questionable, and we continue to use the equilibration in momentum space approximation.

3. *Excluded Volume Force.* The transition from a disordered phase to an ordered one with increasing concentration is a consequence of the hard-body excluded volume interaction that prevents the intersection of two rigid rods. As polymer concentration increases, the intermolecular spacing decreases and the intermolecular interaction becomes stronger; the isotropic state loses stability and order develops spontaneously. The degree of alignment increases further with increase in concentration. Three alternate forms of the potential in nonhomogeneous systems were suggested in Section 4.3.2. These three forms are identical under conditions of spatial homogeneity and reduce to the Maier-Saupe poten-

tial (Maier and Saupe, 1958 & 1959) used by Doi (1981) in the development of his molecular theory.

For an unspecified intermolecular potential $\Phi^{(p)}$, the total excluded volume force on the center of mass of the dumbbell is

$$F^{(r)p} = -\frac{\partial}{\partial r}\Phi^{(p)}. \tag{4.77}$$

Similarly, the generalized excluded volume force is

$$\mathcal{F}_s^{(p)p} = -\frac{\partial}{\partial Q_s}\Phi^{(p)}. \tag{4.78}$$

The effective excluded volume force $\mathcal{F}_\nu^{(p)p}$ can then be derived from Eq. (4.62).

Substituting Eqs. (4.69)-(4.78) into the total and effective force balances (4.59) and (4.61) leads to equations for the momentum space averages $[[\dot{r}]]^p$ and $[[\dot{u}]]^p$ as

$$[[\dot{r}]]^p = v - \frac{kT}{2\zeta\bar{N}}Z \cdot \nabla \ln \Psi_p - \frac{1}{2\bar{N}\zeta}Z \cdot \nabla \Phi^{(p)}, \tag{4.79}$$

$$[[\dot{u}]]^p = \kappa \cdot u - \kappa{:}uuu - \frac{\sigma}{6\lambda}\frac{\partial}{\partial u}\ln f_p - \frac{\sigma}{6\lambda kT}\frac{\partial}{\partial u}\Phi^{(p)} \tag{4.80}$$

where $\lambda \equiv \bar{N}\zeta L^2/(12kT)$ is a time constant associated with the rotation of the rigid dumbbells. The diffusion equation for the concentrated solution of rigid dumbbells obtained by combining Eqs. (4.58), (4.79) and (4.80) is

$$\begin{aligned}
\frac{\partial f_p}{\partial t} = &- \frac{\partial}{\partial r} \cdot \left(v f_p - D_{tr} Z \cdot \nabla f_p - \frac{D_{tr}}{kT}Z \cdot \nabla \Phi^{(p)} f_p \right) \\
&- \frac{\partial}{\partial u} \cdot \left[(\kappa \cdot u - \kappa{:}uuu)f_p - \frac{\sigma}{6\lambda}\frac{\partial f_p}{\partial u} - \frac{\sigma}{6\lambda kT}\frac{\partial \Phi^{(p)}}{\partial u}f_p \right].
\end{aligned} \tag{4.81}$$

Equation (4.81) governs the evolution of the distribution function under the influence of different flow fields.

4.3.3.3 The Mass Flux Vector and The Stress Tensor

The expression for the mass flux Eq. (4.51) when combined with Eqs. (4.79) and (4.80) yields on simplification

$$
\begin{aligned}
j_p = \ & -\frac{kT}{2\bar{N}\zeta}Z\cdot\nabla\rho_p + m^p\left(\frac{3}{2}N\right)\frac{kT}{2\bar{N}\zeta}Z\cdot\left(\nabla\{uu-\frac{\delta}{3}\}\right):\{uu-\frac{\delta}{3}\} \\
& -\frac{L^2 m^p}{4}\nabla\cdot\left(\{uu\}\cdot\kappa^\dagger\right) + \frac{L^2 m^p}{4}\nabla\cdot(\kappa:\{uuuu\}) \\
& +\frac{L^2 m^p}{8\lambda}\nabla\cdot\{uu-\frac{\delta}{3}\} - \frac{L^2 m^p}{8\lambda}N\nabla\cdot\left(\{uu\}\cdot\{uu-\frac{\delta}{3}\}\right) \\
& +\frac{L^2 m^p}{8\lambda}N\nabla\cdot\left(\{uuuu\}:\{uu-\frac{\delta}{3}\}\right).
\end{aligned}
\tag{4.82}
$$

In the above equation, all terms that are multiplied by L^2 result from an explicit treatment of the rigid dumbbell as an extended object in space, as explained in Chapter 3. These terms can be simply ignored, if one is not interested in considering nonhomogeneities in stress and velocity fields across the length of the polymer.

The expression for the stress tensor is simplified to

$$
\pi = \pi_s + 2nkT\delta - 3kT\{uu\} - 6\lambda kT\kappa:\{uuuu\} - \left\{u\frac{\partial\Phi^{(p)}}{\partial u}\right\}.
\tag{4.83}
$$

On subtracting the equilibrium contribution $p\delta = p_s\delta + nkT\delta$, the expression for the total deviatoric stress is

$$
\tau = \tau_s + \tau_p
\tag{4.84}
$$

where the solvent contribution to the stress is

$$
\tau_s = -\eta_s\dot{\gamma}
\tag{4.85}
$$

and the polymeric contribution to the stress is given by

$$
\tau_p = -3kT\{uu - \frac{1}{3}\delta\} - 6\lambda kT\kappa:\{uuuu\} - \left\{u\frac{\partial\Phi^{(p)}}{\partial u}\right\}.
\tag{4.86}
$$

Note that when either $\Phi^{(p)h-r}$ or $\Phi^{(p)Mar}$ are substituted in Eq. (4.86), terms involving

gradients of the structure tensor S are obtained; these terms are the analogue of the *Ericksen stresses* seen in the LEP theory of low-molecular-weight nematics.

The diffusion equation for the configurational distribution function f_p and the expressions for the mass flux vector j_p and the stress tensor τ_p derived in Sections 4.3.3.2 and 4.3.3.3 complete the development of the nonhomogeneous constitutive theory for concentrated rigid rod-like polymeric solutions. These equations can be simultaneously solved with the hydrodynamic equation of motion and the species conservation equation to generate self-consistent stress, velocity and concentration profiles in any fluid mechanical problem.

This theory differs from the nonhomogeneous dilute solution theory for Hookean dumbbell solutions in two significant ways. First, polymer-polymer interactions are considered in the concentrated solution theory. In fact, the isotropic-nematic transition that is the subject of study is a consequence of the hard-rod excluded volume interactions between a pair of rigid rods. A suitable extension of the homogeneous excluded volume potential (Onsager, 1949; Maier and Saupe, 1958 & 1959; Doi, 1981) to nonhomogeneous systems that accounts for the finite spatial extent of the rigid rods was considered, and some alternative forms of the potential were developed. These forms reduce to the same expression under conditions of spatial homogeneity, and differ in their treatment of the range of interaction between interacting rigid rods. The difference between the different forms can be appreciated in studying the nonhomogeneous aspects of the problem; see Chapter 6.

The second difference arises in the use of the governing equations (4.81)-(4.86) for the solution of any flow problem. It is convenient in the development of the theory for Hookean dumbbells to rewrite the diffusion equation for the configurational distribution function in terms of the second moment with respect to the connector vector. A closed set of equations is obtained, and the computational complications associated with solving for the entire distribution function is avoided. The same procedure can be adopted for the rigid-rod solutions, in principle. However, in doing so, a closed set of equations is not achieved; the equation for the second moment involves the fourth moment and so on. Further simplification is achieved by rewriting higher-order mo-

ments in terms of lower-order ones. This technique has been used in Chapter 5 to study the effect of different flow-fields on the I-N transition. The advantages and disadvantages of this approach also are discussed there. The alternative is to either solve for the distribution function numerically or study a linearized system of equations near a known base state. The former allows the study of all aspects of problem, and has been adopted in the study of homogeneous problem (Larson, 1990; Larson and Öttinger, 1991); however, due to the computational intensity only discrete values of the independent variables, such as concentration and deformation rate, can be studied in detail. The application of these techniques to *spatially nonhomogeneous* problems does not seem to be practical with the available computational facilities. The latter alternative is incapable of studying nonlinear phenomena and the effects of large deviations from the base state; however, it provides a viable means of testing the theory that is developed here. This latter approach has been adopted in Chapter 6 for the study of development of structure at the I-N transition point.

Chapter 5

Homogeneous Theory for Liquid Crystalline Polymers: Microstructure and Material Function Predictions

The isotropic-nematic transition with and without flow is studied in this chapter for homogeneous systems. The governing equations are obtained from Eqs. (4.81)-(4.86) by making an assumption of spatial homogeneity. A complete picture of coexisting phases is developed and material functions are obtained in the different phases. This study of a wide range of concentrations and deformation-rates is made possible, in part, by a mathematical simplification whereby the equation for the distribution function is written entirely in terms of the second-order moment with the help of closure approximations. The effect of such approximations on the predictions of the model also is discussed.

5.1 The Constitutive Equation

Making the assumption of spatial homogeneity allows the factorization of the distribution function f_p as

$$f_p(\boldsymbol{r}, \boldsymbol{u}, t) = n f_p(\boldsymbol{u}, t) \tag{5.1}$$

where the number density $n = n_{av}$ is a constant throughout the system. The homogeneous distribution function $f_p(\boldsymbol{u}, t)$ is normalized such that

$$\int f_p(\boldsymbol{u}, t) d\boldsymbol{u} = 1 \tag{5.2}$$

and ensemble averages with respect to $f_p(\boldsymbol{u}, t)$ are defined such that

$$\langle B \rangle \equiv \int B f_p(\boldsymbol{u}, t) d\boldsymbol{u} \tag{5.3}$$

where B is any function of $\boldsymbol{u}$. Although the same notation f_p is used to describe both the spatially-dependent and -independent distribution functions, averages with respect to the two are distinguished by the notation $\{\ \}$ and $\langle\ \rangle$, respectively. It follows from Eq. (5.1) that the two averages are related by

$$\langle B \rangle = \frac{1}{n} \{B\}. \tag{5.4}$$

Thus, the structure tensor in the homogeneous problem is defined as

$$\boldsymbol{S} \equiv \langle \boldsymbol{u}\boldsymbol{u} - \frac{1}{3}\boldsymbol{\delta} \rangle. \tag{5.5}$$

Under the assumption of spatial homogeneity, the three alternative forms of the intermolecular potential (see Table 4.2) reduce to the Maier-Saupe excluded volume potential which is written as

$$\begin{aligned}
\Phi^{(p)\text{M-S}} &= -\frac{3}{2}\mathcal{N}kT(\boldsymbol{u}\boldsymbol{u} - \frac{1}{3}\boldsymbol{\delta}):\langle \boldsymbol{u}\boldsymbol{u} - \frac{1}{3}\boldsymbol{\delta} \rangle \\
&= -\frac{3}{2}\mathcal{N}kT(\boldsymbol{u}\boldsymbol{u} - \frac{1}{3}\boldsymbol{\delta}):\boldsymbol{S}.
\end{aligned} \tag{5.6}$$

By substituting Eq. (5.6) into Eq. (4.81) and factoring the distribution function as indicated in Eq. (5.1), the diffusion equation for the distribution function is written as

$$\frac{\partial f_p}{\partial t} = -\frac{\partial}{\partial u} \cdot \left[(\kappa \cdot u - \kappa{:}uuu)f_p - \frac{\sigma}{6\lambda}\frac{\partial f_p}{\partial u} + \frac{\mathcal{N}\sigma}{4\lambda}\frac{\partial}{\partial u}[(uu - \frac{1}{3}\delta){:}S]f_p \right]. \quad (5.7)$$

The anisotropic drag parameter σ is taken to be a constant, for the sake of simplicity. An evolution equation for the structure tensor $S \equiv \langle uu - \frac{1}{3}\delta \rangle$ is obtained from Eq. (5.7) by taking the second moment over u to yield

$$\langle uu \rangle_{(1)} = -\frac{\sigma}{\lambda}\langle uu - \frac{1}{3}\delta \rangle - 2\kappa{:}\langle uuuu \rangle + \frac{\mathcal{N}\sigma}{2\lambda}\left[\langle uu - \frac{1}{3}\delta \rangle \cdot \langle uu \rangle \right.$$
$$\left. + \langle uu \rangle \cdot \langle uu - \frac{1}{3}\delta \rangle \right] - \frac{\mathcal{N}\sigma}{\lambda}\langle uu - \frac{1}{3}\delta \rangle{:}\langle uuuu \rangle \quad (5.8)$$

where the subscript (1) denotes the contravariant codeformational derivative defined in Eq. (2.25). Equation (5.8) governs the evolution of the structure in liquid crystalline solutions undergoing flow.

Similarly, substituting Eq. (5.6) into Eqs. (4.84)-(4.86) and simplifying for spatial homogeneity yields the expression for the stress tensor in homogeneous systems as

$$\tau = -\eta_s\dot{\gamma} - 3nkT\langle uu - \frac{1}{3}\delta \rangle - 6\lambda nkT\kappa{:}\langle uuuu \rangle$$
$$+ 3\mathcal{N}nkT\langle uu \rangle \cdot \langle uu - \frac{1}{3}\delta \rangle - 3\mathcal{N}nkT\langle uuuu \rangle{:}\langle uu - \frac{1}{3}\delta \rangle. \quad (5.9)$$

Note that because the polymer number density is assumed constant, the equation for the mass flux vector (4.82) is redundant.

Equation (5.7) for the distribution function and expression (5.9) for the stress tensor along with the hydrodynamic equations of motion and continuity form an exact and complete set of equations that can be solved, in principle, for the velocity, stress, pressure and microstructure fields in the system. The numerical solution of Eq. (5.7) is computationally intensive and allows the study of only a few discrete values of concentration and deformation rates; it is preferable to use the moment

equation (5.8) to solve for the structure tensor S. However, both equations (5.8) and (5.9) involve the fourth rank tensor $\langle uuuu \rangle$, which also must be obtained. A closure problem arises because the evolution equation for $\langle uuuu \rangle$ (obtained by taking the fourth moment over u of the diffusion equation) involves the sixth rank tensor $\langle uuuuuu \rangle$. This is a common problem encountered in kinetic theory developments that involve molecular models with constraints, as discussed in Section 2.3.2, and requires closure approximations to express higher-order moments in terms of lower ones. The quadratic closure approximations are made in this development (Doi, 1980 &1981)

$$S{:}\langle uuuu \rangle \approx S{:}\langle uu \rangle \langle uu \rangle;$$

$$\kappa{:}\langle uuuu \rangle \approx \kappa{:}\langle uu \rangle \langle uu \rangle. \tag{5.10}$$

These approximations maintain the trace of the governing equations and are exact in the limit of perfect orientational order. By using these relations, Eqs. (5.8) and (5.9) are written in terms of the homogeneous second moment $\langle uu \rangle$. Rewriting $\langle uu \rangle$ in terms of the structure tensor S given by Eq. (5.5) yields the evolution equation for the structure tensor as

$$S_{(1)} = F(S) + G(S, \kappa), \tag{5.11}$$

where

$$F(S) = -\frac{\sigma}{\lambda} \left[(1 - \frac{\mathcal{N}}{3})S - \mathcal{N}(S \cdot S) + \mathcal{N}(S{:}S)(S + \frac{1}{3}\delta) \right] \tag{5.12}$$

with $\mathcal{N} = Nn$, and

$$G(S, \kappa) = \frac{1}{3}\dot{\gamma} - 2(\kappa{:}S)(S + \frac{1}{3}\delta). \tag{5.13}$$

Equations (5.11)-(5.13) determine the structure tensor for a given flow field. Doi's equation for the structure tensor is recovered by simply replacing the factor (σ/λ) by $(6\bar{D}_r)$, where $\bar{D}_r$ is an averaged rotational diffusion coefficient (Doi, 1981); see Section 4.2.2.

Similarly, on making these transformations in Eq. (5.9) the homogeneous stress

tensor expression is obtained as

$$\tau = -\eta_s\dot{\gamma} - 3nkT\left[(1 - \frac{\mathcal{N}}{3})S - \mathcal{N}(S\cdot S) + \mathcal{N}(S{:}S)(S + \frac{1}{3}\delta) + 2\lambda(\kappa{:}S)(S + \frac{1}{3}\delta)\right].$$
(5.14)

The last term in Eq. (5.14) is the viscous stress term that was dropped in the Doi model; see Section 4.2.2. Equations (5.11)-(5.14) form a complete constitutive theory for homogeneous liquid crystalline polymers, and are identical to the equations derived by Menon (1990). These equations can now be solved together with the equations of motion and continuity for any arbitrary flow field. Menon (1990) has demonstrated this for a flow between two eccentric cylinders.

5.2 Phase Behavior and Microstructure Predictions

The microstructure of the fluid at rest, in simple shear flow, and in shearfree flows is determined by solving Eq. (5.11) numerically using Newton's method with the appropriate kinematics as input. Dimensionless forms of the velocity gradient and stress tensors are defined as

$$\begin{aligned}
\hat{\kappa} &\equiv \frac{\lambda}{\sigma}\kappa, \\
\hat{\tau} &\equiv \frac{\mathcal{N}}{nkT}\kappa.
\end{aligned}$$
(5.15)

Material functions for the fluid are calculated by using the dimensionless form of Eq. (5.14). The choice of the scaling for the velocity gradient ensures that the dimensionless equation for the evolution of S is independent of the parameter σ.

In the following sections, we consider the cases (a) equilibrium, (b) simple shear flow described by the velocity field

$$v_1 = \dot{\gamma}x_2, \quad v_2 = v_3 = 0$$
(5.16)

where $\dot{\gamma}$ is the (dimensional) shear rate, and (c) elongational flows described by the velocity field

$$
\begin{aligned}
v_1 &= \dot{\epsilon} x_1, \\
v_2 &= -\frac{1}{2}\dot{\epsilon} x_2, \\
v_3 &= -\frac{1}{2}\dot{\epsilon} x_3,
\end{aligned}
\tag{5.17}
$$

where $\dot{\epsilon}$ is the (dimensional) elongational rate. Positive values of $\dot{\epsilon}$ correspond to uniaxial elongational flow and negative values of $\dot{\epsilon}$ denote biaxial stretching. In the subsequent discussion, dimensionless shear and elongational rates are denoted as $\hat{\dot{\gamma}}$ and $\hat{\dot{\epsilon}}$, respectively.

5.2.1 Equilibrium Microstructure and Phase Behavior

The predictions of the constitutive equation for the equilibrium phase transition from the isotropic state to the nematic liquid crystalline phases are given by the structure evolution equation, Eq. (5.11), with $v = \kappa = 0$, or

$$
\frac{\partial S}{\partial t} = F(S)
\tag{5.18}
$$

The isotropic state $S = 0$ is spherosymmetric and possesses $SO(3)$ symmetry (Chuang $et\ al.$, 1991). The anisotropic nematic state shows uniaxial symmetry about an arbitrary direction n, $i.e.$, an $O(2)$ type symmetry. However, at equilibrium there is no external field (hydrodynamic or otherwise) for orienting the anisotropic states. Therefore, the solutions to the equilibrium problem are expected to be rotationally invariant; $i.e.$, in the absence of any external field, there is no preferred orientation of the nematic phases.

The director n is unspecified as a consequence of the rotational invariance displayed at equilibrium. This is shown by substituting Eq. (4.25) into Eq. (5.18) and

160

collecting terms in S and n to yield

$$\mathcal{Y}(S)(nn - \tfrac{1}{3}\delta) = S\left[(1 - \tfrac{\mathcal{N}}{3}) - \tfrac{1}{3}\mathcal{N}S + \tfrac{2}{3}\mathcal{N}S^2\right](nn - \tfrac{1}{3}\delta) = 0. \qquad (5.19)$$

The cubic equation $\mathcal{Y}(S) = 0$ admits three distinct solutions which correspond to arbitrary orientations given by n. These solutions for the order parameter S are

$$
\begin{aligned}
S_1 &= 0, \\
S_2 &= \frac{1}{4} + \frac{3}{4}\left[1 - \frac{8}{3\mathcal{N}}\right]^{\frac{1}{2}}, \\
S_3 &= \frac{1}{4} - \frac{3}{4}\left[1 - \frac{8}{3\mathcal{N}}\right]^{\frac{1}{2}}
\end{aligned}
\qquad (5.20)
$$

and are independent of the parameter σ. Doi (1981) also obtained the cubic equation (5.19); however, he considered only solutions S_1 and S_2. These multiple states are represented by the bifurcation diagram shown in Fig. 5-1. Here the two nematic phases given by the solutions S_2 and S_3 make up a transcritical bifurcation from the isotropic base state $S_1 = 0$. Nematic phases that have prolate symmetry with $S > 0$ are referred to as 'Nematic P', and the nematic phases that have oblate symmetry with $S < 0$ are referred to as 'Nematic O'.

The degeneracy of the equilibrium solutions caused by the rotational invariance complicates the analysis of the stability of the nematic phases. In fact, the simple decomposition (4.25) can give misleading conclusions. For example, if only the scalar orientation parameter is taken to be a function of time, *i.e.*, $S = S(t)(nn - \delta/3)$, then the stability of each phase is dictated by the dynamics of the one-dimensional equation $\partial S/\partial t = \mathcal{Y}(S)$. The analysis of a transcritical bifurcation (Iooss and Joseph, 1980) in the one-dimensional system does not portray the correct picture of the stability of the liquid crystalline system, because it completely ignores the destabilizing effects of fluctuations in the director vector n and leads to erroneous results.

The $O(2)$ symmetry inherent in the equilibrium system makes it feasible to apply normal form analysis that exploits this symmetry to give descriptions of the nematic solutions and their stability local to the bifurcation point (Golibutsky and Schaeffer,
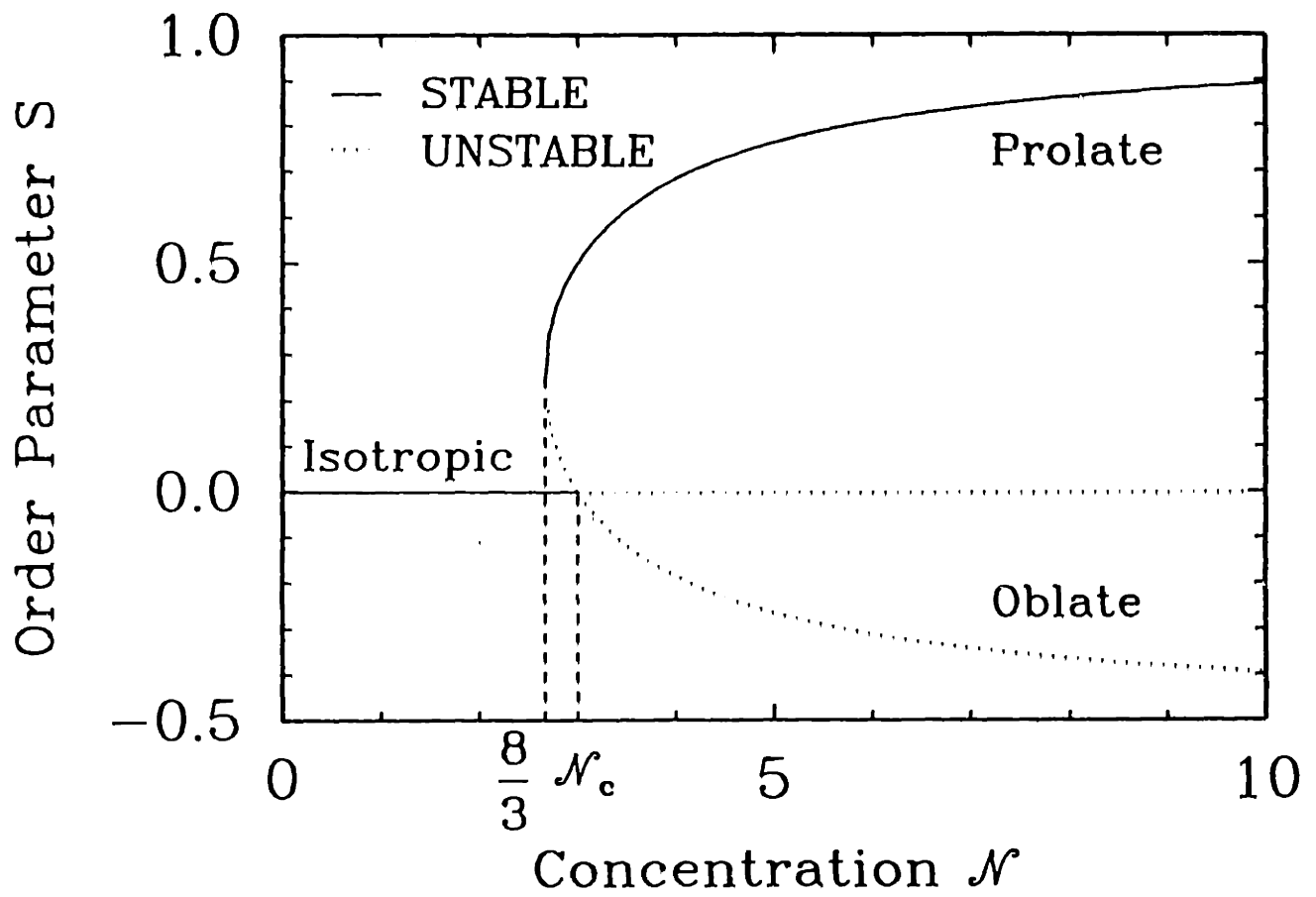
Figure 5-1: Equilibrium phase diagram.

1982; Chossat *et al.*, 1990). However, because of the small size of the equation set (5.11)-(5.13) and our desire to study the nonlinear solutions far from onset, we have chosen instead to compute numerically the equilibrium solutions as a function of $\mathcal{N}$.

Equations (5.11)-(5.13) are written in rectangular Cartesian coordinates. In order to facilitate numerical solution of this set, we arbitrarily set all the off-diagonal elements of the matrix S to zero. Moreover, using the condition that $\text{tr}(S) = 0$ reduces the set to two equations for (S_{11}, S_{22}). These equations are solved by Newton's method and the eigenvalues of the time-dependent set linearized about the equilibrium solution are computed to determine the stability of the state. Setting the off-diagonal elements to zero tacitly assumes that the nematic phases are oriented in the three primary directions x_1, x_2, and x_3. However, it is important to remember that these computed solutions are only three of the infinite number of possibilities, because the director n can be oriented in *any arbitrary direction*. The other orientations of the nematic phase can be accessed by rotation of the three primary solutions.

The isotropic state exists for all concentrations $\mathcal{N}$, but is linearly stable only in the range $0 \leq \mathcal{N} \leq 3$. At $\mathcal{N} = \mathcal{N}_c = 3$, the nematic P and nematic O liquid crystalline phases bifurcate transcritically from the isotropic state, which becomes unstable for $\mathcal{N} > 3$. The critical concentration $\mathcal{N}_c = 3$ is often termed as the *spinodal concentration*, since the *spinodal* denotes the limit of stability of a given phase. As mentioned before, the nematic O phase corresponds to molecules randomly aligned in planes orthogonal to n. This phase evolves with increasing concentration from $\mathcal{N} = 3$ toward the asymptotic limit of $S = -1/2$ for $\mathcal{N} \gg 1$ and is always unstable at equilibrium. This instability is physically reasonable, because orientation along the director is expected to be preferred as $\mathcal{N}$ is increased and the importance of the excluded volume interaction grows. No random molecular arrangement may be supported at high concentrations.

The nematic P phase shown in Fig. 5-1 is initially unstable as it branches from the isotropic state at $\mathcal{N} = 3$ towards lower $\mathcal{N}$. A limit point is reached at $\mathcal{N} = 8/3$, where the nematic phase regains stability and develops towards higher $\mathcal{N}$. In the limit of high $\mathcal{N}$, the nematic P phase tends toward the asymptotic limit $S = 1$, which

corresponds to rods oriented perfectly parallel to the director vector.

The bifurcation analysis indicates that at equilibrium, for $\mathcal{N} < 8/3$, only a stable isotropic phase exists. There are two stable equilibrium phases in the range $8/3 \leq \mathcal{N} \leq 3$, where both the isotropic and nematic P states are stable. For $\mathcal{N} > 3$, only the nematic P phase exists, since the system is unable to support the random in-planar arrangement of the nematic O phase.

5.2.2 Effect of Flow on Bifurcation Diagram: Structural Order

Introducing flow destroys the rotational invariance of the equilibrium states and introduces preferred directions for the alignment of the nematic phases. As shown below, this loss of symmetry breaks the transcritical bifurcation between the isotropic and nematic states and results in smooth transitions between the isotropic-like and nematic states as well as the formation of some parametrically isolated nematic structures. Specific representative initial orientations are investigated to illustrate the effect of the initial, equilibrium orientation on the evolution of S in these flows. The effects of shear and shearfree flows are studied, with kinematics given by Eqs. (5.16) and (5.17), respectively, by solving the nonlinear equations for components (S_{11}, S_{22}, S_{12}). The component S_{33} has been eliminated by using the condition tr$S = 0$. The results are described next for these two types of kinematics.

5.2.2.1 Steady Shear Flow

The liquid crystalline phases can be initially oriented in infinitely many directions with respect to the direction of shear. The multiple orientations for the equilibrium phases suggest that different types of molecular dynamics and structural order will occur depending on the relationship between the direction of shear and the director vector for the equilibrium phase. The three representative initial orientations chosen in this study correspond to selecting the director n as either δ_1, δ_2, or δ_3, that is, as a unit vector in the direction of flow x_1, the direction of velocity variation x_2, or

164

the neutral direction x_3, respectively (cf. Eq. (5.16)). These states are referred to as 1, 2 and 3, respectively, and the results for the three orientations of the director are presented separately.

Director in the 1-direction. Introducing shearing in the direction of the director vector breaks the transcritical bifurcation between the isotropic and nematic phases at equilibrium to give two isolated sequences of states, as shown in Fig. 5-2. The family P1 shown in Fig. 5-2 corresponds to nematic P phases that are oriented with the director in the direction of flow, and the states O1 are nematic O phases with the molecules lying randomly in the plane of shear.

The breaking of the transcritical bifurcation that exists at equilibrium is predicted from the elementary theory of imperfections in bifurcation problems (Iooss and Joseph, 1980). The two broken families P1 and O1 closely follow the equilibrium phase diagram and move apart as $\dot\gamma^{1/2}$ for low shear rates (Menon, 1990). Adding shear flow replaces the abrupt transition at equilibrium with a gradual change in the structural order. The stability of the broken families also follows from the stability of the equilibrium states.

The P1 family emanates from the $\mathcal{N} = 0$ limit and is initially stable. This evolution indicates that shear flow tends to orient the molecules in the direction of flow. At low shear rates, the P1 family loses stability at a turning point $\mathcal{N} = \mathcal{N}_{c2}^s$, regains stability at a second turning point $\mathcal{N} = \mathcal{N}_{c1}^s$, and then evolves stably to higher values of $\mathcal{N}$. Thus, hysteresis is predicted at low shear rates; two stable nematic P phases exist along the P1-family in the range $\mathcal{N}_{c1}^s \leq \mathcal{N} \leq \mathcal{N}_{c2}^s$ with varying degree of order, as shown in Fig. 5-2. As $\mathcal{N}$ is increased, the nematic phases along the P1 family develop perfect prolate symmetry in the 1-direction.

The effect of increasing the shear rate $\dot\gamma$ on the P1 and O1 nematic states is shown in Fig. 5-3. At a critical value of $\dot\gamma$ the two limit points $\mathcal{N}_{c1}^s$ and $\mathcal{N}_{c2}^s$ coalesce, and the hysteresis disappears. The transition in the structural order parameter becomes more gradual with increasing $\dot\gamma$. The behavior at high concentrations is controlled by the intermolecular interaction and resembles closely the equilibrium solution for the

165
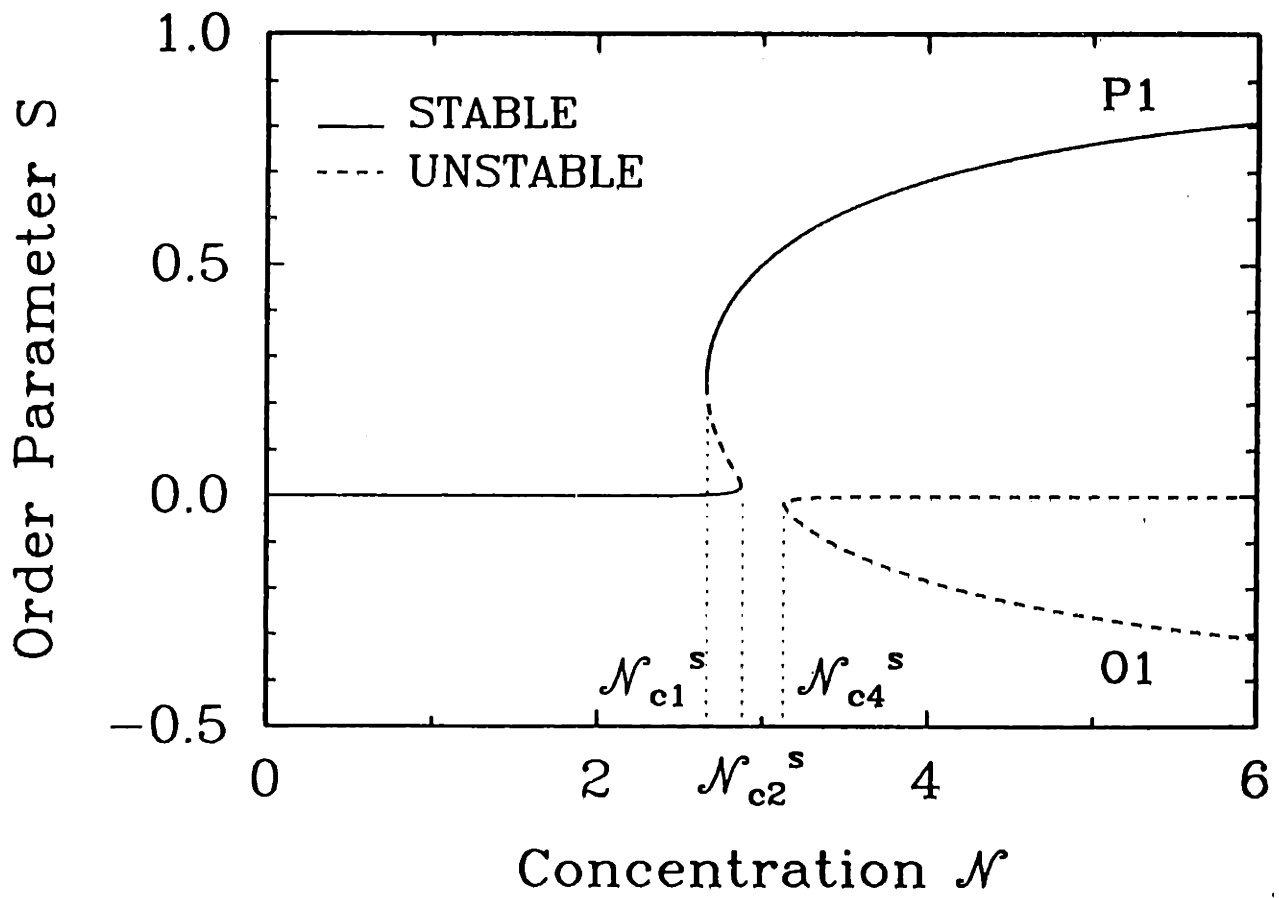
Figure 5-2: Break-up of transcritical bifurcation in the presence of flow for $\hat{\dot{\gamma}} = 0.001$ and initial orientation $n = \delta_1$.
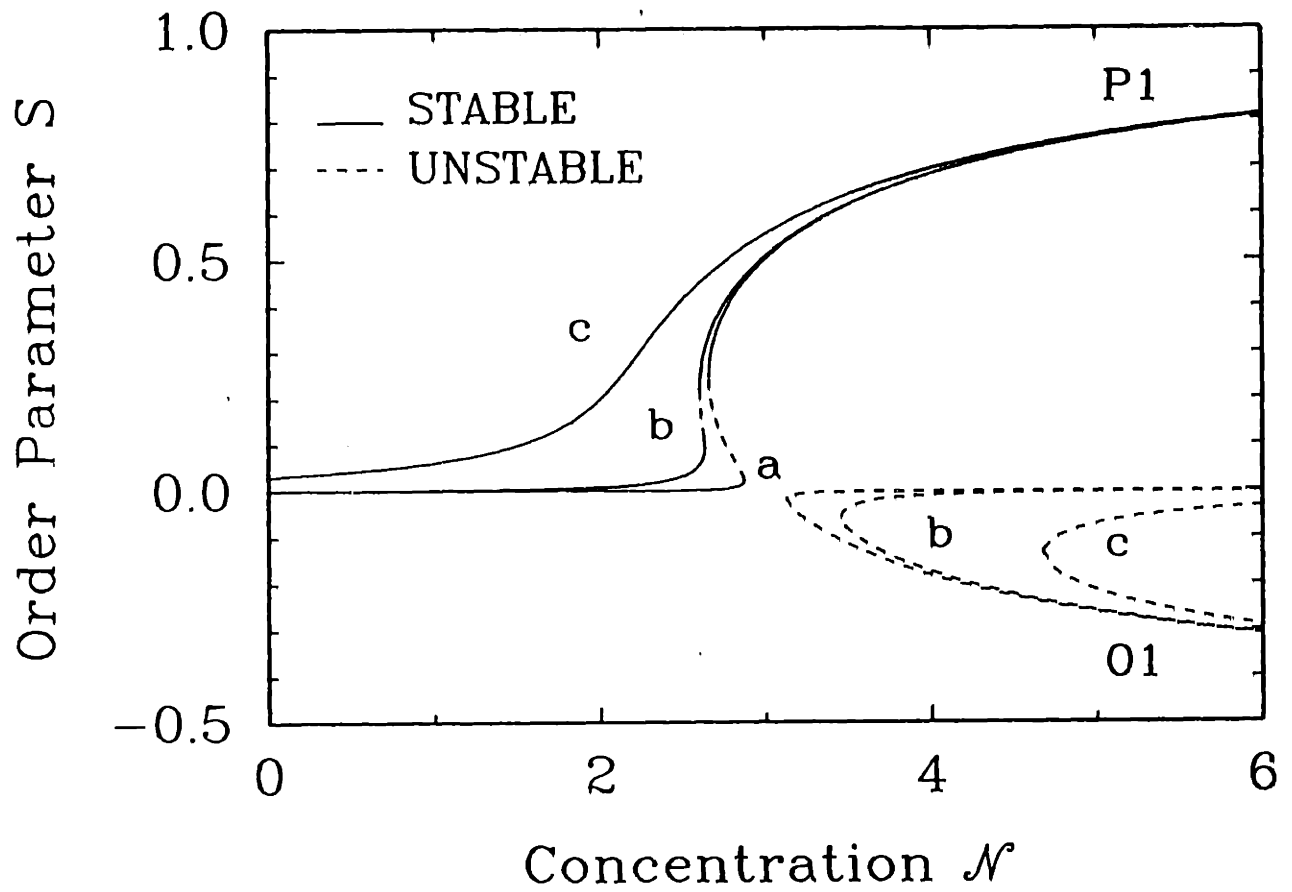
Figure 5-3: Break-up of transcritical bifurcation for $\dot{\gamma}$ of (a) 0.001, (b) 0.01 and (c) 0.1 and initial orientation $n = \delta_1$.

P1 family. The states in the O1 family move to increasing $\mathcal{N}$ with increasing $\dot{\gamma}$ and, being unstable, are of little interest.

Director in the 3-direction. Calculations with increasing $\dot{\gamma}$ also were begun with the nematic phase oriented in the 3-direction at equilibrium. The families of P3 and O3 states are shown in Fig. 5-4 as functions of $\dot{\gamma}$ and $\mathcal{N}$. The phases in the P3 family have prolate symmetry with the molecules oriented in the 3-direction, the direction of vorticity. The P3 phases are stable and develop perfect prolate symmetry for $\mathcal{N} \gg 3$. A limit point $\mathcal{N} = \mathcal{N}_{c3}^s$ is encountered along the P3 family at lower values of $\mathcal{N}$, where the solutions lose stability and evolve to higher values of $\mathcal{N}$ along family O3. The O3 family is composed of nematic O phases, with the molecules lying randomly in the plane of shear; these states are unstable. The limit point $\mathcal{N} = \mathcal{N}_{c3}^s$ evolves to higher $\mathcal{N}$ with increasing $\dot{\gamma}$. For any $\dot{\gamma}$, the P3 phase is stable only for concentrations greater than a critical value $\mathcal{N} = \mathcal{N}_{c3}^s$. Below $\mathcal{N} = \mathcal{N}_{c3}^s$, the P3 states cease to exist and the molecules rotate to align with the flow direction, and the structure is again described by the P1 family.

Recent calculations by Larson and Öttinger (1991) also indicate the existence of the P3 family, referred to as a "log-rolling" configuration by these authors. Their calculations involve a numerical solution of the distribution function, with a slightly different expression for the excluded volume mean-field potential, and avoid the use of any closure approximations. The behavior of the P3 family described above agrees with the calculations of Larson and Öttinger (1991).

Director in the 2-direction. Steady state shear flow calculations were attempted with the equilibrium nematic phases in the direction of the velocity gradient, but failed to find any steady configurations that preserved this orientation. In all cases, the Newton iteration converged to the P1 nematic phase with the appropriate value of $\mathcal{N}$. Not surprisingly, no steady-state nematic phases aligned in the 2-direction are possible in shear flow, which tends to rotate the polymer molecules into the 1-direction. However, calculations by Marrucci and Maffettone (1989) and Larson and
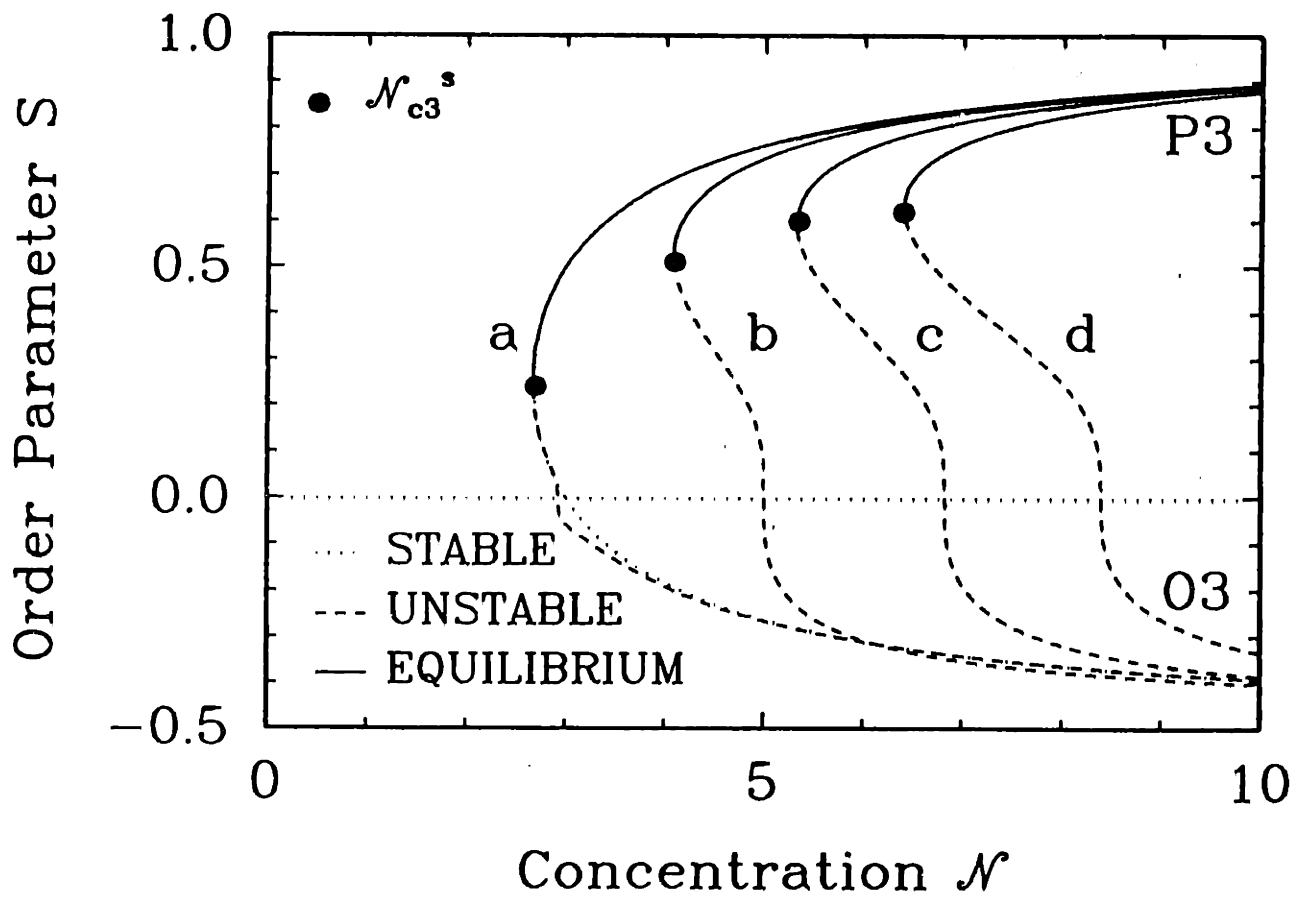
Figure 5-4: Variation of order with concentration for $\hat{\gamma}$ of (a) 0.01, (b) 1.0, (c) 2.0 and (d) 3.0 and initial orientation $n = \delta_3$.

Öttinger (1991) based on direct solution for the distribution function suggest that, at low shear rates, time-periodic states may evolve from equilibrium states with $n = \delta_2$. These states correspond to molecular tumbling in the 12-plane and have been referred to as "tumbling" and "wagging" states (Marrucci and Maffettone, 1989; Larson, 1990; Larson and Öttinger, 1991). Time-periodic states with uniaxial prolate alignment in the 23-plane have also been predicted and are referred to as "kayaking" modes (Larson and Öttinger, 1991). The relevance of molecular tumbling in rheological predictions is discussed at length in Section 5.3.4.

An attempt was made to find the tumbling states by time integration of the equation set (5.11)-(5.13) by starting with a nematic P phase oriented with $n = \delta_2$ and $\dot{\gamma} \ll 1$. No time-periodic states were found. In all transient simulations, the initial equilibrium state $n = \delta_2$ evolved to a stable nematic P phase in the P1 family. Moreover, the initial portion of the transient was monotonic in time and hence showed no signs of unstable oscillation. We can only conclude that the constitutive equation (5.11) cannot predict the tumbling modes. This failure has been ascribed before to the use of the quadratic closure approximations (5.10) in deriving these equations (Larson and Öttinger, 1991; Marrucci and Maffettone, 1989; Larson, 1990; Kuzuu and Doi, 1984), that can be avoided by directly computing the distribution function. However, in a typical fluid mechanics problem in two- or three-dimensions, direct computation of the distribution function even for a simple dumbbell model is computationally intensive (Advani and Tucker, 1987). Instead, alternative closure approximations can be used to overcome the drawbacks of the quadratic closure approximation. These approximations and their advantages and drawbacks are discussed at greater length in Section 5.4.

Depending on the values of $\mathcal{N}$ and $\dot{\gamma}$, multiple phases with different orientation and degree of orientational order are predicted. The different multiphasic regions are plotted in Fig. 5-5 as a function of $\mathcal{N}$ and $\dot{\gamma}$. At low shear rates, several phases are predicted to be stable. At low concentrations, $\mathcal{N} < \mathcal{N}_{c1}^s$, a single P1 phase is stable. In the concentration range, $\mathcal{N}_{c1}^s \leq \mathcal{N} \leq \mathcal{N}_{c2}^s$ and $\mathcal{N} < \mathcal{N}_{c3}^s$, a biphasic mixture is present, with the two flow-aligned nematic P phases having different degrees of
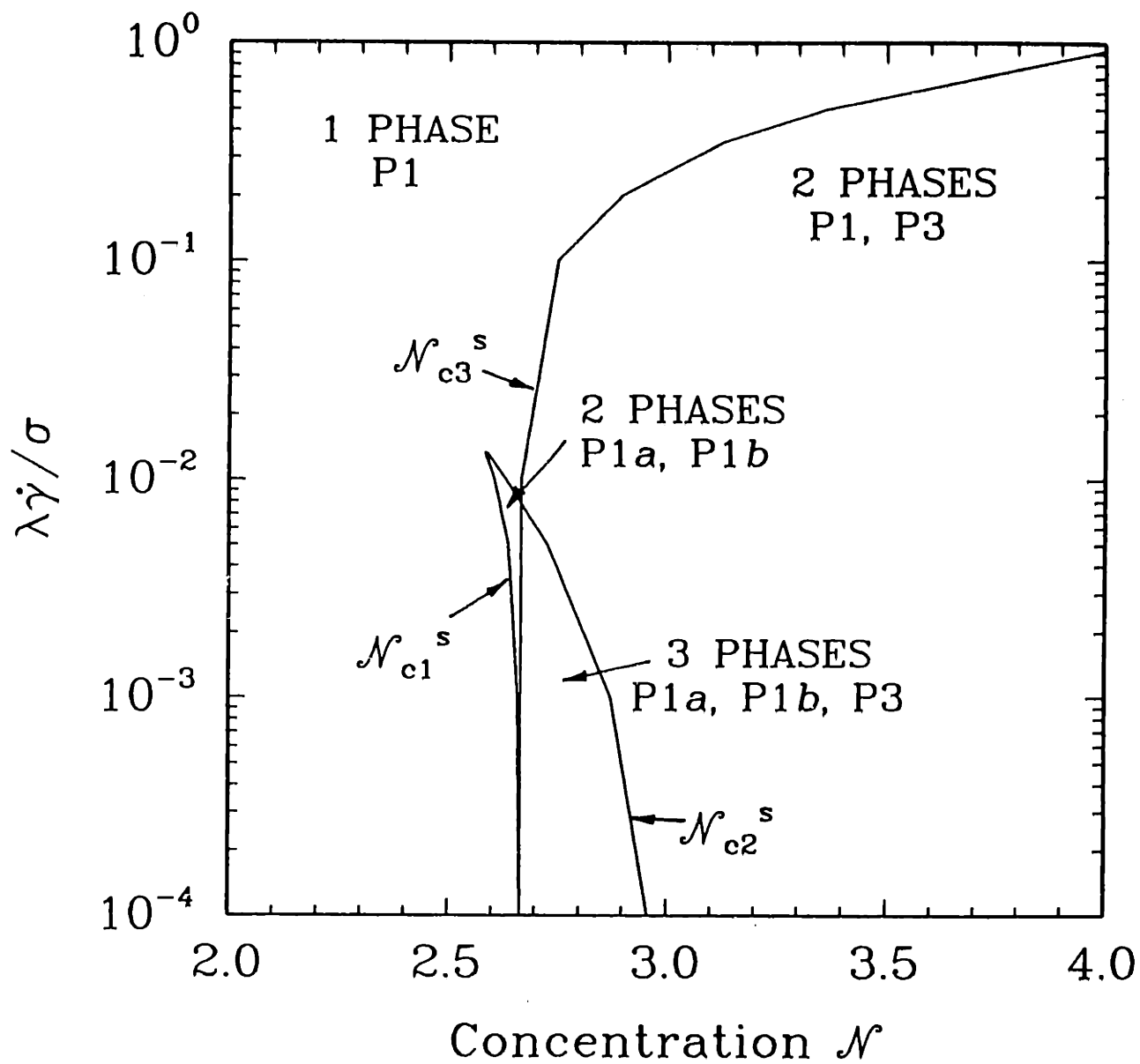
Figure 5-5: Multiphasic regions in simple shear flow.

order. When $\mathcal{N}_{c1}^s \leq \mathcal{N} \leq \mathcal{N}_{c2}^s$ and $\mathcal{N} > \mathcal{N}_{c3}^s$, the log-rolling nematic P phase is also seen, in addition to the two flow-aligned nematic P phases. At higher concentrations, $\mathcal{N} > \mathcal{N}_{c2}^s$, two nematic P phases (log-rolling and flow-aligning) can coexist with a high degree of order. At high rates of shear, family P1 does not display any turning points and proceeds smoothly to high concentrations. At such high shear rates, for a concentration $\mathcal{N} < \mathcal{N}_{c3}^s$, only the flow-aligned nematic P phase exists. At higher concentrations, $\mathcal{N} > \mathcal{N}_{c3}^s$, both the flow-aligned and log-rolling nematic P phases coexist.

High Shear Rate Limit. The only states that exist at all shear rates and all concentrations belong to the P1 family, with the molecules aligned in the flow direction. The effect of shear rate on the degree of order for these states is shown in Fig. 5-6 as a function of concentration. At high $\dot{\gamma}$, the P1 states approach perfect order ($S = 1$) irrespective of concentration. Consequently, the shear rate has a more pronounced effect on the structural order for solutions with low concentrations, where high orientational order cannot be achieved otherwise. Menon (1990) obtained the high shear rate asymptote for the P1 family in terms of a Frobenius series expansion for the variable S

$$S = \sum_{n=0}^{\infty} s_n \dot{\gamma}^{-\alpha_n} \tag{5.21}$$

where $\{s_n\}$ are coefficients in the series and are independent of $\dot{\gamma}$. Computing the first two terms in this series gives

$$S \sim (1 + s_1 \dot{\gamma}^{-2/3} + \ldots). \tag{5.22}$$

This result is useful for determining the rheological properties at high shear rates, and was used by Menon (1990) in comparing the predictions of this model with those of the model developed by Doi.
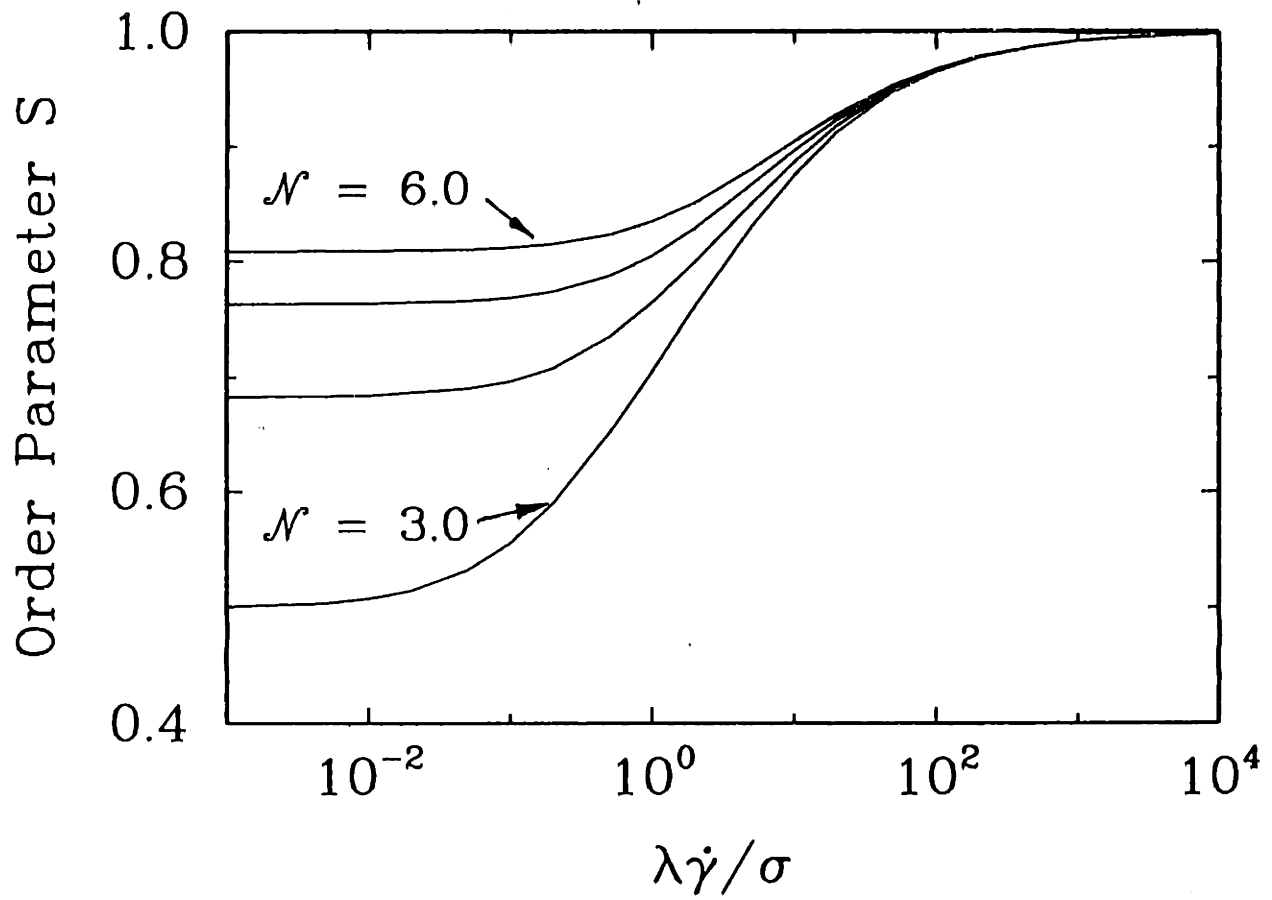
Figure 5-6: Variation of order S with and $\mathcal{N}$ along trajectory P1 for shear flow with $\mathcal{N} = 3.0$, 4.0, 5.0 and 6.0.

5.2.2.2 Shearfree Flows

The effect of steady uniaxial elongational flow ($\dot{\varepsilon} > 0$) and biaxial stretching flow ($\dot{\varepsilon} < 0$) on the orientational order was studied by solving Eqs. (5.11)-(5.13) with the kinematics given by Eq. (5.17). These flows possess uniaxial symmetry about the x_1-axis. Therefore, the nematic phases also display uniaxial symmetry, although not necessarily about the x_1-axis. States also exist with the nematic director in the 23-plane. Using the rotational invariance of the states in the 23-plane, we reduce the equation set by setting S_{23} to zero. A solution with non-zero S_{23} can be obtained by rotation of the x_2 and x_3 axes in the 23-plane.

As for the calculations for shear flows, we pick some representative initial orientations that we study in detail. The two initial orientations that we study correspond to the director in the 1-direction and in the 23-plane, respectively; the results for the two cases are presented separately.

A. Uniaxial Elongational Flow. Three families of nematic states have been computed for uniaxial elongational flow and are plotted in Fig. 5-7. These states are discussed in terms of the two representative equilibrium orientations that we have picked.

Director in the 1-direction. As shown in Fig. 5-7, imposing a uniaxial flow when the molecules are oriented in the primary flow direction 1 breaks the bifurcation between the isotropic and nematic phases into two distinct families, in much the same way as shear flow resulted in the P1 and O1 states. The P1 family evolves from $\mathcal{N} = 0$ and corresponds to phases that are aligned in the 1-direction. The flow strongly orients the polymer solution; for $\mathcal{N} = 3$, the order parameter is $S \simeq 0.6$ for $\dot{\varepsilon} = 0.1$, compared to $S = 0.5$ at rest and $S \simeq 0.55$ for $\dot{\gamma} = 0.1$ in a shear flow.

The qualitative behavior of this P1-family is very similar to the P1 family in shear flow. The family displays turning points $\mathcal{N}_{c1}^{ue}$ and $\mathcal{N}_{c2}^{ue}$ only when $\dot{\varepsilon} \ll 1$. The effect of increasing $\dot{\varepsilon}$ on the degree of order predicted for states in the P1-family is shown in Fig. 5-8 for several values of $\mathcal{N}$. Near perfect order is attained for $\dot{\varepsilon} \gg 1$, irrespective
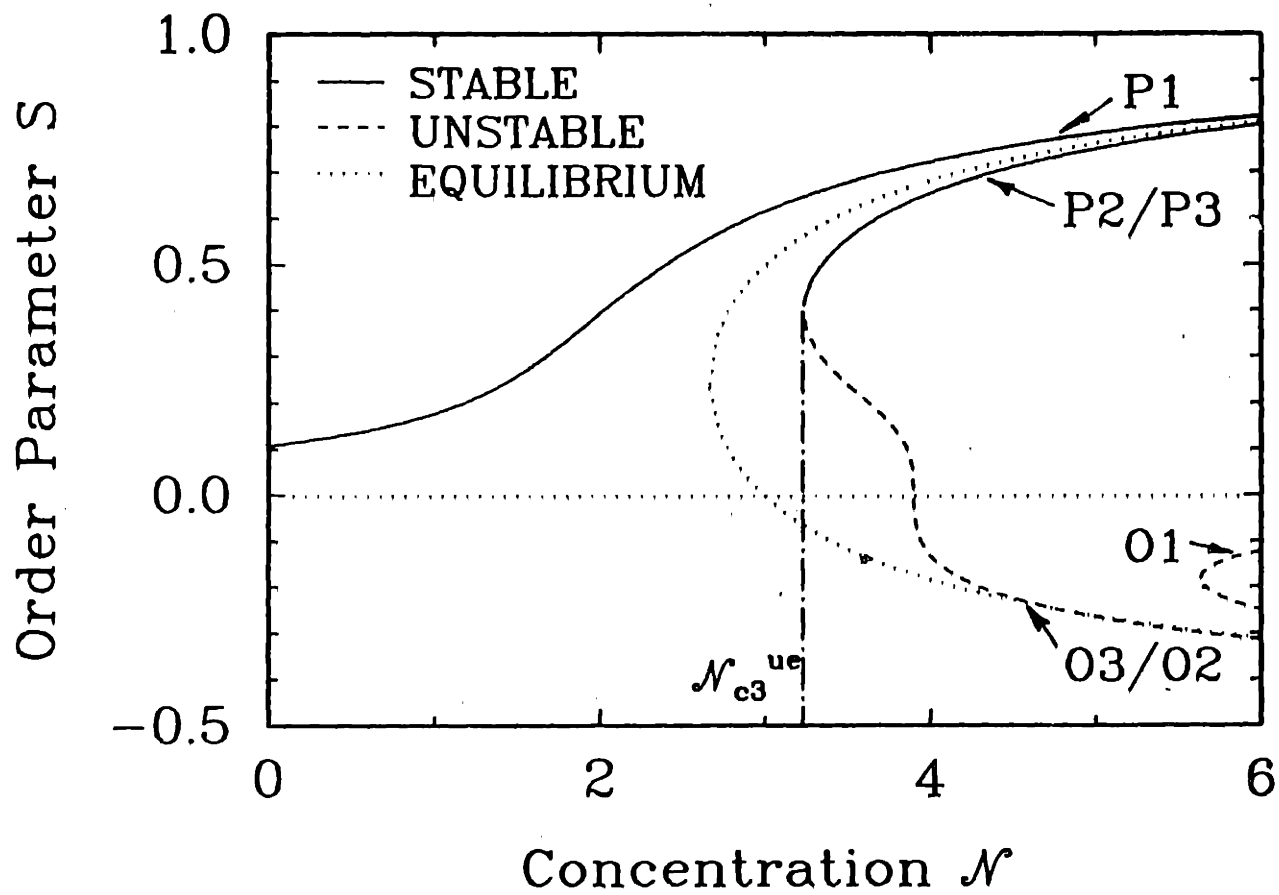
Figure 5-7: Effect of uniaxial elongational flow on transcritical bifurcation for $\dot{\bar{\epsilon}} = 0.1$.
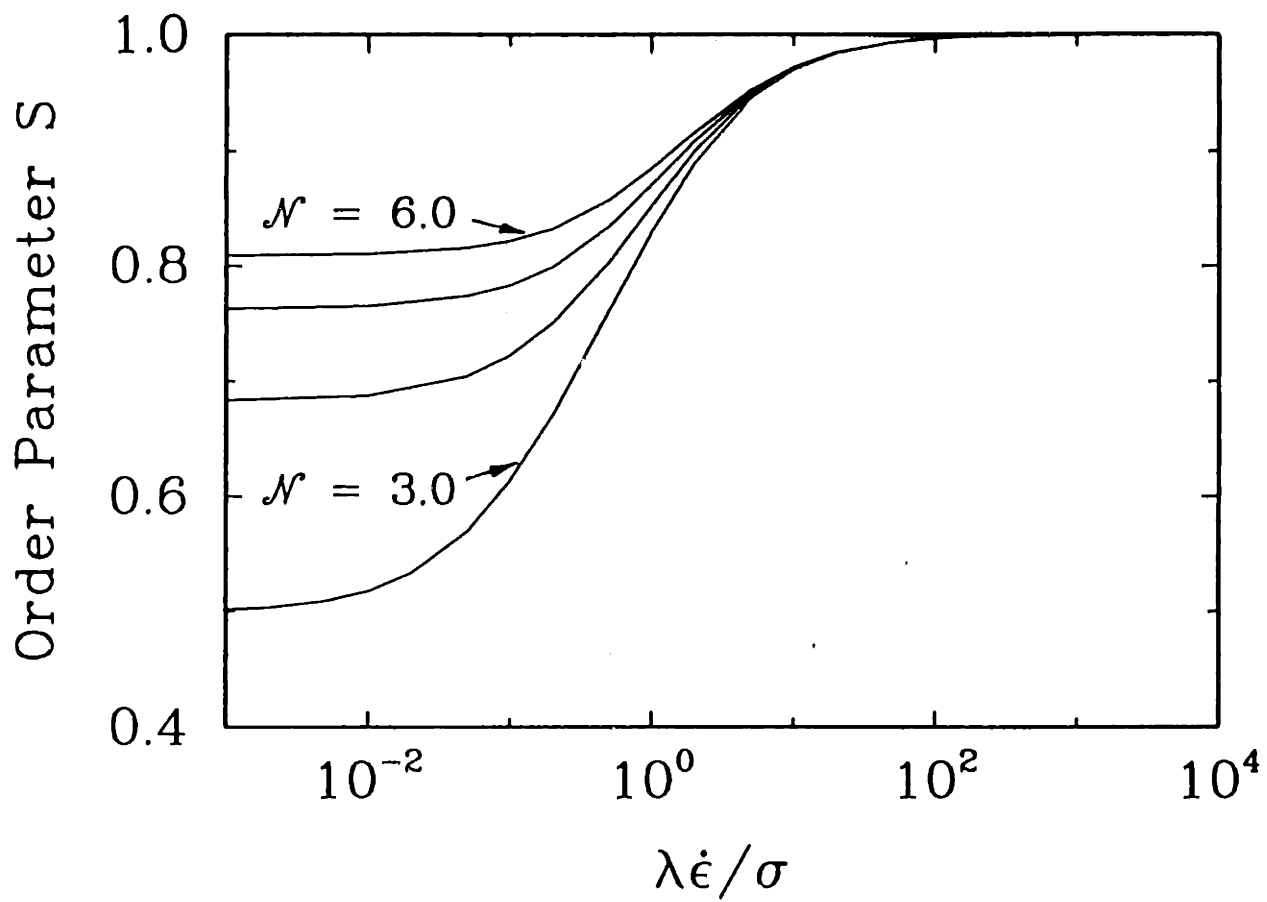
Figure 5-8: Variation of order S with $\dot{\epsilon}$ and $\mathcal{N}$ along trajectory P1 for uniaxial elongational flow with $\mathcal{N} = 3.0$, 4.0, 5.0 and 6.0.

of $\mathcal{N}$. The asymptotic behavior in this limit has been determined by Menon (1990) from a Frobenius series in powers of $\dot{\epsilon}$ as

$$S \sim (1 + s_1 \dot{\epsilon}^{-1} + \ldots) \tag{5.23}$$

Comparing Eqs. (5.22) and (5.23) shows that perfect order is approached more rapidly with increasing strain rate in elongational flow than in shear flow.

The states in the O1 family shown in Fig. 5-7 are composed of molecules oriented in the 23-plane. These states exist only at increasingly higher $\mathcal{N}$ as $\dot{\epsilon}$ is increased and are always unstable, as was the case at equilibrium.

Director in the 23-plane. The rotational symmetry about the 1-direction in the uniaxial elongational flow implies that the interactions of all equilibrium states oriented with the director in the 23-plane with the flow are equivalent. The families computed with $\dot{\epsilon} > 0$ superimpose when represented in terms of the scalar order parameter S, as shown in Fig. 5-7. The nematic states are labelled as P and O, according to the alignment of the molecules relative to the director. All the nematic P states (referred to collectively as P2/P3) develop perfect prolate symmetry for $\mathcal{N} \gg 1$; these states are stable at high $\mathcal{N}$, as indicated in Fig. 5-7. For the sake of clarity, the evolution of a single family P2 that evolves from an initial state with the director $n = \delta_2$ is discussed. On following the P2 states to lower $\mathcal{N}$, a limit point $\mathcal{N}_{c3}^{ue}$ is encountered. The P2 states lose stability at the limit point, and evolve to higher values of $\mathcal{N}$ along the branch O3 (which corresponds to an oblate phase with the director in the 23-plane and perpendicular to the director of the P2 state). All states in this family are unstable. The value of the limit point $\mathcal{N} = \mathcal{N}_{c3}^{ue}$ increases with increasing $\dot{\epsilon}$. Thus, for a given value of $\mathcal{N}$ and $\dot{\epsilon} \gg 1$, only the P1 family has states that may be observable.

As in shear flow, depending on the values of $\mathcal{N}$ and $\dot{\epsilon}$, more than one phase can coexist. The multiphasic regions for uniaxial elongational flow are summarized in Fig. 5-9. Note that the diagram is qualitatively similar to Fig. 5-5 for shear flow, except that the transitions occur at much lower values of $\dot{\epsilon}$, indicating that uniaxial
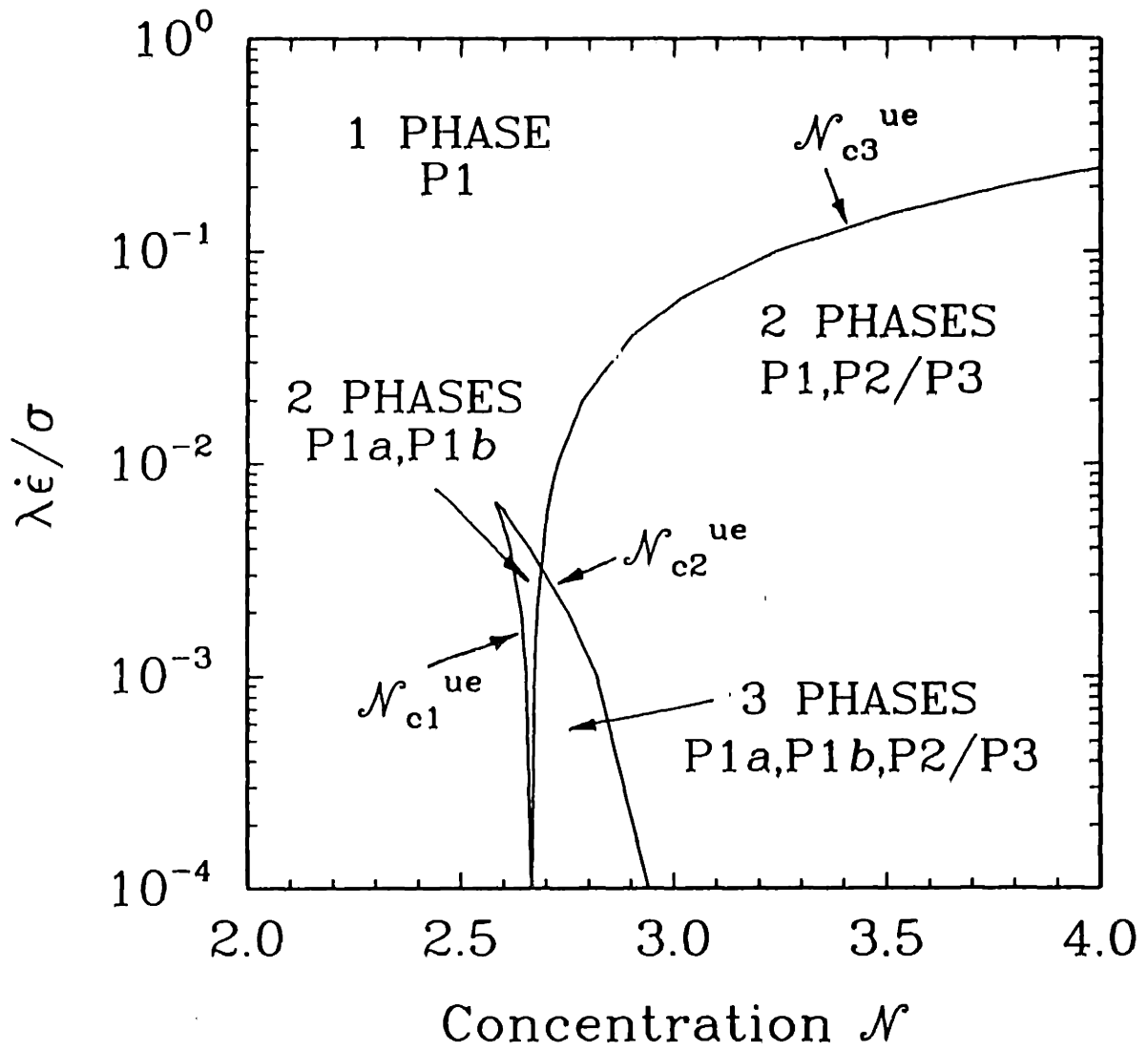
Figure 5-9: Multiphasic regions in uniaxial elongational flow.

elongation is a much stronger flow than simple shear.

B. Biaxial Stretching Flow. When the nematic director is oriented in the x_1-direction at equilibrium, introducing a biaxial stretching flow ($\dot{\epsilon} < 0$) breaks the equilibrium transcritical bifurcation in a unique way. Two isolated families of states denoted as P1 and O1 are obtained, as shown in Fig. 5-10. At low $\mathcal{N}$, the preferred states have the oblate symmetry introduced by the flow. As $\mathcal{N}$ is increased from zero, the structural order parameter S for states in the O1 family becomes increasingly negative, signifying that the molecules tend to lie more nearly in the 23-plane; $S \rightarrow -1/2$ as $\mathcal{N} \rightarrow \infty$. However, the O1 family is not stable at arbitrarily high concentrations. At any given $\dot{\epsilon}$, there is a critical concentration $\mathcal{N}_{c2}^{bs}$ beyond which the random in-plane alignment of the nematic O phase becomes unstable to perturbations that tend to align the molecules in a preferred direction in the 23-plane. This instability is expected because of the tighter packing allowed in the prolate configuration and the preference of the system at equilibrium for these states. The locus of $\mathcal{N}_{c2}^{bs}(\dot{\epsilon})$ is plotted in Fig. 5-11 and decreases with increasing $\dot{\epsilon}$. In the region that lies below the critical concentration curve a stable nematic O family can exist. For concentrations $\mathcal{N}$ less than approximately 1.3, a stable nematic O phase is seen at all values of $\dot{\epsilon}$. Recent calculations by Hu and Ryskin (1991) based on an iterative scheme for calculating the distribution function for an ordered solution of rigid-rod-like molecules also indicate that the oblate states lose stability beyond a critical elongational rate in biaxial extensional flow. These authors suspect a similar transition from oblate to prolate symmetry in the 23-plane, but the results confirming this hypothesis are as yet unpublished.

The other isolated branch that results as a breaking of the bifurcation is the P1 family which corresponds to the nematic P phases aligned in the 1-direction. Along the upper branch of this family, the order parameter $S \rightarrow 1$ as $\mathcal{N} \rightarrow \infty$; these states are stable. Following this branch to lower concentrations, the family turns around at a critical concentration $\mathcal{N}_{c3}^{bs} = \mathcal{N}_{c3}^{bs}(\dot{\epsilon})$, and loses stability before proceeding to $S = 0$, at high concentrations. The locus of these limit points is shown in Fig. 5-11.

179
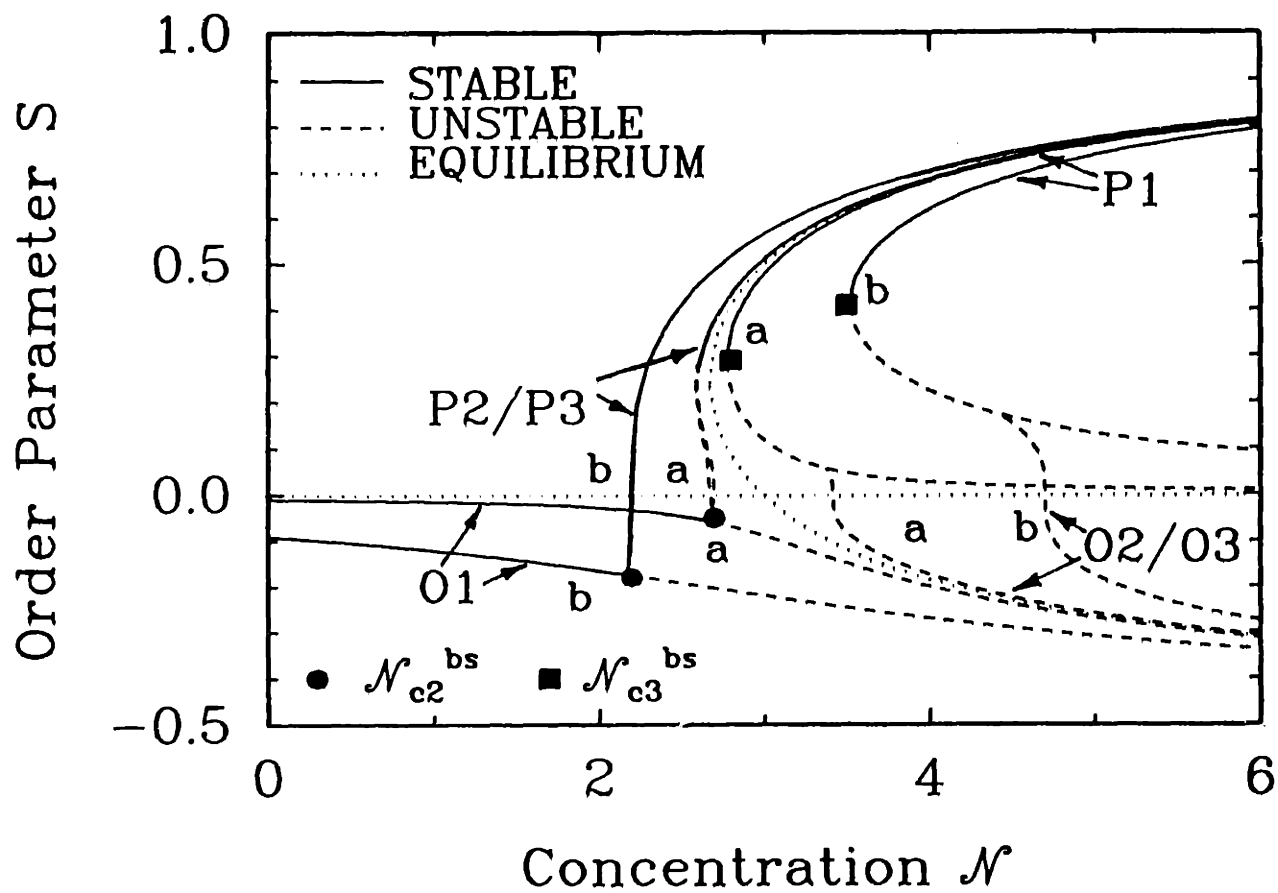
Figure 5-10: Effect of biaxial stretching flow on transcritical bifurcation for $\dot{\epsilon}$ of (a) -0.01 and (b) -0.1.
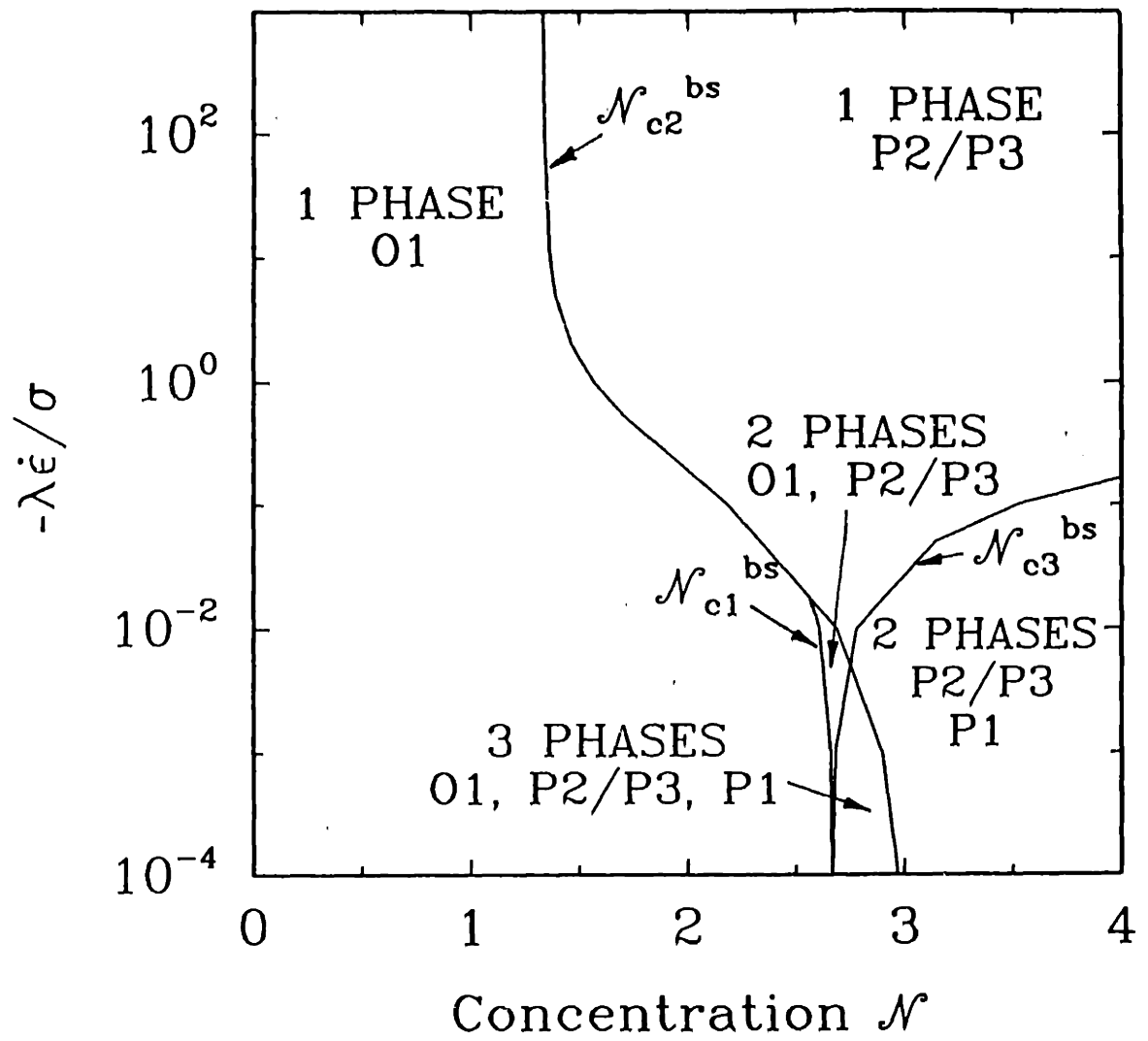
Figure 5-11: Multiphasic regions in biaxial stretching flow.

The critical concentrations $\mathcal{N}_{c3}^{b\hat{s}} = \mathcal{N}_{c3}^{b\hat{s}}(\hat{\epsilon})$ at which the O1 phases lose stability correspond to bifurcations between the O1 family and nematic P states that have evolved from equilibrium nematic phases with the director in the 23-plane. The rotational symmetry of the biaxial stretching flow about the 1-direction makes these states equivalent, and they are collectively denoted as P2/P3. For $\hat{\epsilon} \ll 1$, the P2/P3 states bifurcate subcritically, and then evolve to higher values of $\mathcal{N}$ beyond a limit point $\mathcal{N}_{c1}^{b\hat{s}} = \mathcal{N}_{c1}^{b\hat{s}}(\hat{\epsilon})$. The P2/P3 states are initially unstable, and regain stability beyond this limit point. As $\hat{\epsilon}$ is increased $\mathcal{N}_{c1}^{b\hat{s}}$ approaches $\mathcal{N}_{c2}^{b\hat{s}}$, and the two critical points coalesce at a critical elongational rate $\hat{\epsilon}_c$. For all $\hat{\epsilon} > \hat{\epsilon}_c$, the P2/P3 states bifurcate supercritically and are always stable.

The discussion above indicates that, depending on the values of $\mathcal{N}$ and $\hat{\epsilon}$, nematic P states oriented in the 23-plane may be stable in addition to the P1 and O1 states. The multiphasic regions that are observed in biaxial stretching flow are shown in Fig. 5-11, and are separated by the curves $\mathcal{N}_{c1}^{b\hat{s}}(\hat{\epsilon})$, $\mathcal{N}_{c2}^{b\hat{s}}(\hat{\epsilon})$ and $\mathcal{N}_{c3}^{b\hat{s}}(\hat{\epsilon})$.

The last phases depicted in Fig. 5-10 correspond to states in the O2/O3 family that are separated to form a curve that bifurcates from the unstable branch of the P1 family. These states move to higher values of $\mathcal{N}$ as $\hat{\epsilon}$ is increased and are unstable.

The rotational invariance of of the equilibrium states results in a complex picture of the separation of the different solution branches. A comparison of Figs. 5-5, 5-9 and 5-11 shows that the effect of biaxial extensional flow on the bifurcation diagram is quite different from the effect of shear/uniaxial extensional flows. In all three flows, the primary broken branch corresponds to the primary flow direction; P1 for shear and uniaxial extensional flows and O1 for biaxial extensional flow. Other solution branches are seen that are not broken, and the bifurcation can be said to be only *partially* broken by the effect of flow. However, it is only in the case of biaxial extensional flow that the secondary solution branch (P2/P3) bifurcates from the primary solution branch O1. This transition from a phase with oblate symmetry to one with prolate symmetry is a natural consequence of the increasing importance of the excluded volume interactions with increasing concentration, and shows that even an *in-planar* random distribution of molecules is energetically unfavorable. As such, this oblate-prolate transition may

be viewed as a two-dimensional analogue of the equilibrium isotropic-nematic phase transition. The dependence of the critical concentration $\mathcal{N}_{c2}^{b}$ on the elongation rate $\overset{\wedge}{\dot{\epsilon}}$ provides an additional parameter that can easily be controlled experimentally and allows control of the onset of the oblate-prolate transition. This additional control would be extremely advantageous in experiments seeking to study the dynamics of the isotropic-nematic transition. In such experiments, great care has to be taken in the biphasic region (that just precedes the critical concentration $\mathcal{N}_c$) to avoid nucleation of one phase in another, since this can lead to erroneous results. With the added flexibility of the elongational rate as a control parameter, $\overset{\wedge}{\dot{\epsilon}}$ can be picked to ensure that $\mathcal{N}_{c2}^{b}$ is out of the biphasic region. Extrapolation of results obtained at several elongational rates to zero-elongation can then be used to gain information on the dynamics of the equilibrium isotropic-nematic transition. However, difficulties could be faced in creating a perfectly biaxial flow without end effects and these would first have to be overcome.

5.3 Material Function Predictions

5.3.1 Steady Shear Flow

The effects of shear rate and concentration on the orientational order parameter S have been discussed in Section 5.2.2.1 and presented in Figs. 5-2, 5-3, and 5-4. The viscosity and first normal stress coefficient for steady shear flow are defined as

$$
\begin{aligned}
\eta &= -\frac{\tau_{12}}{\dot{\gamma}}; \\
\Psi_1 &= -\frac{(\tau_{11} - \tau_{22})}{\dot{\gamma}^2}.
\end{aligned}
\tag{5.24}
$$

At low shear rates, families P1, O1, P3 and O3 exist; see Figs. 5-3 and 5-4. The O1 and O3 families are populated by nematic O states with random in-planar molecular arrangement. However, these solutions are always unstable, and are not considered further. The families P1 and P3 represent the flow-aligning and log-rolling nematic

183

P families; see Section 5.2.2.1. Equation (5.14) predicts constant zero-shear-rate viscosities η_0 for these families. The variation of η_0 with concentration in the isotropic and the two possible nematic P families is shown in Fig. 5-12; the viscosity η_0 increases linearly with increasing $\mathcal{N}$ in the isotropic phase. For both nematic P phases, η_0 decreases with increasing concentration. The drop in viscosity is due to the decreasing resistance as the dumbbells develop greater orientational order. For $\sigma = 1$ and at any given concentration, viscosity of the log-rolling nematic P phase is less than the viscosity of the flow-aligning phase. Decreasing the value of σ has a marked effect on the viscosity of the flow-aligning phase, but does not affect the viscosity of the log-rolling phase to any great extent. This is intuitively plausible, if one remembers that decreasing σ has the effect of reducing the resistance to flow in the direction of the dumbbell axis, or, in the flow-aligning case, reducing the resistance in the direction of shearing. However, for the log-rolling phase, reducing the resistance to flow in the vorticity direction does not have much effect on the viscosity, since there is no relative motion in this direction.

As discussed in Section 5.2.2.1, the flow-aligned nematic P states in the P1 family are the only states that exist for all $\dot{\gamma}$ and $\mathcal{N}$. The rheology of these states has been studied in detail by Menon (1990) and some relevant results are presented here. The variation of viscosity in the flow-aligned nematic phase P with is shown in Fig. 5-13 for different concentrations. Shear-thinning with power-law behavior is predicted at high shear rates. Increasing $\mathcal{N}$ lowers η_0 and increases the shear rate at which shear thinning begins so that the curves for different $\mathcal{N}$ intersect at $\dot{\gamma} \approx 0.1$. At high $\dot{\gamma}$ the viscosity predicted actually increases with increasing concentration. This occurs because at these deformation rates an increase in concentration has almost no effect in increasing the degree of order, but results in increasing the hydrodynamic drag force on the molecules.

Asymptotic analysis by Menon(1990) in this limit indicates that the viscosity behaves as

$$\eta - \eta_s \sim (1 - S) \sim \dot{\gamma}^{-2/3},$$

$$(5.25)$$

184
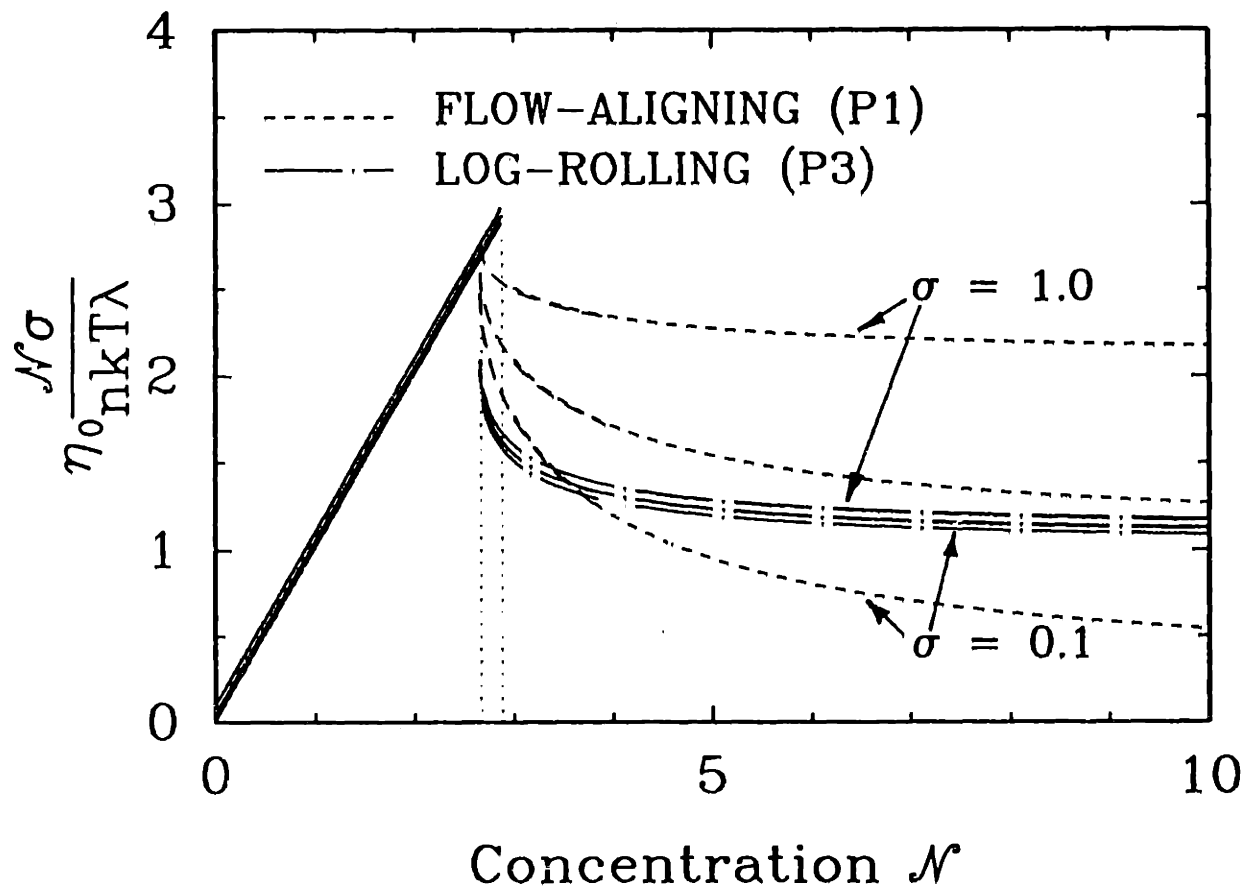
Figure 5-12: Variation of zero-shear-rate viscosity $\eta_0 \mathcal{N}\sigma/(nkT\lambda)$ with $\mathcal{N}$ and σ in the isotropic and nematic phases for $\sigma = 1.0$, 0.5 and 0.1.
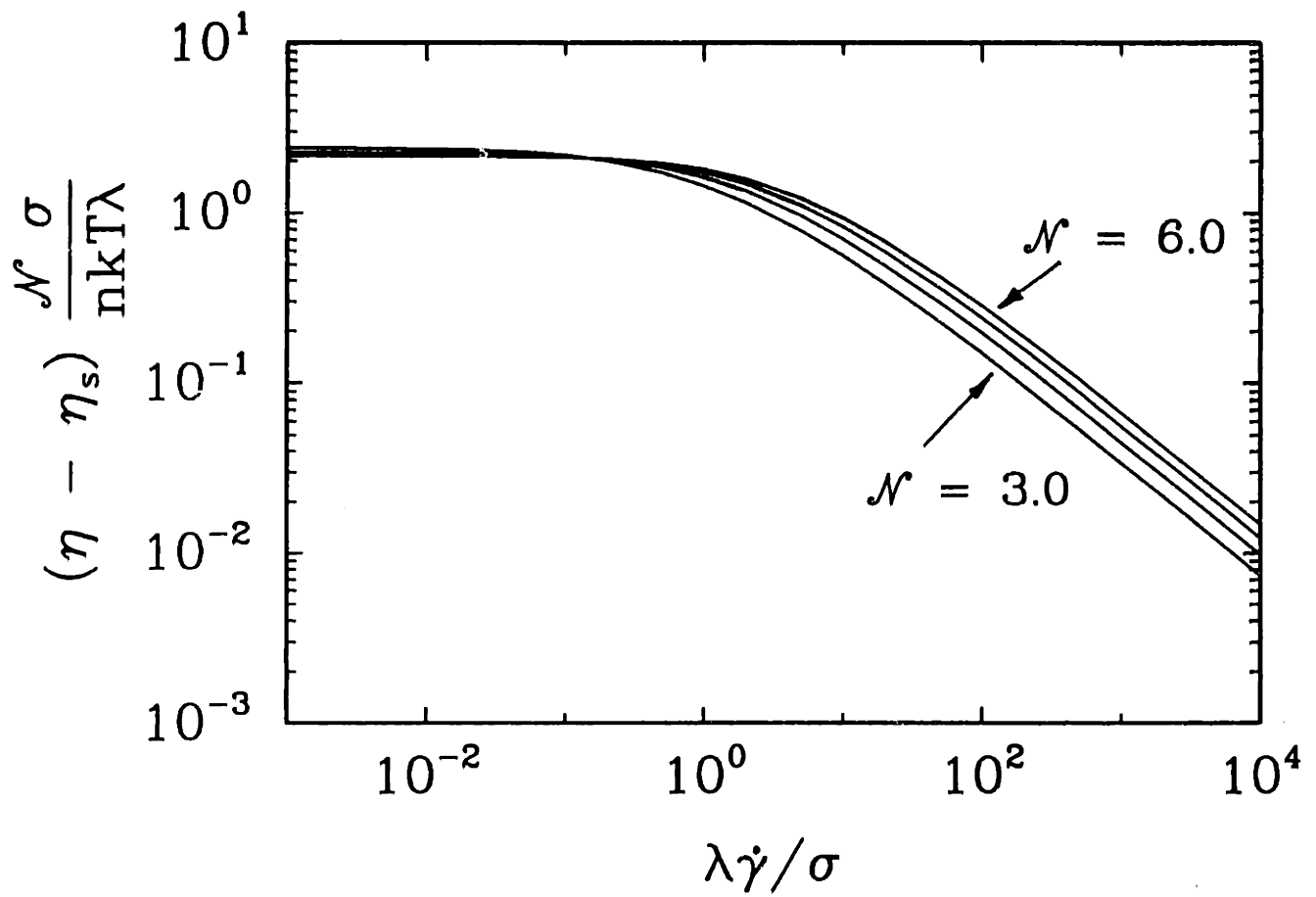
Figure 5-13: Variation of $(\eta - \eta_s)\mathcal{N}\sigma/(nkT\lambda)$ with $\dot{\gamma}$ and $\mathcal{N}$ in the flow-aligned nematic phase P for $\Lambda' = 3.0$, 4.0, 5.0 and 6.0 and $\sigma = 1.0$.

as compared to $\eta - \eta_* \sim (1 - S)^4 \sim \dot{\gamma}^{-8/7}$ for Doi's constitutive equation in this limit. The shear stress for Doi's equations passes through a maximum with increasing $\dot{\gamma}$, which is physically impossible. This is a consequence of neglecting the viscous stress contribution associated with hydrodynamic energy dissipation. Jain and Cohen (1981) and Dahler et al. (1983) have shown that the contribution of this term is non-negligible at high rates of deformation; see Section 4.2.2. The analysis carried out by Menon corroborates these studies and conclusively shows that the excessive shear thinning is a result of neglecting the $\kappa{:}\langle uuuu \rangle$ term from Eq. (5.14) for the stress tensor. The importance of the viscous stress term in the high-shear rate predictions has also been emphasized by Marrucci and Maffettone (1989).

Menon's prediction for viscosity in the high shear rate limit, given by Eq. (5.25) is physically plausible and agrees with the result for dilute solutions of rigid rods (Doi and Edwards, 1986). This is not surprising at high shear rates since the degree of order in the solution is very high irrespective of concentration and hydrodynamic forces dominate over the intermolecular excluded volume forces. However, it is interesting to note that numerical calculations (Stewart and Sørensen, 1972) and perturbation expansion results (Hinch and Leal, 1972 & 1976) of the high shear rate asymptote for dilute rigid-rod solutions in the absence of closure approximations yield a $-1/3$ dependence on the shear rate. This is surprising in that the quadratic closure approximation (which is exact in the limit of perfect order) used in Menon's calculation for liquid crystalline solutions, and in the calculations described by Doi and Edwards (1986) for dilute solutions is expected to be reasonably accurate at higher shear rates, when the degree of order in the solution is high.

A comparison of the viscosity predictions of the model Eqs. (5.11)-(5.14) with the experimental data compiled by Doraiswamy and Metzner (1986) for a 30% w/w solution of hydroxypropyl cellulose in acetic acid was carried out by Bhave et al. (1992) and is shown in Fig. 5-14. The predictions of the Doi model also are shown in order to compare the two theories. The zero-shear-rate viscosity η_0 and the time constant λ are treated as adjustable parameters, and serve to define a reference point in the viscosity-shear-rate curve, leaving the overall shape of the curve unchanged.
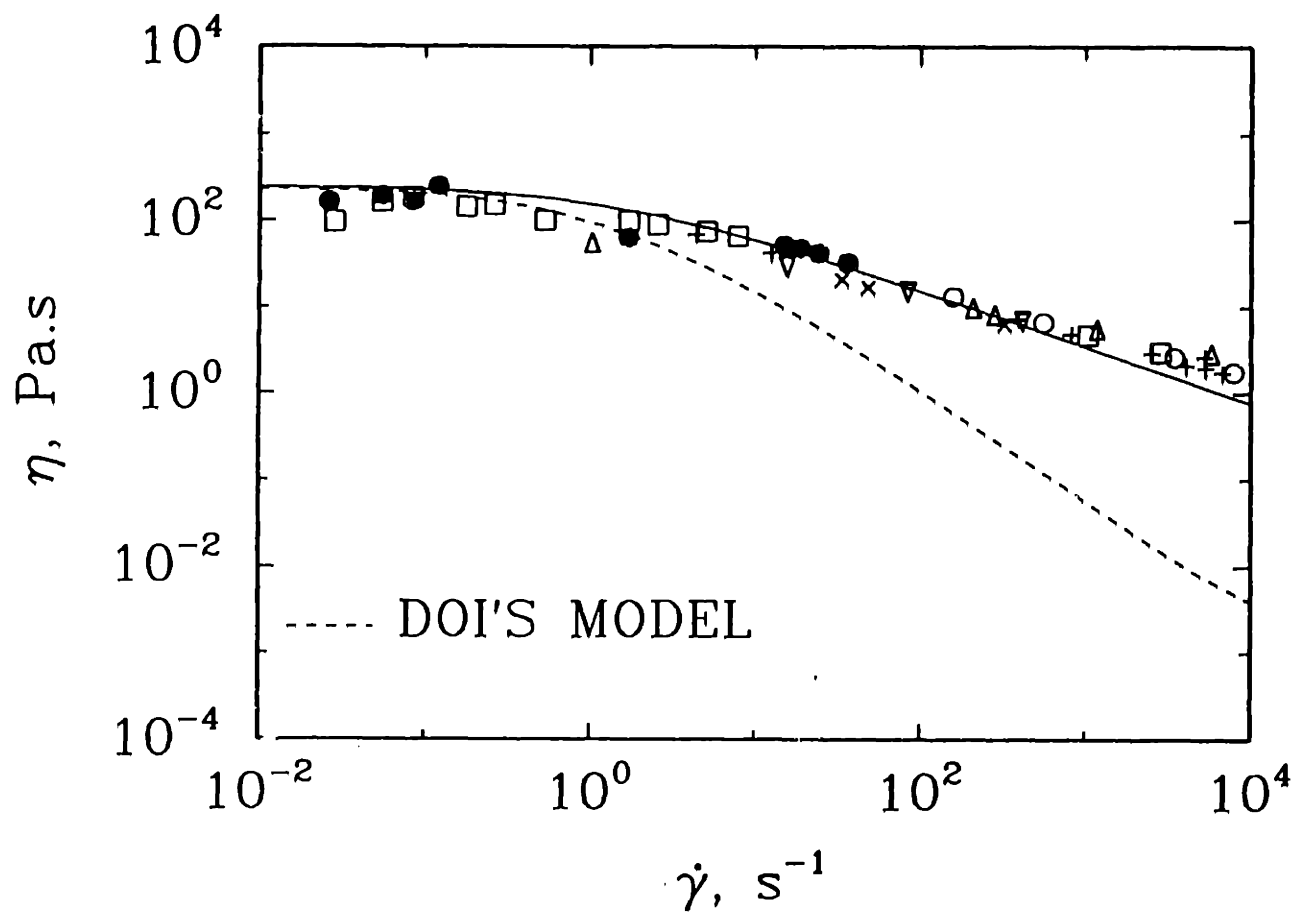
Figure 5-14: Comparison with experimental data of Doraiswamy and Metzner (1986) for a hydroxypropyl cellulose solution in acetic acid with $\mathcal{N} = 4.2$ and $\sigma = 1.0$.

The dimensionless concentration $\mathcal{N}$ is determined from reported phase-transition data (Doraiswamy and Metzner, 1986) by assuming that the transition to a purely nematic phase takes place at $\mathcal{N} = 3$. The solvent viscosity is set to the viscosity of acetic acid, $\eta_s = 0.0012$ Pa·s and $\sigma = 1$. The computed viscosity shows very good agreement with the reported data.

The effect of σ on dimensionless viscosity is shown in Fig. 5-15 for the case $\mathcal{N} = 4.5$. Decreasing σ corresponds to increasing the frictional resistance in directions perpendicular to the dumbbell axis. This effect causes the dumbbells to align and results in lower viscosity. Thus, the viscosity decreases with decreasing σ. The parameter σ has a greater effect at high shear rates, where the hydrodynamic drag (with which σ is associated) is the dominant force on the dumbbells.

The first normal stress coefficient Ψ_1 behaves like the viscosity, except that at low shear rates it is not constant but varies as the reciprocal of the shear rate; see Fig. 5-16. This behavior is predicted by both the Leslie-Ericksen-Parodi theory and the Doi model, and is related to the anisotropic nature of the fluid. It indicates that, at low shear rates, normal stresses are as important as shear stresses. The effect of concentration on Ψ_1 is small, and Ψ_1 increases slightly with increasing $\mathcal{N}$ at all shear rates. The effect of σ on dimensionless Ψ_1 is shown in Fig. 5-16. The first normal stress coefficient decreases with decreasing σ because the normal stress difference decreases as anisotropy in the friction tensor causes the dumbbells to align along the shearing direction. The variation of the stress ratio with shear rate is shown in Fig. 5-17. The stress ratio $S_R \equiv (\tau_{11} - \tau_{22})/\tau_{12}$ is non-zero in the zero-shear-rate limit and asymptotes to a constant value with decreasing shear rate. This is another manifestation of the linear dependence of $\tau_{11} - \tau_{22}$ on $\dot{\gamma}$, and indicates that the fluid is "inherently elastic" because of the alignment of dumbbells, even at vanishingly small shear rates. The stress ratio S_R at low shear rates increases with increasing concentration and is independent of the parameter σ, because the shear stress and normal stress difference have the same dependence on σ.
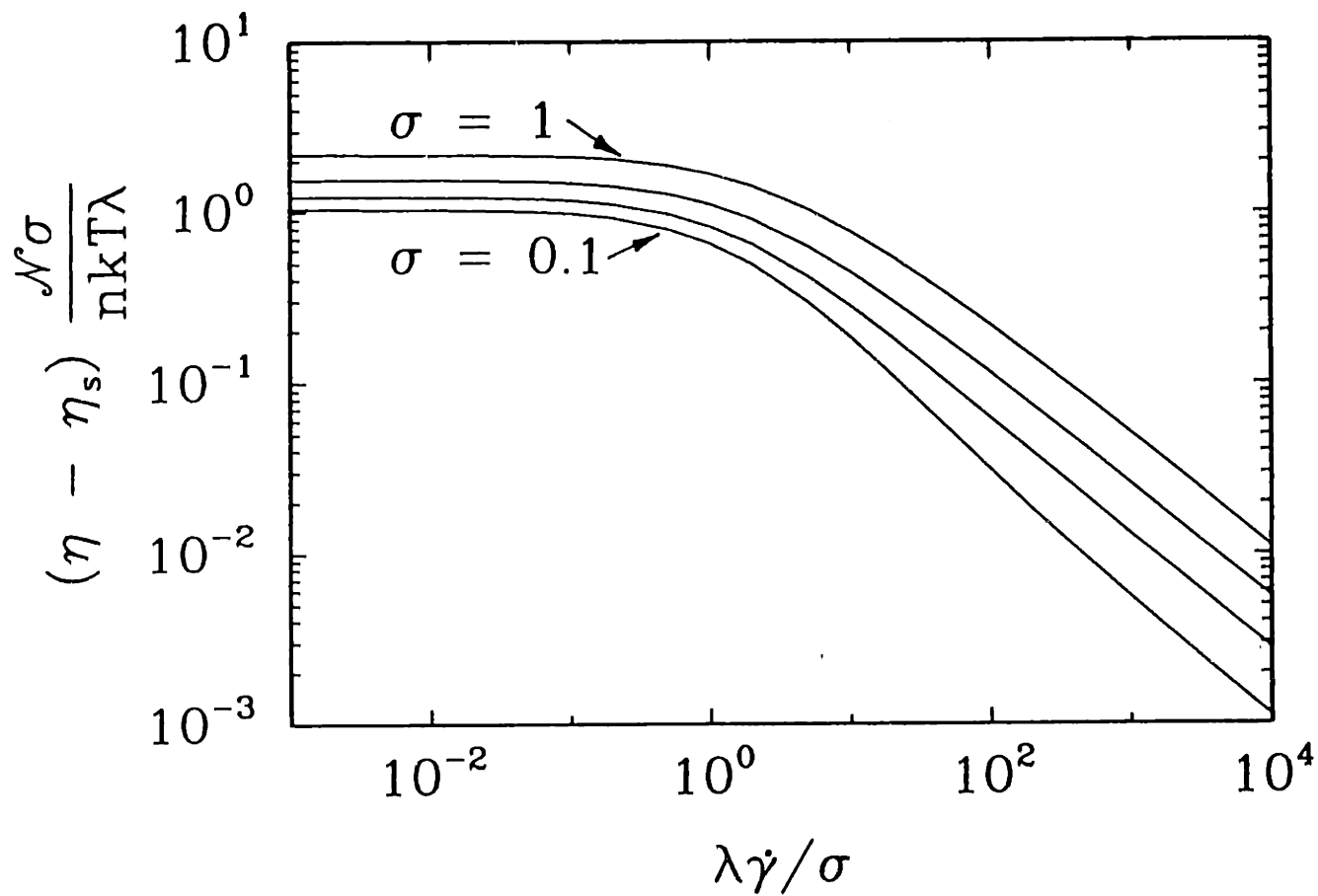
Figure 5-15: Variation of $(\eta - \eta_s)\mathcal{N}\sigma/(nkT\lambda)$ with $\dot{\gamma}$ and parameter σ in the flow-aligned nematic phase for $\mathcal{N} = 4.5$ and $\sigma = 1.0$, 0.5, 0.25 and 0.1.
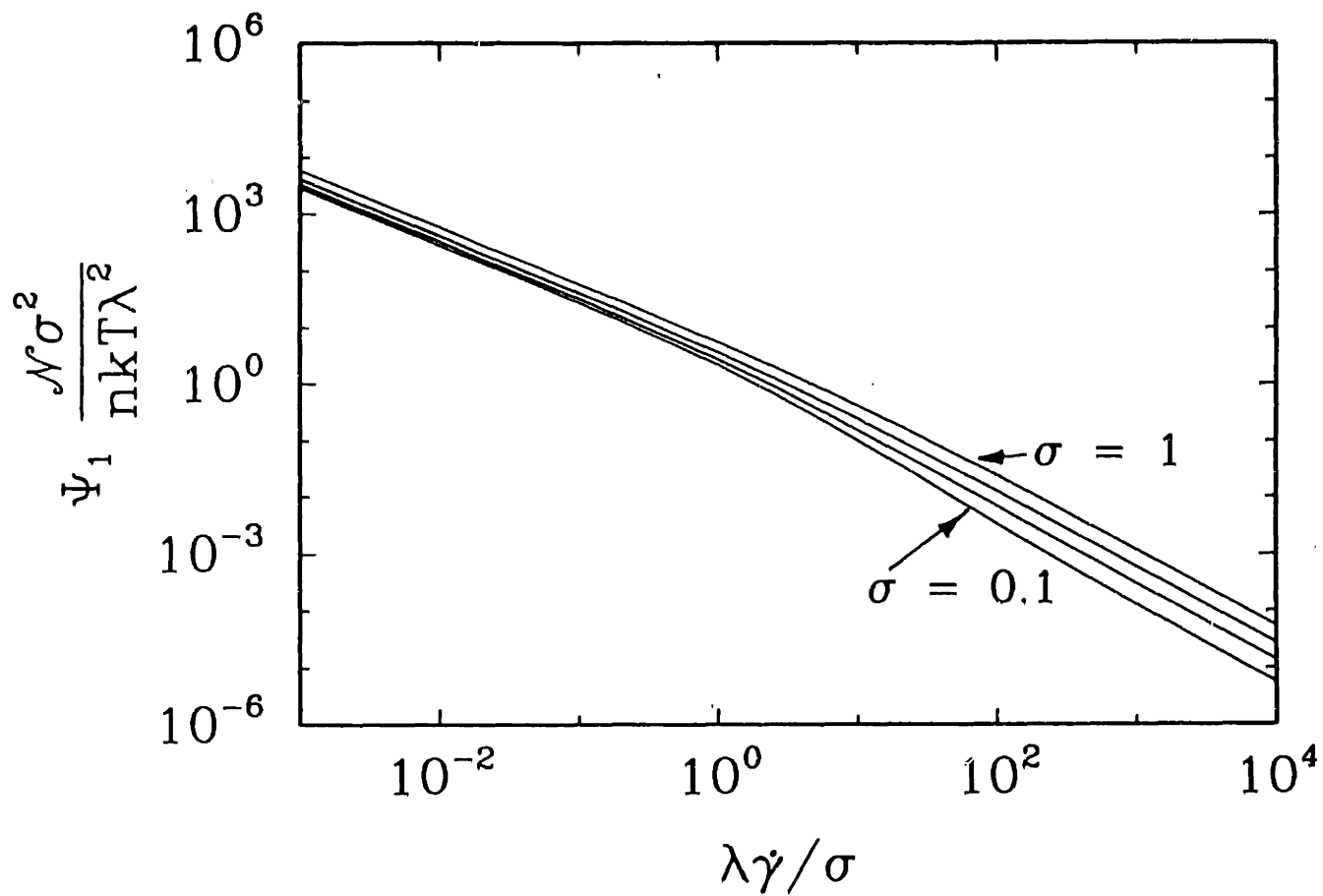
Figure 5-16: Variation of first normal stress coefficient $\Psi_1 \mathcal{N}\sigma^2/(nkT\lambda^2)$ with $\dot{\gamma}$ and parameter σ in the flow-aligned nematic phase P for $\mathcal{N} = 4.5$ and $\sigma = 1.0$, 0.5, 0.25 and 0.1.
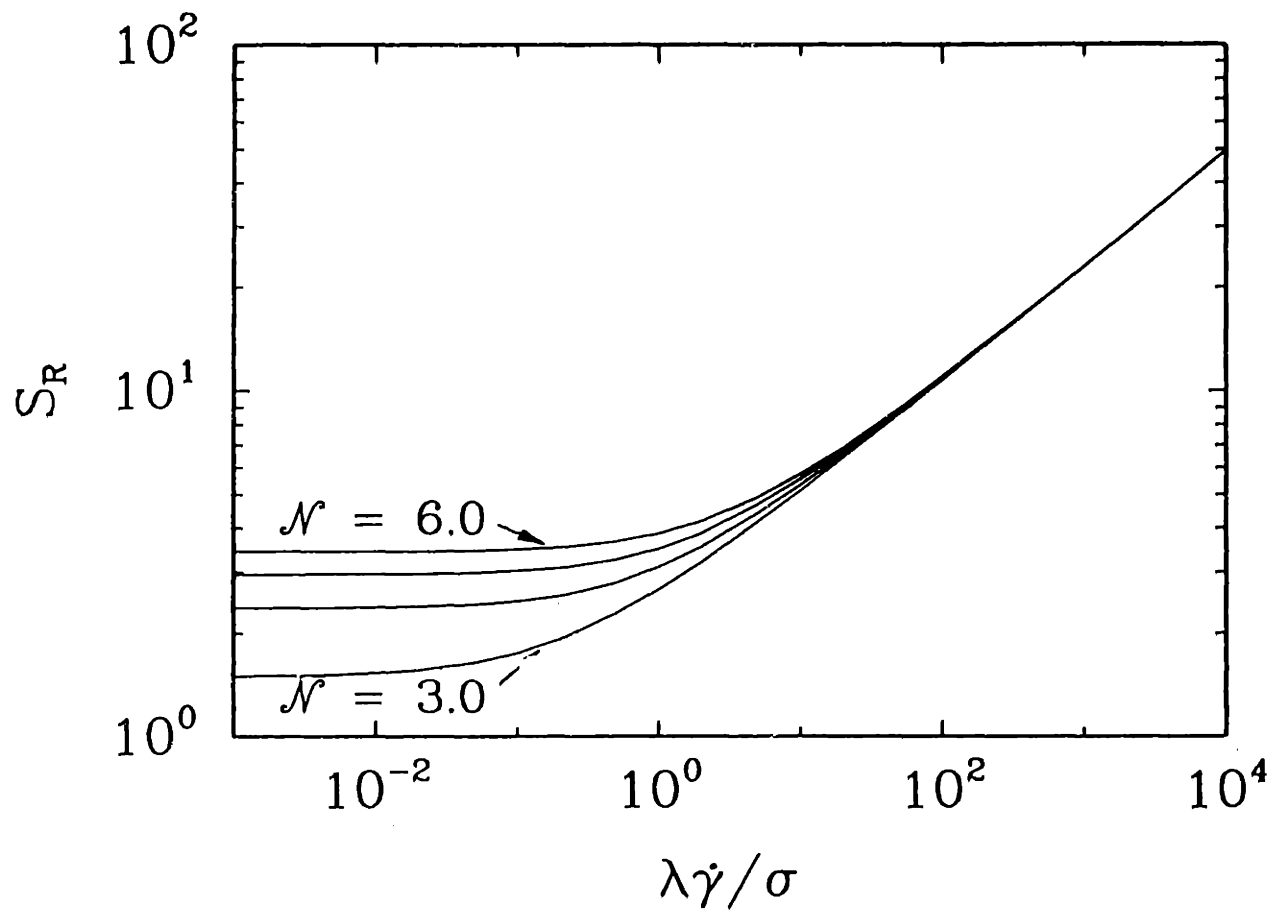
Figure 5-17: Variation of stress ratio with $\dot{\gamma}$ and $\mathcal{N}$ in the flow-aligned nematic phase P for $\mathcal{N}$ = 3.0, 4.0, 5.0 and 6.0 and σ = 1.0.

5.3.2 Transient Shear Flows

Information about the molecular relaxation processes can be obtained by studying the material functions in transient flows. In this section, material functions for stress growth upon inception of steady shear flow are discussed. For this flow, $\dot{\gamma} = 0$ for $t < 0$ and $\dot{\gamma} = \dot{\gamma}_0$ for $t \geq 0$; see Figs. 2.5 and 2.6. The shear stress growth function η^+ is plotted as a function of time in Fig. 5-18, for a dimensionless concentration of $\mathcal{N} = 2$ and for different values of $\dot{\gamma}_0$. The concentration chosen is lower than the lowest concentration at which the nematic phase can exist and the system can be said to be in a concentrated isotropic state. The time variable is made dimensionless with the rotational time constant λ. At low shear rates, η^+ increases monotonically to its steady-state value; at high shear rates, it first goes through a maximum, before reaching its steady state value. The steady-state viscosity η decreases due to shear-thinning as the shear rate increases. The maximum in η^+ occurs at smaller values of dimensionless time on increase in shear rate; the position of the maximum scales very well with strain $\dot{\gamma}_0 t$ as seen in Fig. 5-19. This behavior is characteristic of concentrated polymer solutions and polymer melts (Bird et al., 1987a). It is interesting though that at high shear rates, the η^+ vs. t/λ curves in Fig. 5-18 are not contained within the linear viscoelastic envelope defined by the low shear rate curves. This could be a result of the closure approximations used in deriving the model.

In the ordered phase, initial orientation of the nematic phase with respect to the shearing direction has a significant effect on the transient response; see Fig. 5-20. Three curves are plotted in the figure; the two dashed curves correspond to molecules oriented in the direction of shearing (P1) and in the vorticity direction (P3), respectively. The solid curve represents molecules oriented at the extinction angle χ with respect to the shearing direction. The extinction angle χ is defined as the limiting orientation of the molecules in the limit of zero-shear-rate and can be optically measured. The angle χ is known to be $45°$ in isotropic materials. In the nematic phases, $\chi < 45°$. Doi (1981) has obtained an analytic expression for χ and the corresponding structure tensor S in terms of the equilibrium order parameter S for a given value of $\mathcal{N}$, and the third initial orientation chosen for study is obtained
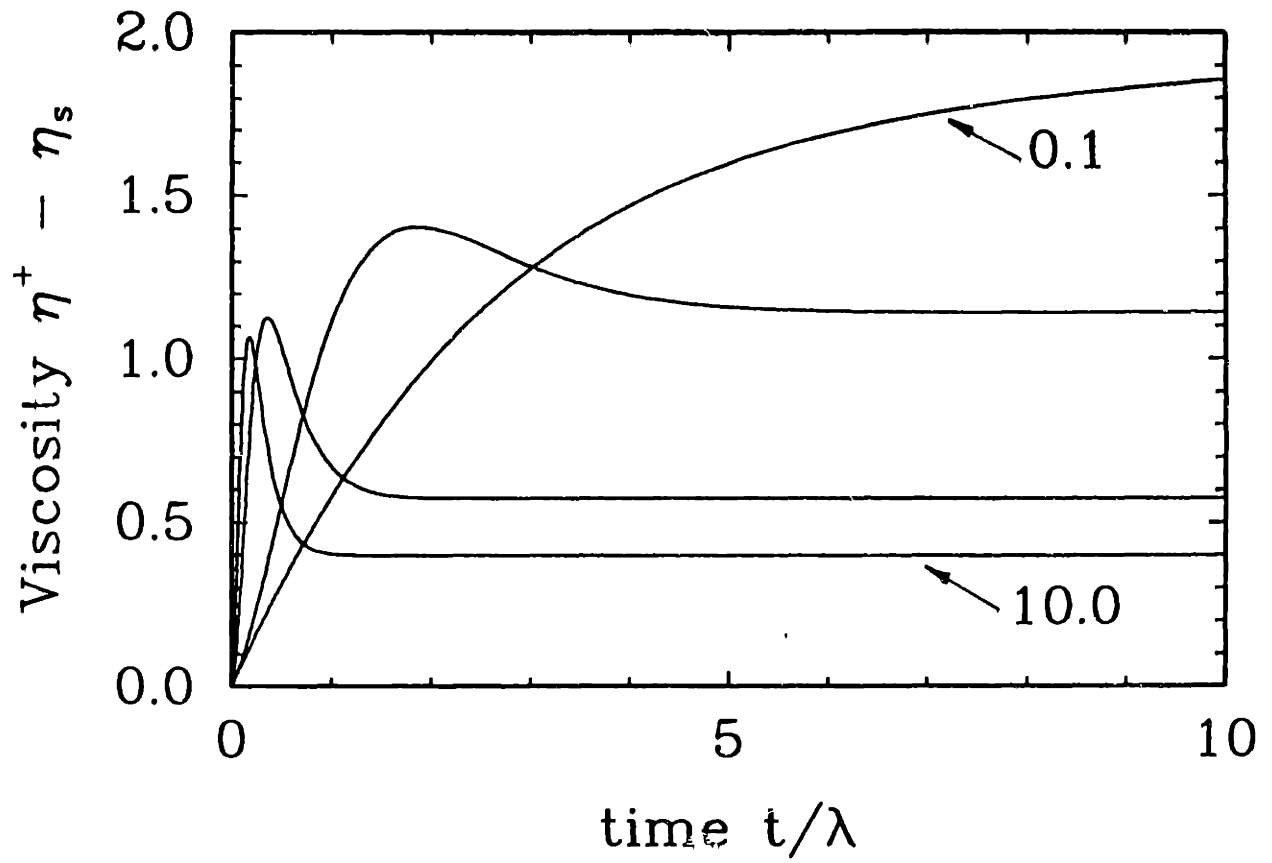
Figure 5-18: Variation of $\eta^+ - \eta_s$ with time t/λ in start-up of steady shear flow for $\mathcal{N} = 2$, $\sigma = 1$ and $\dot{\gamma}_0 = 0.1$, 1, 5 and 10.
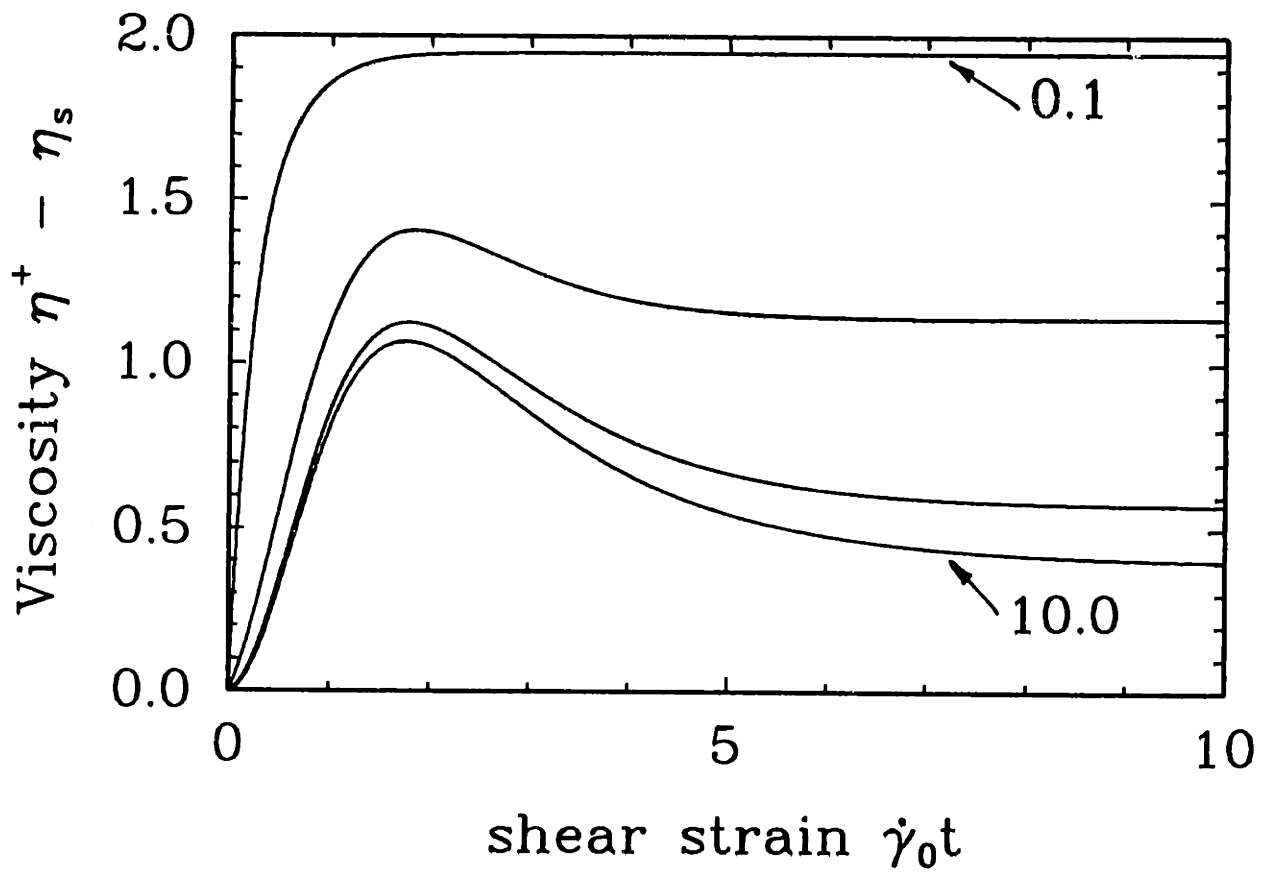
Figure 5-19: Variation of $\eta^+ - \eta_s$ with shear strain $\dot{\gamma}_0 t$ in start-up of steady shear flow for $\mathcal{N} = 2$, $\sigma = 1$ and $\dot{\gamma}_0 = 0.1$, 1, 5 and 10.
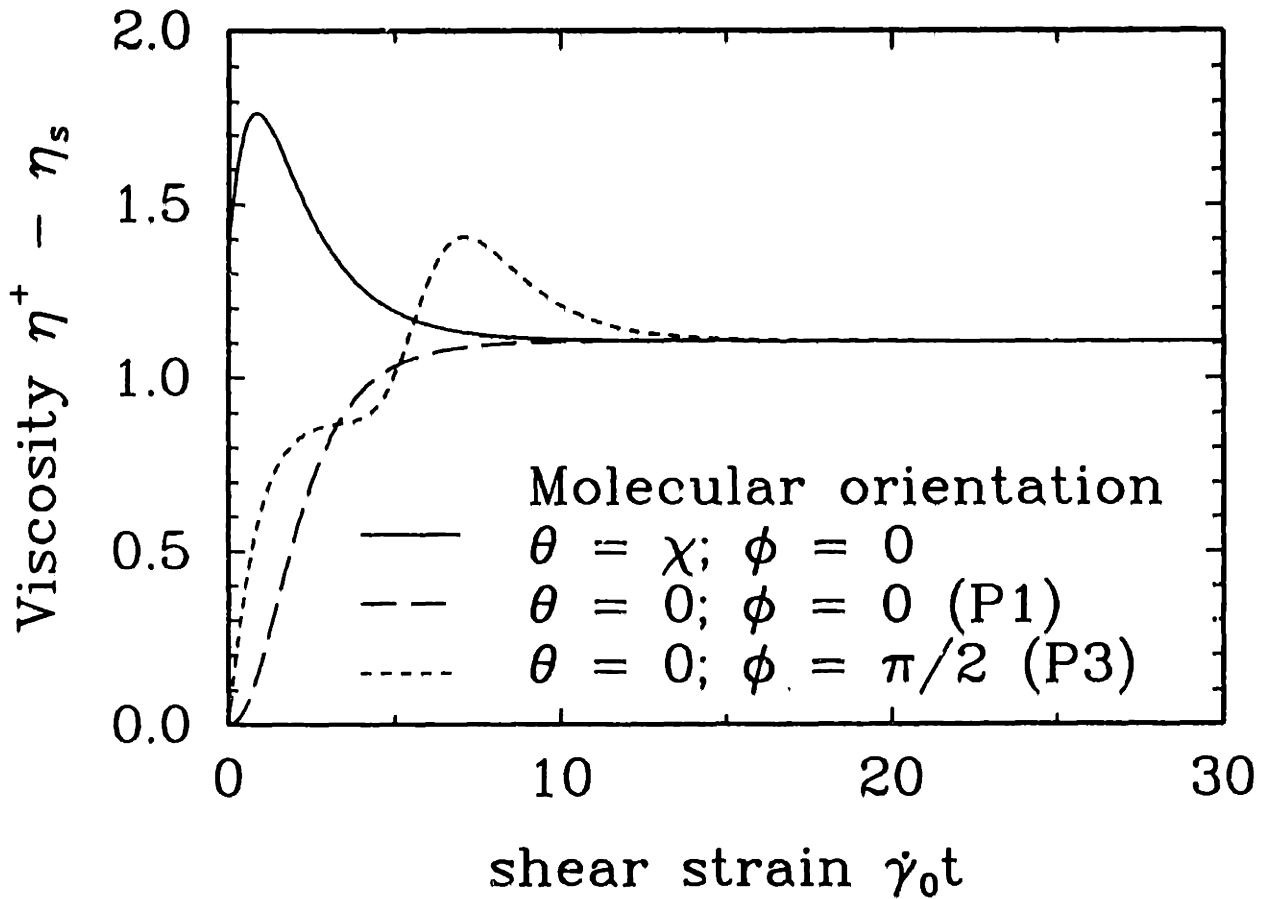
Figure 5-20: Variation of $\eta^+ - \eta_s$ with shear strain $\dot{\gamma}_0 t$ in start-up of steady shear flow for $\mathcal{N} = 4.5$, $\sigma = 1$, $\dot{\gamma}_0 = 5$. The three initial orientations correspond to molecules in the shearing direction (P1), molecules in the direction of vorticity (P3) and molecules aligned at the zero-shear-rate extinction angle χ to the shearing direction as proposed by Doi (1981).

from this result. Very different transient responses are seen in the three cases. For molecules oriented at the extinction angle χ, the non-zero shear stress at $t = 0$ results in a finite viscosity, followed by a sharp maximum. However, molecules oriented along P1 show a longer transient, and η^+ increases monotonically at the same value of $\dot{\gamma}_0$. The P3 state corresponding to the molecules aligned in the vorticity direction cannot exist at the value of $\dot{\gamma}_0$ chosen for the calculation, and rotation of the molecules as they get aligned in the direction of shear manifests itself as a characteristic double-oscillatory behavior that always accompanies the P3-P1 transition.

A recent study of transient material functions in shear and elongational flows has been carried out using a Brownian dynamics simulation (Honerkamp and Seitz, 1987). The results reported here compare well with the Brownian dynamics results. Note also that the Brownian dynamics calculations do not use the closure approximation, and hence these results are unaffected by closure at least in the parameter range studied. It is interesting that in calculations of start-up of shear flow, Honerkamp and Seitz report a non-zero viscosity at $t = 0$ followed by a viscosity maximum, similar to the results obtained by using the initial condition proposed by Doi (1981). They attribute the non-zero viscosity to the molecular rigidity, although in our results it is a consequence of non-zero shear stress at time $t = 0$ due to molecular orientation along the zero-shear-rate extinction angle χ. It is difficult to compare this transient behavior with any experimental data, since information about initial orientation is rarely reported in literature.

5.3.3 Shearfree Flows

For steady shearfree flows the two elongational viscosities $\bar{\eta}_1$ and $\bar{\eta}_2$ are defined as

$$
\bar{\eta}_1 \equiv -\frac{(\tau_{11} - \tau_{22})}{\dot{\epsilon}};
$$
$$
\bar{\eta}_2 \equiv -\frac{(\tau_{22} - \tau_{33})}{\dot{\epsilon}}. \tag{5.26}
$$

Since molecular orientation can cause loss of axisymmetry in the system, $\bar{\eta}_2$ is not necessarily zero for uniaxial elongation and biaxial stretching flows. Hence both $\bar{\eta}_1$

197

and $\bar{\eta}_2$ are calculated.

A. Uniaxial Elongational Flow. Two stable solution trajectories P1 and P2/P3 have been described in Section 5.2.2.2 for uniaxial elongation. Trajectory P1 corresponds to a nematic P family with $n = \delta_1$, and the trajectory P2/P3 represents collectively any nematic P family with the director constrained to lie in the 23-plane. As discussed previously, a limit point is encountered with increasing $\dot{\epsilon}$, for any $\mathcal{N}$ along states given by trajectory P2/P3. Thus these states are important only at low elongational rates, and have not been considered further in computing the material functions. The variation of the order parameter S predicted for the P1 family with $\mathcal{N}$ and $\dot{\epsilon}$ is shown in Figs. 5-7 and 5-8 for uniaxial elongational flow. As expected, $S \to 1$ for $\dot{\epsilon} \gg 1$ or for $\mathcal{N} \to \infty$. The rotational symmetry about the 1-direction is maintained because the molecules are arranged along the 1-direction. Consequently, $\bar{\eta}_2$ is zero for these states. Predictions for the elongational viscosity $\bar{\eta}_1$ as a function of elongational rate and concentration are shown in Fig. 5-21. At low elongation rates Eq. (5.14) predicts a constant elongational viscosity. A slight elongational thickening is predicted for $\sigma = 1$, and a constant high-elongation-rate viscosity $\bar{\eta}_\infty$ is observed. Asymptotic analysis in the $\dot{\epsilon} \gg 1$ limit by Menon (1990) confirms this observation. Asymptotic analysis of Doi's constitutive model in the limit $\dot{\epsilon} \gg 1$ indicates that $\bar{\eta}_\infty - 3\eta_s \sim (1 - S)^3 \sim \dot{\epsilon}^{-1}$, as seen in Fig. 5-21. The zero-elongation-rate elongational viscosity, $\bar{\eta}_0$, satisfies Trouton's relation, $\bar{\eta}_0 = 3\eta_0$, only in the limit $\mathcal{N} = 0$. The effect of σ on dimensionless $\bar{\eta}_1$ is shown in Fig. 5-22. As expected, $\bar{\eta}_1$ decreases with decreasing σ. For $\sigma = 1.0$ the fluid is elongation thickening, but with decreasing σ the fluid becomes elongational thinning.

B. Biaxial Stretching Flow. It was shown for biaxial stretching flow in Section 5.2.2.2 that for any concentration $\mathcal{N} > 3$, the only stable states correspond to trajectory P2/P3 which represents the nematic P phase oriented with the director in the 23-plane. For this family, the rotational symmetry about the 1-direction is not maintained, and both $\bar{\eta}_1$ and $\bar{\eta}_2$ are important material functions. The variations of

198
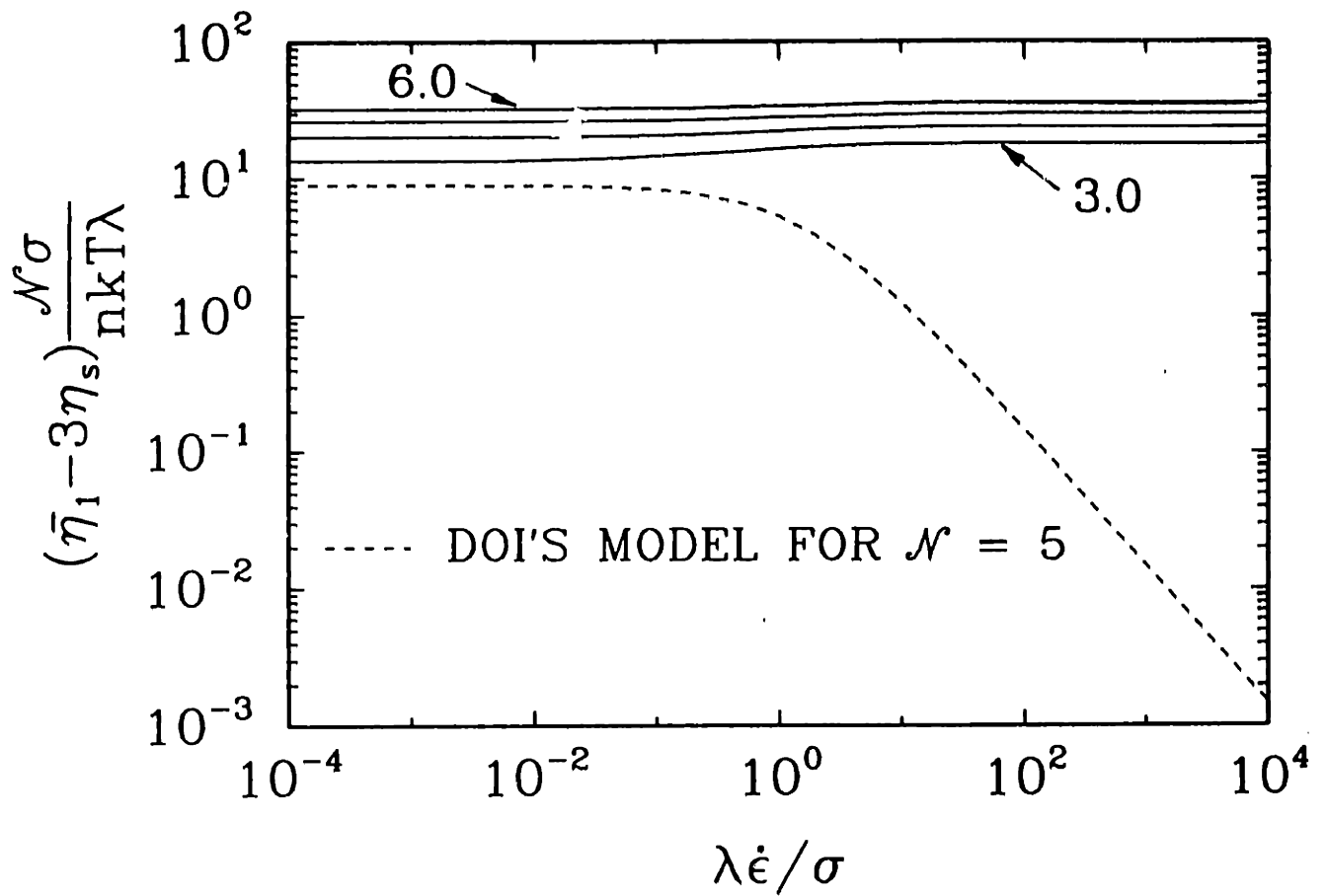
Figure 5-21: Prediction of $(\bar{\eta}_1 - 3\eta_s)\mathcal{N}\sigma/(nkT\lambda)$ in uniaxial elongational flow along trajectory P1 for $\mathcal{N} = 3.0$, 4.0, 5.0 and 6.0 and $\sigma = 1.0$. Predictions of Doi's model for $\mathcal{N} = 5.0$ are shown for comparison.
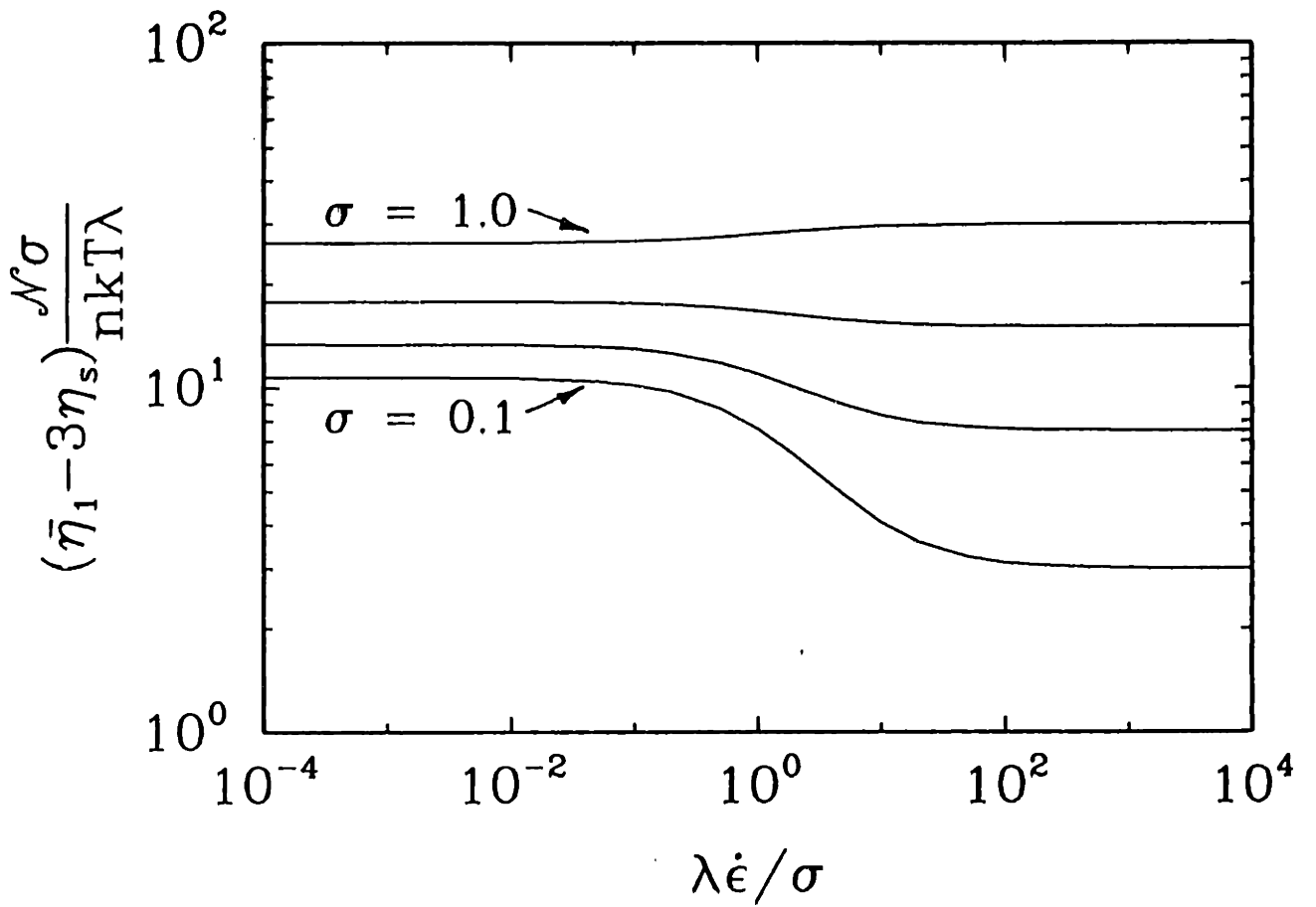
Figure 5-22: Variation of $(\bar{\eta}_1 - 3\eta_s)\mathcal{N}\sigma/(nkT\lambda)$ with σ in uniaxial elongational flow along trajectory P1 for $\mathcal{N} = 5.0$ and $\sigma = 1.0$, 0.5, 0.25 and 0.1.

$\bar{\eta}_1$ and $\bar{\eta}_2$ with $\overset{.}{\epsilon}$ for different concentrations are shown in Figs. 5-23 and 5-24 for the nematic P family with $n = \delta_2$. The effects of the parameter σ on dimensionless $\bar{\eta}_1$ and $\bar{\eta}_2$ are depicted in Figs. 5-25 and 5-26. All the calculations are carried out with zero solvent viscosity.

The predictions of our theory and Doi's theory are markedly different. Equation (5.14) predicts a nearly constant elongational viscosity $\bar{\eta}_1$, whereas Doi's equation predicts pronounced extensional-thinning. Reducing the parameter σ introduces the elongational thinning, as well as a reduction in the magnitude of $(\bar{\eta}_1 - 3\eta_s)\mathcal{N}\sigma/(nkT\lambda)$. The elongational viscosities increase with concentration $\mathcal{N}$.

5.3.4 Discussion of Results

The homogeneous constitutive model developed here predicts a variety of interesting equilibrium and dynamic behavior for solutions of rod-like liquid crystalline materials. Both prolate and oblate nematic phases bifurcate transcritically from the isotropic state with increasing concentration. Both nematic states display rotational invariance.

Introducing either shear or elongational flow breaks this invariance and creates distinct, multiple, steady-state phases that evolve as a function of strain-rate and concentration. The evolution induced by shear and uniaxial elongational flows is qualitatively similar as seen from Figs. 5-5 and 5-9; the bifurcation is broken and prolate states aligned in the direction of flow are favored. The biphasic region where nematic and isotropic phases coexist is seen only below a critical deformation rate. Beyond this, a smooth transition from a less-ordered nematic phase to a highly-ordered nematic phase is observed. Calculations by See *et al.* (1990) show good agreement with these results. Their study is based on calculating the order parameter by using techniques similar to those described in Section 5.2. In addition, See *et al.* have used perturbation methods to obtain predictions at low deformation rates in the absence of closure approximations. However, the calculations by these authors do not capture states such as the P3 family in shear flow or the P2/P3 family in uniaxial elongational flow that have been observed at high concentrations or low deformation rates. The change from a discontinuous isotropic-nematic transition to a continuous
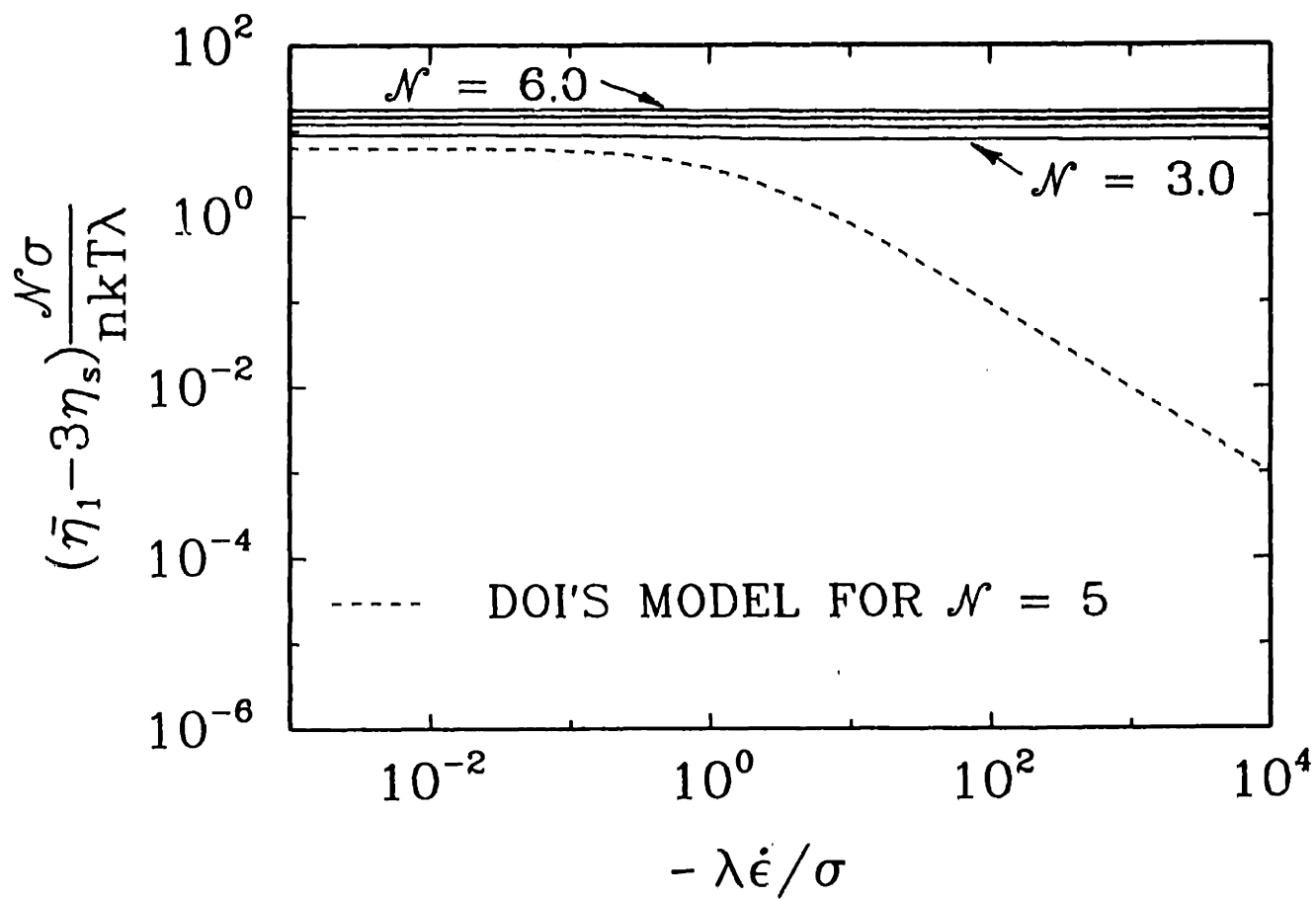
Figure 5-23: Predictions of $(\bar{\eta}_1 - 3\eta_s)\mathcal{N}\sigma/(nkT\lambda)$ in biaxial stretching flow along family P2 for $\mathcal{N} = 3.0$, 4.0, 5.0 and 6.0 and $\sigma = 1.0$. Predictions of Doi's model for $\mathcal{N} = 5.0$ are shown for comparison.
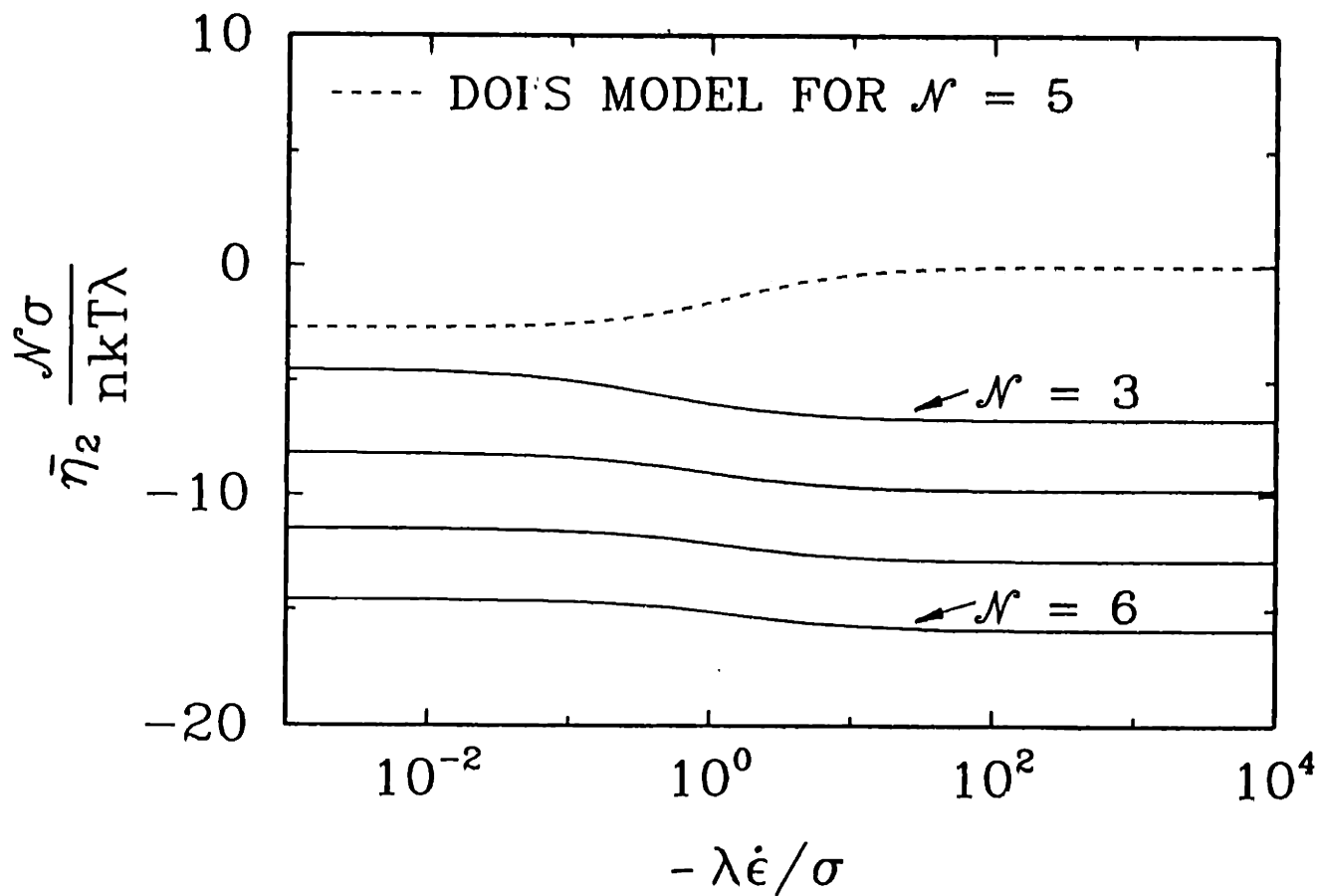
Figure 5-24: Predictions of $\bar{\eta}_2 \mathcal{N}\sigma/(nkT\lambda)$ in biaxial stretching flow along family P2 for $\mathcal{N} = 3.0$, 4.0, 5.0 and 6.0 and $\sigma = 1.0$. Predictions of Doi's model for $\mathcal{N} = 5.0$ are shown for comparison.
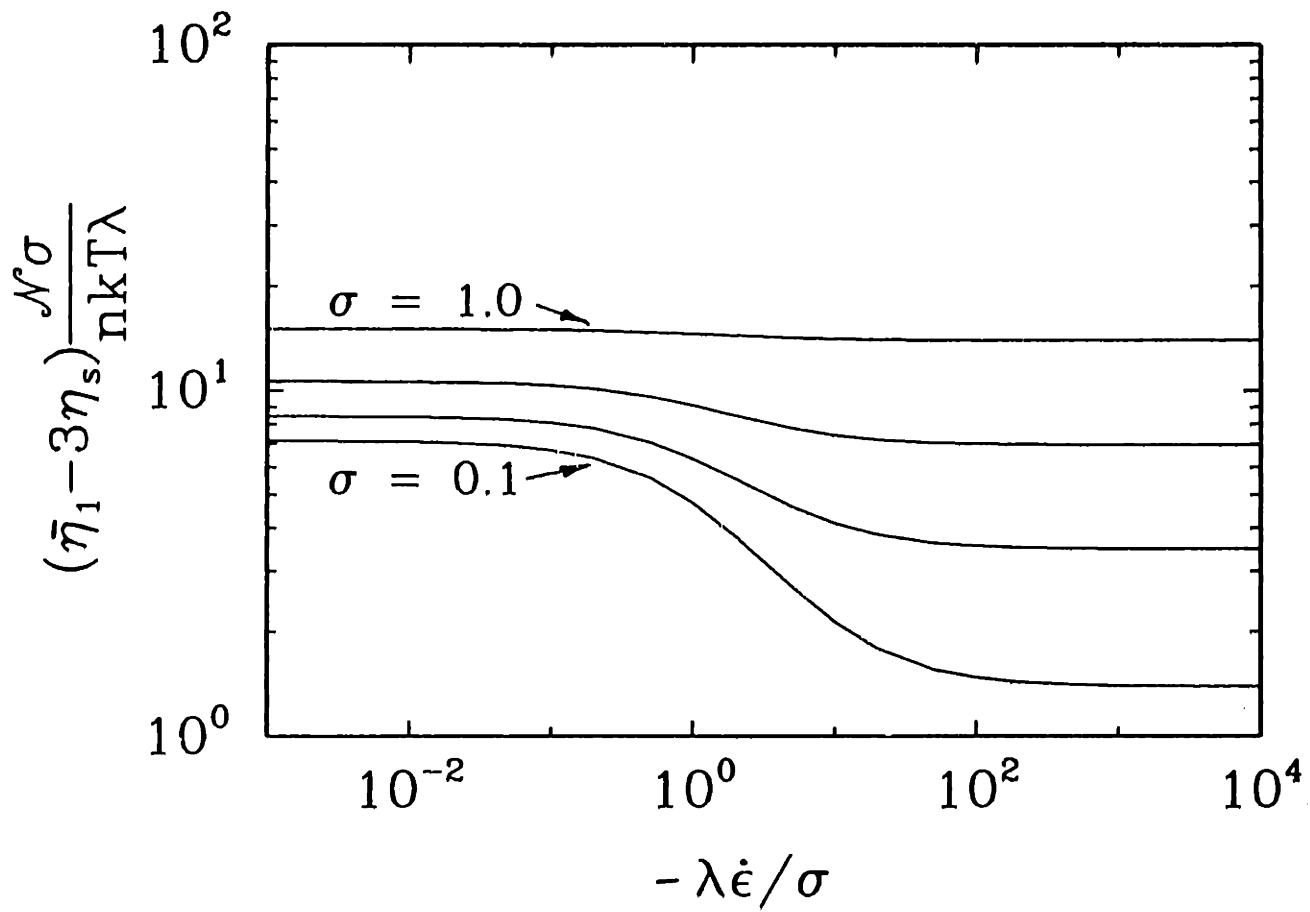
Figure 5-25: Variation of $(\bar{\eta}_1 - 3\eta_s)\mathcal{N}\sigma/(nkT\lambda)$ with σ in biaxial stretching flow along trajectory P2 for $\mathcal{N} = 5.0$ and $\sigma = 1.0$, 0.5, 0.25 and 0.1.
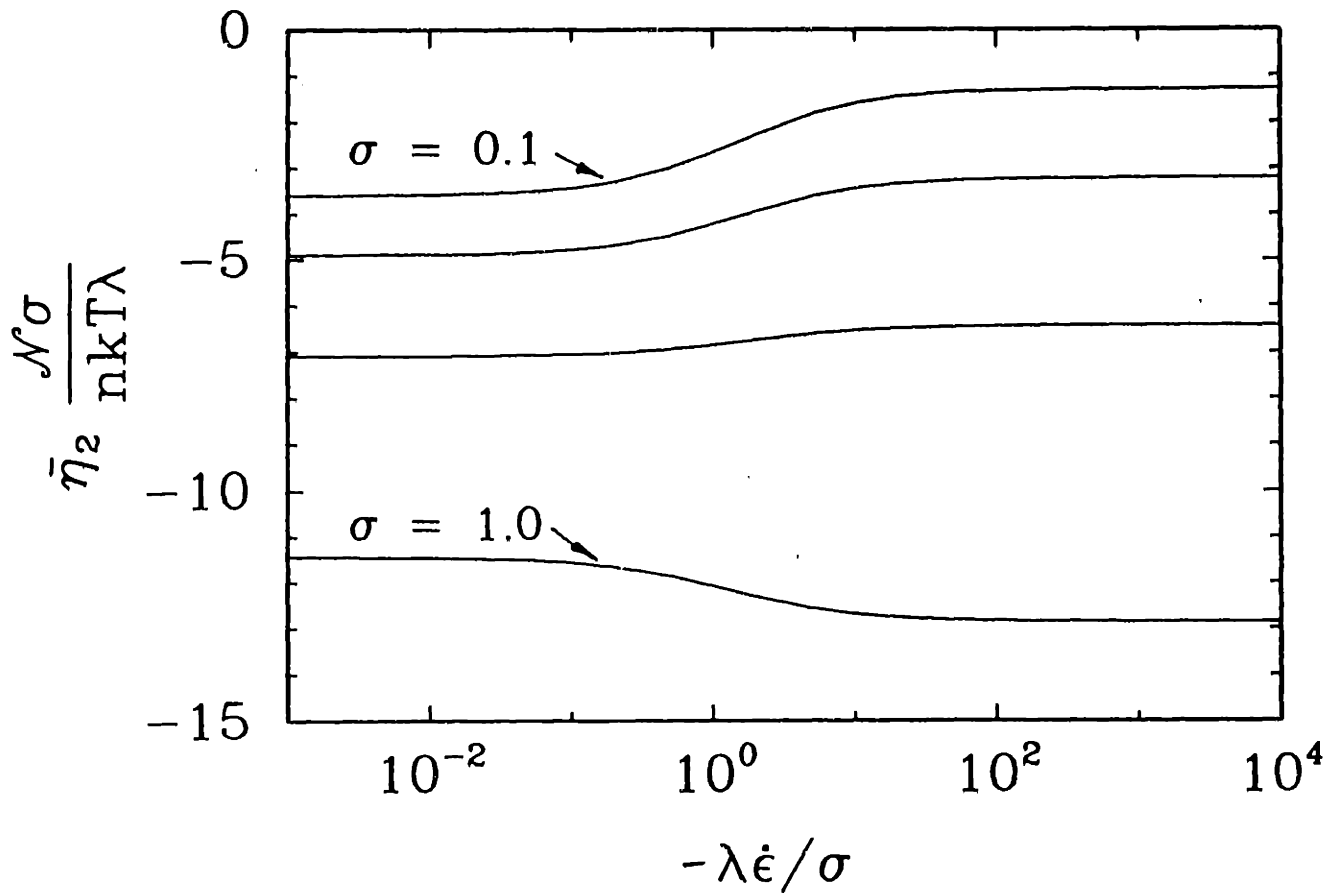
Figure 5-26: Variation of $\bar{\eta}_2 \mathcal{N}\sigma/(nkT\lambda)$ with σ in biaxial stretching flow along trajectory P2 for $\mathcal{N} = 5.0$ and $\sigma = 1.0$, 0.5, 0.25 and 0.1.

205

transition between nematic phases of differing order in the presence of shear flow also has been reported by Olmsted and Goldbart (1990). The calculations of these authors are based on nonequilibrium thermodynamics and are a generalization of the Leslie-Ericksen theory. These authors failed to obtain the P3 family.

An alternative technique that has been used to study the effect of uniaxial elongational flow on the isotropic-nematic transition involves incorporating an additional term in the free-energy expression to account for the elongational flow effects (Thirumalai, 1986; Lee, 1987). Other authors have studied the effect of elongational flows on the isotropic-nematic transition by exploiting the symmetry of the elongational flow (Wang and Gelbart, 1988). The results of these studies are in close agreement with the results for the P1 family in uniaxial elongational flow described in Section 5.2.2.2, but fail to detect solutions such as the P2/P3 families that do not display symmetry about the primary flow direction.

Despite the similarity between uniaxial elongational and biaxial stretching flows, the latter has not been studied previously. As shown in Section 5.2.2.2, biaxial stretching flow uniquely affects the evolution of the microstructure; there is a range of concentrations in which oblate nematic phases are stable with random alignment in the plane orthogonal to the kinematic axis of symmetry. However, due to the importance of excluded volume effects with increasing concentration, such a random, in-planar molecular arrangement is stable only below a critical concentration $\mathcal{N} = \mathcal{N}_{c2}^{bs}(\dot{\epsilon})$; see Fig. 5-14. Beyond this concentration, prolate states perpendicular to the kinematic axis of symmetry are preferred. Such an in-planar, oblate to prolate transition is a two dimensional analogue of the equilibrium isotropic-nematic transition and retains all the essential features of this transition. Since the oblate-prolate transition point is dependent on the elongational rate $\dot{\epsilon}$, it is possible to study the dynamics of the transition outside the biphasic concentration regime $8/3 < \mathcal{N} < 3$. This is an advantage since nucleation effects can be totally avoided in the study of the transition. The only possible drawback is the difficulty in producing and maintaining a perfectly biaxial stretching flow without end effects. The in-planar prolate states that are predicted here have not been observed experimentally, although others have speculated

a similar oblate to prolate transition (Hu and Ryskin, 1991).

By using the homogeneous constitutive theory described in Section 5.1, steady-state and transient material functions in both shear and shearfree flows have been calculated. In shear flow, as expected, the sudden drop in zero-shear-rate viscosity at the isotropic-nematic transition point is predicted. At low shear rates, both normal stresses and the shear stress show a linear dependence on the shear rate. In the high-shear-rate regime, viscosity shows a -2/3 dependence on the shear rate and has been shown to compare well with the experimental data of Doraiswamy and Metzner (1986). Incorporation of the viscous stress term in the stress tensor avoids the excessive shear-thinning inherent in the Doi molecular theory. The predictions of the theory presented in this chapter also compare well with experimental data obtained for the aromatic polyamide *Kevlar* (Ramalingam, 1993). The transient material function calculations, described in Section 5.3.2, illustrate the effect of different initial conditions on the material response. Although these calculations are based on a homogeneous, monodomain theory, they indicate that the rheological response in a polydomain material with different orientations in the different domains will be necessarily complex. As in the case of isotropic concentrated polymer solutions and polymer melts, the stress maxima are seen to scale with the strain imposed on the material. These transient calculations also show that rotation of the molecules from the P3 family to the P1 family is characterized by a double-oscillatory behavior; see Fig. 5-20. These results agree with the Brownian dynamics simulations by Honerkamp and Seitz (1987).

The effect of anisotropic drag on the material function predictions in shear flow has also been studied and is seen to be most pronounced for phases oriented in the direction of flow. However, $\sigma = 1$ (*i.e.*, isotropic drag) appears to agree well with experimental data in simple shear flow. Material functions in uniaxial elongational and biaxial stretching flows have also been obtained. The parameter σ is seen to have a pronounced effect on these predictions. However, due to the lack of experimental data for elongational flows, it is difficult to assess realistically the importance of anisotropic drag on these results. There is a need to gather such data on a variety of

liquid crystalline systems for elongational flows. The choice of a constant value for the parameter σ may not be fully accurate; it may be necessary to incorporate the effect of concentration and the state of order present in the surrounding medium as was discussed in Chapter 4.

The material functions predicted by the homogeneous theories of Doi (1981) and Menon (1990) do not capture the full extent of the complex rheological response characteristic of LCPs. For instance, the theory does not predict the sign changes of the first normal stress difference from positive at low shear rates to negative at intermediate shear rates followed by positive at high shear rates. Such negative first normal stress differences are also accompanied by large second normal stress differences (Magda et al., 1991); this behavior of the second normal stress difference also is not predicted by the present theory. It has been recently demonstrated that such a negative first normal stress difference and the accompanying large second normal stress difference can arise from a molecular tumbling about the vorticity axis; the failure of the homogeneous theories of Doi (1981) and Menon (1990) in predicting this phenomenon has been attributed to the use of the quadratic closure approximation (5.10) (Marrucci and Maffettone, 1989). The theories that do predict the incidence of molecular tumbling and the consequent development of negative first normal stress differences are based on a numerical calculation of the configurational distribution function from the diffusion equation (Marrucci and Maffettone, 1989; Larson, 1990; Larson and Öttinger, 1991). These techniques are computationally intensive, and the studies are therefore restricted to sampling only a few concentration and shear rates. Moreover, although they can be applied to homogeneous problems, rigorous application of these techniques to spatially nonhomogeneous systems that correctly predict a polydomain texture does not seem to be practical with available resources.

Use of closure approximations seems necessary in order to obtain a relatively simple, closed set of governing equations for the solution of complex fluid mechanical problems. The constraints that must be satisfied by any closure approximation and the different closure approximations that have been tried are discussed in the next section.

5.4 Note on Closure Approximations

The diffusion equation (5.7) and the expression for the stress tensor (5.9) can be numerically solved to obtain the rheological properties of the liquid crystalline systems. This technique was first used by Stewart and Sørensen (1972) in studying the rheology of a dilute solution of rigid rods and was adapted by Larson (1990) and Larson and Öttinger (1991) to the study of liquid crystalline systems. The numerical technique involves expanding the distribution function f_p in a series of spherical harmonic functions. Equations for the coefficients of the basis functions can be obtained by exploiting the orthogonality of the basis functions; the resultant set of equations is numerically solved and the distribution function is reconstructed. The number of terms retained in the spherical harmonic expansion is dependent on the degree of accuracy desired in the distribution function; when the distribution function is highly peaked as in liquid crystalline systems as many as 12 terms are needed just beyond the isotropic-nematic transition.

This technique can be applied fairly easily to simple flow fields. However, for more complex flow fields that are encountered in realistic fluid mechanical problems, the problem becomes computationally intensive (Advani and Tucker, 1987). As an illustration, suppose a finite element grid uses 500 nodes. At each nodal point, the distribution function $f_p(u, t)$ must be computed by discretizing the orientation angles (θ, ϕ). Even for a coarse representation, at least 20 nodes each in θ and ϕ are desired, and the total number of variables corresponding to the distribution function alone is $\mathcal{O}(10^5)$! A more compact description of molecular orientation is thus desirable.

The spherical harmonic expansion used in these numerical techniques is based on a moment expansion of the distribution function, where the basis functions are the surface spherical harmonics S_0, S_2, etc. (Bird *et al.*, 1987b), and the corresponding coefficients are the moments of the distribution function with respect to u. The moment expansion for f_p is given by (Onat and Leckie, 1987)

$$f_p(u, t) = \frac{1}{4\pi} + \frac{5}{8\pi} B_2 : S_2 + \frac{3}{32\pi} B_4 \vdots S_4 + \dots \qquad . \qquad (5.27)$$

where the deviatoric form of the second moment B_2 is the familiar structure tensor S defined in Eq. (5.5). Governing equations for B_2, B_4, etc. are obtained by substituting this expansion in the diffusion equation and exploiting the orthogonality of the surface spherical harmonics. The distribution function is reconstructed from these moments in a manner analogous to obtaining f_p numerically from the coefficients of the spherical harmonic basis functions. In practice, only a finite set of even order moments is computed, and this corresponds to the truncation of the series (5.27) after the required number of terms. Moreover, since the primary interest of rheologists lies in computing the stress tensor that involves only the second and fourth order moments, moments higher than the fourth are never considered.

Governing equations for the second and fourth order moments are obtained from the diffusion equation. However, as explained in Section 5.1, a problem of closure occurs at all orders. Thus, the equation for the second moment involves the fourth, the equation for the fourth involves the sixth, and so on. In order to truncate the series after a finite number of moments, it is necessary to approximate the higher order moments in terms of the lower ones. Two choices are available, *viz.*, approximation of the sixth moment in terms of the second and fourth moments, or approximation of the fourth moment in terms of the second moment. The higher the order of the moment that is being approximated, the greater the number of available choices of closure approximations. The number of terms in the simplest approximation of the sixth moment in terms of linear combinations of the second and fourth moments and the unit tensor is 75 (Hand, 1962). If quadratic combinations of the second and fourth moments were allowed, the number of terms would be much higher. Use of such complex approximations is clearly not justified by the marginal information provided by the fourth moment over and above that provided by the second (Advani and Tucker, 1987). The use of closure approximations has therefore been restricted to rewriting the fourth moment in terms of the second moment. Some of the commonly used approximations are discussed below.

There is no unique way of constructing a closure approximation. Any approximation, however, must satisfy the following conditions in order to preserve the symmetry

displayed by the original diffusion equation (Advani and Tucker, 1987).

1. The symmetry of the moment equation with respect to the transposition of the indices on all the terms must be satisfied.

2. The higher order moments satisfy the normalization condition $\langle u_n \rangle : \delta = \langle u_{n-2} \rangle$, where $\langle u_n \rangle$ represents the nth-order moment. The closure approximation must satisfy this normalization condition.

3. The higher order moments are symmetric with respect to the transposition of any pair of indices. This symmetry is of a higher order than the symmetry of the moment equation for the lower order moment. Closure approximations should, ideally, retain this symmetry.

Condition 3 is a stringent condition that is more difficult to satisfy as the order of the moment that is being approximated is increased. If condition 3 is satisfied, conditions 1 and 2 are automatically met.

However, these guidelines are also not sufficient for constructing closure approximations; multiple closure approximations may satisfy the guidelines and must be evaluated based on other considerations. For instance, the distribution function for an isotropic system at equilibrium is exactly known and can be used to check the validity of the closure approximation under equilibrium conditions. In conditions of perfect prolate symmetry, $u = n$ and the different averages are easily evaluated. The accuracy of the closure approximations under these conditions also can be examined. It is necessary to examine the closure approximation under conditions of oblate symmetry to ensure that the predictions are physically meaningful.

Predictions of molecular tumbling by numerical calculations of the distribution function and the importance of this phenomenon in explaining the negative normal stresses displayed by LCPs makes it necessary to understand whether any closure approximation is capable of predicting this tumbling behavior. A quick way of checking the possible incidence of molecular tumbling with a closure approximation has been suggested by Larson (1990). Larson argues that in weak shearing flows, where the scalar order parameter S is not much changed from equilibrium, the structure tensor

$S = S^{eq}[nn - \frac{1}{3}\delta]$. The director vector n can be obtained from the Leslie-Ericksen limit of the Doi theory and is given as

$$\frac{\partial n}{\partial t} = \frac{1}{2}\omega^\dagger \cdot n + \frac{\lambda}{2}(\dot{\gamma} \cdot n - \dot{\gamma}:nnn) \qquad (5.28)$$

where $\dot{\gamma}$ and ω are the rate-of-strain and vorticity tensors, respectively. The parameter λ is a constant that depends on the equilibrium distribution function $f_{p,eq}$ and is a measure of the importance of the straining motion over vorticity. If $\lambda > 1$, straining motion dominates and n tends to a steady-state orientation angle Θ with $\Theta = ((\lambda - 1)/(\lambda + 1))^{1/2}$. If $\lambda < 1$, vorticity dominates; there is no steady-state orientation, and n tumbles continuously. Equating the excluded volume and Brownian motion contributions, and rewriting Eq. (5.8) for the second order moment in terms of n gives

$$S^{eq}\frac{\partial n}{\partial t} = \frac{1}{3}\dot{\gamma} \cdot n + S^{eq}\omega^\dagger \cdot n + \frac{1}{6}S^{eq}\dot{\gamma} \cdot n - \dot{\gamma}:\langle uuuu \rangle \cdot n. \qquad (5.29)$$

In deriving Eq. (5.29), terms that are parallel to n are ignored since they only serve to fix the magnitude of n as $|n| = 1$ and are not otherwise significant. Substituting a closure approximation for the fourth moment $\langle uuuu \rangle$ and comparing the resultant equation with Eq. (5.28) allows the parameter λ to be computed as a function of S^{eq}. It can thus be determined whether a given closure approximation is capable of predicting molecular tumbling.

5.4.1 Comparison of Closure Approximations

Quadratic Closure Approximation. The quadratic closure approximation that was used in this chapter can be written as

$$\langle uuuu \rangle \simeq \langle uu \rangle \langle uu \rangle. \qquad (5.30)$$

This approximation does not fully maintain the symmetry of the fourth order moment. Despite this, the symmetry requirement of the second moment equation and the

212

normalization condition are satisfied due to the low order of the moments involved. The quadratic closure approximation is also exact under conditions of prolate and oblate symmetry. However, the lack of symmetry with respect to transposition of any two indices results in an inexact equilibrium approximation. More specifically, the exact fourth order moment at equilibrium is $1/15(\delta\delta + I + I^{\dagger})$, whereas the quadratic closure approximation predicts it to be $1/9\delta\delta$. The approximation (5.30) is therefore not expected to be accurate near isotropic equilibrium. The parameter λ computed with this approximation is

$$\lambda^{QC} = \frac{2 + S^{eq}}{3S^{eq}}. \tag{5.31}$$

For the entire range $0 \leq S^{eq} \leq 1$, $\lambda < 1$ as shown in Fig. 5-27 and tumbling will not be predicted. This result is in agreement with the numerical calculations presented in Section 5.2.

Hinch and Leal's First Closure Approximation (HL1). Hinch and Leal (1976) tried to overcome the drawbacks of the quadratic closure approximation by constructing an alternative approximation that would be exact in limits of perfect order and under conditions of isotropic equilibrium. Forms of closure that are exact in one of these limits are first constructed and a composite of these forms is obtained. The approximation is presented for $A:\langle uuuu \rangle$ where A is a symmetric, traceless, second-rank tensor, rather than for $\langle uuuu \rangle$. The first composite form developed by Hinch and Leal is

$$
\begin{aligned}
A:\langle uuuu \rangle \quad \simeq \quad A: & \left[\frac{2}{5}(\delta\langle uu \rangle + \langle uu \rangle\delta) - \frac{1}{5}\langle uu \rangle\langle uu \rangle \right. \\
& + \frac{3}{5}(\langle uu \rangle\langle uu \rangle^{2 \to 3} + \langle uu \rangle\langle uu \rangle^{2 \to 4}) \\
& \left. - \frac{2}{5}(\delta\langle uu \rangle \cdot \langle uu \rangle + \langle uu \rangle \cdot \langle uu \rangle\delta) \right]. \tag{5.32}
\end{aligned}
$$

In the above equation, the notation $\Lambda^{2 \to 4}_{ijkl}$ corresponds to a shift of the index in position 2 to position 4, i.e., $\Lambda^{2 \to 4}_{ijkl} \equiv \Lambda_{iklj}$. The approximation HL1 exactly satisfies the conditions of symmetry of the moment equation and normalization. It is also
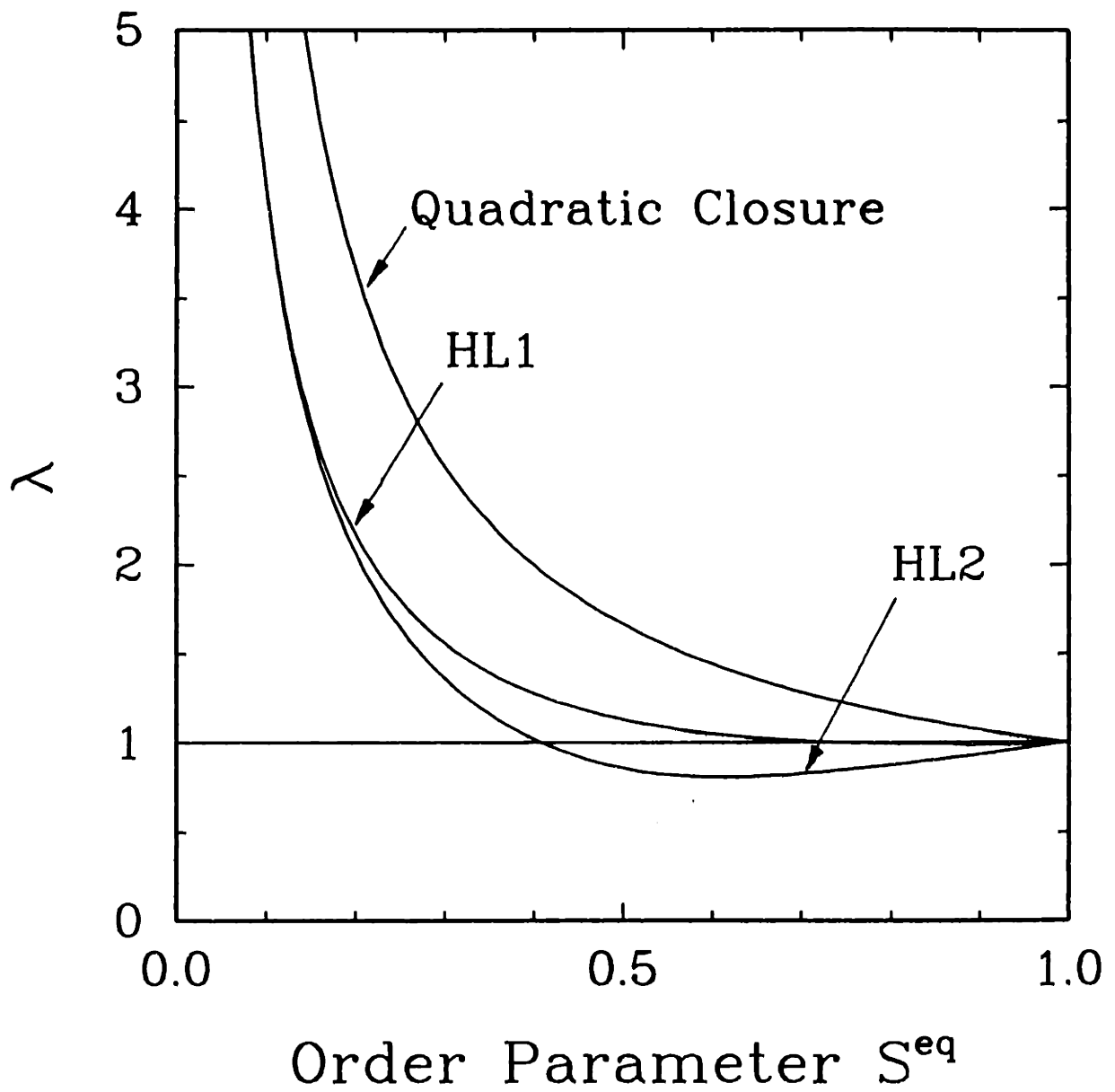
Figure 5-27: The parameter λ plotted as a function of S^{eq} for different closure approximations.

exact in the limit of random disorder with $f_p = 1/4\pi$ *provided* that A is traceless. The condition of prolate symmetry is exactly satisfied. However, under conditions of oblate symmetry, the approximation is inexact and may lead to aphysical results. Thus, for example, if the HL1 approximation is used to derive a closed set of equations, as in Section 5.1, it predicts an oblate phase with an order parameter $S \to -3/4$ at high concentrations, which is physically impossible. Although it could be argued that the oblate phase is unstable at high concentrations and therefore of little interest, this flaw of the HL1 approximation also is manifest in biaxial stretching flows at high extensional rates. Aphysical results using the HL1 approximation in fiber suspension models under biaxial stretching flow were also observed by Advani and Tucker (1990). The HL1 approximation is therefore unsuitable for the study of arbitrary flow fields. For the sake of completeness, the parameter λ predicted by the HL1 approximation is

$$\lambda^{\text{HL1}} = \frac{8S^{\text{eq}2} + S^{\text{eq}} + 6}{15S^{\text{eq}}}. \tag{5.33}$$

This approximation predicts a value of $\lambda < 1$ in the range $0 \le S^{\text{eq}} \le 1$ as shown in Fig. 5-27, and can show periodic tumbling behavior.

Hinch and Leal's Second Closure Approximation (HL2). An alternative composite closure approximation was also suggested by Hinch and Leal (1976) as an improvement over the HL1 approximation and is given as

$$
\begin{aligned}
A{:}\langle uuuu \rangle \;\simeq\; A{:}\Big[&\frac{26}{315}\alpha(\delta\delta + I + I^\dagger) + \frac{16}{63}\alpha(\delta\langle uu\rangle + \langle uu\rangle\delta) \\
&-\frac{4}{21}\alpha((\delta\langle uu\rangle + \langle uu\rangle\delta)^{2\to 3} + (\delta\langle uu\rangle + \langle uu\rangle\delta)^{2\to 4}) \\
&+\langle uu\rangle\langle uu\rangle + \langle uu\rangle\langle uu\rangle^{2\to 3} + \langle uu\rangle\langle uu\rangle^{2\to 4} \\
&-\frac{2}{\langle uu\rangle{:}\langle uu\rangle}\langle uu\rangle\cdot\langle uu\rangle\langle uu\rangle\cdot\langle uu\rangle\Big]
\end{aligned} \tag{5.34}
$$

with

$$\alpha = \exp\left[\frac{2(1 - 3\langle uu\rangle{:}\langle uu\rangle)}{1 - \langle uu\rangle{:}\langle uu\rangle}\right]. \tag{5.35}$$

215

The HL2 approximation maintains the symmetry of the moment equations and satisfies the normalization condition for traceless A. The approximation also is exact at equilibrium and under conditions of prolate ordering with $u = n$. The oblate ordering condition is not exactly satisfied, but the only nonzero terms are scaled with α which decreases exponentially with development of oblate symmetry. The HL2 approximation is thus expected to behave better than the HL1 approximation. However, Advani and Tucker (1990) report that although HL2 behaves quite well in most flows, it displays artificial oscillations in the components of the structure tensor under conditions of strong alignment. It's use is therefore restricted to low deformation rates. Under conditions of such strain rates, the parameter λ obtained by using Larson's criterion is given as

$$\lambda^{\mathrm{HL2}} = \frac{1}{9S^{\mathrm{eq}}}\left[2 - S^{\mathrm{eq}} + 8S^{\mathrm{eq}2} + \frac{56 + 80S^{\mathrm{eq}}}{35}\exp\left(\frac{-6S^{\mathrm{eq}2}}{1 - S^{\mathrm{eq}2}}\right)\right]. \tag{5.36}$$

The parameter λ is less than unity over a large range of order parameter; see Fig. 5-27. Tumbling behavior is thus expected with this approximation.

Hybrid Closure Approximation (HCA). In the context of the liquid crystal problem, one can examine the deficiencies of the quadratic closure approximation that is by far the most reliable closure approximation under all flow rates, and study suitable ways of modifying it. For instance, the quadratic closure approximation which is correct in the limit of perfect prolate order is a suitable approximation at high concentrations. This approximation can be used in the excluded volume terms that are increasingly important at high concentrations. Thus, the predictions of the governing equations at equilibrium would be unchanged. At low deformation rates, when the excluded volume terms nearly balance the Brownian motion terms, the quadratic closure approximation for $S{:}\langle uuuu\rangle$ continues to be valid. However, under such low deformation rates, when the system is close to conditions of isotropic equilibrium, the contribution from terms such as $\kappa{:}(I + I^{\dagger}) = \dot{\gamma}$ is significant. The absence of the cross terms, that lead to $(I + I^{\dagger})$ in the quadratic closure approximation does not capture this contribution in the governing equations.

A possible solution is to let $\kappa{:}\langle uuuu \rangle \simeq \kappa{:}(\langle uu \rangle \langle uu \rangle + C(S)(I + I^\dagger))$, where C is taken to be an arbitrary function of the structure tensor S. This closure approximation changes the coefficient of $\dot{\gamma}$ in Eq. (5.13). There is no *a priori* method for selecting the functional form for $C(S)$. However, the parameter λ is obtained in terms of $C(S)$ as

$$\lambda^{\text{HCA}} = \frac{2 + S^{\text{eq}} - 12C}{3S^{\text{eq}}} \tag{5.37}$$

One possible way of choosing C is to match this expression for λ with those obtained for any of the earlier closure approximations as given by Eqs. (5.31), (5.33) and (5.36), although this choice is not unique. Choosing $C = 0$ corresponds to the quadratic closure approximation and reduces the equation set to the one developed in Section 5.1.

The results of Larson (1990) and Larson and Öttinger (1991) obtained by numerical solution of the exact diffusion equation for the configurational distribution function can be used to compare the results of the hybrid closure scheme for different choices of the function C. These authors show plots of the variable $(S_{22} - S_{33})$ as a function of strain. For molecular alignment in the 12-plane, molecules aligned in the flow direction 1 correspond to $(S_{22} - S_{33}) \simeq 0$; alignment in the 2-direction corresponds to large positive values of $(S_{22} - S_{33})$ that are comparable to S^{eq}. They report a time-periodic behavior of $(S_{22} - S_{33})$ at low shear rates that corresponds to molecular tumbling in the 12-plane. At high shear rates, the oscillatory behavior decays in 2-3 periods. In all cases, the period scales with the imposed shear rate. Out-of-plane orientations in the 23-plane have also been studied (Larson and Öttinger, 1991) and show similar behavior.

In order to compare the predictions of the hybrid closure scheme with the results of Larson (1990) and Larson and Öttinger (1991), time-dependent calculations were carried out. The function C was matched to the HL1 and HL2 approximations that are expected to show tumbling behavior (since $\lambda < 1$). In both cases, time periodic behavior is observed as seen from Figs. 5-28 and 5-29.

In the case where C is chosen to match the HL1 approximation, the time-dependent
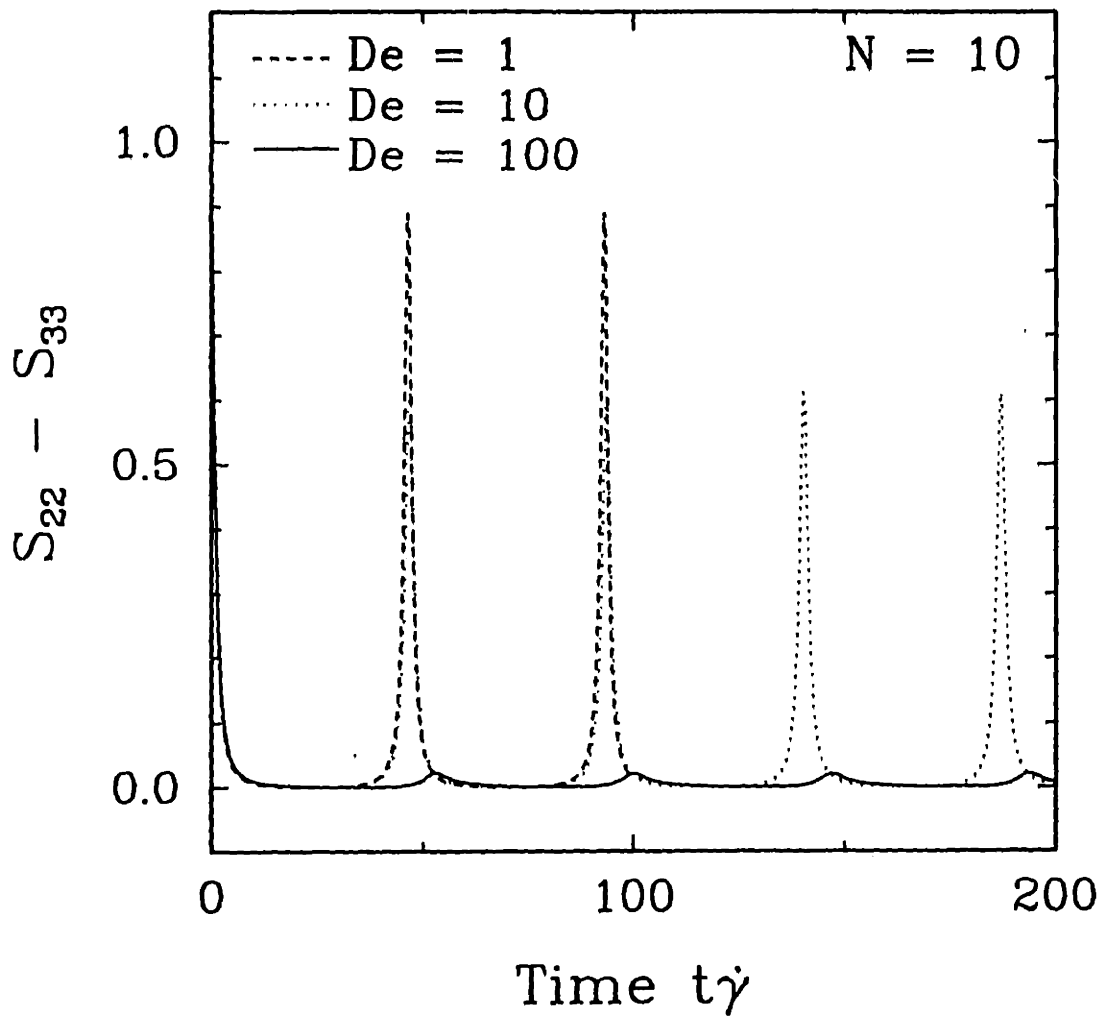
Figure 5-28: Time periodic behavior for the choice of C matched to the HL1 approximation.
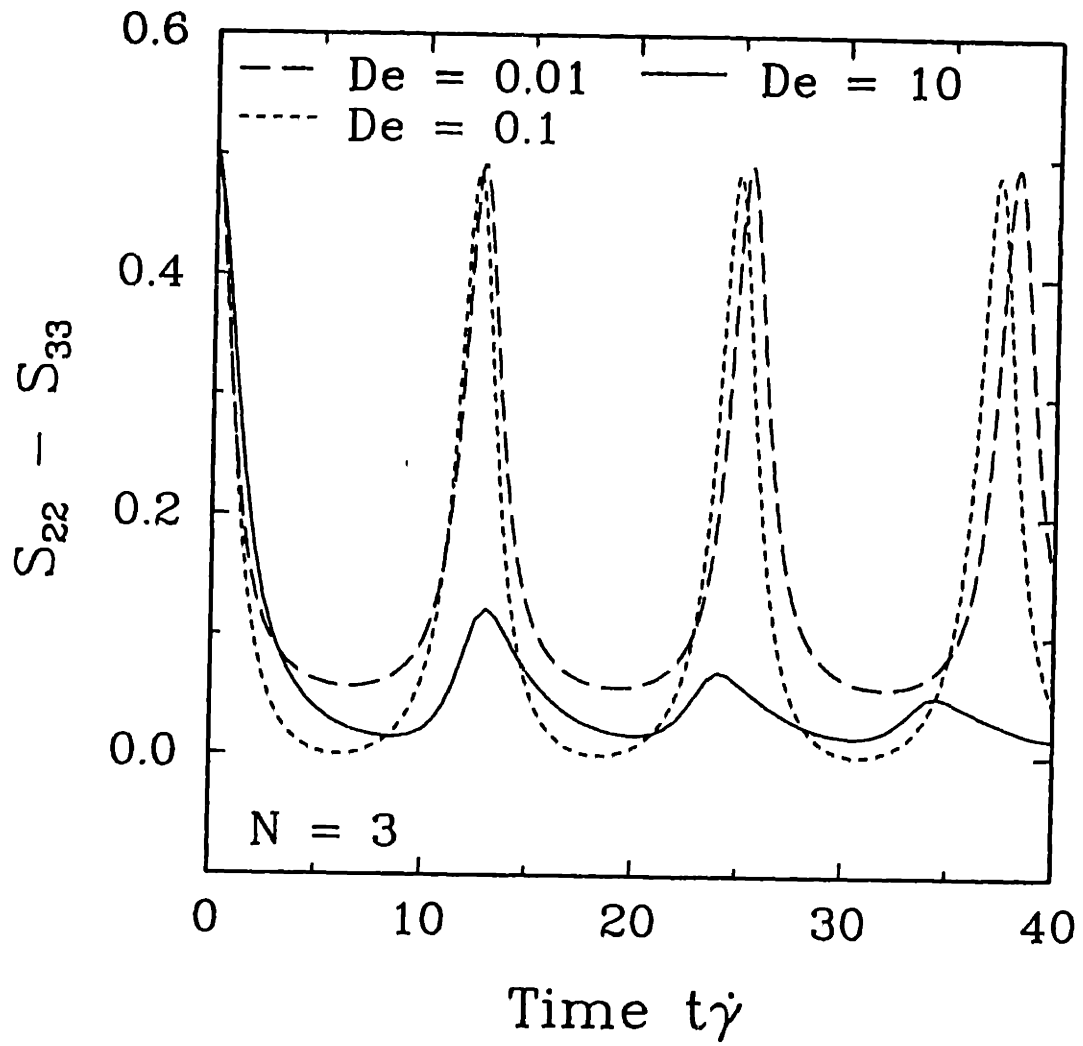
Figure 5-29: Time periodic behavior for the choice of C matched to the HL2 approximation for De = 0.01, 0.1 and 10.

profiles did not compare well with the results of Larson (1990) and Larson and Öttinger (1991). Periodic behavior was observed for values of De $\equiv \lambda\dot{\gamma}/\sigma$ as high as 100 that are much higher than expected from the exact results. Moreover, the oscillations never appear to decay in amplitude over a finite number of periods; rather, the amplitude shows abrupt decrease with increasing shear rate as seen in Fig. 5-28.

In the case of the match to the HL2 approximation, the time-periodic behavior at De < 10 shows reasonably good comparison with the exact results of Larson (1990) and Larson and Öttinger (1991). At low shear rates, the oscillatory behavior persisted for all time, while for the high shear rates > 5, a decay in the oscillations was observed; see Fig. 5-29. However, for values of high De > 50, the amplitude of oscillation increased with increasing De in an aphysical manner as shown in Fig. 5-30. This restricts the applicability of the HL2 approximation only to low shear rates. Similar aphysical oscillations were reported by Advani and Tucker (1990) on using the HL2 approximation for high shear rates.

In summary, the study of the guidelines for constructing closure approximations indicates that there is no unique way of developing closure approximations. Moreover, examination of the different approximations that are commonly used indicates that an approximation that is well-behaved in some flow-fields may develop aphysical characteristics in some other flow as in the case of the HL1 approximation. The process of choosing a suitable closure approximation must, per force, proceed by trial and error, and no closure approximation can be guaranteed to be universally acceptable.
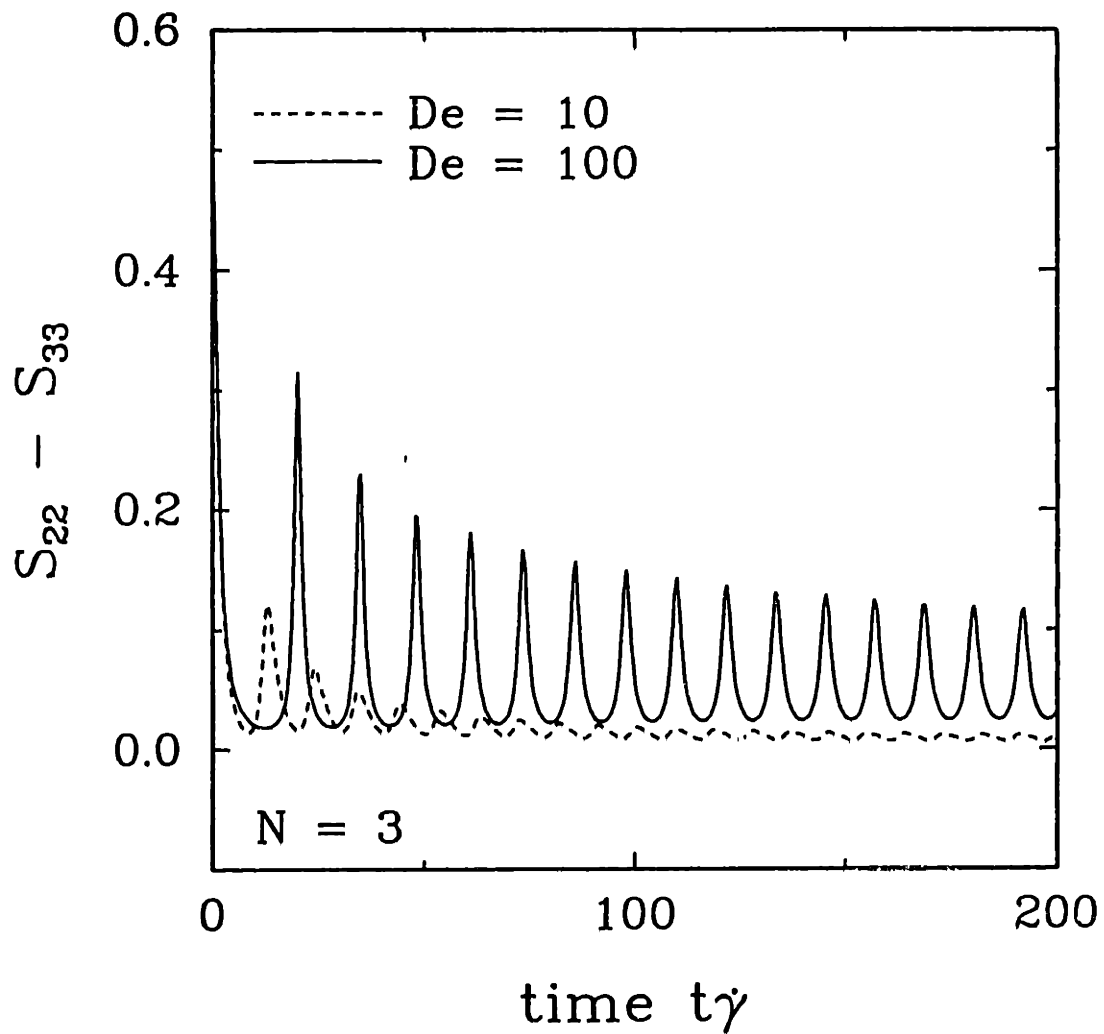
Figure 5-30: Time periodic behavior for the choice of C matched to the HL2 approximation for De = 10 and 100. Large aphysical oscillations are seen at high shear rates.

Chapter 6

Study of Nonhomogeneous Liquid Crystalline Polymer Systems

6.1 Aspects of Nonhomogeneous Liquid Crystalline Polymers

The presence of defe ts and distortions creates polydomains in the liquid crystalline phase. The polydomain texture is initially attributed to the development of structure that occurs at the isotropic-nematic transition point. A schematic drawing of the equilibrium phase transition is shown in Fig. 6-1. In the metastable region both isotropic and nematic prolat. states are linearly stable and coexist. A finite fluctuation is required to render either phase unstable; this fluctuation is the *nucleus*. The nucleus is small in extent but is of large degree, *i.e.*, a nucleus of a prolate nematic phase in a largely isotropic solution will have well-developed orientational order and thus distinctly different material properties from the surrounding isotropic medium. Phase separation, in this case, occurs by *nucleation and growth*. In the unstable region, the isotropic phase is linearly unstable to fluctuations that are infinitesimal in degree but that can be large in extent. No barrier exists for the formation of the stable prolate nematic phase, and a continuous transformation from the disordered phase to the ordered phase is expected. This process is termed *spinodal decomposition.*
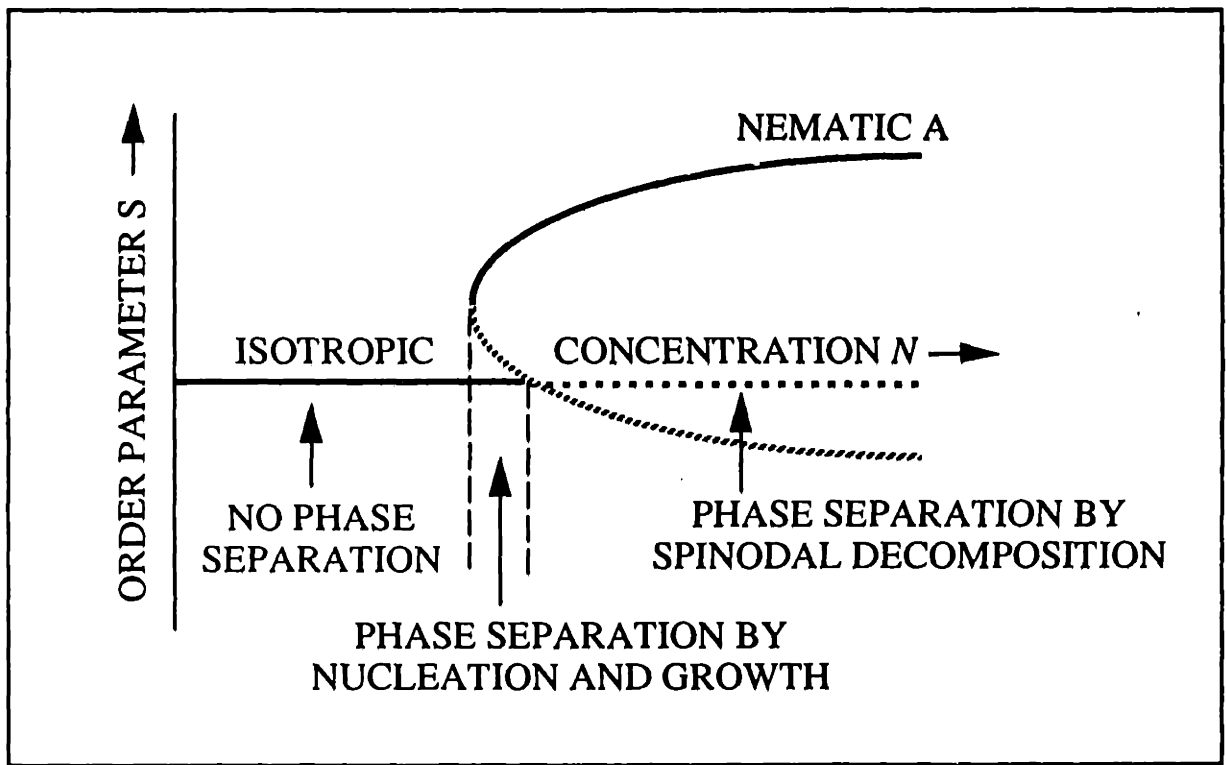
Figure 6-1: The isotropic-nematic phase transition at equilibrium.

Both nucleation and spinodal decomposition eventually lead to the development of a polydomain texture in the liquid crystalline phase. The popular concept of a domain is that of a three-dimensional region of locally-correlated molecular orientation. The orientation between such neighboring domains is uncorrelated, and rapid orientational changes are seen across the surfaces between domains. It is argued by de Gennes (1974) that such surface defects are likely to be unstable and must decay to point and line defects in the system.

The interactions of these defects and distortions with the imposed flow can significantly affect the rheology of LCPs, as suggested by Onogi and Asada (1980); see Section 4.1. A fundamental understanding of the structure formation and its relation to intermolecular interactions needs to be developed. The nonhomogeneous theory of liquid crystalline polymers developed in Chapter 4 is therefore used in this chapter to study the onset of spinodal decomposition at the isotropic-nematic transition point.

Phase separation by spinodal decomposition has been studied in diverse systems ranging from binary alloys and glasses (Cahn, 1961 & 1965) to polymer blends (de Gennes, 1980; Pincus, 1981; Binder, 1983; Chakrabarti *et al.*, 1990; Wang *et al.*, 1991; Kuwahara and Kubota, 1992). The process of spinodal decomposition is qualitatively classified into three time regimes:

1. The early stage, where the spatial fluctuations increase in amplitude while preserving the wavelength of the structure present at onset.

2. The intermediate stage, where both amplitude and wavelength increase with time.

3. The late stage, where the amplitude reaches the equilibrium value and only the wavelength grows in time.

The early stage is characterized by a single dominant wavelength that sets the pattern in the entire system. The direction of molecular ordering is correlated over regions defined by this characteristic wavelength; the dominant wavelength thus defines a characteristic *domain size* at the onset of spinodal decomposition. The degree of orientational order increases with time; but in the early stages, it is just marginally more

than that seen in the isotropic system. The early stages of spinodal decomposition can be easily studied by using a linearized approach, because nonlinear effects are unimportant.

The latter two stages are dominated by intrinsically nonlinear effects such as the coarsening of domains separated by interfaces with thicknesses that are much smaller than the characteristic domain size. Numerical (Chakrabarti et al., 1990) and Monte Carlo simulation methods (Sariban and Binder, 1991) have been used to study the intermediate and late stages in binary polymer blends and block-copolymer systems. In these systems, the separating domains have distinctly different material properties due to differences in composition. In contrast, in liquid crystalline systems, the separating phases differ in orientation alone. Furthermore, since the equilibrium nematic state is rotationally invariant, the molecules within the domains can take up one of infinitely many allowed orientations. This adds enormously to the complexity of the problem, and application of the above numerical techniques to the liquid crystal problem is not yet feasible.

This study of spinodal decomposition in liquid crystals is restricted to the early stages. The large molecular sizes cause a significant slowing down of the phase separation in polymeric systems and this initial stage may last for as long as 100-200 minutes. Therefore, it is possible to get experimental verification of the predicted theoretical results for the onset of spinodal decomposition.

A second problem that deserves study in the nonhomogeneous liquid crystalline systems is the effect of flow fields on the fully-developed polydomain texture. The interest here lies more in understanding the interplay between the texture, distortional elastic stress at the domain boundaries and the imposed flow field, than in understanding the process by which texture initially develops.

A recently proposed *mesoscopic domain theory* (Larson and Doi, 1991) attempts to address this issue. The theory is an extension of the LEP model that is taken to apply within each domain. A short-range order parameter that defines local order within a domain replaces the structure tensor S (defined in Chapter 4) in the development. Assuming the existence of a local director vector n and defining the local order

225

parameter in terms of this director allows the Leslie-Ericksen stress tensor expression to be rewritten in terms of the mesoscopically-averaged local order parameter. However, in this theory, the Frank distortional stresses are not treated exactly; instead, a form for the distortional stress contribution is postulated based on dimensional arguments and a phenomenological parameter a for the average domain size is introduced. A closed system of equations is obtained by postulating a phenomenological growth law for the domain size a, that accounts for the coarsening of domains at equilibrium as well as for the effect of flow on the domains.

Larson and Doi (1991) study the predictions of their model for recoverable strain after cessation of steady-state shearing, and step reversal and step increase of shear rate. The recoverable strain predicted by this mesoscopic theory scales as $t\dot{\gamma}_0$ in agreement with the elastic strain recovery measurements on PBLG solutions (Larson and Mead, 1989). A damped oscillatory response is predicted in the experiments of step reversal and step increase of shear rate. The oscillations are produced by the tendency of the nematic director to tumble at low shear rates, and the decay in the oscillations is a consequence of the phenomenological distortional stress present in the system. Comparison of these results with experimental data (Moldenaers et $al.$, 1990) agrees in a number of features such as the period of oscillation and the increase in damping with increase in concentration. However, in spite of the reasonably good agreement with rheological data, the mesoscopic theory provides little fundamental understanding of the texture formation.

The molecular theory for nonhomogeneous systems that was developed in Chapter 4 can be used, in principle, for the study of texture formation. Solving for the entire distribution function f_p, although feasible in spatially homogeneous systems and simple flow fields, places severe computational demands in nonhomogeneous systems that do not permit tractable calculations at this point. A possible alternative is the use of closure approximations in rewriting the complex diffusion equation for the configurational distribution function f_p entirely in terms of lower order moments. Although the use of such closure approximations is convenient, it can lead to incorrect results in some flow fields as seen in Chapter 5. Furthermore, no unique closure

approximation exists and the validity of any closure scheme is largely dependent on the imposed kinematics. In view of the impact of closure approximations and the complexity of solving the diffusion equation, a linear stability approach was adopted to study the evolution of microstructure from the isotropic state for concentrations in the unstable region. The linear stability analysis entirely avoids the use of closure and is valid for the study of early stages of spinodal decomposition where nonlinear effects are unimportant.

Recently, Shimada et al. (1988) studied the dynamics of the isotropic-nematic transition with a molecular theory approach. Their analysis was carried out using the same form of the hard-rod potential as given in Eq. (4.34). In their treatment, Shimada et al. never derive an explicit form for the mean-field intermolecular potential and present the entire analysis in Fourier space. Consequently, extending their study to nonequilibrium situations is difficult since an expression for the stress tensor cannot be obtained. On the other hand, the development of the stress tensor within our framework using a mean-field form of the potential is straightforward and was described in Chapter 4.

The development in this chapter is an extension of the work by Shimada et al. (1988). The effect of the different forms of the intermolecular potential that were discussed in Chapter 4 on the dynamics of spinodal decomposition is examined. The effects of rotational diffusivity on the phase separation are also studied; these effects were ignored in the analysis of Shimada et al. Moreover, the effects of simple flows on the development of structure at the isotropic-nematic transition point are also studied. Such effects of flow have not been previously considered.

6.2 Spinodal Decomposition: Study of Dynamics at Equilibrium

6.2.1 Development of the Dispersion Relation

In order to study the development of orientational order in a system that is initially isotropic, the diffusion equation for the configurational distribution function f_p (4.81) is first linearized about the isotropic base state $f_{p,eq} = n_{av}/4\pi$ as

$$f_p = \frac{n_{av}}{4\pi} + f_k(u,t)\exp(-\imath k \cdot r) \tag{6.1}$$

and a governing equation for f_k is obtained. The fluctuations in the distribution function f_k are characterized by a spatial wavenumber $k \equiv \sqrt{k \cdot k}$ or a wavelength $\lambda_k \equiv 2\pi/k$. Fluctuations in the concentration n and the order parameter S are defined in terms of the fluctuating part of the distribution function as

$$
\begin{aligned}
n_k &\equiv \int f_k(u,t)du, \\
S_k &\equiv \frac{1}{n_{av}}\int (uu - \frac{1}{3}\delta)f_k(u,t)du.
\end{aligned}
\tag{6.2}
$$

Equations for S_k and n_k can be obtained from the equation for f_k by taking suitable averages over the orientation distribution, as defined by Eq. (6.2). The equation for S_k that is obtained involves fourth moments with respect to f_k. In order to avoid closure approximations in developing a closed set of equations for S_k and n_k, terms involving such higher order moments are approximated by expanding f_k in terms of surface spherical harmonics and truncating the expansion at the second order harmonic as

$$f_k = \frac{n_k}{4\pi} + \frac{15}{8\pi}n_{av}S_k:(uu - \frac{1}{3}\delta). \tag{6.3}$$

The validity of this truncated moment expansion is limited to the early stages of structure development from the isotropic base state.

The closed set of equations thus derived for the fluctuations S_k and n_k can be used

to develop dispersion relations. The dispersion relation is a functional relationship between the growth rate Σ of these fluctuations and the wavenumber k. The system is stable if $\Sigma < 0$ for all wavenumbers k and the condition for marginal stability is obtained when the growth rate corresponding to at least one wavenumber becomes positive. This mode that first loses stability is termed as the most "dangerous" mode.

The procedure described here can be used to develop a set of dispersion relations by starting from the diffusion equation (4.81) for the configurational distribution function f_p. The diffusion equation (4.81) was presented in terms of an arbitrary intermolecular potential $\Phi^{(p)}$. Alternative forms for this mean-field intermolecular potential were presented in Table 4.2. In the subsequent development, we choose $\Phi^{(p)} \equiv \Phi^{(p)\text{Mar}}$ where

$$\Phi^{(p)\text{Mar}} = -\frac{3}{2}NkT(\boldsymbol{uu} - \frac{1}{3}\boldsymbol{\delta}):\{\boldsymbol{uu} - \frac{1}{3}\boldsymbol{\delta}\} - \frac{1}{16}NkT\ell^2\nabla^2(\boldsymbol{uu} - \frac{1}{3}\boldsymbol{\delta}):\{\boldsymbol{uu} - \frac{1}{3}\boldsymbol{\delta}\}. \quad (6.4)$$

This potential is a generalization of the homogeneous mean-field Maier-Saupe potential that accounts for the interactions of a test rod with any other rod within a capsule-like interaction domain that is set by an interaction-range parameter ℓ.

The Fourier transform of Eq. (4.81) is taken with

$$f_k(\boldsymbol{u}, t) \equiv \frac{1}{\mathcal{V}} \int f_p(\boldsymbol{r}, \boldsymbol{u}, t) \exp(\imath \boldsymbol{k} \cdot \boldsymbol{r}) d\boldsymbol{r}. \quad (6.5)$$

On linearizing, the evolution equation for f_k is obtained as

$$\begin{aligned}
\frac{\partial f_k}{\partial t} &= -\left[D_{tr}(k^2\sigma + (1-\sigma)\boldsymbol{kk}{:}\boldsymbol{uu}) - \frac{\sigma}{6\lambda}\frac{\partial}{\partial \boldsymbol{u}} \cdot \frac{\partial}{\partial \boldsymbol{u}} \right] \times \\
&\quad \left[f_k - \frac{3}{2}\frac{\mathcal{N}}{4\pi}n_{av}(1 - \frac{k^2\ell^2}{24})(\boldsymbol{uu} - \frac{1}{3}\boldsymbol{\delta}){:}\boldsymbol{S}_k \right].
\end{aligned} \quad (6.6)$$

In deriving Eq. (6.6), we have assumed that the parameter σ is constant. This is not inconsistent with the Eq. (4.67) for σ, since we are studying only the linearized problem for small fluctuations about the isotropic base state and the denominator in Eq. (4.67) can be approximated as $(1 - (3/2)\boldsymbol{S}{:}\boldsymbol{S})^2 \simeq 1$.

In this problem, the interest lies in obtaining a detailed understanding of the effect of intermolecular forces on the development of structure rather than the effect of changes in the field variables across the length of a single molecule. The development of the intermolecular potential does take into account interactions that result from a finite molecular extension between molecules that are separated by a finite distance. However, nonhomogeneities in stress and velocity fields across the length of the molecule are assumed to be negligible and terms that arise from an explicit treatment of the dumbbell as an extended object in defining the polymer mass density are ignored. Equation (6.7) can thus be obtained by simply averaging Eq. (6.6) over all orientations as

$$\frac{\partial n_k}{\partial t} = -D_{tr}\left[\frac{1}{3}(1+2\sigma)k^2 n_k + n_{av}(1-\sigma)(1-\frac{\mathcal{N}}{5}+\frac{\mathcal{N}}{5}\frac{k^2\ell^2}{24})S_k{:}kk\right].\qquad (6.7)$$

Similarly, multiplying Eq. (6.6) by $(uu-(1/3)\delta)$ and integrating over all orientations yields

$$\begin{aligned}
\frac{\partial S_k}{\partial t} = & -\ (D_{tr}k^2\sigma+\frac{\sigma}{\lambda})\left[1-\frac{\mathcal{N}}{5}+\frac{\mathcal{N}}{5}\frac{k^2\ell^2}{24}\right]S_k\\
& -\ D_{tr}(1-\sigma)\left[\frac{2}{15}\frac{n_k}{n_{av}}kk-\frac{2}{45}\frac{n_k}{n_{av}}k^2\delta+\left(1-\frac{\mathcal{N}}{5}+\frac{\mathcal{N}}{5}\frac{k^2\ell^2}{24}\right)\times\right.\\
& \left.\left(\frac{1}{7}k^2 S_k-\frac{4}{21}(kk{:}S_k)\delta+\frac{2}{7}(S_k\cdot kk+kk\cdot S_k)\right)\right].\qquad (6.8)
\end{aligned}$$

Equations (6.7) and (6.8) form a closed set for the linear evolution of the order parameter and the density.

Let $n_k(t) = \exp(\Sigma t)\hat{n}_k$ and $S_k(t) = \exp(\Sigma t)\hat{S}_k$, where Σ is the characteristic growth rate. By choosing $k = k_z\delta_z$ for the sake of simplicity, a set of dispersion relations is obtained that govern the evolution of the different fluctuation components.

The six independent components of fluctuation are $\hat{S}_{k,xy}$, $\hat{S}_{k,xx}-\hat{S}_{k,yy}$, $\hat{S}_{k,xz}$, $\hat{S}_{k,yz}$, $\hat{S}_{k,zz}$ and $\hat{n}_k$. Note that there are only five independent fluctuation components associated with the structure tensor as a consequence of the condition $trS = 0$. These fluctuation components have been classified by Shimada et al. (1988) into the three distortional modes of *twist*, *splay* and *bend* as illustrated in Fig. 6-2. Most
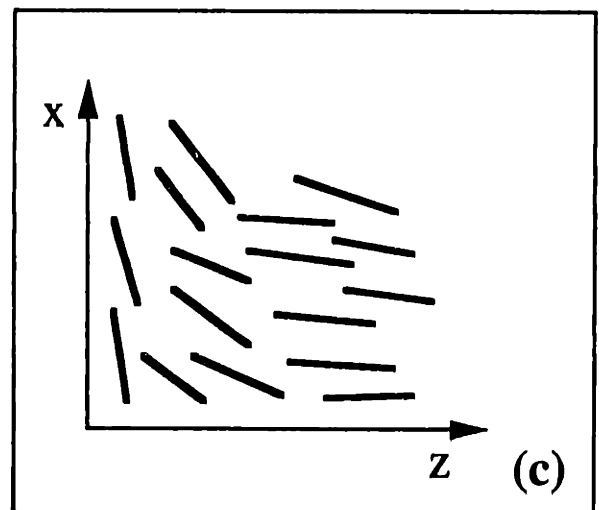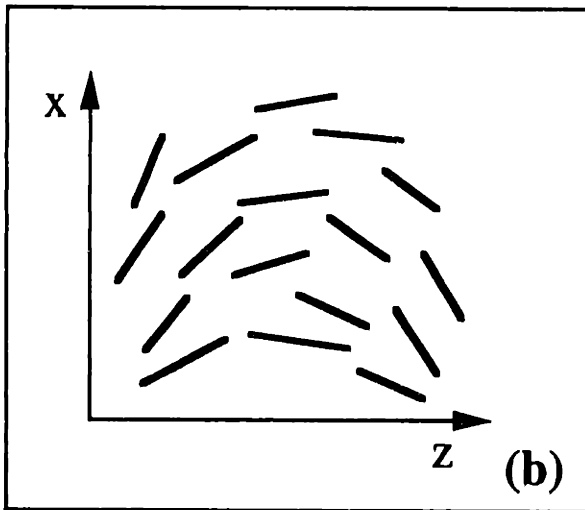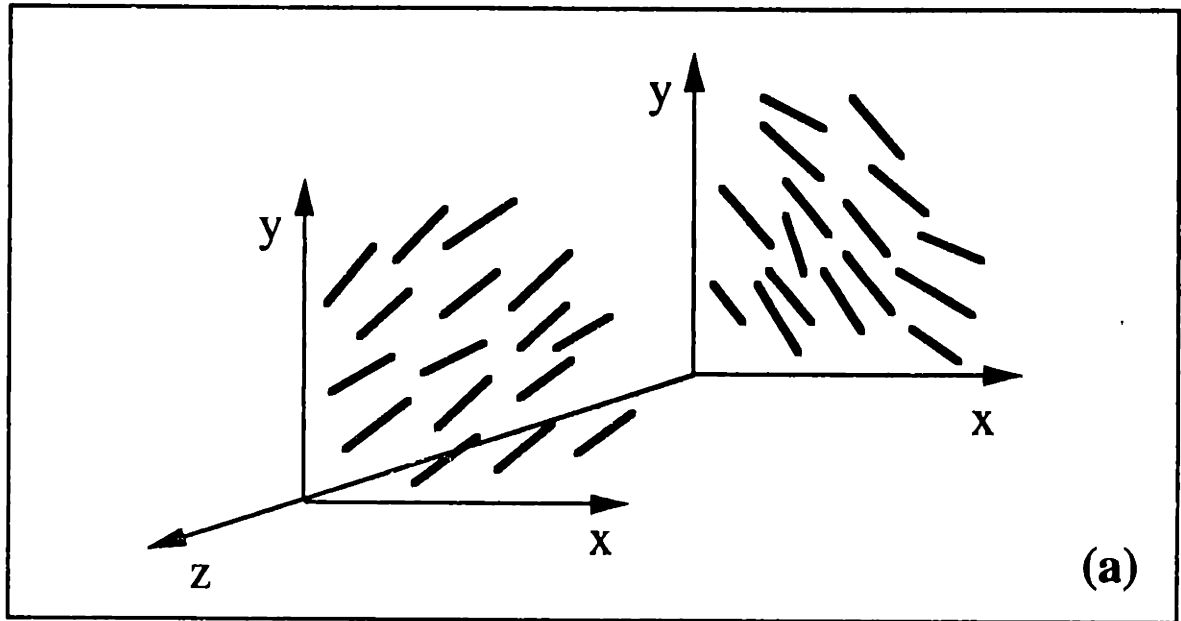
Figure 6-2: Schematic diagrams of each mode of orientation fluctuation. (a) Fluctuation of S_{xy} (twist mode), (b) fluctuation of S_{xz} (bend mode) and (c) fluctuation of S_{zz} (splay mode) (*reproduced from* Shimada *et al.*, 1988).

distortions in reality are combinations of these three modes.

For the choice of $k = k_z \delta_z$, rotational invariance of the equilibrium states causes the dispersion relations for components $\hat{S}_{k,xy}$ and $\hat{S}_{k,xx} - \hat{S}_{k,yy}$ to be identical. These two components correspond to the twist mode, illustrated in Fig. 6-2, and the dispersion relations are given by

$$\Sigma = - \left[D_{tr} k^2 \sigma + \frac{\sigma}{\lambda} + \frac{1}{7} D_{tr} k^2 (1 - \sigma) \right] \left[1 - \frac{\mathcal{N}}{5} + \frac{\mathcal{N}}{5} \frac{k^2 \ell^2}{24} \right] . \qquad (6.9)$$

The dispersion relations for components $\hat{S}_{k,xz}$ and $\hat{S}_{k,yz}$ are identical and are similar in form to Eq. (6.9). These components refer to the bend mode and the dispersion relations are given by

$$\Sigma = - \left[D_{tr} k^2 \sigma + \frac{\sigma}{\lambda} + \frac{3}{7} D_{tr} k^2 (1 - \sigma) \right] \left[1 - \frac{\mathcal{N}}{5} + \frac{\mathcal{N}}{5} \frac{k^2 \ell^2}{24} \right] . \qquad (6.10)$$

The governing equations for $\hat{n}_k$ and $\hat{S}_{k,zz}$ are coupled, and this coupled mode is termed the *splay* mode by Shimada *et al.* (1988); see Fig. 6-2. The equations for $\hat{n}_k$ and $\hat{S}_{k,zz}$ are

$$\hat{n}_k \Sigma = -D_{tr} \left[\frac{1}{3}(1 + 2\sigma) k^2 n_k + n_{av}(1 - \sigma)(1 - \frac{\mathcal{N}}{5} + \frac{\mathcal{N}}{5} \frac{k^2 \ell^2}{24}) \hat{S}_{k,zz} k^2 \right] . \qquad (6.11)$$

and

$$\begin{aligned}
\hat{S}_{k,zz} \Sigma &= - \left[D_{tr} k^2 \sigma + \frac{\sigma}{\lambda} + \frac{11}{21} D_{tr} k^2 (1 - \sigma) \right] \left[1 - \frac{\mathcal{N}}{5} + \frac{\mathcal{N}}{5} \frac{k^2 \ell^2}{24} \right] \hat{S}_{k,zz} \\
&\quad - \frac{4}{45} D_{tr} k^2 \frac{n_k}{n_{av}} (1 - \sigma).
\end{aligned} \qquad (6.12)$$

Equations (6.11) and (6.12) are solved simultaneously to obtain the dispersion relation. The two eigenvalues for this joint mode for $\sigma = 0$ are

$$\Sigma = \frac{1}{6} D_{tr} k^2 \left[-(1 + \frac{11}{7} B) \pm \sqrt{(1 + \frac{11}{7} B)^2 - \frac{108}{35} B} \right] \qquad (6.13)$$

where

$$B = 1 - \frac{\mathcal{N}}{5} + \frac{\mathcal{N}}{5}\frac{k^2\ell^2}{24}. \tag{6.14}$$

The behavior of the eigenvalue associated with the $\hat{S}_{k,zz}$ mode is qualitatively similar to the other two modes.

Equations (6.9)-(6.13) describe the dynamical processes that govern the stability of the isotropic state and the evolution of orientational order beyond the isotropic-nematic transition point. It is clear from the equations that the critical concentration at which the isotropic state loses stability is $\mathcal{N}_{crit} = 5$. Beyond this concentration, the system is unstable to some wavelengths, and the growth rate of these modes is given by Eqs. (6.9)-(6.13).

Both the translational diffusivity D_{tr} and the rotational diffusivity $D_r \equiv \sigma/6\lambda$ may contribute to the development of orientational order in the liquid crystalline system. It has been suggested by Shimada *et al.* (1988) that the rotational diffusivity is infinitesimally small or $D_r \simeq 0$. In our description, this corresponds to $\sigma \simeq 0$. In that case, the rotational and translational diffusivities are given by

$$
\begin{aligned}
D_r &\equiv \frac{\sigma}{6\lambda} \simeq 0, \\
\boldsymbol{D}_{tr} &\equiv D_{tr}(\boldsymbol{uu} + \sigma(\boldsymbol{\delta} - \boldsymbol{uu})) \simeq D_{tr}\boldsymbol{uu},
\end{aligned} \tag{6.15}
$$

respectively, and the molecules are allowed to rotate only by translating along their length. The implications of choosing $\sigma \simeq 0$ are discussed in Section 6.2.3.

The dispersion relation for the "twist" mode for the case $\sigma = 0$ is plotted in Fig. 6-3 for dimensionless growth rate and wavenumber. The dimensionless growth rate and wavenumber are defined as

$$\bar{\Sigma} = \left(\frac{\ell}{L}\right)^2 \lambda\Sigma; \quad \text{and} \quad \bar{k}^2 = \frac{k^2\ell^2}{24}. \tag{6.16}$$

For $\mathcal{N} < \mathcal{N}_{crit}$, the growth rate Σ is negative for all modes, and the system is linearly stable to disturbances of all wavelengths. At $\mathcal{N} = \mathcal{N}_{crit}$, the critical wavenumber is $k = 0$ with $\Sigma = 0$. For all concentrations within the spinodal, *i.e.*, $\mathcal{N} > \mathcal{N}_{crit}$, the
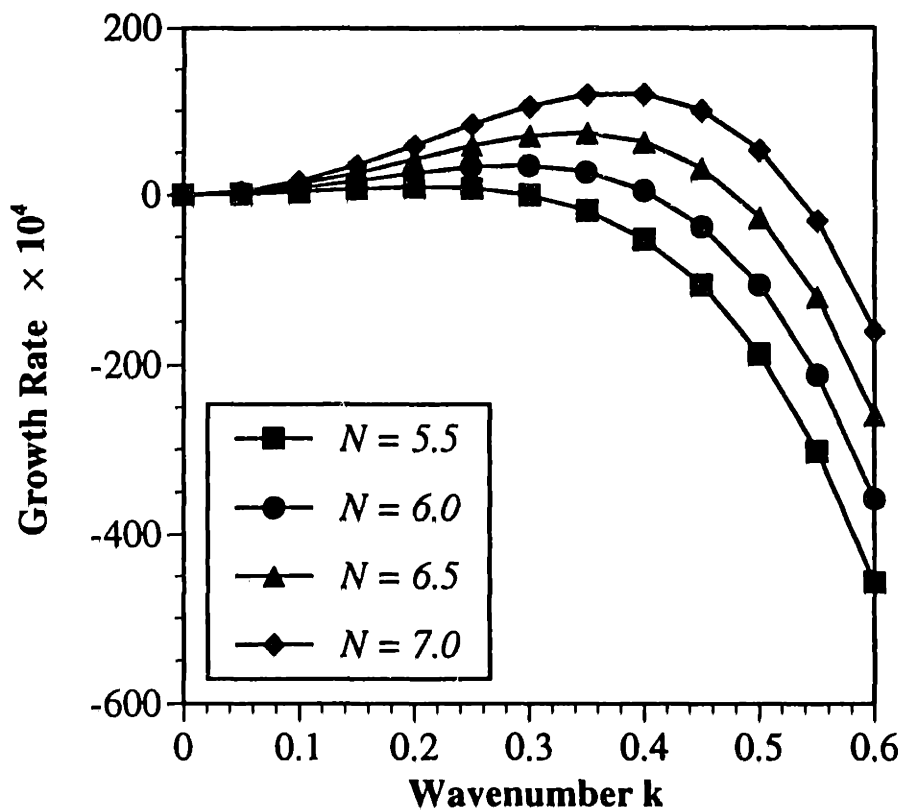
Figure 6-3: Equilibrium dispersion relation for the *twist* mode obtained by using Marrucci's mean-field intermolecular potential.

system is unstable to a number of wavelengths that display positive growth rates. However, as seen from Fig. 6-3, a single wavenumber k_{max} displays a maximum in the growth rate Σ, and since S shows an exponential dependence on Σ, this wavenumber dominates the pattern development at the onset of the transition. The value of k_{max} increases with increasing $\mathcal{N}$, indicating that as we proceed further into the spinodal region, the characteristic domain size decreases. Furthermore, the growth rate associated with k_{max} also increases with $\mathcal{N}$. The behavior described here is qualitatively similar to the classical theory of spinodal decomposition, as described by Cahn (1961 & 1965).

6.2.2 Effect of Intermolecular Potential

Three alternate forms of the intermolecular potential were developed in Section 4.3.2, viz., $\Phi^{(p)M-S}$, $\Phi^{(p)h-r}$ and $\Phi^{(p)Mar}$ and are summarized in Table 4.2. The first form of the potential $\Phi^{(p)M-S}$ neglects effects of finite separation between the interacting rigid rods as explained in Section 4.3.2. The two latter forms of the potential differ only in the terms that involve gradients of the distribution function. In this section, dispersion relations for the three forms are developed and the predictions of characteristic domain sizes are compared. The significance of the gradient terms in the potential is clear from the results for $\Phi^{(p)M-S}$. For the sake of simplicity, σ is set to be zero again.

Following the procedure described in Section 6.2.1, the equations for n_k and S_k for the choice $\Phi^{(p)} \equiv \Phi^{(p)M-S}$ are

$$\frac{\partial n_k}{\partial t} = -D_{tr}\left[\frac{1}{3}(1+2\sigma)k^2 n_k + n_{av}(1-\sigma)(1-\frac{\mathcal{N}}{5})S_k:kk\right].\qquad(6.17)$$

and

$$
\begin{aligned}
\frac{\partial S_k}{\partial t} = &- (D_{tr}k^2\sigma + \frac{\sigma}{\lambda})\left[1 - \frac{\mathcal{N}}{5}\right]S_k \\
&- D_{tr}(1-\sigma)\left[\frac{2}{15}\frac{n_k}{n_{av}}kk - \frac{2}{45}\frac{n_k}{n_{av}}k^2\delta\right. \\
&+ \left.\left(1-\frac{\mathcal{N}}{5}\right)\left(\frac{1}{7}k^2 S_k - \frac{4}{21}(kk:S_k)\delta + \frac{2}{7}(S_k\cdot kk + kk\cdot S_k)\right)\right].(6.18)
\end{aligned}
$$

235

Similarly, choosing $\Phi^{(p)} \equiv \Phi^{(p)h-r}$, the equations for n_k and S_k are

$$\frac{\partial n_k}{\partial t} = -\frac{1}{3}D_{tr}n_k k^2\left(1 + \frac{\mathcal{N}}{5}\frac{k^2 L^2}{90}\right)$$
$$-D_{tr}n_{av}(1 - \frac{\mathcal{N}}{5} + \frac{\mathcal{N}}{5}\frac{29k^2 L^2}{504})S_k{:}kk. \tag{6.19}$$

and

$$\frac{\partial S_k}{\partial t} = -\frac{2}{15}D_{tr}\left[1 + \frac{\mathcal{N}}{5}\frac{11k^2 L^2}{504}\right]\left[n_k kk - \frac{1}{3}n_k k^2\delta\right]$$
$$-\frac{1}{7}D_{tr}\left[1 - \frac{\mathcal{N}}{5}\right]\left[2(S_k\cdot kk + kk\cdot S_k) + k^2 S_k - \frac{4}{3}S_k{:}kk\delta\right]$$
$$-D_{tr}L^2\frac{\mathcal{N}}{210}\left[\frac{3}{7}S_k{:}kkkk + \frac{13}{21}(S_k\cdot kk + kk\cdot S_k)k^2\right.$$
$$\left.+\frac{5}{42}k^4 S_k - \frac{5}{9}S_k{:}kkk^2\delta\right]. \tag{6.20}$$

Following the development in Section 6.2.1, we again set $k = k_z\delta_z$ and obtain the dispersion relation for the different components from Eqs. (6.17)-(6.20). The relations for the twist mode (i.e., $\hat{S}_{k,xy}$ and $\hat{S}_{k,xx} - \hat{S}_{k,yy}$) are presented here to allow comparison to the corresponding relation (6.9). For $\Phi^{(p)M-S}$, the dispersion relation for the twist mode is

$$\Sigma = -\frac{1}{7}D_{tr}k^2\left[1 - \frac{\mathcal{N}}{5}\right]. \tag{6.21}$$

As is apparent from Eq. (6.21), the critical concentration $\mathcal{N}_{crit} = 5$ is unchanged by the form of the potential. However, within the spinodal region for $\mathcal{N} > \mathcal{N}_{crit}$, the fastest growing wavelength corresponds to $k \to \infty$. This implies that the spatial structure breaks up on a very fine scale, which is aphysical. This is a consequence of neglecting the gradient terms in the potential that account for effects of finite separation between the interacting rigid-rods, as explained in Section 4.3.2. It is also clear from the fine structure that develops in the absence of the gradient terms, that these terms are responsible for a finite surface tension between the separating phases.

Similarly, the dispersion relation for the twist mode with the potential $\Phi^{(p)h-r}$ is

$$\Sigma = -\frac{1}{7}D_{tr}k^2\left[1 - \frac{\mathcal{N}}{5} + \mathcal{N}\frac{k^2L^2}{252}\right].\qquad(6.22)$$

Comparing Eqs. (6.22) and (6.9), we note that the form of the dispersion relation is similar for the two forms of the potential and behavior characteristic of classical spinodal decomposition is again observed. However, the two forms of the potential differ significantly in the range of interaction over which one molecule can interact with another. This has a significant impact on the characteristic domain size predicted by the two potentials as shown in Fig. 6-4. In this figure, the growth rates and wavenumbers are made dimensionless by using the scales given in Eq. (6.16). Furthermore, all growth rates are scaled with the maximum growth rate Σ_{max} for the corresponding potential to facilitate an easy comparison between the three potentials. The curve for $\Phi^{(p)h-r}$ is plotted for a choice of $\ell/L = 10$. Comparing the values of k_{max} for the two potentials $\Phi^{(p)h-r}$ and $\Phi^{(p)Mar}$ shown in Fig. 6-4, the characteristic domain size predicted for $\Phi^{(p)Mar}$ is about an order-of-magnitude higher than that for $\Phi^{(p)h-r}$, for the choice of $\ell/L = 10$. Analysis of the dispersion equations indicates that the characteristic domain size λ_{dom} scales as the range of interaction in the intermolecular potential, i.e., $\lambda_{dom} \sim \ell$ for $\Phi^{(p)Mar}$ and $\lambda_{dom} \sim L$ for $\Phi^{(p)h-r}$. The analysis also indicates that the growth rates scale as D_{tr}/λ_{dom}^2 for both potentials.

For typical molecular lengths of 1000 Å, the characteristic domain size predicted for $\Phi^{(p)h-r}$ is $0.2 - 0.3$ μm and for typical $D_{tr} \sim 10^{-10}$ cm^2/s, the growth rate is 0.1 s^{-1}. In contrast, for $\Phi^{(p)Mar}$ with $\ell/L = 10$, the characteristic domain size is predicted to be 3 μm and the growth rate is 10^{-3} s^{-1}. Visual observations of texture in polymeric liquid crystalline systems indicate that characteristic domain sizes are $\mathcal{O}(1)$ μm (Marrucci, 1984). Based on these observations, it is difficult to distinguish between these two forms of the potential. Measurements of growth rates in isotropic polymeric systems indicate that typical growth rates are $\mathcal{O}(10^{-3} - 10^{-4})$ s^{-1} (Kuwahara and Kubota, 1992). Comparing the predicted values of the growth rates for the potentials $\Phi^{(p)h-r}$ and $\Phi^{(p)Mar}$ with these experimental results indicates that the growth rates
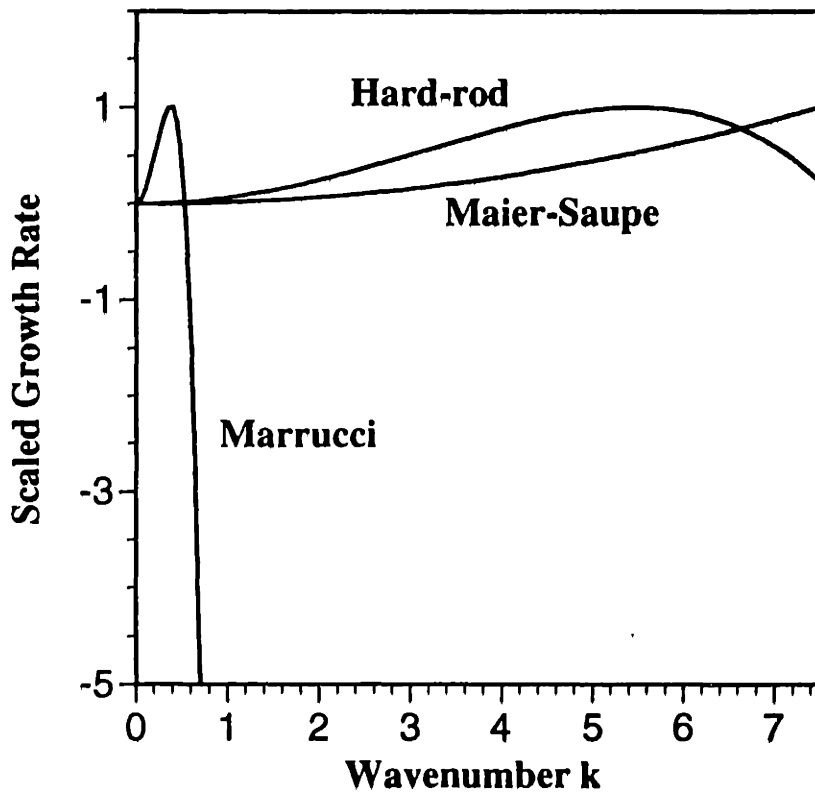
Figure 6-4: Comparison of characteristic domain size predicted by the different inter-molecular potentials.

predicted with $\Phi^{(p)} \equiv \Phi^{(p)h-r}$ are unreasonably high. This is a consequence of the domain of interaction over which the orientations are correlated being comparable to the molecular length L. As a result, orientational order over this small length scale is established with the help of translational diffusion in a very short period of time leading to large growth rates. Therefore the predictions made with $\Phi^{(p)Mar}$ appear to be more reasonable.

6.2.3   Effect of Anisotropic Drag

In the above calculations, it was assumed that $\sigma \simeq 0$. This supposes that the hindrance to molecular rotation experienced by a rigid-rod in a concentrated isotropic solution is very high and results in $D_r \simeq 0$. With this constraint, a change in orientation of the molecules is possible only by translation along the molecular axis for a distance of $\mathcal{O}(L)$. Examining Eqs. (4.67) and (4.68) for the anisotropic drag parameter σ, this is seen to be a reasonable assumption only if $\mathcal{F}(\mathcal{N}) \ll 1$ and is true for the theoretically estimated value of $\beta \sim 10$. However, as discussed in Section 4.3.3.2, some controversy surrounds the magnitude of β (Pecora, 1985). Therefore, it is worthwhile to study the effect of a small but finite value of σ on the kinetics of spinodal decomposition. For nonzero σ, both rotational and translational diffusivities are equally important in determining the development of structure within the spinodal region.

The effect of nonzero σ on the dispersion relation is shown in Fig. 6-5 for $\Phi^{(p)Mar}$ with $\ell/L = 10$ and $\sigma = 0, 10^{-4}, 3 \times 10^{-4}, 10^{-3}$. The growth rate for the $k = 0$ mode is positive for all values of $\sigma \neq 0$. The kinetics of spinodal decomposition can be divided into two concentration regions, $\mathcal{N}_{crit} < \mathcal{N} < \mathcal{N}^*$ and $\mathcal{N} > \mathcal{N}^*$, respectively, where $\mathcal{N}^*$ delineates the two regions of behavior. The first region corresponds to small wavenumbers, and the overall pattern is dominated by the $k = 0$ mode. In this region, the effect of rotational diffusivity is significant, and overall alignment to one preferred direction is accomplished by molecular rotation about a fixed center-of-mass position. For $\mathcal{N} > \mathcal{N}^*$, the results of classical spinodal decomposition are recovered. In this concentration region, although the $k = 0$ mode shows finite growth, a dominant wavenumber exists which shows a maximum in the growth rate. Thus, although
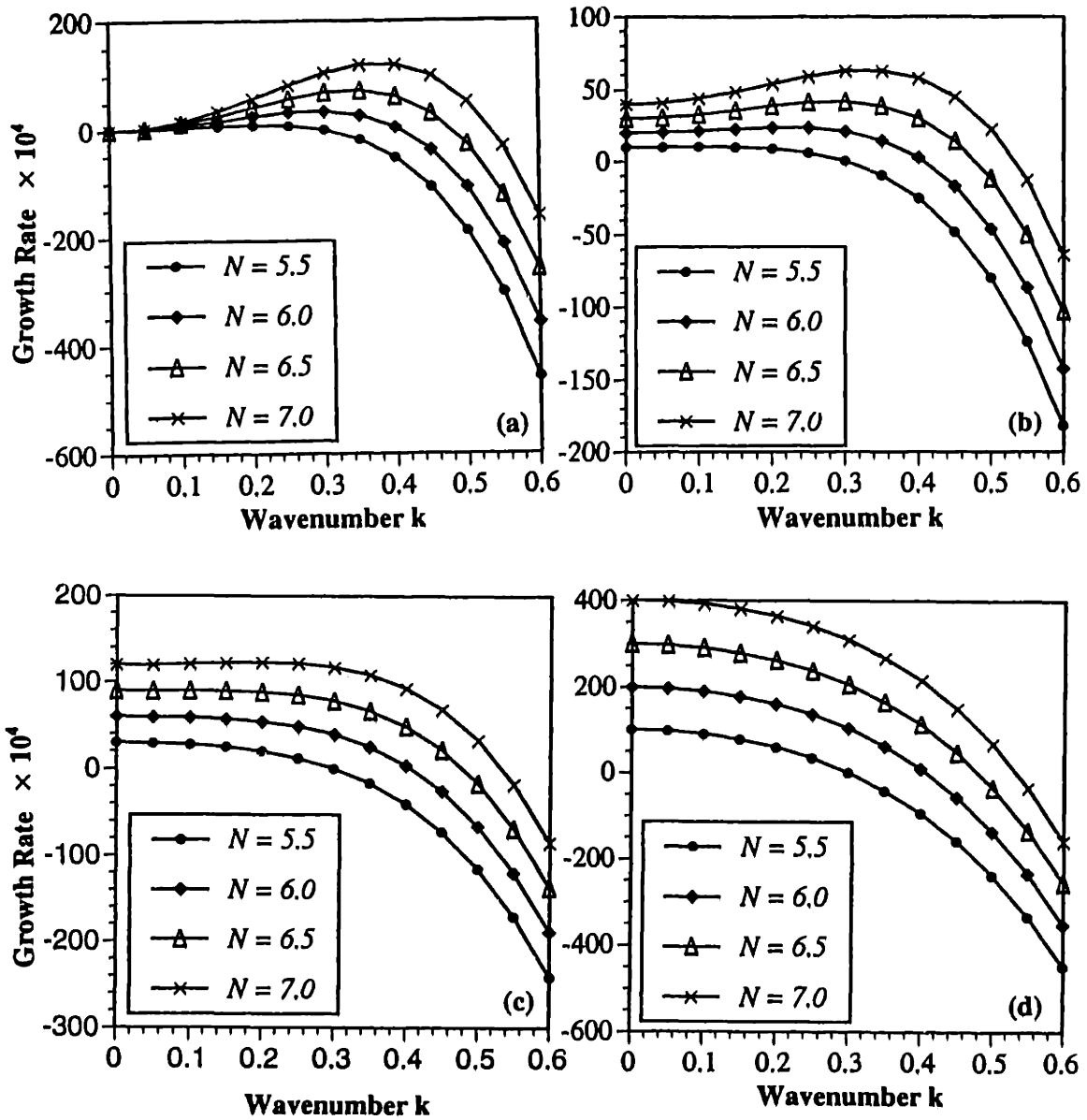
Figure 6-5: Effect of the anisotropic drag parameter σ on dispersion relation for σ of (a) 0, (b) 10^{-4}, (c) 3×10^{-4} and (d) 10^{-3}. In all plots, $\Phi^{(p)} \equiv \Phi^{(p)\text{Mar}}$.

240

rotational diffusivity can contribute to the pattern formation, it is superseded by the effects of translational diffusion. The value of $\mathcal{N}^*$ decreases with decreasing σ and for $\sigma = 0$, $\mathcal{N}^* = \mathcal{N}_{crit}$.

6.3 Effect of Flows on the I-N transition

The linear stability theory described in Section 6.2.1 is extended in this section to account for the effect of flows. It is no longer sufficient to linearize the diffusion equation about the isotropic base state $f_p = n_{av}/4\pi$ as done in Section 6.2.1, since this base state is itself perturbed by the presence of a flow field. Therefore, a regular perturbation about the homogeneous, isotropic base state is first carried out for small values of the deformation rate, by using standard techniques described by Bird *et al.* (1987b). Spatial perturbations are subsequently applied to this state.

The diffusion equation in the homogeneous problem is

$$\frac{\partial f_p}{\partial t} = -D_r \left[\frac{\partial}{\partial u} \cdot \frac{\partial f_p}{\partial u} + \frac{1}{kT} \frac{\partial}{\partial u} \cdot \left(\left(\frac{\partial \Phi^{(p)}}{\partial u} \right) f_p \right) \right] - \frac{\partial}{\partial u} \cdot [(\kappa \cdot u - \kappa : uuu) f_p] \quad (6.23)$$

where $D_r = \sigma/6\lambda$. The homogeneous Maier-Saupe potential $\Phi^{(p)}$ is defined as (Doi, 1981; Bhave *et al.*, 1992)

$$\Phi^{(p)} = -\frac{3}{2} \mathcal{N} kT (uu - \frac{1}{3}\delta) : \int (u'u' - \frac{1}{3}\delta) f_p(u',t) du'. \quad (6.24)$$

Since only small deformation rates are considered, f_p is expanded in a power series as

$$f_p = \frac{1}{4\pi} [1 + \delta\phi_1 + \delta^2 \phi_2 + \ldots] \quad (6.25)$$

where the small parameter δ is taken to be $\dot{\epsilon}/D_r$ and $\dot{\gamma}/D_r$ in elongational and shear flows, respectively. The choice of D_r over the usual choice of λ for nondimensionalizing the deformation rate is deliberate; this choice clarifies that in the perturbation expansion, the small parameter is the ratio $6\lambda\dot{\epsilon}/\sigma$ and not just $\dot{\epsilon}$. Substituting Eq. (6.25) into Eq. (6.23), with $\partial f_p/\partial t = 0$ for steady state and collecting equal orders of the

parameter δ yields the expansion correct to $\mathcal{O}(\delta)$ as

$$f_p^o = \frac{1}{4\pi}[1 + \delta\chi{:}uu + \mathcal{O}(\delta^2)] \qquad (6.26)$$

where

$$\chi \equiv \frac{3}{4(1 - \mathcal{N}/5)}(\delta_z\delta_z - \frac{1}{3}\delta) \qquad (6.27)$$

in elongational flows and

$$\chi \equiv \frac{1}{2(1 - \mathcal{N}/5)}\delta_x\delta_y \qquad (6.28)$$

in shear flows. The regular perturbation shows that the solution for f_p^o is singular at $\mathcal{N} = 5$, unless $\dot{\epsilon} = 0$ (or $\dot{\gamma} = 0$). This regular perturbation is valid *near* the critical point for small values of the parameter δ but does not exist exactly at the critical point. The solution smoothly approaches the unperturbed base state with decreasing δ. The equilibrium analysis of Section 6.2 also indicates the presence of this critical point $\mathcal{N} = 5$ corresponding to the isotropic-nematic transition, and the singularity in the perturbation expansion (6.26) is a consequence of the imperfection of the bifurcation between the isotropic and nematic states in the presence of a flow field. This singular behavior is expected from elementary ideas of effects of imperfection on the bifurcation (Iooss and Joseph, 1980). Note also that the scalar order parameter S obtained from this expansion for f_p^o is of different sign on either side of the critical concentration $\mathcal{N} = 5$, in agreement with the calculations presented in Chapter 5.

The distribution function f_p^o given by Eq. (6.26) is used to define a new base state upon which we impose spatial fluctuations as

$$f_p = n_{av}f_p^o + f_k(u, t)\exp(-\imath k \cdot r). \qquad (6.29)$$

Substituting Eq. (6.29) into the nonhomogeneous diffusion equation (4.81) and linearizing yields the governing equation for f_k as

$$\frac{\partial f_k}{\partial t} = \mathbf{k} \cdot \boldsymbol{\kappa} \cdot \frac{\partial f_k}{\partial \mathbf{k}} - D_{tr}(k^2\sigma + (1-\sigma)\mathbf{kk}{:}\mathbf{uu})f_k$$

$$+ \frac{3}{2}\frac{\mathcal{N}}{4\pi}D_{tr}n_{av}(1 - \frac{k^2\ell^2}{24})(k^2\sigma + (1-\sigma)\mathbf{kk}{:}\mathbf{uu})(S_k{:}\mathbf{uu} + S_k{:}(\bar{\chi}{:}\mathbf{uuuu}))$$

$$+ D_r\frac{\partial}{\partial \mathbf{u}} \cdot \frac{\partial f_k}{\partial \mathbf{u}} - \frac{3}{2}\frac{\mathcal{N}}{15}D_r\frac{\partial}{\partial \mathbf{u}} \cdot \left[\frac{\partial}{\partial \mathbf{u}}(\mathbf{uu}){:}(\bar{\chi} + \bar{\chi}^\dagger)f_k\right]$$

$$- \frac{3}{2}\frac{\mathcal{N}}{4\pi}D_r n_{av}(1 - \frac{k^2\ell^2}{24})\frac{\partial}{\partial \mathbf{u}} \cdot \left[\frac{\partial}{\partial \mathbf{u}}(\mathbf{uu}){:}S_k(1 + \bar{\chi}{:}\mathbf{uu})\right]$$

$$- \frac{\partial}{\partial \mathbf{u}} \cdot [(\boldsymbol{\kappa} \cdot \mathbf{u} - \boldsymbol{\kappa}{:}\mathbf{uuu})f_k] \tag{6.30}$$

where $\bar{\chi} \equiv \chi\delta$ with χ defined by Eqs. (6.27) and (6.28), and δ equals $\dot{\epsilon}/D_r$ and $\dot{\gamma}/D_r$, for elongational and shear flows, respectively. Equations for the fluctuations in concentration and structure tensor are derived from Eq. (6.30). Integrating Eq. (6.30) over all orientations yields the equation for n_k as

$$\frac{\partial n_k}{\partial t} = \mathbf{k} \cdot \boldsymbol{\kappa} \cdot \frac{\partial n_k}{\partial \mathbf{k}} - D_{tr}(k^2\sigma n_k + (1-\sigma)n_{av}\mathbf{kk}{:}S_k + \frac{1}{3}(1-\sigma)k^2 n_k)$$

$$+ \frac{\mathcal{N}}{5}D_{tr}n_{av}(1 - \frac{k^2\ell^2}{24})\left[\frac{1}{2}k^2\sigma S_k{:}(\bar{\chi} + \bar{\chi}^\dagger) + (1-\sigma)\mathbf{kk}{:}S_k\right.$$

$$\left. + \frac{1}{7}(1-\sigma)[2(S_k \cdot \bar{\chi} + \bar{\chi} \cdot S_k){:}\mathbf{kk} + k^2\bar{\chi}{:}S_k]\right]. \tag{6.31}$$

Multiplying Eq. (6.30) by $(\mathbf{uu} - (1/3)\delta)$ and integrating over all orientations yields an evolution equation for S_k as

$$\frac{\partial S_k}{\partial t} = \mathbf{k} \cdot \boldsymbol{\kappa} \cdot \frac{\partial S_k}{\partial \mathbf{k}} - D_{tr}k^2\sigma(1 - \frac{\mathcal{N}}{5} + \frac{\mathcal{N}}{5}\frac{k^2\ell^2}{24})S_k$$

$$- D_{tr}(1 - \sigma)\left[\frac{2}{15}\frac{n_k}{n_{av}}\mathbf{kk} - \frac{2}{45}\frac{n_k}{n_{av}}k^2\delta\right.$$

$$+ \frac{1}{7}\left(1 - \frac{\mathcal{N}}{5} + \frac{\mathcal{N}}{5}\frac{k^2\ell^2}{24}\right)\left(k^2 S_k - \frac{4}{3}(\mathbf{kk}{:}S_k)\delta + 2(S_k \cdot \mathbf{kk} + \mathbf{kk} \cdot S_k)\right)\right]$$

$$+ \frac{\mathcal{N}}{5}D_{tr}(1 - \frac{k^2\ell^2}{24})k^2\sigma\left[\frac{1}{7}(S_k \cdot (\bar{\chi} + \bar{\chi}^\dagger) + (\bar{\chi} + \bar{\chi}^\dagger) \cdot S_k) - \frac{4}{21}(S_k{:}\bar{\chi})\delta\right]$$

$$+ \frac{\mathcal{N}}{5}(1 - \sigma)\frac{1}{63}D_{tr}(1 - \frac{k^2\ell^2}{24})[(S_k{:}\mathbf{kk})(\bar{\chi} + \bar{\chi}^\dagger) + 2(\bar{\chi}{:}\mathbf{kk})S_k + 2(\bar{\chi}{:}S_k)\mathbf{kk}$$

$$+ (S_k \cdot (\bar{\chi} + \bar{\chi}^\dagger) + (\bar{\chi} + \bar{\chi}^\dagger) \cdot S_k)k^2 + 2(\bar{\chi} + \bar{\chi}^\dagger) \cdot (\mathbf{kk} \cdot S_k + S_k \cdot \mathbf{kk})$$

$$+ \quad 2(\boldsymbol{kk} \cdot \boldsymbol{S}_k + \boldsymbol{S}_k \cdot \boldsymbol{kk}) \cdot (\tilde{\chi} + \tilde{\chi}^\dagger)$$

$$+ \quad 2(\boldsymbol{kk} \cdot (\tilde{\chi} + \tilde{\chi}^\dagger) \cdot \boldsymbol{S}_k + \boldsymbol{S}_k \cdot (\tilde{\chi} + \tilde{\chi}^\dagger) \cdot \boldsymbol{kk})]$$

$$- \quad \frac{\mathcal{N}}{5}(1 - \sigma)\frac{2}{63}D_{tr}(1 - \frac{k^2\ell^2}{24})[\boldsymbol{kk}{:}(\boldsymbol{S}_k \cdot (\tilde{\chi} + \tilde{\chi}^\dagger) + (\tilde{\chi} + \tilde{\chi}^\dagger) \cdot \boldsymbol{S}_k)\delta$$

$$+ \quad \tilde{\chi}{:}\boldsymbol{S}_k k^2 \delta]$$

$$- \quad \frac{\sigma}{\lambda}(1 - \frac{\mathcal{N}}{5} + \frac{\mathcal{N}}{5}\frac{k^2\ell^2}{24})\boldsymbol{S}_k + \frac{cal N}{5}\left(\frac{\sigma}{6\lambda}\right)\left[\frac{16}{15}\frac{n_k}{n_{av}}(\tilde{\chi} + \tilde{\chi}^\dagger)\right.$$

$$+ \quad \frac{3}{7}((\tilde{\chi} + \tilde{\chi}^\dagger) \cdot \boldsymbol{S}_k) + \boldsymbol{S}_k \cdot (\tilde{\chi} + \tilde{\chi}^\dagger)) - \frac{4}{7}(\boldsymbol{S}_k{:}\tilde{\chi})\delta\Big]$$

$$+ \quad \frac{\mathcal{N}}{5}\left(\frac{\sigma}{6\lambda}\right)(1 - \frac{k^2\ell^2}{24})\left[\frac{3}{7}((\tilde{\chi} + \tilde{\chi}^\dagger) \cdot \boldsymbol{S}_k) + \boldsymbol{S}_k \cdot (\tilde{\chi} + \tilde{\chi}^\dagger)) - \frac{4}{7}(\boldsymbol{S}_k{:}\tilde{\chi})\delta\right]$$

$$+ \quad \frac{1}{5}n_k(\boldsymbol{\kappa} + \boldsymbol{\kappa}^\dagger) + (\boldsymbol{\kappa} \cdot \boldsymbol{S}_k + \boldsymbol{S}_k \cdot \boldsymbol{\kappa}^\dagger)$$

$$- \quad \frac{2}{7}[(\boldsymbol{\kappa}{:}\boldsymbol{S}_k)\delta + \boldsymbol{S}_k \cdot (\boldsymbol{\kappa} + \boldsymbol{\kappa}^\dagger) + (\boldsymbol{\kappa} + \boldsymbol{\kappa}^\dagger) \cdot \boldsymbol{S}_k]. \tag{6.32}$$

In deriving Eqs. (6.31) and (6.32), closure approximations for higher order moments are avoided by expanding f_k in terms of its moments, as described in Section 6.2.1. Since we are interested in the limit $\sigma \to 0$ with $\dot{\epsilon}/D_r$ (or $\dot{\gamma}/D_r$) as the small parameter of interest, we first scale the terms in $\boldsymbol{\kappa}$ by $D_r \equiv \sigma/6\lambda$ and then take the limit as $\sigma \to 0$ in Eqs. (6.30)-(6.32), to yield

$$\frac{\partial f_k}{\partial t} = - \quad D_{tr}(\boldsymbol{kk}{:}\boldsymbol{uu})f_k$$

$$+ \quad \frac{3}{2}\frac{\mathcal{N}}{4\pi}D_{tr}n_{av}(1 - \frac{k^2\ell^2}{24})(\boldsymbol{kk}{:}\boldsymbol{uu})(\boldsymbol{S}_k{:}\boldsymbol{uu} + \boldsymbol{S}_k{:}(\tilde{\chi}{:}\boldsymbol{uuuu})). \tag{6.33}$$

The governing equation for concentration fluctuations n_k obtained by this method is

$$\frac{\partial n_k}{\partial t} = -D_{tr}\left[\frac{1}{3}k^2 n_k + n_{av}(1 - \frac{\mathcal{N}}{5} + \frac{\mathcal{N}}{5}\frac{k^2\ell^2}{24})(\boldsymbol{S}_k{:}\boldsymbol{kk}) - \frac{1}{7}\frac{\mathcal{N}n_{av}}{5}(1 - \frac{k^2\ell^2}{24})\times\right.$$

$$[\boldsymbol{kk}{:}(\boldsymbol{S}_k \cdot (\tilde{\chi} + \tilde{\chi}^\dagger) + (\tilde{\chi} + \tilde{\chi}^\dagger) \cdot \boldsymbol{S}_k) + \tilde{\chi}{:}\boldsymbol{S}_k k^2]\Big]. \tag{6.34}$$

244

Similarly, the perturbation to the structure tensor is

$$
\begin{aligned}
\frac{\partial S_k}{\partial t} = \; & - \; D_{tr}\left[\frac{2}{15}\frac{n_k}{n_{av}}kk - \frac{2}{45}\frac{n_k}{n_{av}}k^2\delta \right. \\
& + \; \frac{1}{7}\left(1 - \frac{\mathcal{N}}{5} + \frac{\mathcal{N}}{5}\frac{k^2\ell^2}{24}\right)\left(k^2S_k - \frac{4}{3}(kk{:}S_k)\delta + 2(S_k\cdot kk + kk\cdot S_k)\right)\right] \\
& + \; \frac{\mathcal{N}}{5}\frac{1}{63}D_{tr}(1 - \frac{k^2\ell^2}{24})[(S_k{:}kk)(\tilde{\chi} + \tilde{\chi}^\dagger) + 2(\tilde{\chi}{:}kk)S_k + 2(\tilde{\chi}{:}S_k)kk \\
& + \; (S_k\cdot(\tilde{\chi} + \tilde{\chi}^\dagger) + (\tilde{\chi} + \tilde{\chi}^\dagger)\cdot S_k)k^2 + 2(\tilde{\chi} + \tilde{\chi}^\dagger)\cdot(kk\cdot S_k + S_k\cdot kk) \\
& + \; 2(kk\cdot S_k + S_k\cdot kk)\cdot(\tilde{\chi} + \tilde{\chi}^\dagger) \\
& + \; 2(kk\cdot(\tilde{\chi} + \tilde{\chi}^\dagger)\cdot S_k + S_k\cdot(\tilde{\chi} + \tilde{\chi}^\dagger)\cdot kk)] \\
& - \; \frac{\mathcal{N}}{5}\frac{2}{63}D_{tr}(1 - \frac{k^2\ell^2}{24})[kk{:}(S_k\cdot(\tilde{\chi} + \tilde{\chi}^\dagger) + (\tilde{\chi} + \tilde{\chi}^\dagger)\cdot S_k)\delta \\
& + \; \tilde{\chi}{:}S_k k^2\delta].
\end{aligned}
$$

(6.35)

Equations (6.34) and (6.35) form a coupled set from which dispersion relations for the different modes can be derived. Predictions for these different modes in the presence of biaxial stretching, uniaxial elongation and simple shear flows are now examined. Note that since we impose specific kinematics on the system, the equation of motion is not solved. The complexity of the equations makes it difficult to examine the problem in general terms. Hence, with a little judgment, and some knowledge of the breaking of the isotropic-nematic bifurcation obtained from homogeneous theory described in Chapter 5, specific modes are examined for particular one dimensional wave vectors k. Note also that since the bifurcation is destroyed at $\mathcal{N}_{crit} = 5$, it becomes necessary to distinguish between the cases $\mathcal{N} < 5$ and $\mathcal{N} > 5$. The primary interest is in the case $\mathcal{N} < 5$ in studying the effect of flow on the different modes, and predictions for the shift in the critical point on introduction of flow are examined.

The effect of flow on the isotropic-nematic phase transition has also been examined by See et al. (1990) using a homogeneous theory. A perturbation technique is adopted by these authors to study the stability of the isotropic base state with increase in concentration. The shift in the critical point from $\mathcal{N} = 5$ in presence of flow is shown to scale as the square-root of the deformation rate in uniaxial elongation, biaxial stretching and shear flows. However, no information about structure formation is

245

obtained since the theory of See *et al.* is developed for homogeneous systems. A comparison of these results to the linear stability results obtained in the following sections is made at appropriate points.

Biaxial Stretching Flow. Calculations carried out with the homogeneous theory of liquid crystalline polymers indicate that biaxial stretching flow induces an oblate symmetry about the z-axis, *i.e.*, with molecules randomly oriented in the xy-plane. With increasing concentration, this oblate state undergoes a transition to a prolate state, with the molecular axes confined to the xy-plane. In order to study the development of microstructure at this critical point, we choose $k = k_x \delta_x$, and examine the xy-mode for $\mathcal{N} < 5$. Independent study of the xy-mode is feasible since the governing equation for $\hat{S}_{k,xy}$ is decoupled from the remainder of the equation set. The dispersion relation for the xy-mode is

$$\Sigma_{xy} = -\frac{3}{7} D_{tr} k^2 \left[1 - \frac{\mathcal{N}}{5}(1 + \frac{2}{3}\bar{\chi}_{xx}) + \frac{\mathcal{N}}{5}\frac{k^2 \ell^2}{24}(1 + \frac{2}{3}\bar{\chi}_{xx}) \right]. \tag{6.36}$$

It is apparent from Eq. (6.36) that for $1 - \frac{\mathcal{N}}{5}(1 + \frac{2}{3}\bar{\chi}_{xx}) > 0$, the system is stable to disturbances of all wavelengths and for $1 - \frac{\mathcal{N}}{5}(1 + \frac{2}{3}\bar{\chi}_{xx}) < 0$, the system is unstable to some wavelengths. This defines a condition for marginal stability as

$$1 - \frac{\mathcal{N}}{5}(1 + \frac{2}{3}\bar{\chi}_{xx}) = 0. \tag{6.37}$$

Substituting for $\bar{\chi}_{xx}$ from Eq. (6.27) and simplifying yields

$$1 - \frac{\mathcal{N}'}{5} = \left(\frac{\mathcal{N}'}{30}\right)^{1/2} \left(\frac{|\dot{\epsilon}|}{D_r}\right)^{1/2}. \tag{6.38}$$

Thus, from Eq. (6.38), $5 - \mathcal{N}' \sim \mathcal{O}((|\dot{\epsilon}|/D_r)^{1/2})$, in agreement with the perturbation results of See *et al.* (1990). The wavenumber with the maximum growth rate is obtained from Eq. (6.36) as

$$k_{max}^2 \ell^2 = \left[1 - \frac{5}{\mathcal{N}(1 + 2/3\bar{\chi}_{xx})} \right]. \tag{6.39}$$

246

From Eq. (6.39), we see that the dominant wavelength decreases with increasing $|\dot{\epsilon}|$. By substituting for $\tilde{\chi}_{xx}$ from Eq. (6.27) and by using Eq. (6.38), it can be shown that

$$k_{max}^2 \ell^2 |_{\text{flow}} - k_{max}^2 \ell^2 |_{\text{eq}} \sim \left(\frac{|\dot{\epsilon}|}{D_r}\right)^{1/2} \qquad (6.40)$$

The governing equations for uniaxial elongation and shear flows are not as simple as the one shown here for biaxial stretching flow, and obtaining growth rates for individual modes necessitates the simultaneous solution of two or more equations. It is not possible to derive simple analytical expressions for these modes, as in the case of biaxial stretching flow. However, a numerical study of the solutions of these equations reveals the behavior of the critical points, as described below.

Uniaxial Elongational Flow. We examine the mode $\hat{S}_{k,zz}$ with $k = k_z \delta_z$ in uniaxial flow, since we expect it to show the effect of elongation in the z-direction. This mode is coupled with $\hat{n}_k$, as in equilibrium, and the governing equations for $\hat{n}_k$ and $\hat{S}_{k,zz}$ are

$$\hat{n}_k \Sigma = - D_{tr}\left[\frac{1}{3}k^2 n_k + n_{av}(1 - \frac{\mathcal{N}}{5} + \frac{\mathcal{N}}{5}\frac{k^2 \ell^2}{24})k^2 \hat{S}_{k,zz}\right.$$
$$\left. - \frac{1}{7}n_{av}\frac{\mathcal{N}}{5}(1 - \frac{k^2 \ell^2}{24})[\frac{9}{2}\tilde{\chi}_{zz}\hat{S}_{k,zz}k^2]\right]. \qquad (6.41)$$

and

$$\hat{S}_{k,zz}\Sigma = -D_{tr}\left[\frac{11}{21}k^2 \hat{S}_{k,zz}\left[1 - \frac{\mathcal{N}}{5}(1 + \frac{8}{11}\tilde{\chi}_{zz}) + \frac{\mathcal{N}}{5}\frac{k^2 \ell^2}{24}(1 + \frac{8}{11}\tilde{\chi}_{zz})\right]\right.$$
$$\left. + \frac{4}{45}\frac{n_k}{n_{av}}k^2\right]. \qquad (6.42)$$

The two eigenvalues for this coupled mode are

$$\Sigma = \frac{1}{6}D_{tr}k^2 \left[-(1 + \frac{11}{7}B - \frac{12}{7}C) \pm \sqrt{(1 + \frac{11}{7}B - \frac{12}{7}C)^2 - 36(\frac{3}{35}B - \frac{11}{105}C)}\right] \qquad (6.43)$$

247
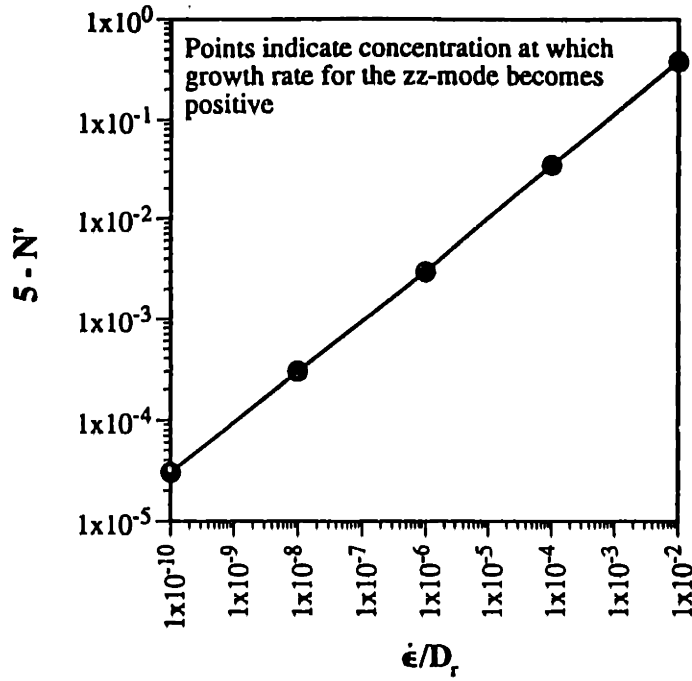
Figure 6-6: Effect of elongation rate on critical concentration $\mathcal{N}'$ in uniaxial elongation flow with $\mathbf{k} = k_z \delta_z$ in the limit of small k.

where

$$B \equiv 1 - \frac{\mathcal{N}}{5} + \frac{\mathcal{N}}{5}\frac{k^2 \ell^2}{24};$$

$$C \equiv \frac{2}{3}\frac{\mathcal{N}}{5}(1 - \frac{k^2 \ell^2}{24})\tilde{\chi}_{zz}. \tag{6.44}$$

This coupled mode is referred to as the *splay* mode at equilibrium; see Fig. 6-2. The introduction of flow is expected to cause only a slight perturbation and hence will not significantly affect the mode. The complexity of the above equations does not permit analytical evaluation of the dependence of the critical point $\mathcal{N}'$ on the elongation rate. Therefore, the critical concentration is numerically evaluated for different elongation rates. Analogous to the equilibrium situation, the system is expected to be unstable only in the small k limit. Therefore, the eigenvalues are evaluated in the small k limit by setting $B \equiv 1 - \mathcal{N}/5$ and $C \equiv 2\mathcal{N}/15\tilde{\chi}_{zz}$. The $\hat{S}_{k,zz}$ mode is found to go unstable at a critical concentration $\mathcal{N}'$ such that $5 - \mathcal{N}' \sim \mathcal{O}((|\dot{\epsilon}|/D_r)^{1/2})$; see Fig. 6-6. This result is in agreement with the perturbation calculations of See et al. (1990) for a homogeneous system. The second eigenvalue corresponding to the concentration

fluctuation $\hat{n}_k$ is always negative, and therefore has no impact on the stability of the system. Both eigenvalues are negative in the high k limit; this limit is thus of little interest and is not studied further.

Shear Flow. The same procedure is followed for shear flow with χ defined by Eq. (6.28) and with $k = k_x \delta_x$, i.e., modes in the shearing direction are examined. The following set of coupled equations are obtained for the modes $(\hat{n}_k, \hat{S}_{k,xx}, \hat{S}_{k,yy}, \hat{S}_{k,xy})$

$$
\hat{n}_k \Sigma = -D_{tr} \left[\frac{1}{3} k^2 n_k + n_{av}(1 - \frac{\mathcal{N}}{5} + \frac{\mathcal{N}}{5} \frac{k^2 \ell^2}{24}) k^2 \hat{S}_{k,xx} \right.
$$
$$
\left. - \frac{3}{7} n_{av} \frac{\mathcal{N}}{5} (1 - \frac{k^2 \ell^2}{24}) \chi_{xy} \hat{S}_{k,xy} k^2 \right] \tag{6.45}
$$

$$
\hat{S}_{k,xx} \Sigma = -D_{tr} \left[\frac{4}{45} \frac{n_k}{n_{av}} k^2 + \frac{11}{21}(1 - \frac{\mathcal{N}}{5} + \frac{\mathcal{N}}{5} \frac{k^2 \ell^2}{24}) \hat{S}_{k,xx} k^2 \right]
$$
$$
+ \frac{\mathcal{N}}{5} \frac{2}{21} D_{tr}(1 - \frac{k^2 \ell^2}{24}) k^2 \chi_{xy} \hat{S}_{k,xy} \tag{6.46}
$$

$$
\hat{S}_{k,yy} \Sigma = -D_{tr} \left[-\frac{2}{45} \frac{n_k}{n_{av}} k^2 + (1 - \frac{\mathcal{N}}{5} + \frac{\mathcal{N}}{5} \frac{k^2 \ell^2}{24})(\frac{1}{7} k^2 \hat{S}_{k,yy} - \frac{4}{21} k^2 \hat{S}_{k,xx}) \right] \tag{6.47}
$$

and

$$
\hat{S}_{k,xy} \Sigma = -D_{tr} \left[\frac{3}{7}(1 - \frac{\mathcal{N}}{5} + \frac{\mathcal{N}}{5} \frac{k^2 \ell^2}{24}) \hat{S}_{k,xy} k^2 \right]
$$
$$
+ \frac{\mathcal{N}}{5} \frac{1}{21} D_{tr}(1 - \frac{k^2 \ell^2}{24})[2k^2 \chi_{xy} \hat{S}_{k,xx} + k^2 \chi_{xy} \hat{S}_{k,yy}]. \tag{6.48}
$$

The growth rates for all modes described by this coupled set of equations are given by the eigenvalues of the matrix

$$
M = \begin{pmatrix}
-1/3 & -B & 0 & 3/7C \\
\\
-4/45 & -11/21B & 0 & 2/21C \\
\\
2/45 & 4/21B & -1/7B & 0 \\
\\
0 & 2/21C & 1/21C & -3/7B
\end{pmatrix}
\tag{6.49}
$$

where

$$
\begin{aligned}
B &\equiv 1 - \frac{\mathcal{N}}{5} + \frac{\mathcal{N}}{5}\frac{k^2\ell^2}{24}; \\
C &\equiv \frac{\mathcal{N}}{5}(1 - \frac{k^2\ell^2}{24})\tilde{\chi}_{xy}.
\end{aligned}
\tag{6.50}
$$

The eigenvalues are again evaluated for different shear rates in the small k limit, as in the case of uniaxial elongational flow, by setting $B \equiv 1 - \mathcal{N}/5$ and $C \equiv \mathcal{N}/5\tilde{\chi}_{xy}$. The critical concentration $\mathcal{N}'$ at which at least one component becomes unstable is calculated numerically. It is found that the xy-mode loses stability, and the critical point again scales as $5 - \mathcal{N}' \sim \mathcal{O}((|\dot{\gamma}|/D_r)^{1/2})$; see Fig. 6-7. This result is in agreement with the results of See *et al.* (1990) obtained by using a homogeneous theory. The other three components of fluctuation, $\hat{S}_{k,xx}$, $\hat{S}_{k,yy}$ and $\hat{n}_k$, do not change their stability and the eigenvalues are always negative. Although this result is expected for n_k, it is surprising for the normal modes $\hat{S}_{k,xx}$ and $\hat{S}_{k,yy}$. This is probably a consequence of truncating the base state expansion (6.26) at $\mathcal{O}(\dot{\gamma}/D_r)$. Note that for the choice $k = k_y\delta_y$, the equations for the modes ($\hat{n}_k$, $\hat{S}_{k,xx}$, $\hat{S}_{k,yy}$, $\hat{S}_{k,xy}$) are identical to Eqs. (6.45)-(6.48) with an interchange of the components $\hat{S}_{xx}$ and $\hat{S}_{yy}$. The overall stability picture is thus unchanged.
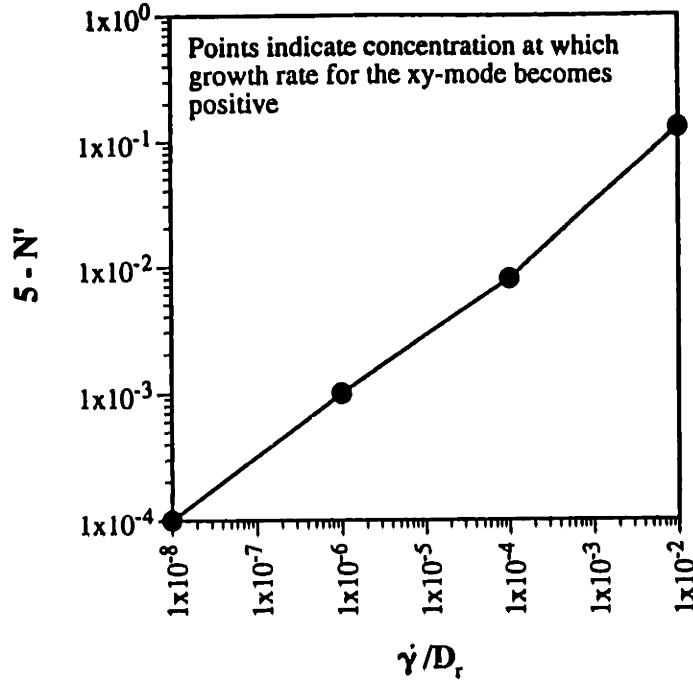
Figure 6-7: Effect of shear rate on the critical concentration $\mathcal{N}'$.

6.4 Summary

The general nonhomogeneous constitutive theory for liquid crystalline polymers developed in Chapter 4 is used to study the development of structure at the isotropic-nematic transition point by using a linear stability approach. In the absence of rotational diffusivity, $\sigma = 0$, we find that the predictions follow the classical theory of spinodal decomposition, as developed by Cahn (1961 & 1965) for a system of binary alloys. Thus, in this limit, for all $\mathcal{N} > 5$, the growth rate of the domains and the dominant wavenumber increase with increasing concentration. The growth rate of the $k = 0$ mode is always zero, in the absence of rotational diffusivity, and the initial pattern development is dominated by a single wavenumber that has a maximum growth rate. However, when rotational diffusivity is significant, the growth rate corresponding to the $k = 0$ mode is nonzero. In this case, the spinodal region can be divided into two regions – for $\mathcal{N}_{crit} < \mathcal{N} < \mathcal{N}^*$, rotational diffusivity dominates and $k = 0$ is the dominant wavenumber, whereas for $\mathcal{N} > \mathcal{N}^*$ classical spinodal decomposition is recovered.

The dominant wavenumber is used to estimate characteristic domain sizes that

251

may be expected in these systems. Two alternative forms of the intermolecular potential are examined, *viz.*, $\Phi^{(p)h-r}$ and $\Phi^{(p)Mar}$. The two forms essentially differ in the range of interaction between interacting molecules; the range is of the order of macromolecular lengths for $\Phi^{(p)h-r}$, whereas it is at least an order of magnitude larger for $\Phi^{(p)Mar}$. In both cases, it is found that the characteristic domain size scales with the domain of interaction of the intermolecular potential in the absence of rotational diffusivity. Although the domain sizes predicted by both forms of the potential are reasonable, the values of the growth rate predicted with $\Phi^{(p)h-r}$ are much higher than those typically seen in polymeric systems. The choice of $\Phi^{(p)Mar}$ therefore appears to be more reasonable.

The effect of biaxial stretching, uniaxial elongation and shear flows on the critical concentration $\mathcal{N}'$ is also examined by using a perturbation theory. In all cases, we find that $5 - \mathcal{N}' \sim \mathcal{O}(\delta^{1/2})$, where $\delta = |\dot{\gamma}|/D_r$ in shear flow and $\delta = |\dot{\epsilon}|/D_r$ in elongational flows. These results are in agreement with the homogeneous theory results of See *et al.* (1990). The characteristic domain size in biaxial stretching flows also was estimated and was found to decrease with increasing elongation rate, such that $k_{max}^2 \ell^2|_{flow} - k_{max}^2 \ell^2|_{eq} \sim \left(\frac{|\dot{\epsilon}|}{D_r}\right)^{1/2}$. Due to the complexity of the equations involved, it is not possible to get a similar scaling for domain size in shear and uniaxial elongational flows.

The linear stability analysis adopted in this chapter is a useful technique that offers insight into the interaction of the intermolecular potential with structure formation at the isotropic-nematic transition point. The theory also can be extended to study the effect of flows on the transcritical bifurcation between the isotropic and prolate nematic states. This technique avoids entirely the problems of closure; this is a consequence of the linearization about the known base state that also restricts the applicability of the theory to the study of only the initial stages of spinodal decomposition. The study of defect structures that can play an important role in determining material properties requires analysis of the full nonlinear set of equations, which is only possible by numerical solution.

Chapter 7

Summary

A general framework for incorporating spatial nonhomogeneities into micromechanical-model-based constitutive theories for viscoelastic solutions was developed by using a phase space kinetic theory. Simple dumbbell models were used to study dilute and concentrated systems, and the coupling between stress, velocity, concentration and microstructure in spatially nonhomogeneous systems was explored. The different aspects of polymer kinetic theory that were addressed in the course of this thesis are summarized in Fig. 7-1.

A consistent nonhomogeneous theory must include:

1. A spatially-dependent distribution function. This makes no assumptions regarding spatial uniformity of polymer concentration and allows the incorporation of configurational anisotropies such as those introduced by rigid boundaries.

2. An explicit description of the distribution of mass at the bead locations. This treatment accounts for the finite spatial extension of the polymer molecule and allows a consistent study of problems in which stress and velocity gradients vary on macromolecular length scales.

3. An accurate description of the finite range of polymer-polymer interaction that also results from the finite spatial extent of polymer molecules. This is essential for a proper description of surfaces and interfaces in the problem.

253

```
┌─────────────────────────────────────────────┐
│     Kinetic Theory of Polymer Solutions     │
│           Using Dumbbell Models             │
└─────────────────────────────────────────────┘
```

Kinetic Theory of Polymer Solutions Using Dumbbell Models

Dilute Solution   **Concentrated Solution**

Flexible Dumbbell   **Rigid Dumbbell**   **Flexible Dumbbell or Multibead Model?**   **Rigid Dumbbell** hard-rod interaction with phase transition to liquid crystalline phase

Homogeneous *(Bird et al., 1987)*

Nonhomogeneous

- Nonsimple fluid theory
- Molecular migration due to concentration, stress and velocity gradients
- Apparent slip and polymer depletion predicted

Homogeneous *Doi, 1981; Menon, 1990; Bhave et al., 1992*

- Multiple phases coexist in shear and shearfree flows
- 2-d oblate-prolate transition seen in biaxial stretching flow

Nonhomogeneous

- Structure develops by spinodal decomposition
- Domain size at onset depends on range of interaction

Figure 7-1: Summary of thesis work. The shadowed boxes highlight the main contributions of the thesis.

A self-consistent dilute solution theory for nonhomogeneities that incorporates the ideas listed here was developed by starting from a simple Hookean dumbbell model of a polymer molecule. The conditions under which behavior of polymer solutions in highly nonhomogeneous flows is influenced by molecular migration caused by concentration, stress and velocity gradients was studied, and a generalized flux expression that accounted for these mechanisms was developed. The resultant constitutive equation describes a nonsimple viscoelastic fluid, with a spatially nonhomogeneous concentration field that results from a balance between the different flux contributions. The importance of this molecular migration and its effect on stress scales with the ratio $De/Pe \equiv \lambda_H D_{tr}/L^2$, which is interpreted as a ratio of the distance a polymer molecule diffuses in one relaxation time to a physical length scale characteristic of macroscopic flow. The small values of D_{tr} in polymeric solutions confines the importance of macromolecular migration to small-scale systems such as narrow pores, to thin boundary layers near solid walls and to regions of very high stress gradients.

The nonhomogeneous theory was used to study a simple problem of rectilinear shear flow. Since stress at a point in the flow is coupled, in a diffusive manner, to stress at any other point, knowledge of stress at the wall is necessary in order to solve this, or any other, problem. Molecular configuration at the wall is set in order to determine the required boundary conditions. Note that this does not set the value of stress since stress also depends on the number density at the wall, which is self-consistently determined as a part of the solution to the problem. Probing molecular length scales in the vicinity of a wall poses immense challenge to experimentalists and little is known yet regarding the detailed molecular orientation at the wall at equilibrium and in presence of flow. There is a need to gain better understanding of the local molecular dynamics that will allow the imposition of more realistic boundary conditions. A significant advantage of the approach taken here is that more sophisticated boundary conditions can easily be incorporated without any change of the governing equations.

In the analysis of rectilinear shear flow, the dumbbell orientation at the wall was taken to be parallel to the wall and in the direction of flow, and any molecular stretching due to local flow was ignored. Even such simplistic boundary conditions

sufficed in predicting the development of polymer-depleted layers adjacent to the wall that scaled as the radius of gyration of the polymer. Apparent slip near the wall was also predicted due to the decreased fluid viscosity in the boundary layer caused by molecular orientation. Both predictions showed reasonably good agreement with available experimental data. The apparent slip coefficient β computed from this theory scaled as $(\mathrm{De}/\mathrm{Pe})^{1/2} \equiv \sqrt{\lambda_H D_{tr}}/L$.

The issue of spatial nonhomogeneities was addressed in this problem primarily with the help of a Taylor series expansion truncated after the first term. This description is inadequate if spatial variation is seen on a submolecular length scale and in such cases, higher order Taylor series terms may be required. Moreover, in order to model such rapid changes on a submolecular length scale, the dumbbell model used in the present development also is inadequate. An extension of the theory to multibead models can overcome this problem. Realistic molecular models such as the Kramers chain or the Rouse-Zimm models could be used, but the associated mathematics will be significantly more complex. It is questionable whether such models are necessary in order to describe nonhomogeneities in dilute solutions. However, for concentrated solutions of flexible molecules, where the effect of chain entanglements and excluded volume polymer-polymer interactions are important, such a multibead description of the polymer molecule is essential. Concentrated solutions of flexible chain molecules have not been considered in this thesis and are a possible avenue for further work.

An extension of the dilute solution flexible model theory to models of rigid polymers is straightforward and will give qualitatively similar results. The analysis of problems for rigid dumbbells is expected to be a bit more complex as a consequence of the constraints in the molecular model. The concepts developed for the nonhomogeneous dilute solution theory also can be extended to the study of other, technologically relevant, nonhomogeneous problems. For instance, the presence of defects and nonhomogeneous polydomain structures in liquid crystalline polymers can strongly affect the fluid rheology and material properties. Such liquid crystalline phases are formed by molecules with rigid backbones and can be modelled using rigid dumbbells. Such an extension of the flexible polymer nonhomogeneous dilute solution theory to

a concentrated system of rodlike polymers was carried out to develop a constitutive theory for nonhomogeneous solutions of rodlike, liquid crystalline polymers. This theory was used to study the phase transition of this system from a randomly-ordered isotropic state to a uniaxially-ordered prolate nematic phase. This development was an extension of the homogeneous theories for liquid crystalline materials developed by Doi (1980 & 1981) and Menon (1990).

The inclusion of pairwise hard-rod excluded volume interactions was shown to result in the isotropic-nematic transition with increasing concentration. The mean-field version of the excluded volume potential accounts for a finite range of interaction by means of terms involving spatial gradients of the structure tensor. In the consistent phase space development adopted here, such an intermolecular potential results in gradient terms in the expression for the stress tensor. These terms are the equivalent of Frank's distortional stresses in the theory for low-molecular-weight nematics.

Using this theory, it was shown that the prolate nematic phase that is stable at high concentrations is rotationally invariant in the absence of any external directing fields. Introduction of flow was shown to destroy the rotational invariance of the equilibrium states. The transcritical bifurcation between the isotropic and prolate nematic states was broken. Multiple nematic states were predicted to be stable, depending on the concentration and deformation rate. The particular orientations that developed were dependent on the kinematics of the applied flow field and the equilibrium orientation. For instance, a randomly ordered fluid developed oblate symmetry under the influence of biaxial stretching flow, whereas shear and uniaxial elongation induced prolate symmetry in the same fluid.

The development of a stable oblate symmetry in the presence of biaxial stretching flow was shown to be possible only at low concentration, and an in-planar transition to prolate symmetry was seen with increasing concentration. The in-planar oblate to prolate transition is a two-dimensional analogue of the three-dimensional equilibrium isotropic-nematic transition. It suggests an interesting way to study experimentally the mechanism of phase transition, since the onset of the transition can be easily controlled by controlling $\dot{\epsilon}$, and the problems presented by the presence of a coexistence

region could be entirely eliminated.

The study of a wide range of concentration and rates-of-deformation for shear, uniaxial elongation and biaxial stretching flows was feasible by the use of a quadratic closure approximation that allowed the complex diffusion equation for the configurational distribution function f_p to be written entirely in terms of the second-order moment. Although the use of such closure approximations is convenient, it may lead to misleading results. For instance, the calculations in shear flow fail to capture the time-periodic molecular tumbling that was predicted by a numerical solution of the diffusion equation (Marrucci and Maffettone, 1989; Larson, 1990). However, calculations in elongational flow appear to be unaffected by the use of quadratic closure. No unique closure approximation exists and the validity of any closure scheme is largely dependent on the imposed kinematics. Closure approximations, when used, must be carefully selected for the required application. Their use can be avoided in the study of homogeneous problems, albeit at the cost of increased numerical complexity. However, a direct numerical solution of the diffusion equation in spatially nonhomogeneous problems does not seem feasible at this time, and future work must be directed towards this goal.

In view of the impact of closure approximations, a linear stability approach was adopted to study the evolution of microstructure from the isotropic state for concentrations in the unstable region. The mechanism of structure development was found to be qualitatively similar to the classical theory for spinodal decomposition (Cahn, 1961 & 1965). The linear stability analysis avoids entirely the use of closure and permits the study of the initial stages of spinodal decomposition, where nonlinear effects are unimportant. Since the initial stage can last for as long as 100-200 minutes in polymeric systems, it is possible to get experimental verification of the predicted theoretical results.

The separation in systems such as binary alloys and glasses is governed by translational diffusion, and the separating domains have distinctly different material properties. In contrast, in the liquid crystalline systems, the separating phases differ in orientation alone, and the separating domains can take infinitely many orientations at

equilibrium. Both rotational and translational diffusivities can potentially influence the process of separation. When the effects of rotational diffusion can be ignored, possibly due to hindered rotational motion in the concentrated isotropic region, the development of structure proceeds by classical spinodal decomposition. The structure development was found to be characterized by a single dominant wavelength λ_{dom} that set the pattern and the characteristic domain size. The wavelength λ_{dom} decreased with increase in concentration, and the growth rate associated with the domains, which scales as D_{tr}/λ_{dom}^2, correspondingly increased. The characteristic initial domain size predicted by this theory scales as the range of interaction in the intermolecular potential. Detailed experimental studies of both characteristic initial domain size and initial growth rate are required in order to differentiate between and to further improve the alternative forms of the intermolecular potential.

The mechanism of phase separation is different when the rotational diffusivity is finite. The unstable concentration region or the spinodal region was divided into two distinct regimes. The first regime corresponding to a range of concentrations just within the spinodal region was dominated by the effects of rotational diffusivity, and the dominant wavenumber was $k = 0$. The development of order in this region is accomplished simply by a molecular rotation with unchanged center-of-mass location; no spatial pattern develops. The second regime is seen at higher concentrations; here the mechanism of classical spinodal decomposition is recovered, and although rotational diffusivity can aid the structure development, the spatial pattern is set by the translational diffusivity alone. The effects of flow on the structure development also were studied, and the breaking of the bifurcation between the isotropic and nematic families on introduction of flow was predicted. The critical concentration $\mathcal{N}'$ at which the near-isotropic state loses stability was found to vary such that $5 - \mathcal{N}'$ scales as the square-root of the deformation rate.

The definition of the domain texture increases as spinodal decomposition progresses, and the late stages are characterized by nonlinear phenomena such as coarsening of the domains. Study of these late stages must be accomplished by using numerical techniques. However, the existence of infinitely many orientations within

different domains adds enormously to the complexity of the problem, and poses a considerable challenge to future analysis. The surfaces between domains eventually decay to line and point defects that are persistent and can significantly affect the rheology of the polymeric liquid crystal. Study of the coupling between defect structures and imposed flow is not possible with the linearized approach used here and merits detailed study. The terms involving gradients of the structure tensor in the expression for the stress tensor also are expected to play an important role in these problems at the boundaries of domains or at defect lines and points. A detailed understanding of these gradient terms and their effect on the fluid rheology also must be developed.

The nonhomogeneous theories for dilute and concentrated solutions developed here incorporate all the features that are judged to be important in an arbitrary, nonhomogeneous fluid mechanical problem. Governing equations for stress, velocity, concentration and microstructure are all derived in a self-consistent manner. These theories have been tested in simple flow problems and are seen to be powerful enough to tie together ideas such as polymer-depletion and apparent slip and to predict microstructure development in phase-separating systems. Detailed numerical solution of complex flow problems using these theories is confounded by the small length scales over which changes in the field variables are predicted to take place. However, the insight provided by these fundamental molecular theories is invaluable in advancing our understanding of nonhomogeneous problems. The nonhomogeneous theories thus are a foundation on which further studies can be based.

Appendix A

Appendix .

This appendix includes all programs and subroutines that were used in calculating the stress, velocity and concentration profiles for the rectilinear shear flow problem; see Section 3.4.

```
        program migration
c**********************************************************************
c     Finite difference scheme to solve for shear flow between
c     parallel plates using the Giesekus-like diffusion constitutive
c     model: Modified equations : uses bornarrow.f from Dr. B
c          subroutines resid.f, dresid.f, jacob.f
c**********************************************************************

        implicit real*8(a-h,o-z)
        dimension b(5010,70),c(5010,8),d(8,5010)
        dimension res(5010,3),x(5010),e(8,8),xprev(5010)


c**********************************************************************

        open(unit=1,file='mig.dat')
        open(unit=2,file='mig.res')
        open(unit=3,file='init.res')
           open(unit=10,file='data.res')
           open(unit=11,file='conclusion')


c**********************************************************************

        read (1,*)tau,n,de,eps,a20,a2fin,da2,icmax,tol
        h=1.d0/dble(n)


c**********************************************************************
c     n: no. of mesh intervals
c     h:  mesh size
c**********************************************************************

        iband=21
        mid=(iband + 1)/2
           iarrow=6
           ntotal=5*n+10
        nod=ntotal-iarrow
        lbd=70
        jn=5010
        ja=8
        jna=5010
        nrhs=2
        lrhs=3


c**********************************************************************
c          define parameters
c**********************************************************************
```

```fortran
          a2=a20
c         eps=de/pe
          pe = de/eps
          boltz=1.3806d-16
          temp=300
          tpolym=1.d-3
          cnav=1.d19
          vs=10.d0
          vratio=vs/(cnav*boltz*temp*tpolym)
          afact=3.d0
          aterm=1.d0+afact
          eqln=500.d0
c         eta_s/eta_p = 0.0241 based on vs=1cp,cnav=1exp16,tpolym=0.1


c********************************************************************
c     give initial guess to the problem
c********************************************************************

          do 100 i=1,ntotal
          read(3,*)x(i)
100       continue

c********************************************************************
c     Setting up the Jacobian matrix and vector of residuals
c********************************************************************

c********************************************************************
c         initialize the jacobian matrix
c********************************************************************

44        icount=0
45    a1=afact*a2
          do 50 k=1,iarrow
                  do 50 l=1,iarrow
                  e(k,l)=0.d0
                  do 50 j=1,nod
                          c(j,k)=0.d0
                          d(k,j)=0.d0
                          do 50 i=1,iband
                                  b(j,i)=0.d0
50        continue

c********************************************************************
c     define residuals vector
```

```
c***************************************************************************

            call resid(res,x,eqln,vratio,a1,a2,de,pe,eps,am,ap,
    1                  adif,dam,dap,dadif,sum1,sum2,h,aterm,afact,n)

c***************************************************************************
c    define derivatives of residuals vector with respect to parameter "a"
c         in order to implement analytic continuation in "a"
c***************************************************************************

            call dresid(res,x,eqln,vratio,a1,a2,de,pe,eps,am,ap,
    1                  adif,dam,dap,dadif,sum1,sum2,h,aterm,afact,n)

c***************************************************************************
c         define jacobian matrix
c***************************************************************************

            call jacob(b,c,d,e,res,x,eqln,vratio,a1,a2,de,pe,eps,am,ap,
    1                  adif,dam,dap,dadif,sum1,sum2,h,aterm,afact,n,mid)


c***************************************************************************
c         jacobian matrix is now completely formed
c***************************************************************************

        sqerr=0.0
            solnorm=0.0
            call arrow(res,b,c,d,e,detlog,isign,tau,jn,iband,lbd,ja,jna,
    1            nrhs,nod,iarrow,lrhs)
            do 70 i=1,ntotal
                sqerr=sqerr + (res(i,1))**2
70      continue
c       error=dsqrt(sqerr/ntotal)
        error=dsqrt(sqerr)
        do 55 i=1,ntotal
            x(i)=x(i)+res(i,1)
55      continue
        do 71 i=1,ntotal
            solnorm=solnorm + x(i)**2
71      continue
            err1=dsqrt(solnorm)
            write(*,*)error,err1
            write(11,*)error,err1
        if(error.lt.tol)goto 65
            icount=icount+1
            if(icount.gt.icmax)goto 90
```

264

```fortran
         go to 45

c**********************************************************************
c         take a small step "da2" in parameter "a2"
c**********************************************************************

65       write(*,*)a2
         write(11,*)a2,isign
         aprev=a2
      do 58 i=1,ntotal
         xprev(i)=x(i)
58    continue
         a2 = a2 + da2
      if(dabs(a2).gt.dabs(a2fin))go to 81
      do 80 i=1,ntotal
         x(i)=x(i)+res(i,2)*da2
80    continue
      go to 44
90       write(*,*)"Newton iteration has not converged"
         write(11,*)"Newton iteration has not converged"
         write(11,*)"Solution has converged to alpha =",aprev
         goto 82
81    write(*,*)"maximum value of alpha has been reached"
      write(11,*)"maximum value of alpha has been reached"

c**********************************************************************
c         write results in file for given value of "a"
c**********************************************************************

82       do 150 i=1,ntotal
                 write(2,*)x(i)
150      continue
         write(10,200)n,de,pe,aprev,a2fin,da2,eqln,icmax
200      format(1x,"Number of intervals:",1x,i5//
     1           1x,"Deborah number:",1x,f5.2//
     1           1x,"Peclet number:",1x,f7.2//
     1           1x,"alpha value reached:",1x,f7.5//
     1           1x,"Maximum alpha:",1x,f7.5//
     1           1x,"Step size in alpha:",1x,f7.5//
     1           1x,"HQ**2/kT:",1x,f6.1//
     1           1x,"maximum Newton iterations allowed:",1x,i3)
         write(11,*)"alpha value reached is",aprev
83       stop
      end
```

```
      subroutine arrow(rhs,b,c,d,e,detlog,isign,tau,
     $         jn,iband,lbd,ja,jna,nrhs,nod,iarrow,lrhs)
      implicit real*8(a-h,o-z)
      dimension b(jn,lbd),c(jn,ja),d(ja,jn),e(ja,ja)
      dimension rhs(jna,lrhs)
c-------------------------------------------------------|
c    written by:  paul thomas   |
c      mit 66-256   |
c      77 massachusetts avenue   |
c      cambridge, ma  02139   |
c         |
c    this subroutine solves the matrix equation: a * x = rhs |
c         |
c    where a is an arrow matrix and rhs,x are vectors.  an arrow |
c    matrix has nonzero elements only in a narrow band centered |
c    on the main diagonal and in the last few columns and rows. |
c         |
c    the matrix a is reduced using gaussian elimination with  |
c    threshold row pivoting.  the column in the band matrix is |
c    searched for the maximum element.  if the diagonal element |
c    is less than a fraction(tau) of the maximum element, then |
c    the rows are exchanged.    |
c         |
c    tau = 1.0 partial pivoting   |
c    tau = 0.2-0.3 recommended range   |
c    tau = 0.0 no pivoting   |
c    tau = -1.0 solves l u x = b.  input is matrix previously |
c      factored with tau = 0.0   |
c         |
c    the program will return the correct  l u decomposition if it |
c    has not pivoted, which is indicated when npiv=0.  this can |
c    be forced by setting tau=0.0, suppressing pivoting.  the |
c    matrix equation is solved for multiple b vectors.  the  |
c    magnitude and sign of the determinant are also calculated. |
c    note: extra storage is required for the band matrix. |
c      b(jn,*), c(jn,*), d(ja,*), e(ja,*), and rhs(jna,*) |
c-------------------------------------------------------|
c-------------------------------------------------------|
c      columns and rows of the arrow  |
c    iband - band width of matrix a, must be odd |
c    iarrow - width of the columns and rows in the arrow |
c    nrhs - number of b vectors  |
c         |
c    tau - minimum ratio of diagonal to maximum element |
c      for no pivoting and  l u, set tau=0.0 |
c      for full pivoting, set tau=1.0  |
```

266

```
c     for solving l u x = b, set tau=-1.0 |
c     detlog - log 10 of the determinant   |
c     isign - sign of the determinant       |
c     npiv - number of times rows have been pivoted |
c          |
c     rhs(nod+iarrow,nrhs) - holds b vectors. the solution |
c         vector x is returned in this vector |
c     e(iarrow,iarrow) - holds the elements in the square |
c         section of the arrow matrix |
c     d(iarrow,nod) - holds the elements of the rows |
c         of the arrow matrix |
c     c(nod,iarrow) - holds the elements of the columns |
c         of the arrow matrix |
c     b(nod, 3*iband-1 ) - banded matrix a. note that the |
c         2 the bandwidth.  |
c----------------------------------------------------------|
      mid=(iband+1)/2
      mex=0
      nex=0
      detlog=0.0d0
      isign=1
      npiv=0
      nodar=nod+iarrow


c          do 500 i=1,4
c          write(*,*)e(i,1),e(i,2),e(i,3),e(i,4)
c500      continue


c----------------------------------------------------------|
c     b(i,mid) contains the diagonal elements of matrix a |
c     mex  keeps track of the maximum row exchange |
c        in the matrix a    |
c     nex  keeps track of the last non-zero element |
c        in the row in matrix a    |
c          |
c     clean out matrix a outside the band width |
c----------------------------------------------------------|
      do 10 i=1,nod
        do 10 j=iband+1,iband+mid-1
          b(i,j)=0.0d0
10    continue
c----------------------------------------------------------|
c     gaussian elimination of matrix a. check the column |
c     for the maximum element. if the diagonal is less than a |
c     fraction, tau, of the maximum element then switch rows. |
c     if tau = 0.0 then no pivoting will take place and the l u |
```

```
c    decomposition will be returned. if tau=1.0 then full row |
c    pivoting will be used. if tau = -1.0 then the l u matrix |
c    will be front-substituted, and then back-substituted.  |
c        |
c----------------------------------------------------------------|
     if (tau.lt.0.0) goto 20
     do 30 i=1,nod-1
       l=i
       big=dabs(b(i,mid))
       do 40 j=i+1,min(l+mid-1,nod)
         if(dabs(b(j,mid+i-j)).lt.big) goto 40
         big=dabs(b(j,mid+i-j))
         l=j
40     continue
       if (dabs(b(i,mid)).ge.tau*big) goto 50
c----------------------------------------------------------------|
c    exchange row i with row l. the vector b and array col are |
c    exchanged. the determinant of the matrix changes sign. |
c----------------------------------------------------------------|
       mex=max(mex,l-i)
       nex=max(nex,l-i)
       k1=min(iband+nex,nod-i+mid)
       call dswap(k1-mid+1,b(i,mid),jn,b(l,mid+i-l),jn)
       call dswap(iarrow,c(i,1),jn,c(l,1),jn)
       call dswap(nrhs,rhs(i,1),jna,rhs(l,1),jna)
       isign=-isign
       npiv=npiv+1
c----------------------------------------------------------------|
c    the lower band matrix is eliminated and replaced with the |
c    pivots for the l u decomposition. the b vector and the |
c    array col is updated.    |
c----------------------------------------------------------------|
50     diag=b(i,mid)
       if(diag.eq.0.0d0) then
         write(6,*) 'stopping in arrow, zero pivot,i,mid',i,mid
         stop
       endif
       nex=max(l-i,nex-1)
       j1=max(1,i+mid-nod)
       j2=max(1-nex,i+mid-nod)
       do 30 j=mid-1,j1,-1
         i1=mid+i-j
         piv=b(i1,j)/diag
         b(i1,j)=piv
         call daxpy(nrhs,-piv,rhs(i,1),jna,rhs(i1,1),jna)
         call daxpy(iarrow,-piv,c(i,1),jn,c(i1,1),jn)
```

```
            call daxpy(mid-j2,-piv,b(i,mid+1),jn,b(i1,j+1),jn)
30    continue
c--------------------------------------------------------------|
c     the array row is eliminated except for the last column and |
c     replaced with the pivot for the l u decomposition. the b |
c     vector and the array head are updated.    |
c--------------------------------------------------------------|
      do 110 i=1,nod-1
        diag=b(i,mid)
        j1=min(i+mid-1+mex,nod) ·
        do 110 j=1,iarrow
          piv=d(j,i)/diag
          d(j,i)=piv
          call daxpy(nrhs,-piv,rhs(i,1),jna,rhs(nod+j,1),jna)
          call daxpy(j1-i,-piv,b(i,mid+1),jn,d(j,i+1),ja)
          call daxpy(iarrow,-piv,c(i,1),jn,e(j,1),ja)
110   continue
c--------------------------------------------------------------|
c     the final element of the banded matrix a is checked to see |
c     if it is large enough. if it is too small, it is pivoted |
c     with an element from the last column of the array row.  |
c--------------------------------------------------------------|
      big=dabs(b(nod,mid))
      do 140 j=1,iarrow
        if(dabs(d(j,nod)).lt.big) goto 140
        big=dabs(d(j,nod))
        l=j
140   continue
      if(dabs(b(nod,mid)).ge.tau*big) goto 150
      call dswap(nrhs,rhs(nod,1),jna,rhs(nod+l,1),jna)
      call dswap(iarrow,c(nod,1),jn,e(l,1),ja)
      call dswap(1,b(nod,mid),1,d(l,nod),1)
      isign=-isign
      npiv=npiv+1
c--------------------------------------------------------------|
c     the last column of the array row is eliminated. the b |
c     vector and the array head are updated.    |
c--------------------------------------------------------------|
150   diag=b(nod,mid)
      do 180 i=1,iarrow
        piv=d(i,nod)/diag
        d(i,nod)=piv
        call daxpy(nrhs,-piv,rhs(nod,1),jna,rhs(nod+i,1),jna)
        call daxpy(iarrow,-piv,c(nod,1),jn,e(i,1),ja)
180   continue
c--------------------------------------------------------------|
```

```
c   the array head is eliminated using threshold row pivoting. |
c   if the diagonal element is less than a fraction, tau, of the |
c   maximum column element, then the rows are exchanged. as the |
c   column is eliminated, the b vector and the array head are |
c   updated.      |
c------------------------------------------------------------------|
      do 200 i=1,iarrow-1
        big=dabs(e(i,i))
        do 210 j=i+1,iarrow
          if(dabs(e(j,i)).lt.big) goto 210
          big=dabs(e(j,i))
          l=j
210     continue
        if (dabs(e(i,i)).ge.tau*big) goto 220
        call dswap(nrhs,rhs(nod+i,1),jna,rhs(nod+l,1),jna)
        call dswap(iarrow,e(i,1),ja,e(l,1),ja)
        isign=-isign
        npiv=npiv+1
220     diag=e(i,i)
        if(dabs(e(i,i)).lt.0.00000001) then
          write(6,*) 'i,j,iarrow,e(i,i)',i,j,iarrow,diag
          stop
          endif
        do 200 j=i+1,iarrow
          piv=e(j,i)/diag
          e(j,i)=piv
          call daxpy(nrhs,-piv,rhs(nod+i,1),jna,rhs(nod+j,1),jna)
          call daxpy(iarrow-i,-piv,e(i,i+1),ja,e(j,i+1),ja)
200   continue
      goto 260
c------------------------------------------------------------------|
c   if tau < 0 the matrix is not decomposed, and the previous |
c   l u matrix is used. the lower matrix l is forward |
c   substituted.    |
c------------------------------------------------------------------|
20    do 270 i=1,nod
        il=min(i+mid-1,nod)
        do 270 n=1,nrhs
          piv=rhs(i,n)
          call daxpy(il-i,-piv,b(i+1,mid-1),1-ja,rhs(i+1,n),1)
          call daxpy(iarrow,-piv,d(1,i),1,rhs(nod+1,n),1)
270   continue
      do 290 i=1,iarrow
        do 290 n=1,nrhs
          piv=rhs(nod+i,n)
          call daxpy(iarrow-i,-piv,e(i+1,i),1,rhs(nod+i+1,n),1)
```

```
290   continue
c------------------------------------------------------------------|
c   the upper matrix u containing the arrow is back-substituted |
c   for the solution vectors x.  the magnitude and sign of the |
c   matrix are calculated.      |
c------------------------------------------------------------------|
260   do 300 i=iarrow,1,-1
      diag=e(i,i)
      detlog=detlog+dlog10(dabs(diag))
      if(diag.lt.0.0) isign=-isign
      do 300 n=1,nrhs
        piv=rhs(nod+i,n)/diag
        rhs(nod+i,n)=piv
        call daxpy(i-1,-piv,e(1,i),1,rhs(nod+1,n),1)
        call daxpy(nod,-piv,c(1,i),1,rhs(1,n),1)
300   continue
c------------------------------------------------------------------|
c   the upper matrix u containing the banded matrix a is back- |
c   substituted for the solution vectors x.  the magnitude and |
c   sign of the determinant are calculated.   |
c------------------------------------------------------------------|
      do 320 i=nod,1,-1
        diag=b(i,mid)
        detlog=detlog+dlog10(dabs(diag))
        if(diag.lt.0.0) isign=-isign
        j1=max(1,i-mid-1-mex)
        do 320 n=1,nrhs
          piv=rhs(i,n)/diag
          rhs(i,n)=piv
          do 320 j=i-1,j1,-1
            rhs(j,n)=rhs(j,n)-b(j,mid+i-j)*piv
c         j2=mid+i-j1
c         call daxpy(i-j1,-piv,b(j1,j2),jn-1,rhs(j1,n),jna)
320   continue
      return
      end
```

Subroutine: jacob.f

```fortran
                    subroutine jacob(b,c,d,e,res,x,eqln,vratio,a1,a2,de,pe,eps,am,ap,
       1                    adif,dam,dap,dadif,sum1,sum2,h,aterm,afact,n,mid)
                    implicit real*8(a-h,o-z)
                    dimension b(5010,70),c(5010,8),d(8,5010)
                    dimension res(5010,3),x(5010),e(8,8)

                    b(1,mid)=1.d0
                    b(1,mid+4)=-1.d0/de*(1.d0-eqln)
                    b(2,mid)=1.d0
                    b(2,mid+3)=-1.d0/de
                    b(3,mid)=1.d0
                    b(3,mid+2)=-1.d0/de
                    b(4,mid)=1.d0
                    do 20 i=2,n
                            ii=5*i
c                           am=1.d0 + a2*vratio/x(ii)*(x(ii-4)+x(ii-3)
c      1                            +x(ii-2))
c                           ap=1.d0 + a2*vratio/x(ii)*(x(ii-4)+
c      1                            aterm*x(ii-3)+x(ii-2))
c                           adif=a2*vratio*((x(ii+1)+aterm*x(ii+2)+x(ii+3))/
c      1                            x(ii+5) - (x(ii-9)+aterm*x(ii-8)+x(ii-7))/
c      1                            x(ii-5))
c                           dam=vratio/x(ii)*(x(ii-4)+x(ii-3)+x(ii-2))
c                           dap=vratio/x(ii)*(x(ii-4)+
c      1                            aterm*x(ii-3)+x(ii-2))
c                           dadif=vratio*((x(ii+1)+aterm*x(ii+2)+x(ii+3))/
c      1                            x(ii+5) - (x(ii-9)+aterm*x(ii-8)+x(ii-7))/
c      1                            x(ii-5))
                            b(ii-5,mid-4)=-eps
                            b(ii-5,mid-3)=-eps
                            b(ii-5,mid+1)=h**2 + 2.d0*eps
                            b(ii-5,mid+2)=2.d0*eps
                            b(ii-5,mid+4)=-2.d0*de*x(5*n+8)**2
       1                            *(1.d0 + 2.d0*vratio*x(ii-1))*h**2
                            b(ii-5,mid+6)=- eps
                            b(ii-5,mid+7)=- eps
                            c(ii-5,4)=-4.d0*de*x(5*n+8)*x(ii-1)*h**2
       1                            *(1.d0 + vratio*x(ii-1))
                            b(ii-4,mid-4)=-2.d0*eps
                            b(ii-4,mid+1)=h**2 + 4.d0*eps
                            b(ii-4,mid+6)=-2.d0*eps
                            b(ii-3,mid-5)=-eps
                            b(ii-3,mid-4)=-eps
                            b(ii-3,mid)=2.d0*eps
                            b(ii-3,mid+1)=h**2 + 2.d0*eps
                            b(ii-3,mid+5)=-eps
```

```fortran
                                b(ii-3,mid+6)=-eps
                                b(ii-2,mid-4)=-eps*vratio
                                b(ii-2,mid-1)=-de*x(ii-1)*h**2
                                b(ii-2,mid+1)=vratio*h**2 - de*x(ii-3)*h**2
     1                                    + 2.d0*eps*vratio + x(ii)*h**2
                                b(ii-2,mid+2)=x(ii-1)*h**2
                                b(ii-2,mid+6)=-eps*vratio
                                b(ii-1,mid-7)=de
                                b(ii-1,mid-4)=1.d0
                                b(ii-1,mid-2)=-2.d0*de
                                b(ii-1,mid+1)=-2.d0
                                b(ii-1,mid+3)=de
                                b(ii-1,mid+6)=1.d0
   20           continue
                in=5*n
                c(in-1,1)=b(in-1,mid+6)
                b(in-1,mid+6)=0.d0
                b(in,mid-3)=-de
                b(in,mid)=-1.d0
                c(in,3)=1.d0
                c(in,6)=de
                b(in+1,mid)=1.d0
                c(in+1,1)=-1.d0/de*(1.d0-eqln)
                b(in+2,mid-5)=de
                b(in+2,mid-2)=1.d0
                b(in+2,mid)=-2.d0*de
                c(in+2,1)=-2.d0
                c(in+2,3)=1.d0
                c(in+2,6)=de
                b(in+3,mid)=1.d0
                c(in+3,1)=-1.d0/de
                b(in+4,mid)=1.d0
                d(1,5)=h/2.d0
                do 21 j=2,n
                        d(1,5*j)=h
   21           continue
                e(1,1)=h/2.d0
                d(2,2)=-2.d0*de
                d(2,5)=-2.d0
                d(2,7)=de
                d(2,10)=1.d0
                e(2,2)=1.d0
                e(2,5)=de
                d(3,in+2)=1.d0
                e(3,1)=-1.d0/de
                d(4,4)=x(in+8)*h/2.d0
```

273

```fortran
      do 40 j=2,n
               d(4,5*j-1)=x(in+8)*h
40    continue
      d(4,in+4)=x(in+8)*h/2.d0
      e(4,4)=h/2.d0*sum2
      d(5,2)=h**2 + 4.d0*eps
      d(5,7)=-2.d0*eps
      e(5,5)=-2.d0*eps
      d(6,in-3)=-2.d0*eps
      d(6,in+2)=h**2 + 4.d0*eps
      e(6,6)=-2.d0*eps
      return
      end
```

```
              subroutine resid(res,x,eqln,vratio,a1,a2,de,pe,eps,am,ap,
     1                 adif,dam,dap,dadif,sum1,sum2,h,aterm,afact,n)
              implicit real*8(a-h,o-z)
              dimension res(5010,3),x(5010)

          res(1,1)=-(x(1)-x(5)/de*(1.d0-eqln))
              res(2,1)=-(x(2)-x(5)/de)
              res(3,1)=-(x(3)-x(5)/de)
              res(4,1)=-(x(4)+1.d0/vratio)
              do 5 i=2,n
              ii=5*i
c                 am=1.d0 + a2*vratio/x(ii)*(x(ii-4)+x(ii-3)+
c    1                    x(ii-2))
c                 ap=1.d0 + a2*vratio/x(ii)*(x(ii-4)+
c    1                    aterm*x(ii-3)+x(ii-2))
c                 adif=a2*vratio*((x(ii+1)+
c    1                    aterm*x(ii+2)+x(ii+3))/x(ii+5)-
c    1                    (x(ii-9)+aterm*x(ii-8)+x(ii-7))/
c    1                    x(ii-5))
              res(ii-5,1)=-(x(ii-4)*h**2
     1                    - 2.d0*de*x(5*n+8)**2*(1.d0 + vratio*
     1                    x(ii-1))*x(ii-1)*h**2
     1                    - eps*(x(ii+1)-2.d0*x(ii-4)+x(ii-9))
     1                    - eps*(x(ii+2)-2.d0*x(ii-3)+x(ii-8)))
              res(ii-4,1)=-(x(ii-3)*h**2
     1                    - 2.d0*eps*(x(ii+2)-2.d0*x(ii-3)+x(ii-8)))
              res(ii-3,1)=-(x(ii-2)*h**2
     1                    - eps*(x(ii+3)-2.d0*x(ii-2)+x(ii-7))
     1                    - eps*(x(ii+2)-2.d0*x(ii-3)+x(ii-8)))
              res(ii-2,1)=-((1.d0 + vratio*x(ii-1))*h**2
     1                    - de*x(ii-3)*x(ii-1)*h**2
     1                    - eps*vratio*(x(ii+4)-2.d0*x(ii-1)+x(ii-6))
     1                    + h**2*x(ii)*x(ii-1))
              res(ii-1,1)=-((x(ii+5)-2.d0*x(ii)+x(ii-5))
     1                    + de*(x(ii+2)-2.d0*x(ii-3)+x(ii-8)))
5         continue
          res(5*n,1)=-(x(5*n+7)-x(5*n) + de*(x(5*n+10)-x(5*n-3)))
          res(5*n+1,1)=-(x(5*n+1)-x(5*n+5)/de*(1.d0-eqln))
          res(5*n+2,1)=-((x(5*n+7)-2.d0*x(5*n+5)+x(5*n))
     1                 + de*(x(5*n+10)-2.d0*x(5*n+2)+x(5*n-3)))
          res(5*n+3,1)=-(x(5*n+3)-x(5*n+5)/de)
          res(5*n+4,1)=-(x(5*n+4)+1.d0/vratio)
          sum1=0.d0
          sum2=0.d0
          do 10 i=1,n
                  inum=5*i
```

```
                    sum1=sum1+(x(inum)+x(inum+5))
                    sum2=sum2+(x(inum-1)+x(inum+4))      .
10      continue
        res(5*n+5,1)=-(h/2.d0*sum1 - 1.d0)
        res(5*n+6,1)=-((x(10)-2.d0*x(5)+x(5*n+6))
1              + de*(x(7)-2.d0*x(2)+x(5*n+9)))
        res(5*n+7,1)=-(x(5*n+2)-x(5*n+5)/de)
        res(5*n+8,1)=-(x(5*n+8)*h/2.d0*sum2-1.d0)
        res(5*n+9,1)=-(x(2)*h**2
1              - 2.d0*eps*(x(7)-2.d0*x(2)+x(5*n+9)))
        res(5*n+10,1)=-(x(5*n+2)*h**2
1              - 2.d0*eps*(x(5*n+10)-2.d0*x(5*n+2)+x(5*n-3)))

        return
        end
```

```fortran
      subroutine dresid(res,x,eqln,vratio,a1,a2,de,pe,eps,am,ap,
     1            adif,dam,dap,dadif,sum1,sum2,h,aterm,afact,n)
      implicit real*8(a-h,o-z)
      dimension res(5010,3),x(5010)

      go to 100
      res(1,2)=0.0
      res(2,2)=0.0
      res(3,2)=0.0
      res(4,2)=0.0
      do 60 i=2,n
      ii=5*i
          dam=vratio/x(ii)*(x(ii-4)+x(ii-3)+x(ii-2))
          dap=vratio/x(ii)*(x(ii-4)+
     1            aterm*x(ii-3)+x(ii-2))
          dadif=vratio*((x(ii+1)+
     1            aterm*x(ii+2)+x(ii+3))/x(ii+5)-
     1            (x(ii-9)+aterm*x(ii-8)+x(ii-7))/
     1            x(ii-5))
          res(ii-5,2)=-(dam*x(ii-4)*h**2
     1            + afact*vratio*h**2/x(ii)*(x(ii-4)**2
     1            + x(5*n+8)**2*(1.d0 + x(ii-1))**2)
     1            - eps*dap*(x(ii+1)-2.d0*x(ii-4)+x(ii-9))
     1            - eps*dadif*(x(ii+1)-x(ii-9))/4.d0)
          res(ii-4,2)=-(dam*x(ii-3)*h**2
     1            + afact*vratio*h**2/x(ii)*(x(ii-3)**2
     1            + x(5*n+8)**2*(1.d0 + x(ii-1))**2)
     1            - eps*dap*(x(ii+2)-2.d0*x(ii-3)+x(ii-8))
     1            - eps*dadif*(x(ii+2)-x(ii-8))/4.d0)
          res(ii-3,2)=-(dam*x(ii-2)*h**2
     1            + afact*vratio*h**2/x(ii)*x(ii-2)**2
     1            - eps*dap*(x(ii+3)-2.d0*x(ii-2)+x(ii-7))
     1            - eps*dadif*(x(ii+3)-x(ii-7))/4.d0)
          res(ii-2,2)=-(dam*(1.d0 + x(ii-1))*h**2
     1            + afact*vratio/x(ii)*(1.d0 + x(ii-1))*
     1            (x(ii-4)+x(ii-3))*h**2
     1            - eps*dap*(x(ii+4)-2.d0*x(ii-1)+x(ii-6))
     1            - eps*dadif*(x(ii+4)-x(ii-6))/4.d0)
          res(ii-1,2)=-(dap/pe*(x(ii+5)-2.d0*x(ii)+x(ii-5))
     1            + dadif/pe*(x(ii+5)-x(ii-5))/4.d0)
60    continue
      res(5*n,2)=0.0
      res(5*n+1,2)=0.0
      res(5*n+2,2)=0.0
      res(5*n+3,2)=0.0
      res(5*n+4,2)=0.0
```

```
        res(5*n+5,2)=0.0
        res(5*n+6,2)=-(1.d0/pe*(vratio/x(5)*
   1            (x(1)+aterm*x(2)+x(3)))*
   1            (x(10)-2.d0*x(5)+x(5*n+6))
   1            + vratio/pe*((x(11)+aterm*x(12)+x(13))/x(15)-
   1            (x(1)+aterm*x(2)+x(3))/x(5))*(x(10)-x(5*n+6))/4.d0)
        res(5*n+7,2)=-(1.d0/pe*(vratio/x(5*n+5)*
   1            (x(5*n+1)+aterm*x(5*n+2)+x(5*n+3)))*
   1            (x(5*n+7)-2.d0*x(5*n+5)+x(5*n))
   1            + vratio/pe*((x(5*n+1)+aterm*x(5*n+2)
   1            +x(5*n+3))/x(5*n+5)-
   1            (x(5*n-9)+aterm*x(5*n-8)+x(5*n-7))/x(5*n-5))
   1            *(x(5*n+7)-x(5*n))/4.d0)
        res(5*n+8,2)=0.0
100     do 150 i=1,5*n+10
            res(i,2)=0.d0
150     continue
        return
        end
```

```
                program initguess

c*****************************************************************************
c      program for generating initial guess to the non-linear
c           problem, using finite differences and subroutine arrow
c*****************************************************************************

                implicit real*8(a-h,o-z)
                dimension b(10000,6),c(10000,1),d(1,10000)
          dimension rhs(10000,1),xx(10000),e(1,1)
                dimension tx(10000),ty(10000),tz(10000),cn(10000)
                dimension grad(10000),velgrad(10000),x(50000)


c*****************************************************************************

                open(unit=1,file='mig.dat')
                open(unit=2,file='init.res')


c*****************************************************************************

                read (1,*)tau,n,de,eps,a20,a2fin,da2,icmax
                h=1.d0/n


c*****************************************************************************
c      n: no. of mesh intervals on each side
c      h:  mesh size
c*****************************************************************************


c*****************************************************************************
c           define parameters
c*****************************************************************************

                pe=de/eps
                delta=dsqrt(eps)
                large=1.d0/delta
                boltz=1.3806d-16
                temp=300
                tpolym=1.d-3
                cnav=1.d19
                vs=10.d0
                vratio=vs/(cnav*boltz*temp*tpolym)
                tyywall=1.d0
                eqln=500.0


c*****************************************************************************
c           generate initial values of ty(i), tz(i), and cn(i)
```

```
c**********************************************************************
        do 10 i=1,n+1
        xx(i)=(i-1)*h
        ty(i)=tyywall/vratio*(1.d0-dexp(-1.d0*large))/
1               (1.d0-dexp(-2.d0*large))*
1               (dexp(-1.d0*large*(1.d0-xx(i)))
1             + dexp(-1.d0*large*xx(i)))
        tz(i)=ty(i)
        cn(i)=1.d0
10      continue

c**********************************************************************
c       generate initial guess to grad(i)
c**********************************************************************

        iband=3
        mid=(iband + 1)/2
        nod=(n + 1)
        lbd=6
        jn=10000
        ja=1
        jna=10000
        nrhs=1
        lrhs=1
        iarrow=0
        do 20 i=2,n
                b(i,mid)=-2.d0*eps-h**2*(1.d0+de/vratio-de*ty(i))
        b(i,mid-1)=eps
        b(i,mid+1)=eps
                rhs(i,1)=h**2
20      continue
        b(1,mid)=1.d0
        rhs(1,1)=-1.d0
        b(n+1,mid)=1.d0
        rhs(n+1,1)=-1.d0
      call arrow(rhs,b,c,d,e,detlog,isign,tau,jn,iband,lbd,ja,jna,
1           nrhs,nod,iarrow,lrhs)
        do 30 i=1,n+1
                grad(i)=rhs(i,1)
30      continue

c**********************************************************************
c       generate initial value of shear and velgrad(i)
c       shear is obtained using trapezoid rule of integration
c**********************************************************************
```

```
            sum1=0.0
            do 40 i=1,n
                    sum1 = sum1 + (grad(i)+grad(i+1))
40          continue
            shear=2.d0/(h*sum1)
            do 50 i=1,n+1
                    velgrad(i)=shear*grad(i)
50          continue
```

c**
c   generate initial value of tx(i) using arrow
c**

```
        iband=3
        mid=(iband + 1)/2
        nod=(n + 1)
        lbd=6
        jn=10000
        ja=1
        jna=10000
        nrhs=1
        lrhs=1
            iarrow=0
        do 60 i=2,n
                    b(i,mid)=-2.d0*eps - h**2
            b(i,mid-1)=eps
            b(i,mid+1)=eps
                    rhs(i,1)=-2.d0*de*h**2*shear*velgrad(i)
     1                      -2.d0*de*h**2*velgrad(i)**2
60      continue
            b(1,mid)=1.d0
            rhs(1,1)=1.d0/vratio*(1.d0-eqln)
            b(n+1,mid)=1.d0
            rhs(n+1,1)=1.d0/vratio*(1.d0-eqln)
        call arrow(rhs,b,c,d,e,detlog,isign,tau,jn,iband,lbd,ja,jna,
     1          nrhs,nod,iarrow,lrhs)
            do 70 i=1,n+1
                    tx(i)=rhs(i,1)
70          continue
```

c**
c   write global values of the variables in file init.res
c**

```
        do 80 i=1,n+1
```

```
                       ii=5*i
                       x(ii-4)=tx(i)
                       x(ii-3)=ty(i)
                       x(ii-2)=tz(i)
                       x(ii-1)=grad(i)
                       x(ii)=cn(i)
80         continue
           go to 83
c*****************************************
           do 81 i=1,n+1
                       ii=5*i
                       x(ii-3)=0.d0
                       x(ii)=1.5d0
81         continue
           do 82 j=1,3
                       x(5*j)=5.d-1
                       x(5*(j+n-2))=5.d-1
                       x(5*j-3)=1.d0/vratio
                       x(5*(j+n-2)-3)=1.d0/vratio
82         continue
83         x(5*n+6)=1.d0
           x(5*n+7)=1.d0
c          x(5*n+6)=5.d-1
c          x(5*n+7)=5.d-1
           x(5*n+8)=shear
           x(5*n+9)=1.d0/vratio
           x(5*n+10)=1.d0/vratio
           do 90 i=1,5*n+10
                       write(2,*)x(i)
90         continue

       stop
       end
```

Subroutine: post.f

```fortran
program postprocess
implicit real*8(a-h,o-z)
dimension x(50000),xx(10000)

open(2,file='mig.res')
open(1,file='mig.dat')
open(10,file='tx.res')
open(11,file='ty.res')
open(12,file='tz.res')
open(13,file='grad.res')
open(14,file='cn.res')
open(15,file='shear.res')

read(1,*)tau,n,de,pe,a20,a2fin,da2,icmax
do 10 i=1,5*n+8
          read(2,*)x(i)
10        continue
h=1.d0/n

do 20 i=1,n+1
          xx(i)=(i-1)*h
          ii=5*i
          write(10,*)xx(i),x(ii-4)
          write(11,*)xx(i),x(ii-3)
          write(12,*)xx(i),x(ii-2)
          write(13,*)xx(i),x(ii-1)
          write(14,*)xx(i),x(ii)
20        continue
shear=x(5*n+8)
write(15,200)shear
200       format(1x,"Shear stress in the gap is :",1x,f10.4)

stop
end
```

Subroutine: vel.f

```fortran
              program velocity

              implicit real*8(a-h,o-z)
              dimension grad(1010),vel(1010),y(1010)

              open(unit=1,file='grad.res')
              open(unit=2,file='shear.dat')
              open(unit=3,file='vel.dat')
              open(unit=10,file='vel.res')

              read(3,*)n
              h=1.d0/n
              do 10 i=1,n+1
                      read(1,*)y(i),grad(i)
10            continue
              read(2,*)shear

              vel(1)=0.d0
              do 20 i=2,n+1
                      vel(i)=vel(i-1) +
     1                shear*h/2.d0*(grad(i-1)+grad(i))
20            continue

              do 30 i=1,n+1
                      write(10,*)y(i),vel(i)
30            continue
              stop
              end
```

Bibliography

[1] Standard and Poor's Industry Surveys: Chemicals Basic Analysis, Vol. 157, No. 44, November 1989.

[2] S. G. Advani and C. L. Tucker. The Use of Tensors to Describe and Predict Fiber Orientation in Short Fiber Composites. *J. Rheol.*, 31(8):751–784, 1987.

[3] S. G. Advani and C. L. Tucker. Closure Approximations for Three-Dimensional Structure Tensors. *J. Rheol.*, 34(3):367–386, 1990.

[4] R. C. Armstrong. Kinetic Theory and Rheology of Dilute Solutions of Flexible Macromolecules-I. Steady State Behavior. *J. Chem. Phys.*, 60:724–728, 1974.

[5] R. C. Armstrong. Kinetic Theory and Rheology of Dilute Solutions of Flexible Macromolecules-II. Linear Viscoelasticity. *J. Chem. Phys.*, 60:729–733, 1974.

[6] J. H. Aubert, S. Prager, and M. Tirrell. Macromolecules in Nonhomogeneous Velocity Gradient Fields-II. *J. Chem. Phys.*, 73(8):4103–4112, 1980.

[7] J. H. Aubert and M. Tirrell. Macromolecules in Nonhomogeneous Velocity Gradient Fields. *J. Chem. Phys.*, 72(4):2694–2701, 1980.

[8] J. H. Aubert and M. Tirrell. Effective Viscosity of Dilute Polymer Solutions Near Confining Boundaries. *J. Chem. Phys.*, 77(1):553–561, 1982.

[9] D. Ausserre, J. Edwards, J. Lecourtier, H. Hervet, and F. Rondelez. Hydrodynamic Thickening of Depletion Layers in Polymer Solutions. *Europhys. Lett.*, 14(1):33–38, 1991.

[10] P. Baldwin and E. Helfand. Dilute Polymer Solution in Steady Shear Flow-Non-Newtonian Stress. *Phys. Rev. A*, 41:6772–6785, 1990.

[11] A. N. Beris and B. J. Edwards. Poisson-Bracket Formulation of Viscoelastic Flow Equations of Differential Type - A Unified Approach. *J. Rheol.*, 34(4):503–538, 1990.

[12] A. V. Bhave, R.C. Armstrong, and R. A. Brown. Kinetic Theory and Rheology of Dilute, Nonhomogeneous Polymer Solutions. *J. Chem. Phys.*, 95(4):2988–3000, 1991.

[13] A. V. Bhave, R.K. Menon, R.C. Armstrong, and R. A. Brown. A Constitutive Equation for Liquid Crystalline Polymer Solutions. submitted for publication in J. Rheol.

[14] R. B. Bird. Experimental Tests of Generalized Newtonian Models containing a Zero-Shear Viscosity and a Characteristic Time. *Can. J. Chem. Eng.*, 43:161–167, 1965.

[15] R. B. Bird. Use of simple molecular models in the study of the mechanical behavior of solutions of flexible macromolecules. Technical Report 53, The University of Wisconsin Rheology Research Center, 1978.

[16] R. B. Bird, R. C. Armstrong, and O. Hassager. *Dynamics of Polymeric Liquids,* Vol. I. Fluid Mechanics. John Wiley & Sons, New York, second edition, 1987.

[17] R. B. Bird, C. F. Curtiss, R. C. Armstrong, and O. Hassager. *Dynamics of Polymeric Liquids,* Vol. II. Kinetic Theory. John Wiley & Sons, New York, second edition, 1987.

[18] R. B. Bird and J. R. DeAguiar. An Encapsulated Dumbbell Model for Concentrated Polymer Solutions and Melts-I. Theoretical Development and Constitutive Equation. *J. Non-Newt. Fluid Mech.*, 13:149–160, 1983.

[19] R. B. Bird and H. C. Öttinger. Transport Properties of Polymeric Liquids. *Ann. Rev. Phys. Chem.*, 43, 1992.

[20] R. B. Bird, W. E. Stewart, and E. N. Lightfoot. *Transport Phenomena*. John Wiley and Sons, Inc., New York, 1960.

[21] I. Bitsanis and G. Hadziioanou. Molecular Dynamics Simulations of the Structure and Dynamics of Confined Polymer Melts. *J. Chem. Phys.*, 92(6):3827–3847, 1990.

[22] J. Brandrup, E. H. Immergut, and W. McDowell, editors. *Polymer Handbook*. John Wiley & Sons, second edition, 1975.

[23] R. A. Brown, R. C. Armstrong, A. N. Beris, and P. W. Yeh. Galerkin Finite Element Analysis of Complex Viscoelastic Flows. *Comput. Meth. Appl. Engg.*, 58:201–226, 1986.

[24] P. O. Brunn. The Effect of a Solid Wall for the Flow of Dilute Macromolecular Solutions. *Rheol. Acta*, 15:23–29, 1976.

[25] P. O. Brunn. Hydrodynamically Induced Cross-Stream Migration of Dissolved Macromolecules (Modelled as Nonlinearly Elastic Dumbbells). *Int. J. Multiphase Flow*, 9(2):187–202, 1983.

[26] P. O. Brunn and S. Chi. Macromolecules in Nonhomogeneous Flow Fields: A General Study for Dumbbell Model Macromolecules. *Rheol. Acta*, 23:163–171, 1984.

[27] P. O. Brunn and S. Grisafi. Kinetic Theory of a Dilute Polymer Solution in a Small Channel: Equilibrium Results. *Chem. Eng. Comm.*, 36:367–383, 1985.

[28] W. R. Burghardt and G. G. Fuller. Role of Director Tumbling in the Rheology of Polymer Liquid Crystal Solutions. *Macromolecules*, 24(9):2546–2555, 1991.

[29] J. W. Cahn. Phase Separation by Spinodal Decomposition. *J. Chem. Phys.*, 42(1):93–99, 1961.

[30] J. W. Cahn. On Spinodal Decomposition. *Acta Metallurgica*, 9:795–801, 1965.

[31] S. Chandrasekhar. *Liquid Crystals*. Cambridge University Press, New York, 1977.

[32] G. Chauveteau. Rodlike Polymer Solution Flow Through Fine Pores: Influence of Pore Size on Rheological Behavior. *J. Rheol.*, 26(2):111–142, 1982.

[33] M. D. Chilcott and J. M. Rallison. Creeping Flow of Dilute Polymer Solutions Past Cylinders and Spheres. *J. Non-Newt. Fluid Mech.*, 29:381–432, 1988.

[34] P. Chossat, R. Lauterbach, and I. Melbourne. Steady-State Bifurcation with O(3) Symmetry. *Arch. Rat. Mech. Anal.*, 113:313–376, 1990.

[35] I. Chuang, N. Turok, and B. Yurke. Late-Time Coarsening Dynamics in a Nematic Liquid Crystal. *Phys. Rev. Lett.*, 66(19):2472–2475, 1991.

[36] A. Ciferri, W. R. Krigbaum, and R. B. Meyer. *Polymer Liquid Crystals*. Academic Press, New York, 1982.

[37] P. J. Coates. *Simulation of the Flow of Viscoelastic Fluids in Contraction Geometries*. PhD thesis, Massachusetts Institute of Technology, May 1992.

[38] P. J. Coates, R. C. Armstrong, and R. A. Brown. Calculation of Steady-State Viscoelastic Flow Through Axisymmetric Contractions with the EEME Formulation. *J. Non-Newt. Fluid Mech.*, 42:141–188, 1992.

[39] Y. Cohen and A. B. Metzner. Slip Phenomena in Polymeric Solutions Flowing Through Small Channels. *AIChE Symp. Ser.*, 78(212):77–85, 1982.

[40] Y. Cohen and A. B. Metzner. Apparent Slip Flow of Polymer Solutions. *J. Rheol.*, 29:67–102, 1985.

[41] Y. Cohen and A. B. Metzner. An Analysis of Apparent Slip Flow of Polymer Solutions. *Rheol. Acta*, 25(1):28–35, 1986.

[42] C. F. Curtiss and R. B. Bird. A Kinetic Theory for Polymer Melts-I. The Equation for the Single-Link Orientational Distribution Function. *J. Chem. Phys.*, 74(3):2016–2025, 1981.

[43] C. F. Curtiss and R. B. Bird. A Kinetic Theory for Polymer Melts-II. The Stress Tensor and the Rheological Equation of State. *J. Chem. Phys.*, 74(3):2026–2033, 1981.

[44] J. S. Dahler, S. Fesciyan, and N. Xystris. Rheological Properties of a Semidilute Solution of Rodlike Macromolecules. 2. Transient Flows. *Macromolecules*, 16:1673–1677, 1983.

[45] P. -G. de Gennes. Reptation of a Polymer Chain in Presence of Fixed Obstacles. *J. Chem. Phys.*, 55:572–579, 1971.

[46] P. -G. de Gennes. *The Physics of Liquid Crystals*. Clarendon Press, Oxford, 1974.

[47] S. R. de Groot and P. Mazur. *Non-Equilibrium Thermodynamics*. Dover Publications, Inc., New York, 1984.

[48] J. J. de Pablo, H. C. Öttinger, and Y. Rabin. Hydrodynamic Changes of the Depletion Layer of Dilute Polymer Solutions Near a Wall. *AIChE J.*, 38(2):273–283, 1992.

[49] J. R. DeAguiar. An Encapsulated Dumbbell Model for Concentrated Polymer Solutions and Melts-II. Calculation of Material Functions and Experimental Comparisions. *J. Non-Newt. Fluid Mech.*, 13:161–179, 1983.

[50] W. R. Dean and P. E. Montagnon. On the Steady Motion of Viscous Liquid in a Corner. *Proc. Camb. Phil. Soc.*, 45:389–394, 1949.

[51] M. M. Denn. Issues in Viscoelastic Fluid Mechanics. *Ann. Rev. Fluid Mech.*, 22:13–34, 1990.

[52] M. Doi. Rheological Properties of Rodlike Polymers in Isotropic and Liquid Crystalline Phases. *Ferroelectrics*, 30:247–254, 1980.

[53] M. Doi. Molecular Dynamics and Rheological Properties of Concentrated Solutions of Rod-Like Polymers in Isotropic and Liquid Crystalline Phases. *J. Polym. Sci.: Polym. Phys. Ed.*, 19:229–243, 1981.

[54] M. Doi and S. F. Edwards. Dynamics of Concentrated Polymer Systems. 1. Brownian Motion in Equilibrium State. *J. Chem. Soc., Faraday Trans. II*, 74(10):1789–1801, 1978a.

[55] M. Doi and S. F. Edwards. Dynamics of Concentrated Polymer Systems. 2. Molecular Motion Under Flow. *J. Chem. Soc., Faraday Trans. II*, 74(10):1802–1817, 1978b.

[56] M. Doi and S. F. Edwards. Dynamics of Concentrated Polymer Systems. 3. Constitutive Equation. *J. Chem. Soc., Faraday Trans. II*, 74(10):1818–1832, 1978c.

[57] M. Doi and S. F. Edwards. Dynamics of Concentrated Polymer Systems. 4. Rheological Properties. *J. Chem. Soc., Faraday Trans. II*, 75(1):38–54, 1979.

[58] M. Doi and S. F. Edwards. *The Theory of Polymer Dynamics*. Clarendon Press, Oxford, 1986.

[59] M. Doi, T. Shimada, and K. Okano. Concentration Fluctaution of Stiff Polymers. II. Dynamical Structure Factor of Rod-Like Polymers in the Isotropic Phase. *J. Chem. Phys.*, 88(6):4070–4075, 1988.

[60] D. Doraiswamy and A. B. Metzner. The Rheology of Polymeric Liquid Crystals. *Rheol. Acta*, 25:580–587, 1986.

[61] E. Duering and Y. Rabin. Polymers in Shear Flow near Repulsive Boundaries. *Macromolecules*, 23:2232–2237, 1990.

[62] A. El-Kareh and L. G. Leal. Existence of Solutions for All Deborah Numbers for a Non-Newtonian Model Modified to Include Diffusion. *J. Non-Newt. Fluid Mech.*, 33:257–287, 1989.

[63] J. L. Ericksen. Anisotropic Fluids. *Arch. Rat. Mech. Anal.*, 4(3):231-237, 1960.

[64] J. L. Ericksen. Conservation Laws for Liquid Crystals. *Trans. Soc. Rheol.*, 5:23-34, 1961.

[65] J. L. Ericksen. A Thermodynamic View of Order Parameters for Liquid Crystals. In J. L. Ericksen, editor, *Orienting Polymers*, pages 27-36. Springer-Verlag, New York, 1984.

[66] X. J. Fan. *Acta Mech. Sinica*, 5:216-226, 1989.

[67] J. D. Ferry. *Viscoelastic Properties of Polymers*. John Wiley & Sons, New York, second edition, 1980.

[68] M. Fixman. Dynamics of Polymer Chains. *J. Chem. Phys.*, 42:3831, 1965.

[69] P. J. Flory. *Statistical Mechanics of Chain Molecules*. Wiley-Interscience, New York, 1969.

[70] F. C. Frank. On the Theory of Liquid Crystals. *Disc. Faraday Soc.*, 25:19-28, 1958.

[71] H. Giesekus. A Simple Constitutive Equation for Polymer Fluids Based on the Concept of Deformation-Dependant Tensorial Mobility. *J. Non-Newt. Fluid Mech.*, 11:69-109, 1982.

[72] J. T. Gleeson, R. G. Larson, D. W. Mead, G. Kiss, and P. E. Cladis. Image Analysis of Shear-Induced Textures in Liquid-Crystalline Polymers. *Liq. Cryst.*, 11(3):341-364, 1992.

[73] M. Golibutsky and D. Schaeffer. Bifurcations with O(3) Symmetry Including Application to the Bénard Problem. *Comm. Pure Appl. Math.*, 35:81-111, 1982.

[74] F. Greco and G. Marrucci. Molecular Structure of the Hedgehog Point Defect in Nematics. *Mol. Cryst. Liq. Cryst.*, 210:129-141, 1992.

[75] F. Greco and G. Marrucci. Rodlike Molecule Dynamics. The Tumbling Regime. *Mol. Cryst. Liq. Cryst.*, 212:125–137, 1992.

[76] G. L. Hand. A Theory of Anisotropic Fluids. *J. Fluid Mech.*, 13(1):33–46, 1962.

[77] E. Helfand and G. H. Fredrickson. Large Fluctuations in Polymer Solutions under Shear. *Phys. Rev. Lett.*, 62(21):2468–2471, 1989.

[78] E. J. Hinch and L. G. Leal. The Effect of Brownian Motion on the Rheological Properties of a Suspension of Non-Spherical Particles. *J. Fluid Mech.*, 52(4):683–712, 1972.

[79] E. J. Hinch and L. G. Leal. Constitutive Equations in Suspension Mechanics. Part 2. Approximate Forms for a Suspension of Rigid Particles Affected by Brownian Rotations. *J. Fluid Mech.*, 76(1):187–208, 1976.

[80] J. Honerkamp and R. Seitz. Transient Behavior of Liquid Crystalline Polymers. *J. Chem. Phys.*, 87(5):3120–3126, 1987.

[81] T. D. Hu and G. Ryskin. Numerical Simulation of Rodlike Polymers in a Uniaxial Extensional Flow: The Distribution-Function Version vs. The Order-Parameter Version of Doi's Theory. *J. Chem. Phys.*, 95(8):6042–6049, 1991.

[82] G. Iooss and D. D. Joseph. *Elementary Stability and Bifurcation Theory*. Springer-Verlag, New York, 1980.

[83] S. Jain and C. Cohen. Rheology of Rodlike Molecules in Semidilute Solutions. *Macromolecules*, 14:759–765, 1981.

[84] R. Keunings. On the High Weissenberg Number Problem. *J. Non-Newt. Fluid Mech.*, 20:209–226, 1986.

[85] J. G. Kirkwood and P. L. Auer. *J. Chem. Phys.*, 19:281–, 1951.

[86] G. Kiss and R. S. Porter. Rheology of Concentrated Solutions of poly-(γ-benzyl-glutatmate). *J. Polym. Sci., Polym. Symp.*, 65:193–211, 1978.

[87] W. Kozicki, S. N. Pasari, A. R. K. Rao, and C. Tiu. Anomalous Effects in Laminar Capillary Flow of Polymer Solutions. *Chem. Eng. Sci.*, 25(1):41, 1970.

[88] H. A. Kramers. The Behavior of Macromolecules in Inhomogeneous Flow. *J. Chem. Phys.*, 14(7):415–424, 1946. translated from *Physica*, 11:1-19, 1944.

[89] N. Kuzuu and M. Doi. Constitutive Equation for Nematic Liquid Crystals under Weak Velocity Gradient derived from a Molecular Kinetic Equation. *J. Phys. Soc. Japan*, 52(10):3486–3494, 1983.

[90] N. Kuzuu and M. Doi. Constitutive Equation for Nematic Liquid Crystals under Weak Velocity Gradient derived from a Molecular Kinetic Equation. II.Leslie Coefficients for Rodlike Polymers. *J. Phys. Soc. Japan*, 53(3):1031–1040, 1984.

[91] R. G. Larson. *Constitutive Equations for Polymer Melts and Solutions*. Butterworths, Boston, 1988.

[92] R. G. Larson. Arrested Tumbling in Shearing Flows of Liquid Crystal Polymers. *Macromolecules*, 23:3983–3992, 1990.

[93] R. G. Larson and M. Doi. Mesoscopic Domain Theory for Textured Liquid Crystalline Polymers. *J. Rheol.*, 35(4):539–563, 1991.

[94] R. G. Larson, D. W. Mead, and J. T. Gleeson. Texture of a Liquid Crystalline Polymer During Shear. In *Proc. XIth Intl. Congress on Rheology, Brussels, Belgium*, pages 65–69, 1992.

[95] R. G. Larson and H. C. Öttinger. Effect of Molecular Elasticity on Out-of-Plane Orientations in Shearing Flows of Liquid-Crystalline Polymers. *Macromolecules*, 24:6270–6282, 1991.

[96] S. -D. Lee. Comment on Effects of Elongational Flow on the Isotropic-Nematic Phase Transition of Rod-Like Systems. *J. Chem. Phys.*, 86(11):6567–6568, 1987.

[97] F. M. Leslie. Some Constitutive Equations for Anisotropic Fluids. *Quart. J. Mech. Appl. Math.*, 19:357, 1966.

[98] F. M. Leslie. Some Constitutive Equations for Liquid Crystals. *Arch. Rat. Mech. Anal.*, 28:265, 1968.

[99] G. G. Lipscomb, R. Keunings, and M. M. Denn. Implications of Boundary Singularities in Complex Geometries. *J. Non-Newt. Fluid Mech.*, 24:85–96, 1987.

[100] A. S. Lodge. *Body Tensor Fields in Continuum Mechanics*. Academic Press, New York, 1974.

[101] A. S. Lodge. On Using Rubber as a Guide for Understanding Polymeric Liquid Behavior. In A. S. Lodge, M. Renardy, and J. A. Nohel, editors, *Viscoelasticity and Rheology*, pages 181–208. Academic Press, 1985.

[102] J. J. Magda, S. –G. Baek, K. L. DeVries, and R. G. Larson. Shear Flows of Liquid Crystal Polymers: Measurements of the Second Normal Stress Differnce and the Doi Molecular Theory. *Macromolecules*, 24(15):4460–4468, 1991.

[103] W. Maier and A. Saupe. Eine Einfache Molekulare Theorie des Nematischen Kristallinflussigen Zustandes. *Z. Naturforsch*, 13a:561–566, 1958.

[104] W. Maier and A. Saupe. Eine Einfache Molekular-Statistische Theorie der Nematischen Kristallinflussigen Phase. *Z. Naturforsch*, 14a:882–889, 1959.

[105] K. V. Mansfield and D. N. Theodorou. Interfacial Structure and Dynamics of Macromolecular Liquids: A Monte Carlo Simulation Approach. *Macromolecules*, 22:3143–3152, 1989.

[106] J. M. Marchal and M. J. Crochet. A New Mixed Finite Element for Calculating Viscoelastic Flow. *J. Non-Newt. Fluid Mech.*, 26:77–114, 1987.

[107] G. Marrucci. Prediction of Leslie Coefficients for Rodlike Polymer Nematics. *Mol. Cryst. Liq. Cryst. (Lett.)*, 72:153–161, 1982.

[108] G. Marrucci. Remarks on the viscosity of polymeric liquid crystals. In *Proc. IX Intl. Congress on Rheology, Mexico*, pages 441–448, 1984.

[109] G. Marrucci and F. Greco. The Elastic Constants of Maier-Saupe Rodlike Molecule Nematics. *Mol. Cryst. Liq. Cryst.*, 206:17–30, 1991.

[110] G. Marrucci and P. L. Maffettone. Description of Liquid-Crystalline Phase of Rodlike Polymers at High Shear Rates. *Macromolecules*, 22:4076–4082, 1989.

[111] V. G. Mavrantzas and A. N. Beris. Modelling of the Rheology and Flow-Induced Concentration Changes in Polymer Solutions. *Phys. Rev. Lett.*, 69(2):273–276, 1992.

[112] V. G. Mavrantzas and A. N. Beris. Theoretical Study of the Wall Effects on the Rheology of Dilute Polymer Solutions. *J. Rheol.*, 36(1):175–213, 1992.

[113] R. K. Menon. *Kinetic Theory, Rheology and Complex Flows of Liquid-Crystalline Polymers*. PhD thesis, Massachusetts Institute of Technology, September 1990.

[114] A. B. Metzner, Y. Cohen, and C. Rangel-Nafaile. Inhomogeneous Flows of Non-Newtonian Fluids: Generation of Spatial Concentration Gradients. *J. Non-Newt. Fluid Mech.*, 5:449–462, 1979.

[115] H. K. Moffatt. Viscous and Resistive Eddies Near a Sharp Corner. *J. Fluid Mech.*, 18:1–18, 1964.

[116] P. Moldenaers and J. Mewis. Relaxational Phenomena and Anisotropy in Lyotropic Polymeric Liquid Crystals. *J. Non-Newt. Fluid Mech.*, 34:359–374, 1990.

[117] J. G. Oldroyd. On the Formulation of Rheological Equations of State. *Proc. Roy. Soc.*, A200:523–541, 1950.

[118] J. G. Oldroyd. An Approach to Non-Newtonian Fluid Mechanics. *J. Non-Newt. Fluid Mech.*, 14:9–46, 1984.

[119] P. D. Olmsted and P. Goldbart. Theory of the Nonequilibrium Phase Transition for Nematic Liquid Crystals Under Shear Flow. *Phys. Rev. A.*, 41(8):4578–4581, 1990.

[120] E. T. Onat and F. A. Leckie. Representation of Mechanical Behavior in the Presence of Changing Internal Structure. *J. Appl. Mech.*, 55(1):1–10, 1988.

[121] S. Onogi and T. Asada. Rheology and Rheo-Optics of Polymer Liquid Crystals. In G. Astarita, G. Marrucci, and L. Nicolais, editors, *Rheology. Vol. 1: Principles*, pages 127–148. ˙ lenum Press, 1980.

[122] L. Onsager. The Effects of Shape on the Interaction of Colloidal Particles. *Ann. N. Y. Acad. Sci.*, 51:627–659, 1949.

[123] H. C. Öttinger. Consistently Averaged Hydrodynamic Interaction for Rouse Dumbbells in Steady Shear Flow. *J. Chem. Phys.*, 83(12):6535–6536, 1985.

[124] H. C. Öttinger. Consistently Averaged Hydrodynamic Interaction for Rouse Dumbbells: Series Expansions. *J. Chem. Phys.*, 84(7):4068–4073, 1986.

[125] H. C. Öttinger. Consistently Averaged Hydrodynamic Interaction for Rouse Dumbbells: Translational Diffusivity. *J. Chem. Phys.*, 87(10):6185–6190, 1987.

[126] H. C. Öttinger. Diffusivity of Polymers in Dilute Solutions Undergoing Homogeneous Flows. *AIChE Journal*, 35(2):279–286, 1989.

[127] H. C. Öttinger. Renormalization-Group Calculation of Excluded-Volume Effects on the Viscometric Functions for Dilute Polymer Solutions. *Phys. Rev. A*, 40(5):2664–2671, 1989.

[128] H. C. Öttinger. Renormalization of Various Quantities for Dilute Polymer Solutions Undergoing Shear Flow. *Phys. Rev. A*, 41(8):4413–4420, 1990.

[129] H. C. Öttinger. A Class of Multiparticle Constitutive Equations. *J.Rheol.*, 35(6):1275–1301, 1991.

[130] H. C. Öttinger. Incorporation of Polymer Diffusivity and Migration into Constitutive Equations. *Rheol. Acta*, 31:14-21, 1992.

[131] A. C. Ouano and J. Biesenberger. Diffusional Phenomena in Dilute Polymer Solutions Flowing in Capillaries. *J. Chromat.*, 55:145-154, 1971.

[132] O. Parodi. Stress Tensor for a Nematic Liquid Crystal. *J. de Physique (Paris)*, 31(7):581-584, 1970.

[133] R. Pecora. Dynamics of Rodlike Macromolecules in Semidilute Solutions. *J. Polym. Sci., Polym. Symp.*, 73:83-91, 1985.

[134] S. Ramalingam. *Fiber Spinning and Rheology of Liquid Crystalline Polymers.* PhD thesis, Massachusetts Institute of Technology, 1993.

[135] A. V. Ramamurthy. Wall Slip in Viscous Fluids and Influence of Materials of Construction. *J. Rheol.*, 30(2):337-357, 1986.

[136] M. Reiner. The Deborah number. *Phys. Today*, 17:62, 1964.

[137] M. Renardy. Short Wave Instabilities Resulting From Memory Slip. *J. Non-Newt. Fluid Mech.*, 35:73-76, 1990.

[138] M. Renardy, W. J. Hrusa, and J. A. Nohel. *Mathematical Problems in Viscoelasticity.* Longman Scientific & Technical, 1987.

[139] F. Rondelez, D. Ausserre, and H. Hervet. Experimental Studies of Polymer Concentration Profiles at Solid-Liquid and Gas-Liquid Interfaces by Optical and X-Ray Evanescent Wave Techniques. *Ann. Rev. Phys. Chem.*, 38:317-347, 1987.

[140] P. E. Rouse. *J. Chem. Phys.*, 21:1272-1280, 1953.

[141] R. H. Schaefer, N. Laiken, and B. H. Zimm. Molecules in Cylindrical Flow. 1. Theory of Free-Draining Model. *Biophys. Chem.*, 2(2):180-184, 1974.

[142] J. D. Schieber and H. C. Öttinger. The Effects of Bead Inertia on the Rouse Model. *J. Chem. Phys.*, 89(11):6972–6981, 1988.

[143] W. R. Schowalter. The Behavior of Complex Fluids at Solid Boundaries. *J. Non-Newt. Fluid Mech.*, 29:25–36, 1988.

[144] H. See, M. Doi, and R. G. Larson. The Effect of Steady Flow Fields on the Isotropic-Nematic Phase Transition of Rigid Rod-Like Polymers. *J. Chem. Phys.*, 92(1):792–800, 1990.

[145] G. Sekhon, R. C. Armstrong, and M. S. Jhon. The origin of polymer migration in a nonhomogeneous flow field. *J. Polymer Sci. Polymer Phys. Ed.*, 20:947–952, 1982.

[146] M. Srinivasrao and G. C. Berry. Rheo-Optical Studies of Aligned Nematic Solutions of a Rodlike Polymer. *J. Rheol.*, 35(3):379–397, 1991.

[147] H. E. Stanley. *Introduction to Phase Transitions and Critical Phenomena.* Oxford University Press, New York, 1971.

[148] M. J. Stephen and J. P. Straley. Physics of Liquid Crystals. *Rev. Mod. Phys.*, 46(4):617–704, 1974.

[149] W. E. Stewart and J. P. Sørensen. Hydrodynamic Interaction Effects in Rigid Dumbbell Suspensions. II. Computations for Steady Shear Flow. *Trans. Soc. Rheol.*, 16(1):1–13, 1972.

[150] J. P. Straley. Frank Elastic Constants of the Hard-Rod Liquid Crystal. *Phys. Rev. A*, 8(4):2181–2183, 1973.

[151] D. N. Theodorou. Lattice Models for Bulk Polymers at Interfaces. *Macromolecules*, 21(5):1391–1400, 1988.

[152] D. N. Theodorou. Structure and Thermodynamics of Bulk Homopolymer/Solid Interfaces: A Site Lattice Model Approach. *Macromolecules*, 21(5):1400–1410, 1988.

[153] N. Thérien, B. Coupal, and J. L. Corneille. Experimental Confirmation of Film Thickness for Non-Newtonian Liquids in Gravity Flow on Inclined Planes. *Can. J. Chem. Eng.*, 48:17, 1970.

[154] D. Thirumalai. Effect of Elongational Flow on the Isotropic-Nematic Phase Transition of Rod-Like Systems. *J. Chem. Phys.*, 84(10):5869–5873, 1986.

[155] M. Tirrell and M. F. Malone. Stress-Induced Diffusion of Macromolecules. *J. Polym. Sci.: Polym. Phys. Ed.*, 15:1569–1583, 1977.

[156] V. Tsvetkov. *Acta Physicochim. (USSR)*, 16:132, 1942.

[157] S. Wang and W. M. Gelbart. Effect of Elongational Flow on the Orientational Order Phase Transitions and Viscosity of Hard Rod Fluids. *J. Chem. Phys.*, 90(1):597–598, 1988.

[158] H. R. Warner. Kinetic Theory and Rheology of Dilute Suspensions of Finitely Extendible Dumbbells. *Ind. Eng. Chem. Fundamentals*, 11:379–387, 1972.

[159] L. E. Wedgewood, D. N. Ostrov, and R. B. Bird. A Finitely Extensible Bead-Spring Chain Model for Dilute Polymer Solutions. *J. Non-Newt. Fluid Mech.*, 40:119–139, 1991.

[160] L. R. Whitlock and R. S. Porter. Experimental Investigation of Concept of Molecular Migration Within Sheared Polystyrene. *J. Polym. Sci. A-2*, 10:877, 1972.

[161] K. F. Wissbrun. Rheology of Rod-Like Polymers in the Liquid Crystalline State. *J. Rheol.*, 26:619–662, 1981.

[162] A. Yethiraj and C. K. Hall. Monte Carlo Simulations of Polymers Confined between Flat Plates. *Macromolecules*, 23(6):1865–1872, 1990.

[163] B. H. Zimm. Dynamics of Polymer Molecules in Dilute Solutions – Viscoelasticity, Flow Birefringence and Dielectric Loss. *J. Chem. Phys.*, 24(2):269–278, 1956.